The Dissertation Committee for Joshua David Engstrom certifies that this is the approved version of the following dissertation:

Stable Submicron Protein Particles: Formation, Properties, and Pulmonary Applications

Committee:

Keith P. Johnston, Supervisor

Robert O. Williams III, Co-Supervisor

Thomas M. Truskett

Krishnendu Roy

Nicholas A. Peppas

Venkat Ganesan

Stable Submicron Protein Particles: Formation, Properties, and Pulmonary Applications

by

Joshua David Engstrom, B.S.

Dissertation

Presented to the Faculty of the Graduate School of

The University of Texas at Austin

in Partial Fulfillment

of the Requirements

for the Degree of

Doctor of Philosophy

The University of Texas at Austin

August 2007

Dedication

To my loving wife and children

Acknowledgements

I want to give special thanks to my wife, Jenalyn, for her patience, love, caring, and support throughout our graduate school experience in Austin. Her excitement and encouragement for my pursuit of a graduate degree was always very motivating and inspired me to continually push forward. I also want to thank my parents for their undeviating support and encouragement.

I am grateful for the educators who guided and inspired me to pursue my educational ambitions. Special thanks are given to my high school chemistry teacher, Mrs. Marian DeWane, who helped me build a strong foundation in chemistry and encouraged me to pursue a career in chemical engineering. I also want to thank Professor Thomas Fletcher from my undergraduate days at Brigham Young University who introduced me to undergraduate research and guided me toward graduate school.

Special thanks are given to Professors Keith P. Johnston and Robert O. Williams III for their guidance and advice throughout my graduate career. This work would not have been possible without the countless hours we spent discussing and crafting exciting research ideas for my educational and professional development. I also want to give special thanks to Professor G. Barrie Kitto whose help was invaluable for my initial work in proteins.

I am especially grateful for the labmates with whom I had the opportunity to work. Their support greatly accelerated this work. Specifically I would like to thank Dale Simpson, Jasmine Tam, Andrea Mazuski, Edwina Lai, Baltej Ludher, Kirk Overhoff, and Bo Chen whose help resulted in the final products shown in Chapters 2-6 of this dissertation. I would also like to thank Michal Matteucci and Todd Crisp for their insightful conversations.

Stable Submicron Protein Particles: Formation, Properties, and Pulmonary Applications

Publication No._____

Joshua David Engstrom, Ph.D.

The University of Texas at Austin, 2007

Supervisors: Keith P. Johnston and Robert O. Williams III

The spray freezing into liquid (SFL) and thin film freezing (TFF) processes were utilized to produce 300 nm protein particles with surface areas on the order of 31 - 73 m^2/g and 100% protein activities. Despite a cooling rate of ~10^2-10^3 K/s in SFL and TFF, the particle sizes and surface areas were similar to those observed in the widely reported process, spray freeze-drying (SFD), where cooling rates reach 10^6 K/s. In SFL and TFF, the thin liquid channels between the ice domains were sufficiently thin and freezing rates of the thin channels sufficiently fast to achieve the similar particle morphologies. Therefore, the extremely rapid cooling rate in the SFD process was not necessary to form the desired submicron protein particles.

In SFL and TFF the surface area/volume ratio of the gas-liquid formed on the liquid protein formulations (46-600 cm^{-1}) was 1-2 orders of magnitude lower than in SFD (6000 cm^{-1}), leading to far less protein adsorption and aggregation. This larger exposure to the gas-liquid interface resulted in lower protein activities in SFD. Although protein stabilities are high in conventional lyophilization, cooling rates are on the order of 1

K/min resulting in large 30 to 100 μm sized particles. Thus, the intermediate cooling rate regime for SFL and TFF, relative to SFD and lyophilization, offers a promising route to form stable submicron protein particles of interest in pulmonary and parenteral delivery applications.

The rod-shaped protein particles produced by SFL and TFF are beneficial for forming suspensions stable against settling in hydrofluoroalkanes (HFA) for pressurized metered dose inhaler (pMDI) delivery. The flocculated rods are templated by atomized HFA droplets that evaporate and shrink to form particles with optimal aerodynamic diameters for deep lung delivery. Fine particle fractions of 38-48% were achieved. This novel concept for forming stable suspensions of flocs of rod shaped particles, and templating and shrinking the flocs to produce particles for efficient pMDI deep lung delivery is applicable to a wide variety of drugs.

Table of Contents

List of Tables

List of Figures

Chapter 1: Introduction

1.1 DELIVERY METHODS FOR PROTEIN THERAPEUTICS-THE NEED FOR HIGH SURFACE AREA PARTICLES

Advances in recombinant DNA technology have led to a large number of novel therapeutic proteins (1). To minimize cost of production and increase ease of handling by the end user it is preferred to formulate aqueous solutions of proteins (2). However, proteins are readily denatured by the numerous stresses that can occur in solutions such as heating, agitation, freezing, pH changes, and exposure to interfaces or denaturants (3). These stresses often result in inactive protein molecules or aggregates which compromise efficacy and increase the risk of adverse side effects (3). Proteins can also be degraded by chemical reactions such as hydrolysis and deamidation in solution (1, 3). Although protein solutions could be frozen, the requisite storage and shipping conditions can become uneconomical (2, 3).

To overcome the instabilities proteins encounter in solution, an alternative approach has been to remove the water to form dehydrated protein formulations which potentially may have a long shelf life at ambient temperatures (1, 2, 4-9). Lyophilization has been the most common method for preparing dry stable protein formulations (2, 8). In lyophilization the liquid protein formulation is slowly cooled until frozen and then water is removed through the process of sublimation under vacuum (6, 8). The protein formulation after drying has the form of a porous solid cake (2, 6). The low specific surface area powder produced by lyophilization is typically reconstituted and delivered parenterally which has been met with poor patient compliance (10, 11). Therefore, noninvasive delivery routes or minimizing the frequency of injection delivery has received increasing attention (9).

Alternative protein delivery routes to parenteral include pulmonary, transdermal, subcutaneous, and intramuscular depot delivery which can benefit from the formation of stable high surface area micron or sub-micron sized protein particles (9, 11-18). For example, in pulmonary delivery it is necessary to have particles that have an aerodynamic diameter between 1-5 μm sufficient to reach the deep lung (9, 18). In depot delivery it is beneficial to produce submicron protein particles (300-500 nm) that can be uniformly encapsulated into micron sized polymer spheres to avoid burst release (14, 16, 19). The production of high surface area protein particles with the proper physical characteristics offers new opportunities for alternative delivery routes, but it is challenging to produce stable submicron protein particles when the powder surface area exceeds 10 m^2/g (14, 20, 21), relative to the less than 1 m^2/g for powders produced by lyophilization. Although lyophilized protein cakes could be pulverized by milling to break the cake into micron sized particles, the milling process significantly reduces process yield and its control on particle size distribution is very poor (9). Since lyophilization does not produce high surface area particles, dry protein particles must be formed with alternate drying processes (9).

Protein particles may be precipitated from aqueous solution by a variety of processes including spray-drying (6, 22-24), supercritical CO_2-assisted aerosolization and bubble drying (scCO_2A-BD) (25), spray freeze-drying (SFD) (6, 9, 20, 21), spray freezing into liquids (SFL) (7, 26, 27), and thin film freezing (TFF) (28, 29). The spraying, freezing and drying steps in these processes must be designed to minimize stresses that cause physical destabilization to the protein structure (2, 4, 5, 8). Loss in stability may be characterized in terms of protein denaturation (protein unfolding), aggregation, and loss of enzyme activity upon rehydration (5, 6, 30). During spraying and freezing, stresses arise from changes in solute concentration and pH in the remaining

unfrozen solution, as well as exposure of protein to gas-liquid and/or ice-liquid interfaces (4, 8). During drying, dehydration stress from removal of water molecules can subsequently lead to protein unfolding (2, 4, 31). Stabilizers, such as disaccharide sugars often increase the thermodynamic stability of the native folded protein during freezing and prevent the protein from unfolding during drying through replacement of hydrogen bonds to the protein upon loss of water (2, 8, 31-33). The stability of the protein after processing can be sensitive to the interfaces present in the various particle formation techniques.

1.2 MORPHOLOGY OF PROTEINS PRODUCED BY LYOPHILIZATION AND RAPID FREEZING PROCESSES

To understand why lyophilization only produces low specific surface area (<1 m^2/g) powder whereas rapid cooling processes such as spray freeze-drying (SFD), spray freezing into liquid (SFL), and thin film freezing (TFF) produce powders with specific areas that range from 30-150 m^2/g, the effect of cooling rate on the resulting dry powder morphology must be understood. The morphology of an aqueous solution in the frozen state depends on the cooling rate in that as the degree of supercooling increases so does the nucleation rate of ice particles (34). The freezing mechanism of slow cooling, such as in lyophilization, is explained with the aid of Fig. 1.1 which shows a phase diagram for sucrose, a non-crystallizing solute in water (34-37). Protein and sugar solutions subjected to slow cooling rates on a temperature controlled shelf in a tray lyophilizer have a low degree of supercooling beneath the equilibrium freezing curve (37). The water in the supercooled solution nucleates and forms crystalline ice (34). The latent heat of crystallization causes the temperature of the supercooled solution to rise to the equilibrium freezing curve (34, 37). Globular proteins and most sugars remain in the unfrozen solution known as the freeze concentrate and are usually kinetically hindered

from crystallizing (34). As liquid water moves from the unfrozen phase to the ice phase during freezing, the composition of the freeze concentrate follows the equilibrium freezing curve toward T_g', the point where the solution is maximally freeze concentrated (Fig. 1.1) (37). At this point the unfrozen domains become sufficiently viscous that they vitrify over 20-30 minutes (37). After drying the powder specific surface areas are typically below 1 m^2/g regardless of protein concentration in solution. SEMs (not shown) of the powder morphology revealed large irregularly shaped particles that ranged in size from 30-100 μm.

Rapid cooling rates of aqueous solutions do not follow the equilibrium path as described above (34, 36). Rapid freezing minimizes the time for the formation and growth of ice crystals as the aqueous solution passes through the critical temperature zone (7, 38, 39), which is the region between the equilibrium freezing curve and the T_g curve where liquid water can nucleate to form crystalline ice. The degree of supercooling can be so great that the temperature may pass below the T_g curve fast enough to minimize, or even fully prevent, nucleation of ice crystals (34). When a supercooled aqueous solution passes through the critical temperature zone, the solute may become supersaturated from a decrease in solubility before the water vitrifies. As shown in Fig. 1.1, the solubility curve decreases with decreasing temperature and ends at the eutectic temperature, T_e. For temperatures well below T_e, it is not possible to measure a true equilibrium sucrose solubility in liquid water. However, for rapid non-equilibrium supercooling of the water without time to freeze, the solubility of sucrose in hypothetical supercooled liquid water would be expected to decrease with temperature. For example, the ideal solubility of a solid in a liquid decreases as the difference between the melting point of the solid and the temperature increases. Furthermore, the decrease in solubility with temperature is evident in Fig. 1.1 above T_e.

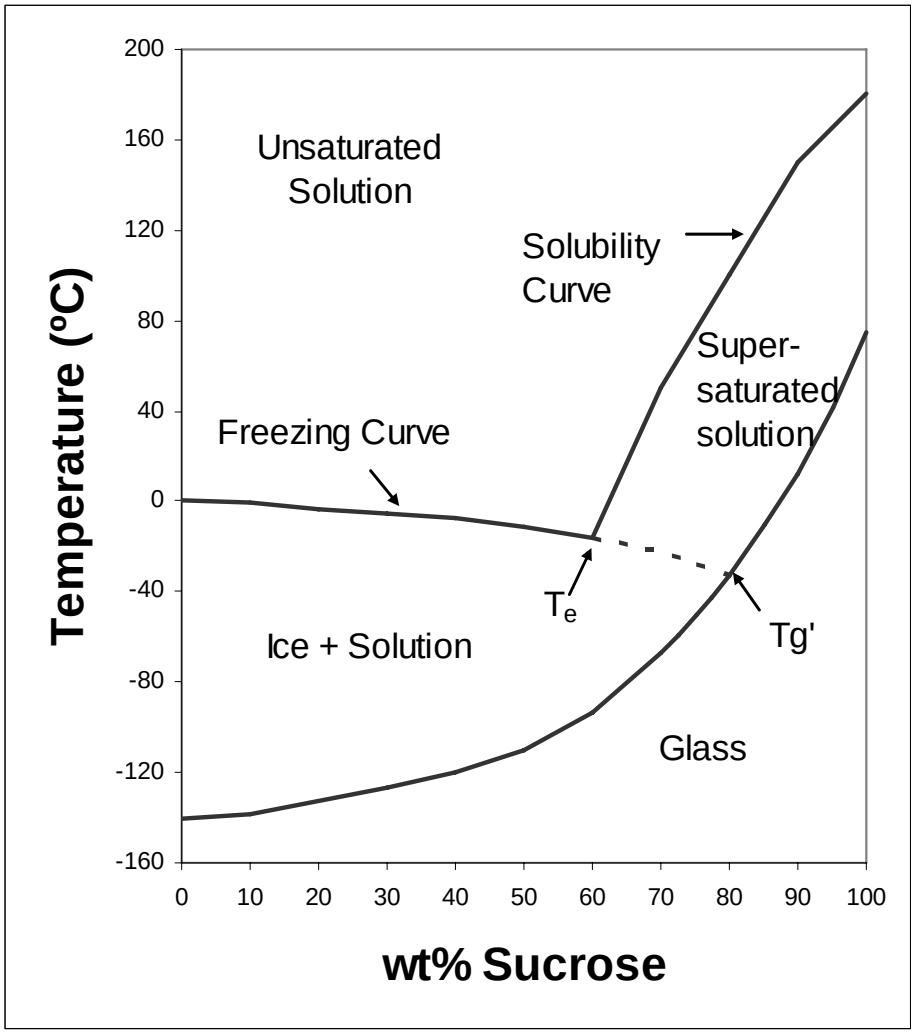

Figure 1.1: Solid-liquid diagram for the sucrose-water system. Adapted from Fig. 7 of Nail et al. (48).

The decrease in solubility with temperature will lead to supersaturation and nucleation and growth of solute from the unfrozen solution even before a significant amount of vitrification of water occurs. Unlike lyophilization, the high degree of supercooling in the rapid cooling processes rapidly leads to temperatures far below the T_g curve in Fig. 1.1. Vitrified water domains form as relatively few water molecules have enough time to reach the crystalline state. The expected morphologies for lysozyme or bovine serum albumin (BSA) solutions subjected to rapid cooling rates (10^2 - 10^6 K/s) and the slower cooling rates (~10^{-1} K/s) of lyophilization are shown schematically in Fig. 1.2. For the slower cooling rate fewer ice nuclei form leaving larger unfrozen channels between the growing nucleated ice particles. The lysozyme particles are then shown to precipitate in the channels of the unfrozen liquid (Fig. 1.2). A detailed explanation of the effect of cooling rate on powder morphology of Fig. 1.2 is given in Chapters 2, 4, and 5 of this dissertation.

1.3 STABILITY OF PROTEINS PROCESSED BY RAPID AND INTERMEDIATE FREEZING PROCESSES

The spray freeze-drying (SFD) process (Fig. 1.3B) has been successful in forming desired particle sizes for alternate delivery routes, but has been hampered by protein stability and processing challenges. In order for alternate delivery routes to be viable the protein particle size must be small enough while maintaining adequate protein stability. The shortcomings of the SFD process, suggest the need for the alternate particle forming processes spray freezing into liquid (SFL) (Fig. 1.3A) and thin film freezing (TFF) (Fig. 1.4).

In SFD, an aqueous solution containing dissolved protein and stabilizers is atomized into the cold gas above a cryogenic liquid (Fig. 1.3) (20, 21, 40-42). The 10-50 μm droplets travel through the cryogenic gas, where they may begin to freeze (38), and then freeze completely after contact with the liquid cryogen. By systematically studying

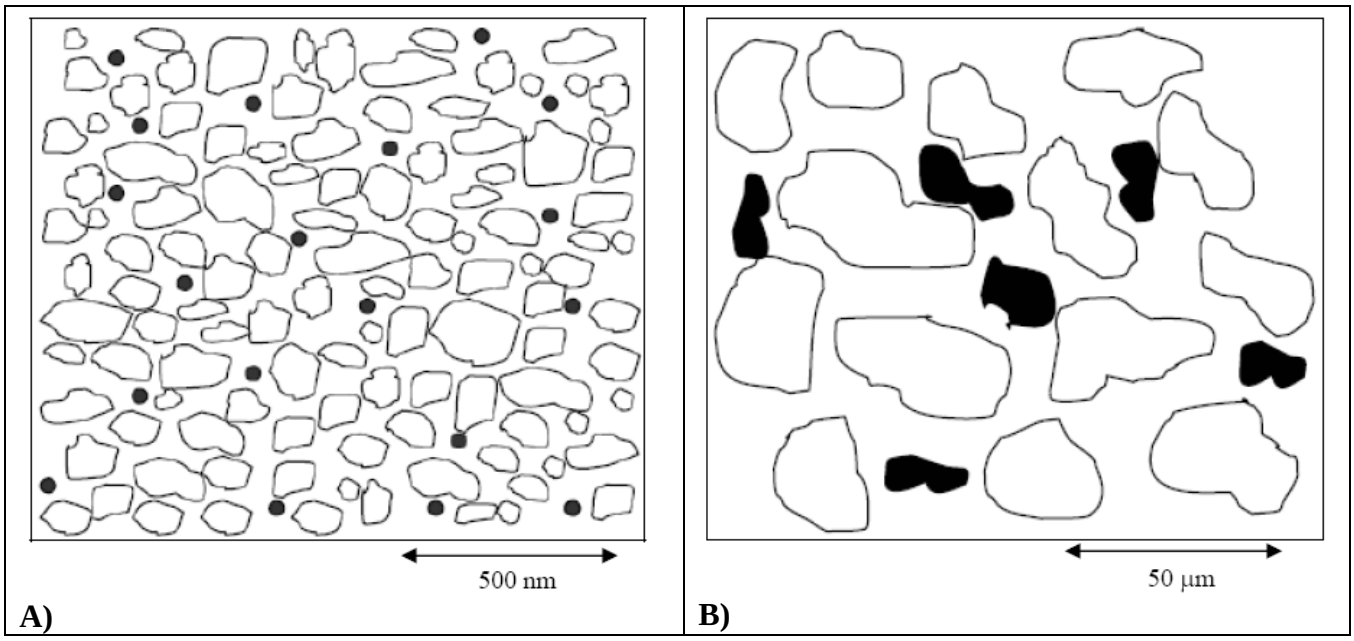

Figure 1.2: Nucleation and growth of protein particle in unfrozen channels between glassy frozen water domains with high supercooling (A), and with low supercooling in shelf lyophilization (B). Ice particles are represented as white domains and solute precipitate as solid black dots or regions.

the effects of the separate spraying, freezing and drying steps in SFD, it was shown that the large gas-liquid interface (6000 cm^{-1}) in the spraying step was the primary cause of protein aggregation for recombinant human interferon γ (rhIFN-γ) (21), lysozyme (26), and more recently lactate dehydrogenase (LDH) (43). The protein adsorbs at this interface and subsequently unfolds and forms aggregates (21, 44). The freezing and drying steps had a minimal effect on protein stability. For rhIFN-γ, Webb et al. (21) reported that a protein in the freeze concentrate during rapid freezing would not have sufficient time to diffuse to the ice-liquid interface and denature before being trapped in an amorphous glass (21). Therefore, the formation of high SSA protein powder by SFD has often resulted in an undesirable degree of denaturation and aggregation for a variety of proteins (6, 9, 20-22).

The alternative SFL (Fig. 1.3) process was developed to minimize exposure of protein to the gas-liquid interface and yet sustain rapid freezing rates to produce high SSA powder (7, 26, 27) (Fig. 1.5). As shown in Fig. 1.3, the feed nozzle is immersed under the cryogen surface to minimize exposure to nitrogen gas-liquid interface (7, 26, 27). The SFL process has used LN2 nearly exclusively as the cryogen (6, 7, 9, 14, 20-23, 26, 27, 30, 41, 42, 45-47). The boiling point of LN2 is low, only -196ºC, which is desirable for rapid freezing. It is environmentally friendly, nonflammable and it does not remain as a residue in the product (48). In spite of its low boiling point, LN2 has been shown to produce slower cooling rates than cryogens with higher freezing points such as isopentane (*i*-C5) (fp = -160ºC) and propane (C3) (fp = -190ºC) (49, 50). The lower LN2 cooling rate is well known to result from boiling of the LN2 around an inserted object, or sprayed fluid, forming an insulating gas, a phenomenon referred to as the Leidenfrost effect (49). The jet dimensions formed ~100 μm droplets which lead to a cooling rate of ~10^3 K/s as a result of the Leidenfrost effect (43, 49, 51). The cooling rate was

sufficiently fast to arrest the growth of submicron protein particles, without the need for ultra rapid cooling rates of 10^6 K/s in SFD (51). Despite exposure of the freezing liquid jet in SFL to gas-liquid interface the modification resulted in less protein adsorption, denaturation and aggregation, and consequently, higher enzymatic activities than in SFD (7, 26, 27, 43). The evaporating liquid nitrogen prevents the liquid jet from atomizing forming larger droplets (~100 μm) with much lower gas-liquid interface exposure ($600 cm^{-1}$).

Although higher protein stabilities are achieved with SFL over SFD, the SFL process has significant challenges. The Leidenfrost effect in SFL makes it difficult to form a controlled cooling environment. Another challenge is that aqueous formulations can freeze in the capillary nozzle (ID 63 μm) during the spray and stop the flow. Protein recovery is challenging in SFL since a large amount of liquid cryogen (1 L) is required to process 1-20 mL protein formulation volumes. Removal of the LN2 cryogen can lead to losses of frozen ice particles decreasing protein recovery. Therefore, it is desirable to have a process that gives high protein stabilities, as observed in SFL, but with greater control over the cooling rate. Because therapeutic proteins often cost thousands of dollars per milligram it would also be desirable to design a process for small volumes of protein formulation, as low as 1 mL.

The TFF process overcomes the challenges in SFL in that the cooling rate is controlled much more effectively and much smaller amounts of protein may be recovered after freezing. In the TFF process (Fig. 1.1) liquid droplets fall from a given height and impact, spread, and freeze on a cooled solid substrate with maximum exposure to the gas-liquid interface of ($46 cm^{-1}$) (Fig. 1.5). Recently TFF was used to form high SSA powder (25-29 m^2/g) of the poorly water soluble drug danazol (29). Liquid droplets (~2-4 mm in

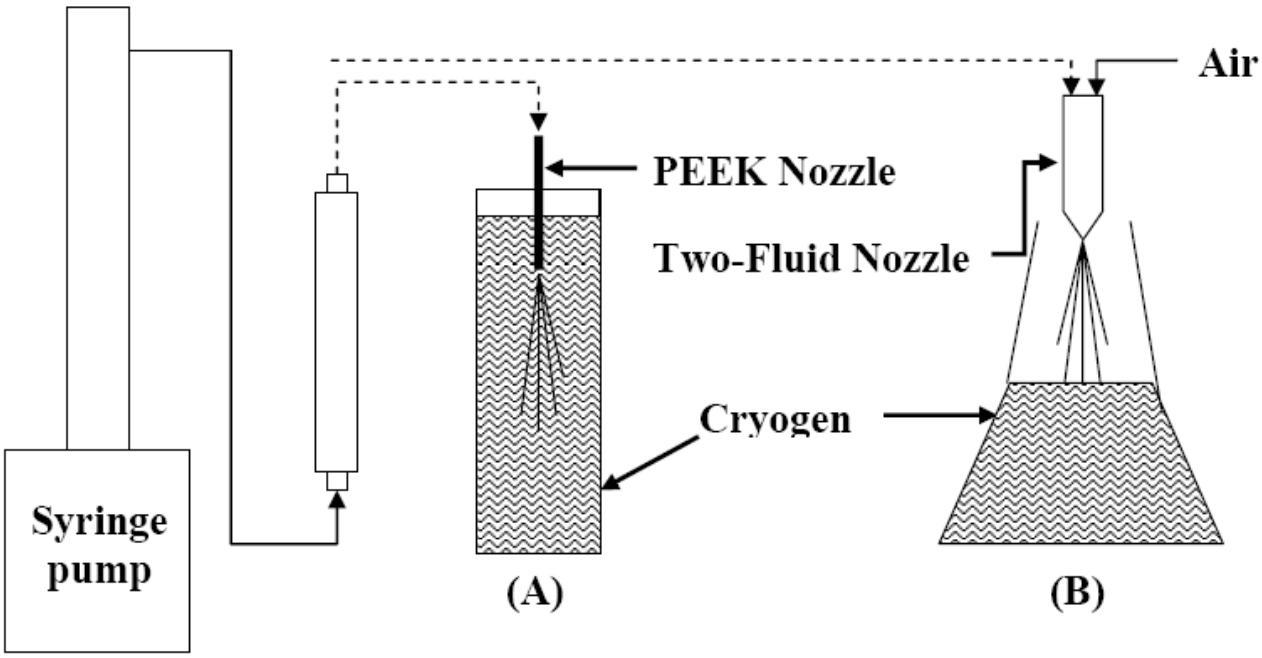

Figure 1.3: Experimental apparatus for SFL (A) and SFD (B) sprays. For SFL the nozzle is immersed below the cryogen surface while for SFD the liquid jet is atomized above the liquid cryogen surface with a two-fluid nozzle.

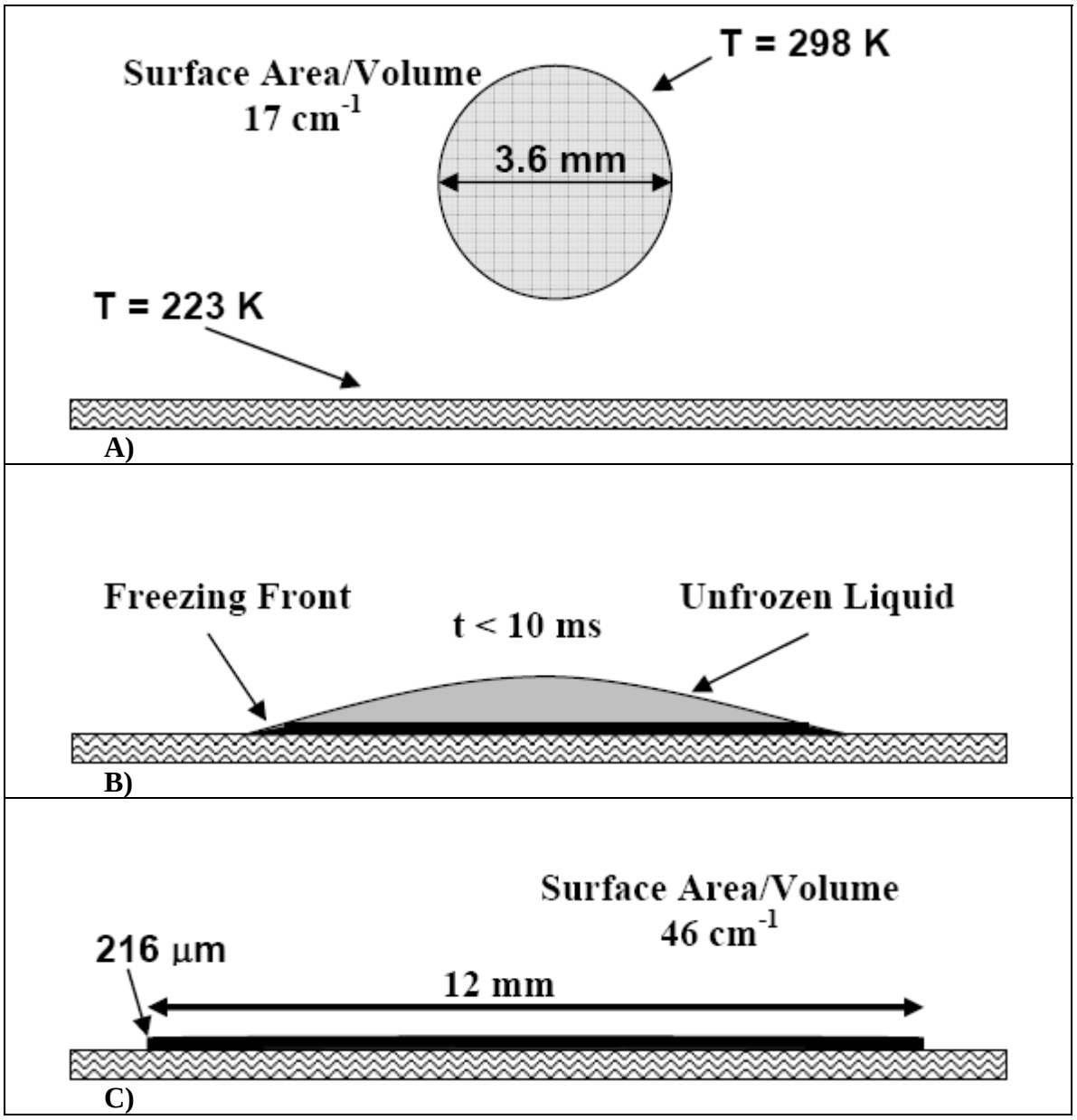

Figure 1.4: Diagram of the thin film freezing process displaying the falling droplet (A), spreading after impact on the stainless steel surface (B), and during cooling and freezing as a thin film (C) (drawn to scale).

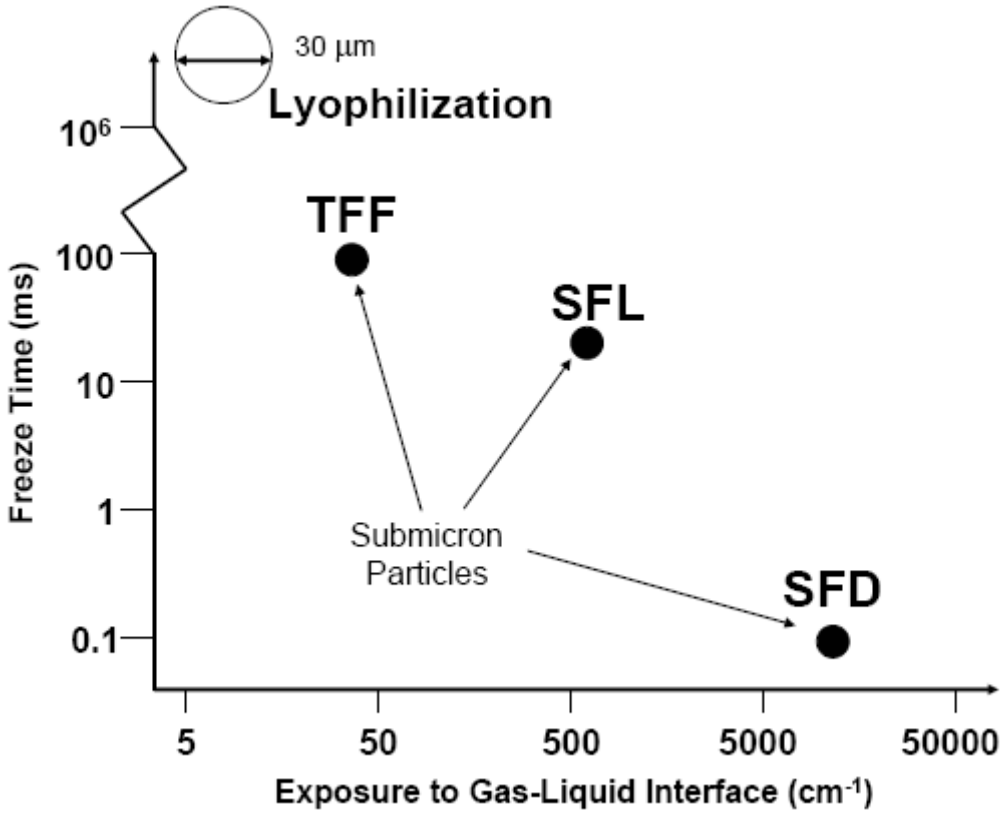

Figure 1.5: Freezing time versus exposure to gas-liquid interface for lyophilization, thin film freezing (TFF), spray freezing into liquid (SFL), and spray freeze-drying (SFD).

diameter) were dispensed from a pipet above a cryogenically cooled metal surface (52, 53). Upon impact, the droplets spread out into thin films (~100-400 μm) that froze on time scales of 70 to 1000 ms, which corresponds to a cooling rate of ~10^2 K/s (53-66). The cooling rates predicted with a 1-D heat transfer model were in agreement with experimental measurements with an infrared (IR) camera (29). Since the cooling rates in TFF and SFL are comparable, TFF will be shown in Chapter 5 of this dissertation to be a desirable process for forming high surface area protein particles.

1.4 PULMONARY DELIVERY OF SUBMICRON PROTEIN PARTICLES

Until recently, the delivery of protein therapeutics has been largely limited to parenteral delivery due to the chemical and physical instabilities of many therapeutic proteins (67). As an alternative to parenteral delivery, non-invasive routes including transdermal, oral, and pulmonary have been pursued (68). Comparatively, pulmonary delivery has been shown to provide higher bioavailabilities for proteins and peptides than the other non-invasive delivery routes (68-70). Further advantages include a well established delivery route, large alveolar surface absorption (~100 m^2), rapid absorption across thin alveolar epithelium (0.1-0.5 μm), and avoidance of first pass metabolism (67, 70-74).

Drugs can be delivered to the lungs by dry powder inhalers (DPI), nebulizers, and pressurized metered dose inhalers (pMDI) (70, 75). Comparatively, the pMDI remains the most popular delivery device because of its low cost, portability, and disposability (70). Although pMDIs are popular, many drugs, including proteins, have very low solubilities in the hydrofluoroalkane (HFA) propellants approved by the FDA (76). Therefore, pMDIs are often formulated as suspensions (76, 77). Protein pMDI delivery, as opposed to DPI delivery, has not been widely explored due to fear of the protein

denaturing in the presence of the HFAs (70). On the contrary, studies have shown that protein stability is maintained for a variety of proteins including insulin, lysozyme, catalase and rhDNase I (78-80).

For effective drug delivery to the lungs it has been shown that aerosolized particles with aerodynamic diameters between 1-5 μm have the highest deposition in the deep lung (81). The formation of protein particles within the optimal aerodynamic size range has been achieved by milling (76, 80), spray drying (72, 82-84), and spray freeze-drying (SFD) (9, 23), but there are disadvantages to each process. The milling process can generate significant amounts of heat on localized areas of the protein particle which can lead to denaturation (6, 9). In the spray drying and SFD processes the large gas-liquid interface created upon atomization increases interfacial protein adsorption leading to denaturation and aggregation (6, 20, 21, 24, 41). Although additional excipients such as surfactants can increase protein stability in the spray drying and SFD processes (9, 22, 24), the low processing efficiencies for spray drying (50-70%) (22, 23) and SFD (~80%) (6, 22, 23) can have costly consequences for highly valuable proteins. Consequently, the production of protein particles with optimal aerodynamic diameters, high stability, and over 90% processing yield has been difficult to achieve.

Along with high protein stability, good suspension stability of non-porous 1-5 μm diameter protein particles in HFAs with <1-5% (w/w) mass loadings has been difficult to achieve (76). Increasing the mass loading above 5% (w/w) can lead to aggregation of particles within aerosolized droplets and a decrease in fine particle fraction (FPF) (76, 85). Suspended spherical particles formed by milling or spray drying often flocculate and settle in less than 1 minute which can lead to irreversible particle aggregation and variable dosing between actuations (84, 86). Consequently, pMDIs are relatively inefficient with typical FPFs between 5-30% (87). Although surfactants and cosolvents,

such as ethanol, could potentially stabilize the suspension, the surfactants currently approved by the FDA for inhalation are insoluble in HFAs and thus provide no stabilization (88) and cosolvents can chemically destabilize drugs (84). To slow flocculation and settling hollow sphere or porous particles of drugs formed by spray drying were shown to be stable for at least 4 hours when suspended in HFAs and had respirable fractions as high as 68% (84, 89). For suspended porous particles, the HFA enters the particle pores which significantly decreases the density difference of the particle with the surrounding HFA media and reduces van der Waals attractive forces between particles (84). Although the porous particles greatly increase suspension stability, reports of protein stability of porous protein particles are limited (18, 84, 89).

The intermediate cooling processes SFL (7, 26, 27, 43, 51) and (28) have been shown to produce high surface area stable submicron (300 nm) protein particles. High protein stability is achieved in both the SFL and TFF processes by minimizing the gas-liquid interfacial exposure of the protein (28, 43). In spite of the slower cooling rate compared to the rapid cooling SFD process (~10^6 K/s), the intermediate SFL and TFF cooling rates (~10^2 – 10^3 K/s) produce high surface area (>30 m^2/g) powders comparable to SFD (28). Studies by Maa et al. demonstrated that high surface area SFD particles had higher respirable fractions compared to spray dried particles when delivered by a DPI (23). In Chapter 6 of this dissertation the advances of utilizing rod particles produced by SFL or TFF for pMDI delivery are discussed.

1.5 OBJECTIVES

The ability to produce stable high surface area protein particles, with diameters on the order of 100 to 500 nm would offer new opportunities for a variety of non-invasive protein delivery options. In this dissertation, the first overall goal is to demonstrate that

the freezing processes SFL and TFF can form high surface area sub-micron protein particles (>30 m^2/g) and to understand the mechanisms of protein destabilization and how they can be minimized. Here, the two key objectives are to investigate: (1) the nucleation, growth and morphology of protein particles formed by SFL and TFF processes as a function of the cooling rate, (2) the protein stability of particles prepared by SFL and TFF followed by lyophilization.

The second overall goal is to form stable suspensions (against settling) of protein particles in HFA 227 without stabilizing surfactants or cosolvents in order to achieve high fine particle fractions (>30%) in pMDI delivery. The approach is fundamentally the opposite of previous ones, in that the particles are purposely flocculated in the HFA to prevent settling. Asymmetric particles, such as rods, may be expected to pack less efficiently to form much lower density flocs with greater free volume than spheres. Rods can be produced by SFL or TFF. The flocculation concept for achieving stable suspensions and high fine particles fractions without the need for surfactants is of practical interest for wide classes of low and high molecular weight pharmaceuticals and biopharmaceuticals that may be formed into nanorods.

1.6 DISSERTATION OUTLINE

Chapter 2 presents the mechanisms for the formation of high surface area lysozyme particles in spray freezing processes described as a function of spray geometry and atomization, solute concentration and the calculated cooling rate. In the spray freeze-drying (SFD) process, droplets are atomized into a gas and then freeze upon contact with a liquid cryogen. In the spray freezing into liquid (SFL) process, a solution is sprayed directly into the liquid cryogen below the gas-liquid meniscus. A wide range of feed concentrations is examined for two cryogens, liquid nitrogen (LN2) and isopentane (*i*-

C5). The particle morphologies are characterized by SEM micrographs and BET measurements of specific surface area. As a result of boiling of the cryogen (Leidenfrost effect), the cooling rate for SFL into LN2 is several orders of magnitude slower than for SFL into *i*-C5 and for SFD in the case of either LN2 or *i*-C5. For 50 mg/mL concentrated feed solutions, the slower cooling of SFL into LN2 leads to a surface area of 34 m^2/g. For the other three cases with more rapid cooling rates, surface areas were greater than 100 m^2/g. The ability to adjust the cooling rate to vary the final particle surface area is beneficial for designing particles for controlled release applications.

Chapter 3 presents enzyme activities determined for lactate dehydrogenase (LDH) powder produced by lyophilization, and two fast freezing processes, spray freeze-drying (SFD) and spray freezing into liquid (SFL) nitrogen. The 0.25 mg/mL LDH aqueous feed solutions included either 30 or 100 mg/mL trehalose. The SFL process produced powders with very high enzyme activities upon reconstitution, similar to lyophilization. However, the specific surface area of 13 m^2/g for SFL was an order of magnitude larger than for lyophilization. In SFD activities were reduced in the spraying step by the long exposure to the gas-liquid interface for 0.1 to 1 s, versus only 2 ms in SFL. The ability to produce stable high surface area submicron particles of fragile proteins such as LDH by SFL is of practical interest in protein storage and in various applications in controlled release including encapsulation into bioerodible polymers. The SFL process has been scaled down for solution volumes <1 mL to facilitate studies of therapeutic proteins.

Chapter 4 presents an ultra-rapid freezing (URF) technology, otherwise known as thin film freezing (TFF), which has been developed to produce high surface area powders composed of solid solutions of an active pharmaceutical ingredient (API) and a polymer stabilizer. A solution of API and polymer excipient(s) is spread on a cold solid surface to form a thin film that freezes in 50 ms to 1s. This study provides an understanding of how

the solvent's physical properties and the thin film geometry influence the freezing rate and consequently the final physicochemical properties of URF processed powders. Theoretical calculations of heat transfer rates are shown to be in agreement with infrared images with 10 ms resolution. Danazol (DAN)/polyvinylpyrrolidone (PVP) powders, produced from both acetonitrile (ACN) and tert-butanol (T-BUT) as the solvent, were amorphous with high surface areas (~28-30 m^2/g) and enhanced dissolution rates. However, differences in surface morphology were observed and attributed to the cooling rate (film thickness) as predicted by the model. Relative to spray freezing processes that use liquid nitrogen, URF also offers fast heat transfer rates as a result of the intimate contact between the solution and cold solid surface, but without the complexity of cryogen evaporation (Leidenfrost effect). The ability to produce amorphous high surface area powders with submicron primary particles with a simple ultra rapid freezing process is of practical interest in particle engineering to increase dissolution rates, and ultimately bioavailability.

Chapter 5 presents highly stable, submicron lactate dehydrogenase (LDH) and lysozyme particles that may be produced by thin film freezing (TFF) of aqueous solutions followed by lyophilization. The LDH activity was determined by measuring the decrease in absorbance of NADH over time for the reaction of pyruvate to lactate. For lysozyme the particle morphology was determined by scanning electron microscopy (SEM) and compared with the specific surface area (BET) and the particle size, as measured by laser light scattering. Protein particles with an average diameter of 300 nm and 100% enzyme activity upon reconstitution (for LDH) were formed by TFF. Droplets of protein solutions, 3.6 mm in diameter, spread upon impact with 223 and 133 K metal surfaces to form cylindrical disks with thicknesses of 200-300 μm. Calculated cooling rates of the disks of 10^2 K/s were confirmed experimentally with infrared measurements. The

cooling rates of 10^2 K/s, intermediate to those in lyophilization (1 K/min) and spray freeze-drying (SFD) (10^6 K/s), were sufficiently fast to produce sub-micron protein particles with surface areas of 31-73 m^2/g, an order of magnitude higher than in lyophilization. In addition, the low surface area/volume ratio (32-45 cm^{-1}) of the gas-liquid interface led to minimal protein adsorption and denaturation relative to SFD.

Chapter 6 presents a novel concept for the formation of stable suspensions composed of very low density flocs of rod-shaped drugs in hydrofluoroalkane propellants for pressurized meter dose inhalers (pMDI), and for templating the flocs to achieve high fine particle fractions in pulmonary delivery. The flocculated suspensions in HFA 227 are stable against settling for one year. Bovine serum albumin (BSA) nanorods, 50 nm in diameter and 480 nm in length, produced by thin film freezing (TFF), are shown by theory and experiment to form space filling flocs with protein particle volume fractions of only 0.0020, which are one order of magnitude lower than for flocs composed of spheres. The rods are flocculated reversibly, as they were found to break up into individual submicron primary rod particles in a polar solvent acetonitrile. Actuation of the HFA suspension with a pMDI produces high fine particle fractions (38-48%) with an emitted dose of 0.7 mg for particles with 3-4 μm aerodynamic diameters (d_a), as determined with an Andersen cascade impactor (ACI). The atomized 25 μm HFA droplets break apart and template the highly open flocs, which are held together by extremely weak van der Waals forces. Upon evaporation of the HFA, capillary forces shrink the ~25 μm templated flocs resulting in porous particles with optimal d_a = 3-4 μm for deep lung delivery. The corresponding geometric diameters d_g are on the order of 10 μm, as shown by SEM and static light scattering measurements. This novel concept for forming extremely stable suspensions of open flocs of rod shaped particles, and templating and shrinking the flocs to produce particles for efficient pMDI deep lung

delivery is applicable to a wide variety of drugs without the need for surfactants or cosolvents to stabilize the primary particles.

1.7 REFERENCES

1. M. C. Manning, K. Patel, and R. T. Borchardt. Stability of protein pharmaceuticals. *Pharm. Res.* **6:**903-918 (1989).

2. J. F. Carpenter, B. S. Chang, W. Garzon-Rodriguez, and T. W. Randolph. Rational design of stable lyophilized protein formulations: theory and practice. In J. F. Carpenter and M. C. Manning (eds.), *Pharmaceutical Biotechnology. 13. Rational Design of Stable Protein Formulations*, Kluwer Academic/Plenum Press, New York, 2002, pp. 109-133.

3. J. F. Carpenter, K.-i. Izutsu, and T. W. Randolph. Freezing- and drying-induced perturbations of protein structure and mechanisms of protein protection by stabilizing additives. In L. Rey and J. C. May (eds.), *Drugs and the Pharmaceutical Sciences. 137. Freeze-Drying/Lyophilization of Pharmaceutical and Biological Products*, Marcel Dekker, Inc., New York, 2004, pp. 147-186.

4. M. J. Pikal. Mechanisms of protein stabilization during freeze-drying and storage: the relative importance of thermodynamic stabilization and glassy state relaxation dynamics. *Drugs Pharm. Sci.* **137:**63-107 (2004).

5. R. A. DePaz, D. A. Dale, C. C. Barnett, J. F. Carpenter, A. L. Gaertner, and T. W. Randolph. Effects of drying methods and additives on the structure, function, and storage stability of subtilisin: role of protein conformation and molecular mobility. *Enzyme Microb. Technol.* **31:**765-774 (2002).

6. Y.-F. Maa and S. J. Prestrelski. Biopharmaceutical powders: particle formation and formulation considerations. *Curr. Pharm. Biotechnol.* **1:**283-302 (2000).

7. Z. Yu, T. L. Rogers, J. Hu, K. P. Johnston, and R. O. Williams III. Preparation and characterization of microparticles containing peptide produced by a novel process: spray freezing into liquid. *Eur. J. Pharm. Biopharm.* **54:**221-228 (2002).

8. W. Wang. Lyophilization and development of solid protein pharmaceuticals. *Int. J. Pharm.* **203:**1-60 (2000).

9. Y.-F. Maa and H. R. Costantino. Spray freeze-drying of biopharmaceuticals: applications and stability considerations. In H. R. Costantino and M. J. Pikal (eds.), *Biotechnology: Pharmaceutical Aspects. 2. Lyophilization of Biopharmaceuticals*, American Association of Pharmaceutical Scientists, Arlington, 2004, pp. 519-561.

10. K. A. Johnson. Preparation of peptide and protein powders for inhalation. *Adv. Drug Deliv. Rev.* **26:**3-15 (1997).

11. S. J. Shire, Z. Shahrokh, and J. Liu. Challenges in the development of high protein concentration formulations. *J. Pharm. Sci.* **93:**1390-1402 (2004).

12. Y.-F. Maa, L. Zhao, L. G. Payne, and D. Chen. Stabilization of alum-adjuvanted vaccine dry powder formulations: mechanism and application. *J. Pharm. Sci.* **92:**319-332 (2003).

13. X. M. Lam, E. T. Duenas, A. L. Daugherty, N. Levin, and J. L. Cleland. Sustained release of recombinant human insulin-like growth factor-I for treatment of diabetes. *J. Control. Release* **67:**281-292 (2000).

14. W. T. Leach, D. T. Simpson, T. N. Val, E. C. Anuta, Z. Yu, R. O. Williams III, and K. P. Johnston. Uniform encapsulation of stable protein nanoparticles produced by spray freezing for the reduction of burst release. *J. Pharm. Sci.* **94:**56-69 (2005).

15. O. L. Johnson, W. Jaworowicz, J. L. Cleland, L. Bailey, M. Charnis, E. Duenas, C. Wu, D. Shepard, S. Magil, T. Last, A. J. S. Jones, and S. D. Putney. The stabilization and encapsulation of human growth hormone into biodegradable microspheres. *Pharm. Res.* **14:**730-735 (1997).

16. X. M. Lam, E. T. Duenas, and J. L. Cleland. Encapsulation and stabilization of nerve growth factor into poly(lactic-co-glycolic) acid microspheres. *J. Pharm. Sci.* **90:**1356-1365 (2001).

17. M. R. Prausnitz. Microneedles for transdermal drug delivery. *Adv. Drug Deliv. Rev.* **56:**581-587 (2004).

18. D. A. Edwards, J. Hanes, G. Caponetti, J. Hrkach, A. Ben-Jebria, M. L. Eskew, J. Mintzes, D. Deaver, N. Lotan, and R. Langer. Large porous particles for pulmonary drug delivery. *Science* **276:**1868-1871 (1997).

19. J. L. Cleland, E. T. Duenas, A. Park, A. Daugherty, J. Kahn, J. Kowalski, and A. Cuthbertson. Development of poly-(d,l-lactide-co-glycolide) microsphere formulations containing recombinant human vascular endothelial growth factor to promote local angiogenesis. *J. Control. Release* **72:**13-24 (2001).

20. H. R. Costantino, L. Firouzabadian, K. Hogeland, C. C. Wu, C. Beganski, K. G. Carrasquillo, M. Cordova, K. Griebenow, S. E. Zale, and M. A. Tracy. Protein spray-freeze drying. Effect of atomization conditions on particle size and stability. *Pharm. Res.* **17:**1374-1383 (2000).

21. S. D. Webb, S. L. Golledge, J. L. Cleland, J. F. Carpenter, and T. W. Randolph. Surface adsorption of recombinant human interferon-γ in lyophilized and spray-lyophilized formulations. *J. Pharm. Sci.* **91:**1474-1487 (2002).

22. X. C. Nguyen, J. D. Herberger, and P. A. Burke. Protein powders for encapsulation: a comparison of spray-freeze drying and spray drying of darbepoetin alfa. *Pharm. Res.* **21:**507-514 (2004).

23. Y.-F. Maa, P.-A. Nguyen, T. Sweeney, S. J. Shire, and C. C. Hsu. Protein inhalation powders: spray drying vs spray freeze drying. *Pharm. Res.* **16:**249-254 (1999).

24. M. Adler and G. Lee. Stability and surface activity of lactate dehydrogenase in spray-dried trehalose. *J. Pharm. Sci.* **88:**199-208 (1999).

25. S. P. Sellers, G. S. Clark, R. E. Sievers, and J. F. Carpenter. Dry powders of stable protein formulations from aqueous solutions prepared using supercritical CO(2)-assisted aerosolization. *J. Pharm. Sci.* **90:**785-797 (2001).

26. Z. Yu, K. P. Johnston, and R. O. Williams III. Spray freezing into liquid versus spray-freeze drying: Influence of atomization on protein aggregation and biological activity. *Eur. J. Pharm. Sci.* **27:**9-18 (2006).

27. Z. Yu, A. S. Garcia, K. P. Johnston, and R. O. Williams III. Spray freezing into liquid nitrogen for highly stable protein nanostructured microparticles. *Eur. J. Pharm. Biopharm.* **58:**529-537 (2004).

28. J. D. Engstrom, E. S. Lai, B. Ludher, B. Chen, T. E. Milner, G. B. Kitto, R. O. Williams III, and K. P. Johnston. Formation of stable submicron protein particles by thin film freezing. *Pharm. Res.* (Submitted).

29. K. A. Overhoff, J. D. Engstrom, B. Chen, T. L. Rogers, K. P. Johnston, and R. O. Williams III. Novel ultra-rapid freezing particle engineering process to enhance the dissolution rates of poorly water-soluble drugs. *Eur. J. Pharm. Biopharm.* **65:**57-67 (2007).

30. M. C. Heller, J. F. Carpenter, and T. W. Randolph. Protein formulation and lyophilization cycle design: prevention of damage due to freeze-concentration induced phase separation. *Biotechnol. Bioeng.* **63:**166-174 (1999).

31. M. J. Akers, V. Vasudevan, and M. Stickelmeyer. Formulation development of protein dosage forms. In S. L. Nail and M. J. Akers (eds.), *Pharmaceutical Biotechnology. 14. Development and Manufacture of Protein Pharmaceuticals*, Kluwer Academic/Plenum Press, New York, 2002, pp. 47-127.

32. T. F. O'Connor, P. G. Debenedetti, and J. D. Carbeck. Simultaneous determination of structural and thermodynamic effects of carbohydrate solutes on the thermal stability of ribonuclease A. *J. Am. Chem. Soc.* **126:**11794-11795 (2004).

33. C. A. Angell and L.-M. Wang. Hyperquenching and cold equilibration strategies for the study of liquid-liquid and protein folding transitions. *Biophys. Chem.* **105:**621-637 (2003).

34. F. Franks. *Biophysics and Biochemistry at Low Temperatures*, Cambridge University Press, New York, 1985.

35. C. A. Angell. Liquid fragility and the glass transition in water and aqueous solutions. *Chem. Rev.* **102:**2627-2649 (2002).

36. A. P. MacKenzie. Non-equilibrium freezing behavior of aqueous systems. *Philos. Trans. R. Soc. London, B: Biol. Sci.* **278:**167-189 (1977).

37. S. L. Nail, S. Jiang, S. Chongprasert, and S. A. Knopp. Fundamentals of freeze-drying. In S. L. Nail and M. J. Akers (eds.), *Pharmaceutical Biotechnology. 14. Development and Manufacture of Protein Pharmaceuticals*, Kluwer Academic/Plenum Publishers, New York, 2002, pp. 281-360.

38. Z. H. Chang and J. G. Baust. Ultra-rapid freezing by spraying/plunging: pre-cooling in the cold gaseous layer. *J. Microsc.* **161:**435-444 (1991).

39. M. C. Heller, J. F. Carpenter, and T. W. Randolph. Application of a thermodynamic model to the prediction of phase separations in freeze-concentrated formulations for protein lyophilization. *Arch. Biochem. Biophys.* **363:**191-201 (1999).

40. J. D. Andya, Y.-F. Maa, H. R. Costantino, P.-A. Nguyen, N. Dasovich, T. D. Sweeney, C. C. Hsu, and S. J. Shire. The effect of formulation excipients on protein stability and aerosol performance of spray-dried powders of a recombinant humanized anti-IgE monoclonal antibody. *Pharm. Res.* **16:**350-358 (1999).

41. Y.-F. Maa and P.-A. Nguyen. Method of spray freeze drying proteins for pharmaceutical administration. United States Patent. 6,284,282 (2001).

42. H. R. Costantino, L. Firouzabadian, C. C. Wu, K. G. Carrasquillo, K. Griebenow, S. E. Zale, and M. A. Tracy. Protein spray freeze drying. 2. Effect of formulation variables on particle size and stability. *J. Pharm. Sci.* **91:**388-395 (2002).

43. J. D. Engstrom, D. T. Simpson, C. Cloonan, E. Lai, R. O. Williams III, G. B. Kitto, and P. Johnston Keith. Stable high surface area lactate dehydrogenase particles produced by spray freezing into liquid nitrogen. *Eur. J. Pharm. Biopharm.* **65:**163-174 (2007).

44. S. Magdassi and A. Kamyshny. Surface activity and functional properties of proteins. In S. Magdassi (ed.), *Surface Activity of Proteins*, Marcel Dekker, New York, 1996, pp. 1-38.

45. J. Hu, T. L. Rogers, J. Brown, T. Young, K. P. Johnston, and R. O. Williams III. Improvement of dissolution rates of poorly water soluble APIs using novel spray freezing into liquid technology. *Pharm. Res.* **19:**1278-1284 (2002).

46. J. Hu, K. P. Johnston, and R. O. Williams III. Rapid dissolving high potency danazol powders produced by spray freezing into liquid process. *Int. J. Pharm.* **271:**145-154 (2004).

47. T. L. Rogers, J. Hu, Z. Yu, K. P. Johnston, and R. O. Williams III. A novel particle engineering technology: spray-freezing into liquid. *Int. J. Pharm.* **242:**93-100 (2002).

48. T. L. Rogers, A. C. Nelsen, J. Hu, J. N. Brown, M. Sarkari, T. J. Young, K. P. Johnston, and R. O. Williams III. A novel particle engineering technology to enhance dissolution of poorly water soluble drugs: spray-freezing into liquid. *Eur. J. Pharm. Biopharm.* **54:**271-280 (2002).

49. H. Sitte, L. Edelmann, and K. Neumann. Cryofixation without pretreatment at ambient pressure. In R. A. Steinbrecht and K. Zierold (eds.), *Cryotechniques in Biological Electron Microscopy*, Springer-Verlag, Berlin, 1987, pp. 87-113.

50. M. J. Costello and J. M. Corless. The direct measurement of temperature changes within freeze-fracture specimens during rapid quenching in liquid coolants. *J. Microsc.* **112:**17-37 (1978).

51. J. D. Engstrom, D. T. Simpson, E. Lai, R. O. Williams III, and K. P. Johnston. Morphology of protein particles produced by spray freezing of concentrated solutions. *Eur. J. Pharm. Biopharm.* **65:**149-162 (2007).

52. J. Fukai, M. Tanaka, and O. Miyatake. Maximum spreading of liquid droplets colliding with flat surfaces. *J. Chem. Eng. Jpn.* **31:**456-461 (1998).

53. M. Pasandideh-Fard, R. Bhola, S. Chandra, and J. Mostaghimi. Deposition of tin droplets on a steel plate : simulations and experiments. *Int. J. Heat Mass Transfer* **41:**2929-2945 (1998).

54. M. Pasandideh-Fard, S. Chandra, and J. Mostaghimi. A three-dimensional model of droplet impact and solidification. *Int. J. Heat Mass Transfer* **45:**2229-2242 (2002).

55. J. Fukai, T. Ozaki, H. Asami, and O. Miyatake. Numerical simulation of liquid droplet solidification on substrates. *J. Chem. Eng. Jpn.* **33:**630-637 (2000).

56. D. Sivakumar and H. Nishiyama. Numerical analysis on the impact behavior of molten metal droplets using a modified splat-quench solidification model. *J. Heat Transf.-Trans. ASME* **126:**1014-1022 (2004).

57. B. Kang, Z. Zhao, and D. Poulikakos. Solidification of liquid metal droplets impacting sequentially on a solid surface. *J. Heat Transfer* **116:**436-45 (1994).

58. J. Madejski. Solidification of droplets on a cold surface. *Int. J. Heat Mass Transfer* **19:**1009-1013 (1976).

59. C. Sanmarchi, H. Liu, E. J. Lavernia, R. H. Rangel, A. Sickinger, and E. Muehlberger. Numerical analysis of the deformation and solidification of a single droplet impinging onto a flat substrate. *J. Mater. Sci.* **28:**3313-21 (1993).

60. G. X. Wang and E. F. Matthys. Modeling of heat transfer and solidification during splat cooling: effect of splat thickness and splat/substrate thermal contact. *Int. J. Rapid Solid.* **6:**141-74 (1991).

61. G. X. Wang and E. F. Matthys. Numerical modeling of phase change and heat transfer during rapid solidification processes: use of control volume integrals with element subdivision. *Int. J. Heat Mass Transfer* **35:**141-53 (1992).

62. H. Zhang, X. Y. Wang, L. L. Zheng, and X. Y. Jiang. Studies of splat morphology and rapid solidification during thermal spraying. *Int. J. Heat Mass Transfer* **44:**4579-4592 (2001).

63. Z. Zhao, D. Poulikakos, and J. Fukai. Heat transfer and fluid dynamics during the collision of a liquid droplet on a substrate. I. Modeling. *Int. J. Heat Mass Transfer* **39:**2771-2789 (1996).

64. Z. Zhao, D. Poulikakos, and J. Fukai. Heat transfer and fluid dynamics during the collision of a liquid droplet on a substrate. II. Experiments. *Int. J. Heat Mass Transfer* **39:**2791-2802 (1996).

65. T. Bennett and D. Poulikakos. Splat-quench solidification: estimating the maximum spreading of a droplet impacting a solid surface. *J. Mater. Sci.* **28:**963-970 (1993).

66. G. Trapaga and J. Szekely. Mathematical modeling of the isothermal impingement of liquid droplets in spraying processes. *Metall. Trans. B* **22B:**901-14 (1991).

67. R. U. Agu, M. I. Ugwoke, M. Armand, R. Kinget, and N. Verbeke. The lung as a route for systemic delivery of therapeutic proteins and peptides. *Respiratory Research* **2:**198-209 (2001).

68. J. S. Patton and P. R. Byron. Inhaling medicines: delivering drugs to the body through the lungs. *Nature Reviews Drug Discovery* **6:**67-74 (2007).

69. V. Codrons, F. Vanderbist, R. K. Verbeeck, M. Arras, D. Lison, V. Preat, and R. Vanbever. Systemic delivery of parathyroid hormone (1-34) using inhalation dry powders in rats. *J. Pharm. Sci.* **92:**938-950 (2003).

70. S. A. Shoyele and A. Slowey. Prospects of formulating proteins/peptides as aerosols for pulmonary drug delivery. *Int. J. Pharm.* **314:**1-8 (2006).

71. A. L. Adjei and P. K. Gupta. *Inhalation Delivery of Therapeutic Peptides and Proteins*, 1997.

72. S. White, D. B. Bennett, S. Cheu, P. W. Conley, D. B. Guzek, S. Gray, J. Howard, R. Malcolmson, J. M. Parker, P. Roberts, N. Sadrzadeh, J. D. Schumacher, S. Seshadri, G. W. Sluggett, C. L. Stevenson, and N. J. Harper. EXUBERA: Pharmaceutical Development of a Novel Product for Pulmonary Delivery of Insulin. *Diabetes Technology & Therapeutics* **7:**896-906 (2005).

73. H. M. Courrier, N. Butz, and T. F. Vandamme. Pulmonary drug delivery systems: recent developments and prospects. *Critical Reviews in Therapeutic Drug Carrier Systems* **19:**425-498 (2002).

74. M. J. Kwon, J. H. Bae, J. J. Kim, K. Na, and E. S. Lee. Long acting porous microparticle for pulmonary protein delivery. *Int. J. Pharm.* **333:**5-9 (2007).

75. L. Garcia-Contreras and H. D. C. Smyth. Liquid-spray or dry-powder systems for inhaled delivery of peptide and proteins? *American Journal of Drug Delivery* **3:**29-45 (2005).

76. P. Rogueda. Novel hydrofluoroalkane suspension formulations for respiratory drug delivery. *Expert Opinion on Drug Delivery* **2:**625-638 (2005).

77. D. Traini, P. Young, P. Rogueda, and R. Price. The Use of AFM and Surface Energy Measurements to Investigate Drug-Canister Material Interactions in a Model Pressurized Metered Dose Inhaler Formulation. *Aerosol Science and Technology* **40:**227-236 (2006).

78. E. A. Quinn, R. T. Forbes, A. C. Williams, M. J. Oliver, L. McKenzie, and T. S. Purewal. Protein conformational stability in the hydrofluoroalkane propellants tetrafluoroethane and heptafluoropropane analyzed by Fourier transform Raman spectroscopy. *Int. J. Pharm.* **186:**31-41 (1999).

79. M. J. Oliver, L. McKenzie, W. D. Graffiths, G. R. Morgan, and N. O'Kelly. Initial assessment of a protein formulated in pressurized mdis for pulmonary delivery, *RDD VII*, 2000.

80. C. Benfait. Kos reports achievement of new research and development milestones. *Kos Press Release* (2004).

81. J. Heyder, J. Gebhart, G. Rudolf, C. F. Schiller, and W. Stahlhofen. Deposition of particles in the human respiratory tract in the size range 0.005-15 μm. *J. Aerosol Sci.* **17:**811-825 (1986).

82. A. Ben-Jebria, D. Chen, M. L. Eskew, R. Vanbever, R. Langer, and D. A. Edwards. Large porous particles for sustained protection from carbachol-induced bronchoconstriction in guinea pigs. *Pharm. Res.* **16:**555-561 (1999).

83. N. Tsapis, D. Bennett, B. Jackson, D. A. Weitz, and D. A. Edwards. Trojan particles: large porous carriers of nanoparticles for drug delivery. *Proc. Natl. Acad. Sci. U. S. A.* **99:**12001-12005 (2002).

84. L. A. Dellamary, T. E. Tarara, D. J. Smith, C. H. Woelk, A. Adractas, M. L. Costello, H. Gill, and J. G. Weers. Hollow porous particles in metered dose inhalers. *Pharm. Res.* **17:**168-174 (2000).

85. I. Gonda. Development of a systematic theory of suspension inhalation aerosols. I. A framework to study the effects of aggregation on the aerodynamic behavior of drug particles. *Int. J. Pharm.* **27:**99-116 (1985).

86. Y.-H. Liao, M. B. Brown, S. A. Jones, T. Nazir, and G. P. Martin. The effects of polyvinyl alcohol on the in vitro stability and delivery of spray-dried protein particles from surfactant-free HFA 134a-based pressurised metered dose inhalers. *Int. J. Pharm.* **304:**29-39 (2005).

87. M. Keller. Innovations and perspectives of metered dose inhalers in pulmonary drug delivery. *Int. J. Pharm.* **186:**81-90 (1999).

88. R. P. S. Peguin, P. Selvam, and S. R. P. da Rocha. Microscopic and Thermodynamic Properties of the HFA134a-Water Interface: Atomistic Computer Simulations and Tensiometry under Pressure. *Langmuir* **22:**8826-8830 (2006).

89. R. Vanbever, J. D. Mintzes, J. Wang, J. Nice, D. Chen, R. Batycky, R. Langer, and D. A. Edwards. Formulation and physical characterization of large porous particles for inhalation. *Pharm. Res.* **16:**1735-1742 (1999).

Chapter 2: Morphology of Protein Particles Produced by Spray Freezing of Concentrated Solutions

The mechanisms for the formation of high surface area lysozyme particles in spray freezing processes are described as a function of spray geometry and atomization, solute concentration and the calculated cooling rate. In the spray freeze-drying (SFD) process, droplets are atomized into a gas and then freeze upon contact with a liquid cryogen. In the spray freezing into liquid (SFL) process, a solution is sprayed directly into the liquid cryogen below the gas-liquid meniscus. A wide range of feed concentrations is examined for two cryogens, liquid nitrogen (LN2) and isopentane (*i*-C5). The particle morphologies are characterized by SEM micrographs and BET measurements of specific surface area. As a result of boiling of the cryogen (Leidenfrost effect), the cooling rate for SFL into LN2 is several orders of magnitude slower than for SFL into *i*-C5 and for SFD in the case of either LN2 or *i*-C5. For 50 mg/mL concentrated feed solutions, the slower cooling of SFL into LN2 leads to a surface area of 34 m^2/g. For the other three cases with more rapid cooling rates, surface areas were greater than 100 m^2/g. The ability to adjust the cooling rate to vary the final particle surface area is beneficial for designing particles for controlled release applications.

2.1 INTRODUCTION

Spray-freezing processes may be used for rapid cooling of solutions containing a therapeutic peptide or protein to produce high specific surface area (SSA) powders intended for pulmonary, transdermal, or depot delivery routes (1). In some cases loss in protein activity in spray freezing processes has been a significant limitation (1-3). In the spray freeze-drying (SFD) process, an aqueous solution containing dissolved protein and

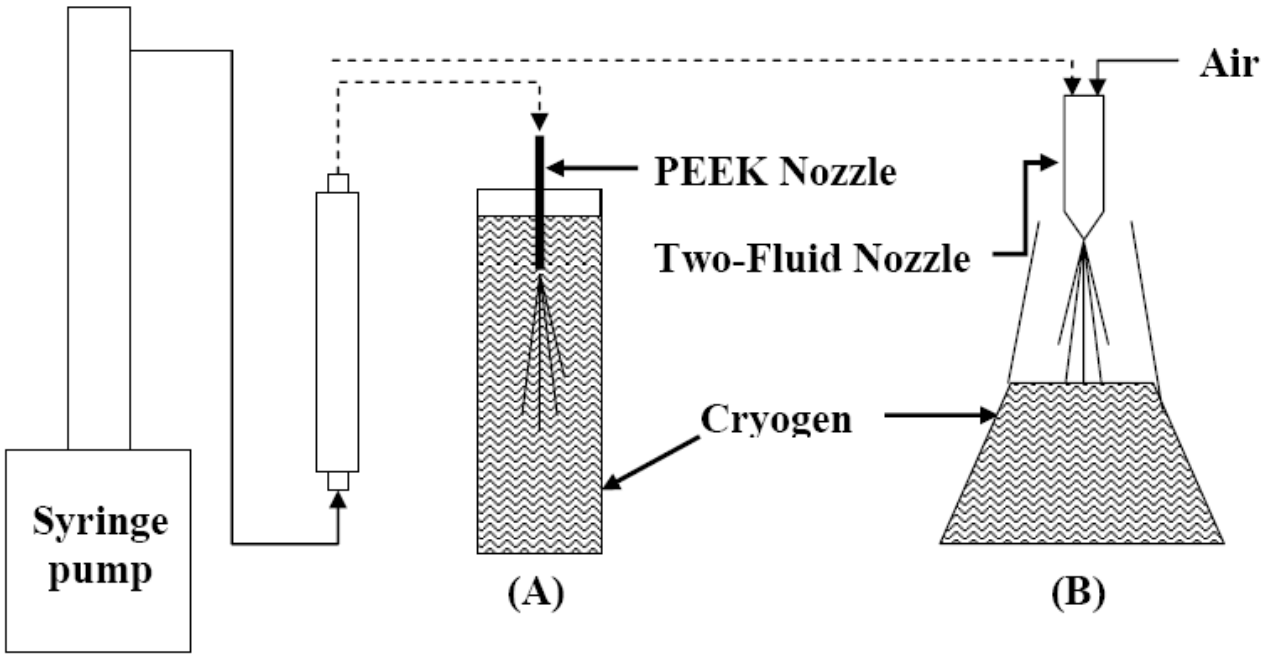

Figure 2.1: Experimental apparatus for SFL (A) and SFD (B) sprays. For SFL the nozzle is immersed below the cryogen surface while for SFD the liquid jet is atomized above the liquid cryogen surface with a two-fluid nozzle.

excipients is atomized into the cold gas above a cryogenic liquid (Fig. 2.1) (4-8). The micron-sized droplets travel through the cryogenic gas, where they may begin to freeze (9), and are then completely frozen after contact with the liquid cryogen. The frozen droplets are then lyophilized leaving behind dry particles of protein and excipients. The SSA of SFD powders increases with an increase in cooling rate produced by a decrease in the aqueous droplet size (1, 6, 10). High SSA particles are of practical interest as they may be micronized into sub-micron particles for uniform encapsulation into bioerodible polymer microspheres for controlled release (6, 11, 12).

The atomization step in SFD in the ambient gas creates a large gas-liquid interfacial area for protein adsorption and unfolding (8). In addition, the rapid cooling of the liquid droplets produces a large ice-liquid interface which may also denature proteins (6, 13). For the protein recombinant human interferon-γ (rhIFN-γ), Webb et al. (8) demonstrated that the gas-liquid interface is more damaging than the ice-liquid interface. Their calculations showed that a protein in the freeze concentrate during rapid cooling would not have sufficient time to diffuse to the ice-liquid interface and denature before being trapped in an amorphous glass (8). To minimize the area of the gas-liquid interface in the SFD process the atomized droplet size may be increased, but at the expense of the SSA of the powder (1, 6).

In the alternative spray freezing into liquid (SFL) process, the feed nozzle is immersed under the cryogen surface. Freezing occurs upon impingement of the feed solution with the cryogenic liquid (Fig. 2.1) (14). The SFL process has been used in freezing dilute organic solutions of poorly water soluble drugs (15-18) to produce powders with high SSA and thus enhanced dissolution rates. It has also been used to spray aqueous peptide and protein solutions to achieve powders with SSA values greater than 100 m^2/g (17, 19-21). Lysozyme was shown to be more stable when produced by

SFL versus SFD as a result of reduced denaturation in the spray freezing step. The improvement in stability resulted from reduced exposure to the gas-liquid interface (20).

Both the SFL and SFD processes have used liquid nitrogen (LN2) nearly exclusively as the cryogen (1-8, 11, 14-17, 19-22). The boiling point of LN2 is low, only -196ºC, which is desirable for rapid cooling. It is environmentally friendly, nonflammable and it does not remain as a residue in the product (18). In spite of its low boiling point, LN2 has been shown to produce slower cooling rates than cryogens with higher freezing points such as isopentane (*i*-C5) (fp = -160ºC) and propane (C3) (fp = -190ºC) (23, 24). The lower LN2 cooling rate is well known to result from boiling of the LN2 around an inserted object, or sprayed fluid, forming an insulating gas, a phenomenon referred to as the Leidenfrost effect (23). The influence of the Leidenfrost effect on cooling rates in SFD and SFL and on jet breakup in SFL has received little attention. Furthermore, relatively few spray freezing studies have investigated feed solutions with concentrations greater than 5 mg/mL. Scanning electron microscopy (SEM) micrographs of trehalose and sucrose powders prepared from 20% (w/v) solutions by SFD into liquid propane (SFD-C3) and into LN2 (SFD-LN2) showed very slight differences in powder morphology (25) indicating that the cooling rates in each cryogen may have been similar; however, SSA data were not available to confirm this result (25).

For SFL of dilute polyethylene glycol (PEG) solutions into liquid CO_2 at -50ºC (26) vaporization of the pressurized CO_2 was not possible and the liquid-liquid impingement readily broke up the jet into droplets (27). For proteins including BSA and lysozyme, powders with SSAs on the order of 134 m^2/g have been produced for the SFL-LN2 process for dilute feed concentrations up to 5 mg/mL (11, 21). However, for PEG solutions, increasing the feed concentration increased the solution viscosity and inhibited liquid jet breakup resulting in slower cooling rates and larger particle sizes and eventually

fibers (26). In addition, the SSA decreases with an increase in the volume fraction of solute in the feed solution, and hence in the frozen solution (26).

The objectives of this study were to investigate morphologies (SEMs and SSAs) of protein particles, produced by both SFL and SFD into *i*-C5 and LN2 for dilute and concentrated feed solutions, in terms of jet break up, cooling rates, and nucleation and growth mechanisms. An important objective was to determine if cooling rates may be slowed down by the formation of a Leidenfrost insulating gas layer and how this influences particle morphology. Alternatively, in order to minimize solvent evaporation and to increase jet atomization, the cryogen isopentane (*i*-C5) was chosen for its low melting temperature of -160ºC, high thermal conductivity and viscosity, and high heat of vaporization and boiling point of 27ºC (23). The differences in spray geometry and thus cooling rates will be shown to influence the SSA of the product, particularly for more concentrated solutions. Previous work with SFL in a dewer flask with metal walls did not provide flow visualization of the jet and the frozen particles (20). In this work, flow visualization experiments are used to show that a low viscosity turbulent gaseous N_2 cone about the sprayed jet reduces the degree of jet atomization and consequently the SSA. Thus, the SSA may be tuned by varying the cooling rate. A better mechanistic description of cooling rate and particle formation in the SFL and SFD processes will be useful for further understanding stabilities of protein powders in previous SFL and SFD studies and in a companion study of lactate dehydrogenase (28).

2.2 MATERIALS AND METHODS

2.2.1 Materials

Trehalose and lysozyme were purchased from Sigma Chemical Company (St. Louis, MO) and isopentane (*i*-C5) (>99% Purity) from GFS Chemicals (Powell, OH).

The water was deionized by flowing distilled water through a series of 2x7 L mixed bed DI vessels (Water and Power Technologies, Salt Lake City, UT) containing 60:40 anionic:cationic resin blends.

2.2.2 Freeze procedures

2.2.2.1 SFL into liquid nitrogen (SFL-LN2)

The SFL process was modified slightly from a previous study (19). The liquid flow rate was 10 mL/min resulting in a pressure drop of 17.2 MPa through a 63 um ID poly-ether-ether-ketone (PEEK) nozzle 5 cm in length (Upchurch Scientific, Oak Harbor, WA) (Fig. 2.1). A 2 L Erlenmeyer flask containing a 2.54 cm length, 0.952 cm diameter octagonal magnetic stir bar (Fisher Scientific, Somerville, NJ) was filled with LN2 and placed in a 4 L insulated bucket (Fisher Scientific, Somerville, NJ) also filled with LN2. The ice bucket was placed on a stir plate. The depth of the LN2 vortex was approximately 2.5 cm and the nozzle was placed 2.5 cm beneath the minimum LN2 vortex level. Once the spray was completed, stirring was stopped allowing the frozen slurry to settle. Excess LN2 was decanted, and the slurry was then transferred to a 250 mL glass beaker using a spatula pre-cooled in LN2. The beakers were held in a -80°C freezer to remove residual LN2 before transfer to the pre-cooled lyophilizer shelf.

2.2.2.2 SFL into isopentane (SFL-i-C5)

The spray apparatus was based on the SFL-LN2 process, except that it was contained in a vacuum hood with care taken to eliminate all ignition sources (Fig. 2.1). The *i*-C5 was cooled to 4°C in an ice-water bath. A 400 mL Pyrex® beaker was filled with 300 mL of the chilled *i*-C5, corresponding to a height of 8 cm. A smaller volume of *i*-C5 was used relative to LN2 since *i*-C5 losses due to boiling were minimal compared to LN2 during the spray. The beaker filled with *i*-C5 was placed in a LN2 bath contained in the above 4 L bucket with an inside diameter of 15 cm. The *i*-C5 was further cooled

under vigorous stirring with a 2.54 cm length, 0.952 cm diameter octagonal magnetic stir bar (Fisher Scientific, Somerville, NJ). The surface of the *i*-C5 was 1.5 cm below the surface of the LN2 in the ice bucket. With a Type K thermocouple (Eutech Instruments, Vernon Hills, IL) it was found that the temperature of the *i*-C5 varied 5ºC from the center to the side of the beaker. It varied less than 1ºC as the thermocouple was positioned at different points between the top surface of the *i*-C5 in the beaker and the bottom. When the temperature in the center of the beaker reached -155ºC, the nozzle was immersed 1 cm below the cryogen surface. Solid *i*-C5 coated the inside of the beaker before and during the spray. The temperature varied less than 5^{o}C during the spray, as only 10-20 mL of aqueous solution was sprayed into the large thermal mass of *i*-C5.

In order to minimize the amount of *i*-C5 placed in the lyophilizer the excess *i*-C5 was filtered. An Edwards RV8 Dual-Mode Vacuum Pump (Scientific Instrument Services, Inc., Ringoes, NJ) was connected to a 1000 mL Pyrex® filtering flask (Fisher Scientific, Somerville, NJ) fitted with a porcelain Büchner funnel (Coors®, Fisher Scientific, Somerville, NJ) with an inside diameter of 11.4 cm and a circular cellulose fiber filter with a diameter of 11 cm and 1-5 μm pores (Fisher Scientific, Somerville, NJ). When the spray was complete, the ice crystal suspension in *i*-C5 was filtered for 30 seconds, after which the ice crystals with residual *i*-C5 were rapidly transferred to a 250 mL Pyrex® beaker filled with LN2 using a pre-cooled spatula. The residual *i*-C5 on the ice crystals was evaporated from the beakers on a lyophilizer shelf held at -60°C under vacuum for 2 hrs with a LN2 trap. At -60°C, liquid *i*-C5 has a vapor pressure of 1.08 kPa, far above a value of only 1.11 Pa for ice. The heat of vaporization of the *i*-C5 cooled the frozen slurry. Completion of the *i*-C5 evaporation was recognized by a sharp drop in the vacuum chamber pressure.

2.2.2.3 SFD sprays into liquid nitrogen (SFD-LN2) and isopentane (SFD-i-C5)

The SFL apparatus described above was modified for SFD (Fig. 2.1). The aqueous feed solution was sprayed with a 0.7 mm diameter two-fluid nozzle (Büchi, Laboratory-Techniques, Switzerland) at a constant flow rate of 10 mL/min resulting in a pressure drop of 0.827 MPa (Fig. 2.1). Droplet sizes were tuned by varying the air flow rates. Droplet size distributions were measured by static light scattering (Malvern Mastersizer-S, Malvern Instruments, Ltd.,Worcestershire, UK) (Fig. 2.2) by mounting the nozzle 10 cm above the laser beam (λ = 633 nm) and spraying the droplets normal to the laser beam. A 300 mm lens (PN 33544/777, Malvern Instruments, Ltd., Worcestershire, UK) was mounted to the detector and the sprayed droplets entered the laser beam 10-12 cm in front of the lens. Care was taken to minimize stray light entering the chamber with the laser beam. Obscuration values were between 8-12%.

The SFD setup was comparable to that of Maa et al.(4), who used a flow rate of 15 mL/min, and droplet sizes were similar (Table 2.1). The SFD nozzle was mounted 10 cm above the surface of the cryogen. Cryogen preparation and post-spray slurry collection were performed as presented in the SFL spray section, with the exception that 1 L of LN2 was utilized in a 2 L Erlenmeyer flask and 300 mL of *i*-C5 in a1 L flask. A greater amount of LN2 was required to compensate for the 200 mL loss of LN2 after a 20 mL spray, due to excessive boiling whereas the losses for *i*-C5 were minimal. For SFD air flow rates of 250 mL/s, the LN2 splashed around violently inside the Erlenmeyer flask which quickly dropped the gas temperature surrounding the air plume to -196ºC 10 cm above the cryogen surface. Reducing the air flow rates to 50 mL/s decreased LN2 splashing and increased the gas temperature to -140ºC. For no air flow, the gas temperature above the LN2 was -30ºC. For the *i*-C5 spray, the temperature of the *i*-C5 gas at a position 5 cm above the cryogen surface was -90ºC. The nomenclature for the

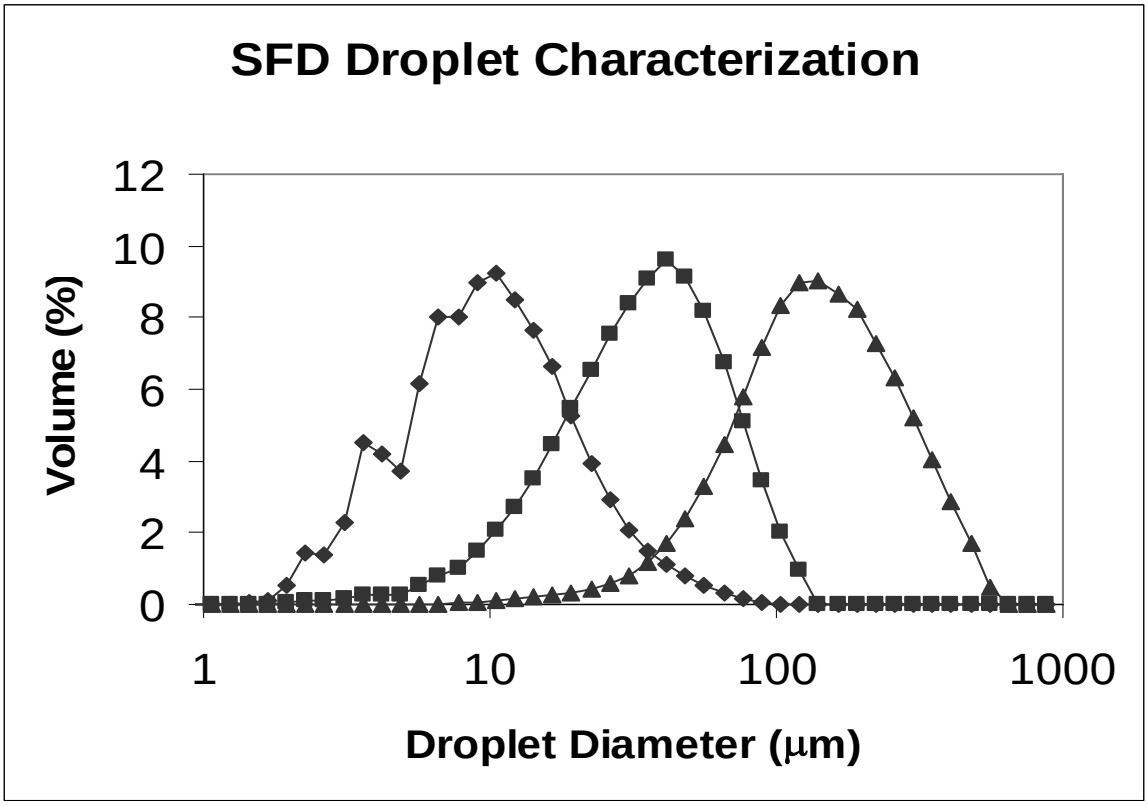

Figure 2.2: Water droplets formed by SFD nozzle were measured by static light scattering with the Malvern Mastersizer for a constant water flow rate at 10 mL/min and air flow rates at (◆) 250, (■) 150, and (▲) 50 mL/s.

Table 2.1: Droplet diameters formed from SFD sprays

SFD Air Flow Rate (mL/s)	SFD Liquid Flow Rate (mL/min)	d(v,50) (μm)	Span[a]
250	10	9	2.4
290[b]	15[b]	7[b]	1.4[b]
150	10	37	2.0
167[b]	15[b]	19[b]	1.6[b]
50	10	129	2.0

[a] Span calculated as $(d_{90}-d_{10})/d_{50}$
[b] Values from Maa et als. (3, 4).

spray configurations is as follows: spray technique-cryogen-d(v,50) (e.g. SFD-LN2-10 refers to the SFD configuration, with LN2 as the cryogen, and an air-flow rate that gives a droplet size d(v,50) = 10 μm.

2.2.2.4 Falling droplets into liquid nitrogen (falling droplet-LN2) and isopentane (falling droplet-i-C5)

The aqueous feed solution was passed through a 127 μm ID, 1.59 mm OD PEEK nozzle at a flow rate of 2 mL/min producing 3.6 mm diameter droplets. The nozzle was held 10 cm above a beaker of the stirred cryogen.

2.2.3 Drying and shelf loading

A Virtis Advantage Lyophilizer (The Virtis Company, Inc., Gardiner, NY) was used to dry the frozen slurries. The beakers containing the frozen slurries were covered with a single layer Kim-wipe held in place by a rubber-band in order to prevent powder from leaving the vial. Primary drying was carried out at -40ºC for 36 hrs at 300 mTorr and secondary drying at 25ºC for 24 hrs at 100 mTorr. A 12 hour linear ramp of the shelf temperature from -40°C to +25°C was used at 100 mTorr.

2.2.4 Transfer and storage of dried powders

After the lyophilization cycle was complete, the lyophilizer was purged with nitrogen. The beakers were then rapidly transferred to a dry box held at 14% RH, and the powders were transferred to 20 mL scintillation vials. The vials were then covered with 24 mm Teflon® Faced Silicone septa (Wheaton, Millville, NJ) which were held in place by open-top screw cap lids (VWR Scientific Products, Austin, TX). Vials were purged with dry nitrogen for 2 minutes by inserting a needle from a dry nitrogen source through the septa with an additional needle for the gas effluent.

2.2.5 Surface area measurement

Surface areas of dried powders were measured with a Quantachrome Nova 2000 (Quantachrome Corporation, Boynton Beach, FL) BET apparatus. Dried powders were transferred to the glass BET sample cells in a dry box. Samples were then degassed under vacuum for a minimum of 12 hours. The Brunauer, Emmett, and Teller (BET) equation (29) was used to fit adsorption data of nitrogen at 77 K over a relative pressure range of 0.05-0.30. The samples were measured two times.

2.2.6 Residual moisture content

Aliquots of methanol were dispensed through the septum of the scintillation vials to form a suspension concentration of 10-100 mg/mL. Vials were then placed in a tub sonicator (Mettler Electronics, Anaheim, CA) for 5 minutes at maximum power to insure complete suspension of the powder. Moisture content was measured for a 200 μL aliquot with an Aquatest 8 Karl-Fischer Titrator (Photovolt Instruments, Indianapolis, IN). The moisture values were corrected with a 200 μL methanol blank. All samples had a moisture content between 2-3% (w/w) after drying which compared well to the residual moisture contents of 2-7% (w/w) for BSA prepared by SFD as presented by Costantino et al. (6).

2.2.7 Particle size analysis

The size distribution of dried powders was measured by multiangle laser light scattering with a Malvern Mastersizer-S (Malvern Instruments, Ltd.,Worcestershire, UK). A mass of 30-100 mg of powder was suspended in 10 mL of acetonitrile and the suspension was then sonicated on ice for 1 minute using a Branson Sonifier 450 (Branson Ultrasonics Corporation, Danbury, CT) with a 102 converter and tip operated in pulse mode at 35 W. Typical obscuration values ranged from 11-13%. Aliquots of the sonicated suspension were then dispensed into a 500 mL acetonitrile bath for analysis.

2.2.8 Scanning electron microscopy

SEM images were collected on a Hitachi Model S-4500 scanning electron microscope (Hitachi Ltd, Tokyo, Japan). The samples were prepared in a dry-box. Aluminum stages fitted with double adhesive carbon conducting tape were gently dipped into sample vials until covered by powder. Stages were then placed in septum capped vials and purged with nitrogen for transfer. To minimize the time samples were exposed to atmospheric moisture the stages were rapidly transferred to a Pelco Model 3 sputter-coater. A conductive gold layer was applied and the samples were then quickly transferred to the SEM. Total exposure to the atmosphere was less than 1 minute.

2.3 RESULTS

2.3.1 SFL

Solutions containing lysozyme and trehalose were sprayed at different feed concentrations into both LN2 and *i*-C5 (Table 2.2). For a lysozyme feed concentration of 5 mg/mL extremely high SSAs were obtained for both cryogens. The SSA for 5 mg/mL lysozyme in LN2 was comparable to previous values for SFL of bovine serum albumin (BSA) (11, 20). Concentrated lysozyme samples at 50 mg/mL and above had SSAs 3-4 times higher when sprayed in *i*-C5 relative to LN2. For 50 mg/mL solutions sprayed in *i*-C5, surface areas were above 100 m^2/g. To validate that the lysozyme SSA values achieved in Table 2.2 were not affected by moisture exposure the residual moisture contents of the dried powders of all lysozyme formulations were determined by Karl Fischer titration. For residual moisture contents up to 7-8% (w/w) the known glass transition temperature (T_g) for lysozyme is ~50-60ºC (30), and for lower moisture contents the T_g is expected to be higher. The low moisture contents of 2-3% (w/w) measured for all dry powder samples, as mentioned in section 2.2.6, shows that the

Table 2.2: Specific surface area measurements and particle size distributions of lysozyme and trehalose powders processed by SFL

		SSA (m^2/g)		Size (μm)[a]	
Component	**Feed Concentration (mg/mL)**	**LN2**	***i*-C5**	**LN2**	***i*-C5**
BSA[b]	5	134	--	0.050-1.0 (92%) 1.0-2.0 (8.0%)	--
Lysozyme	5	114 ± 11	164 ± 8	0.050-1.0 (85%) 2.0-10 (15%)	--
Lysozyme	50	34 ± 2	124 ± 15	0.050-1.0 (48%) 4.0-12 (52%)	0.050-1.0 (80%) 3.0-11 (20%)
Lysozyme	100	38 ± 2	111 ± 4	0.050-1.0 (29%) 6.0-40 (71%)	0.050-1.0 (76%) 3.5-11 (24%)
Trehalose	50	14 ± 2	84 ± 11	--	--
Trehalose	100	13 ± 1	70 ± 6	--	--

[a] Particle size distribution of powders measured with a Malvern Mastersizer after sonication.
[b] Values from Leach et al. (11).

drying protocol was sufficient to produce lysozyme powders with a T_g much higher than room temperature. Therefore, it was expected that loss in lysozyme powder SSA due to moisture exposure would be negligible. As a further comparison and control concentrated 50 and 100 mg/mL trehalose feed concentrations processed by SFL had SSAs nearly 5 times greater in i-C5 than in LN2. The ability to achieve high surface areas for trehalose, which is hygroscopic, suggests that our sample transfer procedures did not cause significant losses in SSA from increases in molecular diffusion due to exposure to moisture.

As the lysozyme feed concentration increased from 5 to 100 mg/mL for SFL-LN2 sprays, the submicron particle content after sonication decreased from 85 to 29% on a volume percentage basis (Table 2.2). The SFL-i-C5 submicron content remained 76% even for a high feed concentration of 100 mg/mL. Selected sonicated size distribution peaks are given in Fig. 2.3 and showed that the submicron d(v,50) peak for all powders was approximately 300 nm. Similar particle sizes for sonicated BSA powder prepared by SFD-LN2 for 20 mg/mL formulations were measured by Costantino et al. (6). However, a second peak with much larger sizes was present for the SFL-LN2 spray at 50 mg/mL (Fig. 2.3).

In SFL-LN2 (Fig. 2.4A) the nozzle tip was hidden by a large gaseous froth at the surface yet a narrow liquid jet was observed to penetrate at least 10 cm into the cryogen without breakup. To better visualize the ice particles a dyed solution was sprayed through the SFL nozzle. Large dyed ice crystals appeared to emanate from the bottom of the jet and subsequently were circulated in the flask by the large gas flux of evaporating LN2. Following the spray, large, dense crystals were suspended in the quiescent LN2. For the SFL-i-C5 spray, it was easy to observe the spray, since evaporation of cryogen was minimal. A wide jet angle was apparent at the tip of the nozzle and the jet break up

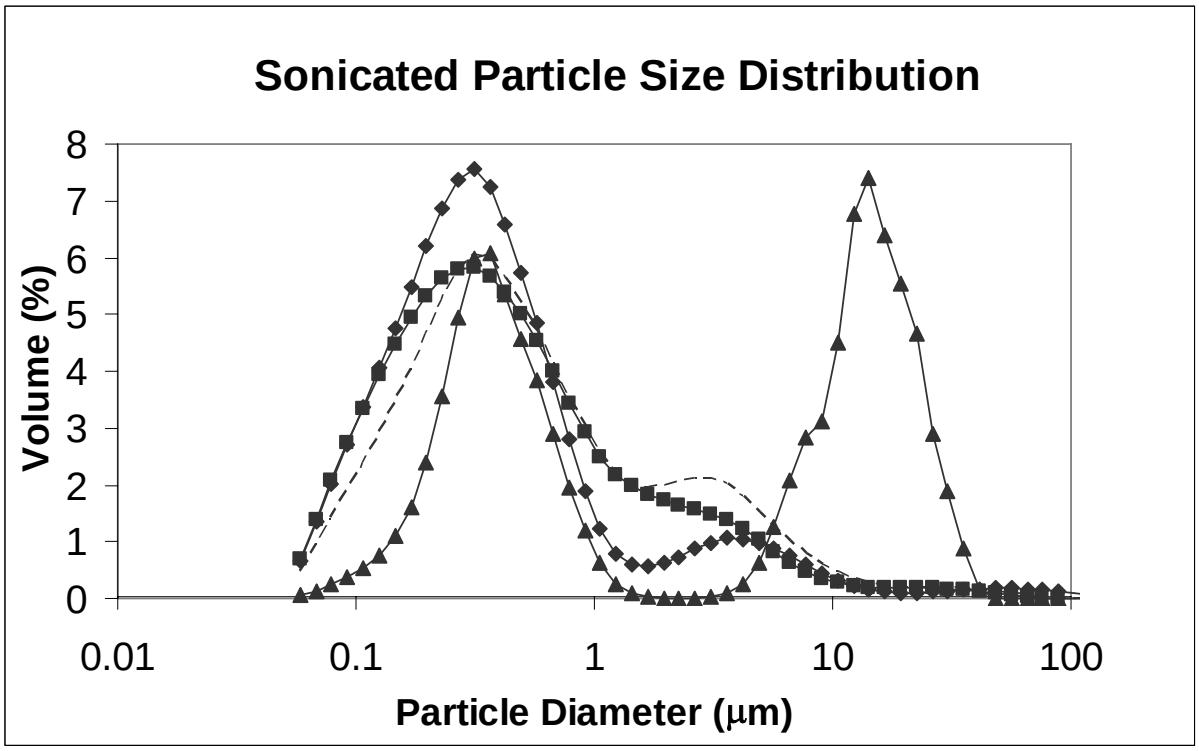

Figure 2.3: Particle size distributions of lysozyme samples processed at (◆) 5 mg/mL in SFL-LN2, and 50 mg/mL in (▲) SFL-LN2, (■) SFL-*i*-C5, and (---) SFD-LN2-10 after sonication as measured by static light scattering.

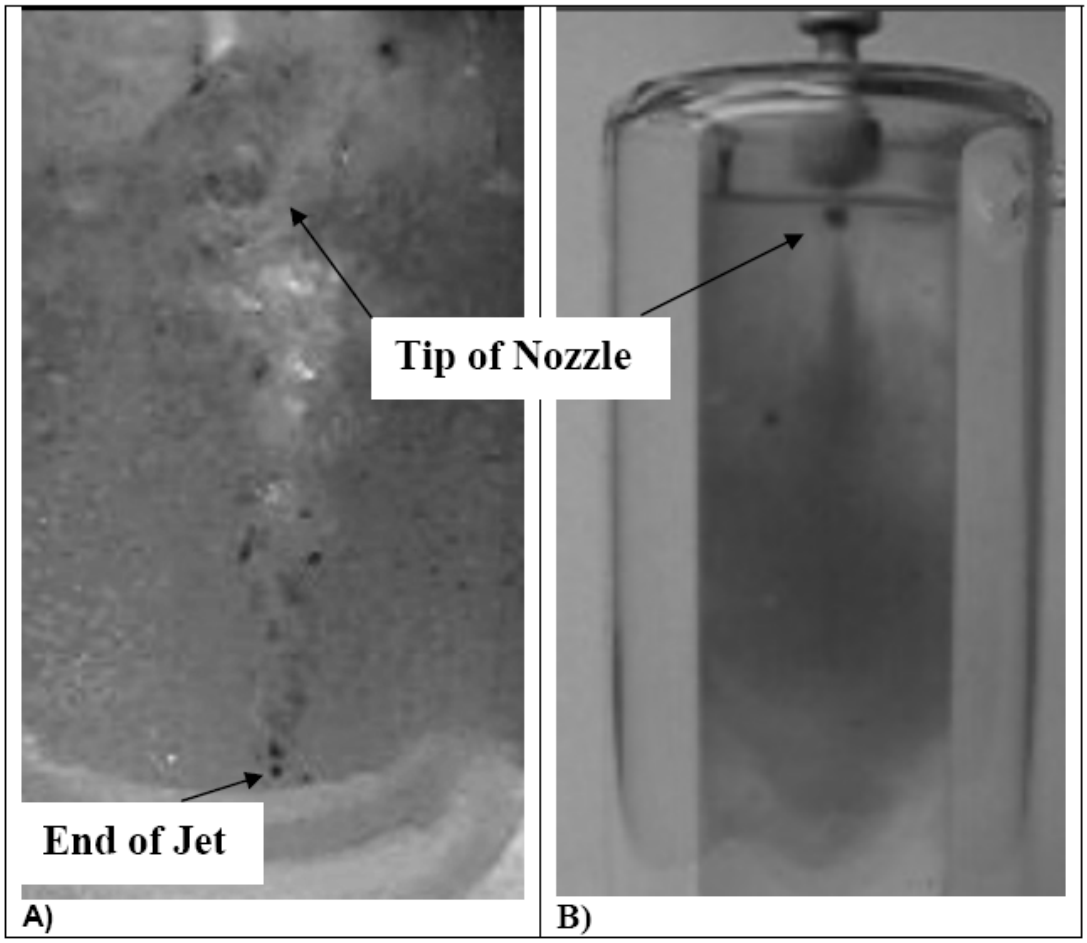

Figure 2.4: SFL of dye solution sprayed at 10 mL/min as seen through a double glass dewar in LN2 (A) and i-C5 (B). i-C5 temperature is -100°C.

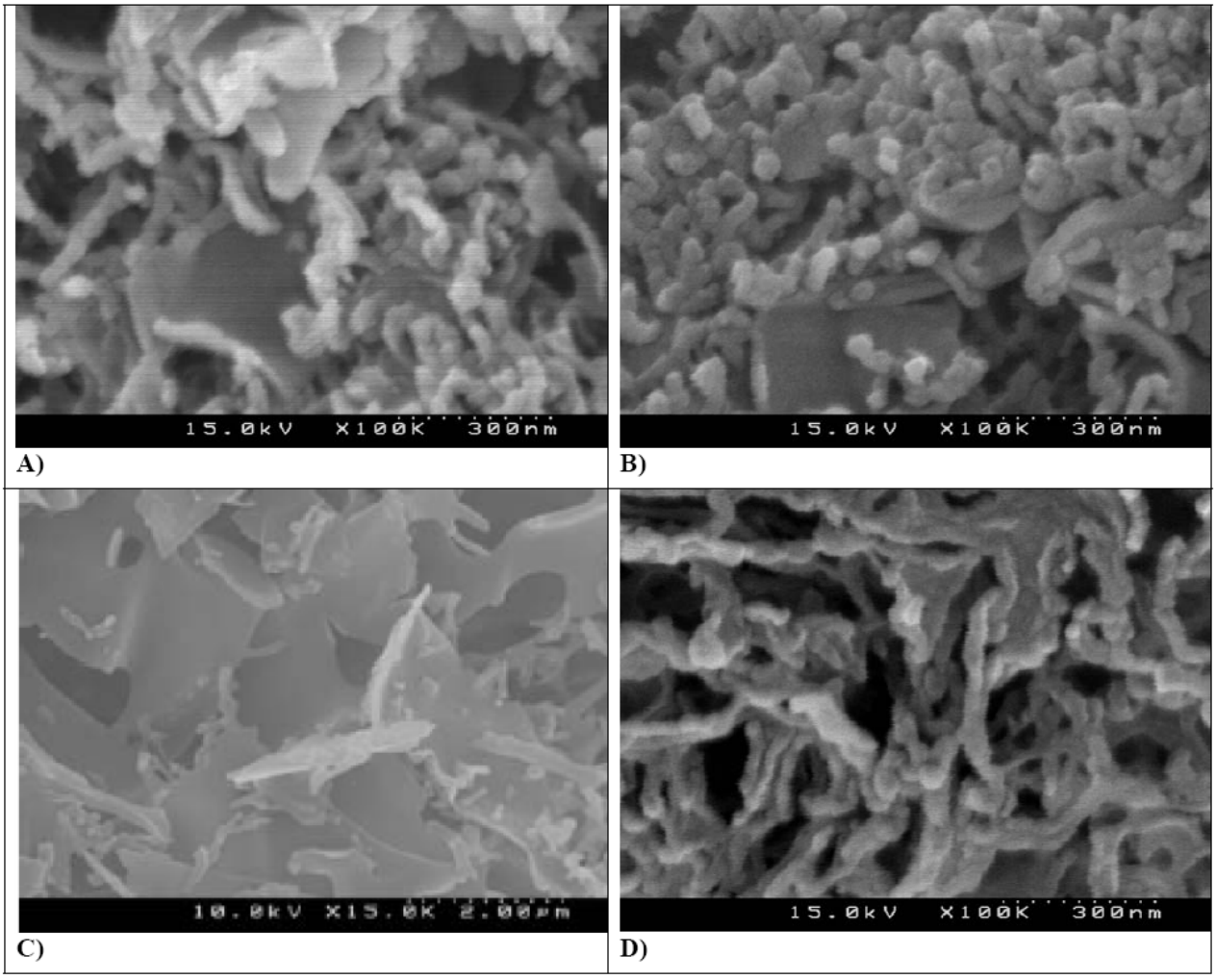

Figure 2.5: SEM's of 5 mg/mL lysozyme formulations for SFL-LN2 (A), SFL-i-C5 (B), and 50 mg/mL lysozyme formulations for SFL-LN2 (C), and SFL-i-C5 (D). Liquid flow rate was 10 mL/min.

length was less than 0.5 cm. The intense jet atomization led to a fine dispersion of ice particles (Fig. 2.4B). After stopping the spray, the particles remained suspended for approximately 1 minute. Selected SEM images from the results in Table 2.2 are shown in Fig. 2.5 for the 5 and 50 mg/mL lysozyme formulations. Both the 5 mg/mL SFL-LN2 and SFL-i-C5 particles (Fig. 2.5A and B) were extremely fine showing spherical particle structures approximately 50 nm in diameter that were joined together. For 50 mg/mL SFL-LN2 (Fig. 2.5C), large sheets were observed with morphological features greater than 1μm. The 50 mg/mL SFL-i-C5 primary particles were extremely fine, 100 nm in diameter, with necks between the aggregated primary particles (Fig. 2.5D). This type of morphology has been observed for SFL-LN2 sprays of 5-10 mg/mL BSA feed concentrations (11). The calculated SSA for 100 nm diameter nonporous spheres assuming a particle density of 1 g/cm^3 is 60 m^2/g and the measured SSA for the SFL-*i*-C5 for a 50 mg/mL lysozyme feed concentration was 124 m^2/g, indicated limited internal porosity. The powder SSA for the 50 mg/mL lysozyme SFL-LN2 spray was 34 m^2/g, consistent with the much larger features in the SEM micrograph.

2.3.2 SFD

For 50 mg/mL lysozyme sprayed by SFD-LN2, there was a substantial decrease in SSA and decrease in the volume percentage of submicron particles for an increase in aqueous solution droplet size (Table 2.3). For SFD-*i*-C5 the SSA was moderately larger for 10 μm droplets relative to 40 or 130 μm droplets. The particle size distribution was similar for 10 and 130 μm droplets. For the 10 and 40 μm droplets, the SSAs and particle size distributions were similar for both cryogens. However, sprays into *i*-C5 resulted in a much larger SSA and particle size relative to LN2 for the 130 μm droplets. As mentioned for SFL, the SFD sprays follow the same pattern for volume percentage of submicron sonicated particles versus droplet size as presented by Costantino et al.(6) As

Table 2.3: Specific surface area measurements and particle size distributions of lysozyme powders processed by SFD and SFL

		SSA (m^2/g)		Size (μm)[a]	
Freeze Process	**Droplet Size (μm)**	**LN2**	***i*- C5**	**LN2**	***i*-C5**
SFD	10	126 ± 5	129 ± 2	0.050-1.0 (74%) 1.0-10 (26%)	0.050-1.0 (64%) 3.0-11 (36%)
SFD	40	87 ± 3	68 ± 2	0.050-1.0 (52%) 3.0-12 (48%)	0.050-1.0 (47%) 3.5-12 (53%)
SFD	130	26 ± 1	90 ± 2	0.050-1.0 (38%) 5.0-11 (62%)	0.050-1.0 (74%) 3.0-10 (26%)
Falling Droplet	3600	4.2 ± 0.02	22 ± 0.3	0.20-1.0 (23%) 3.5-13 (77%)	0.050-2.0 (65%) 4.0-11 (35%)
SFL	--	34 ± 2	124 ± 5	0.050-1.0 (48%) 4.0-12 (52%)	0.050-1.0 (80%) 3.0-11 (20%)

Lysoyzme feed concentration was 50 mg/mL for all sprays.
[a]Particle size distribution of powders measured with a Malvern Mastersizer after sonication.

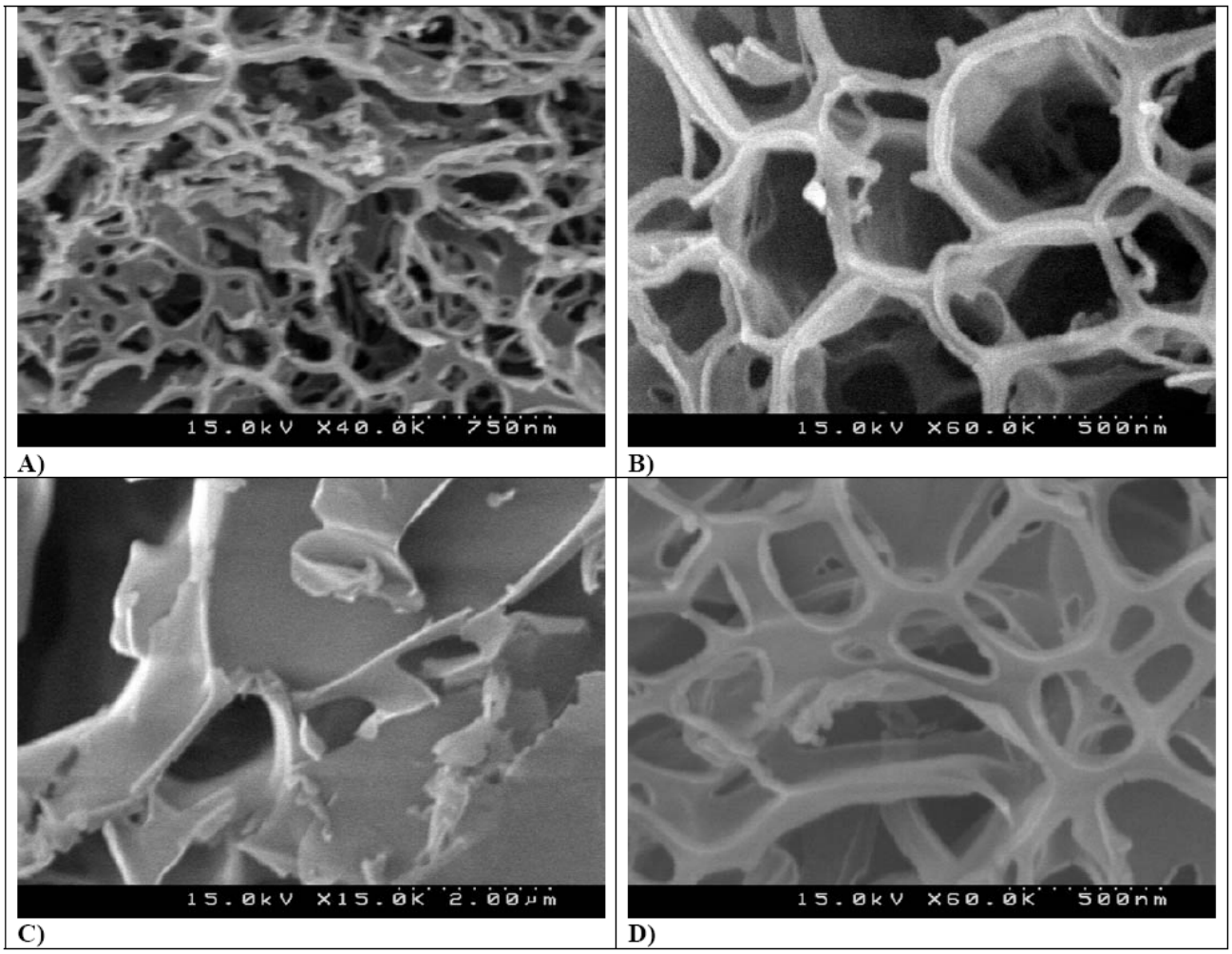

Figure 2.6: SFD sprays of 50 mg/mL lysozyme formulations for 10 μm diameter droplets processed by SFD-LN2-10 (A), SFD-*i*-C5-10 (B), and for 130 μm diameter droplets processed by SFD-LN2-130 (C), SFD-*i*-C5-130 (D).

shown in Fig. 2.3, the d(v,50) for the SFD submicron peak was 0.3 mm.

SEM micrographs of SFD powder formed from 10 μm aqueous droplets frozen over *i*-C5 and LN2 had similar morphologies (Fig. 2.6A and B) with 100 nm diameter necks between the aggregated primary particles. These morphologies resemble the 50 mg/mL SFL-*i*-C5 (Fig. 2.5D) lysozyme spray. For 50 mg/mL solutions, the SFL-LN2 particles (Fig. 2.5C) are 10 times larger compared to the particles prepared by SFD (Fig. 2.6A and B) or SFL with *i*-C5 (Fig. 2.5D). The SFD-LN2-130 (Fig. 2.6C) spray formed large sheets with 1 μm sized morphological features similar to the SFL-LN2 spray in Fig. 2.5C. The SFD-*i*-C5-130 spray had morphologies more similar to the 10 μm droplet SFD sprays with 200 nm necks between aggregated primary particles.

Additional experiments were performed with lysozyme concentrations held at 50 mg/mL, while trehalose was added to form the appropriate formulation ratios shown in Table 2.4. The SFD sprays were conducted at an air flow rate of 250 mL/s to form 10 μm droplets (Table 2.1, Fig. 2.2). For each lysozyme:trehalose formulation in Table 2.4, powder SSAs were large, above 100 m^2/g despite the high feed concentration of over 50 mg/mL. The SSA decreased modestly with increasing trehalose content. The SSAs were independent of cryogen type. The lysozyme:trehalose SSAs were compared to the rhDNase:trehalose powders presented in Maa et als. (3, 4) where the same two-fluid nozzle and protein:sugar ratios were used. For high protein:trehalose ratios, the SSAs for the lysozyme:trehalose and rhDNase:trehalose formulations were both above 100 m^2/g, but the SSAs decreased well below 100 m^2/g with increasing sugar content for the rhDNase:trehalose formulations. The discrepancy may be attributed to the difference in lyophilization protocols. Maa et al. performed the primary drying step at a shelf temperature of -25ºC (4) which is slightly above the measured T_g' of trehalose at -31ºC (31). Meltback of trehalose during drying may have caused a significant decrease in

Table 2.4: Specific surface area measurements of protein and sugar powders processed by SFD for 10 μm. diameter droplets over *i*-C5 and LN2

Loading Ratio of Protein:Trehalose in spray formulation	SSA (m^2/g)		
	Lysozyme-*i*-C5	**Lysozyme-LN2**	**rhDNase-LN2[a]**
80:20	162 ± 4	147 ± 4	111
60:40	134 ± 3	131 ± 3	71
40:60	120 ± 2	113 ± 2	5

Lysozyme feed concentration was 50 mg/mL for all formulations
[a] Values from Maa et al. for the protein rhDNase (3).

powder SSA with an increase in trehalose content. In our study, the shelf temperature during primary drying was -40ºC and was sufficiently cold to prevent meltback of trehalose during drying, to preserve a high surface area.

2.3.3 Falling droplet

The SSA for falling droplet-*i*-C5 was approximately 5 times greater than for falling droplet-LN2 (Table 2.3). During the cooling process for falling droplet-LN2 the spherical liquid droplet impacted the LN2 and then floated on the LN2 surface due to surface tension. After approximately 30 seconds the boiling around the frozen droplet ceased as the droplet was fully solidified, and the droplet sank to the bottom of the beaker. During cooling in the LN2 two droplets occasionally coalesced into a larger droplet. Therefore, ice formation may not be completed for at least 30 seconds after the liquid droplet impacts the LN2 surface.

For the falling droplet-*i*-C5 process the drop impacted the *i*-C5 surface and then immediately sank without boiling. Impaction with *i*-C5 caused the 3.6 mm diameter droplet to deform into a 4-5 mm diameter dish shape (Fig. 2.7). The greater deformation of the droplet is consistent with the much smaller interfacial tension between water and *i*-C5 versus water and LN2. The resulting volume percentage of submicron particles formed by falling droplet-*i*-C5 was much greater at 80% than for falling droplet-LN2 at 48%, and approached values observed for the spray freezing processes, despite lower SSAs.

2.4 DISCUSSION

2.4.1 Jet breakup

The breakup of liquid jets has been studied for jets sprayed into a gaseous atmosphere (32, 33), into liquids (34), and into supercritical fluids (27, 35-38). For liquid

jets sprayed into a gas at atmospheric pressure, Rayleigh and atomization jet breakup boundaries have been characterized using the Ohnesorge number Oh (viscous to surface tension forces) $= \mu_j / (\rho_j D_o \sigma)^{1/2}$, and $\mathrm{Re}_j = \rho_j U D_o / \mu_j$, where the subscript j stands for liquid jet and μ, ρ, D_o, and σ are the viscosity, density, jet diameter, and interfacial tension, respectively (32, 33). For jets sprayed into a quiescent gas or a liquid such as in SFL, U is the jet velocity whereas for the SFD sprays with a two-fluid nozzle U is the relative velocity of the air to the liquid jet (32). As either Re and/or Oh increases, the liquid jet breakup mechanism crosses the boundary from the Rayleigh regime to the atomization regime (33, 39). In the Rayleigh breakup regime the droplet sizes are slightly larger than the liquid jet diameter and jet breakup occurs far downstream from exiting the nozzle. In the atomization regime, droplet diameters are an order of magnitude smaller than the jet diameter and jet breakup occurs immediately upon exiting the nozzle (33).

For sprays into gases at low pressures, typically the shear stress at the fluid interface is neglected (36). Experimentally, it has been shown for liquid jet sprays into dense gaseous atmospheres (38) and into liquids (34), the much larger ambient values of μ_a and ρ_a facilitate jet breakup at lower U. The above correlation for sprays into gases is no longer valid (38, 39). The Weber number We (inertial to interfacial forces) $= \rho_a U^2 D_o / \sigma$ has been used for liquid jets sprayed into gases of varying density (32) and into supercritical fluids (27, 35) to correlate jet breakup length. To account for the effects of ρ_a and μ_a, Czerwonatis et al. have modified the Oh number to form a new dimensionless number, Z^{**}, which is defined as (38):

$$Z^{**} = Oh \cdot \sqrt{We} \cdot \sqrt{\frac{\mu_a}{\mu_j}} = \frac{\mu_j \cdot U}{\sigma} \cdot \sqrt{\frac{\rho_a}{\rho_j}} \cdot \sqrt{\frac{\mu_a}{\mu_j}} \qquad (1)$$

On the basis of experiments with liquid jets in pressurized nitrogen and carbon dioxide,

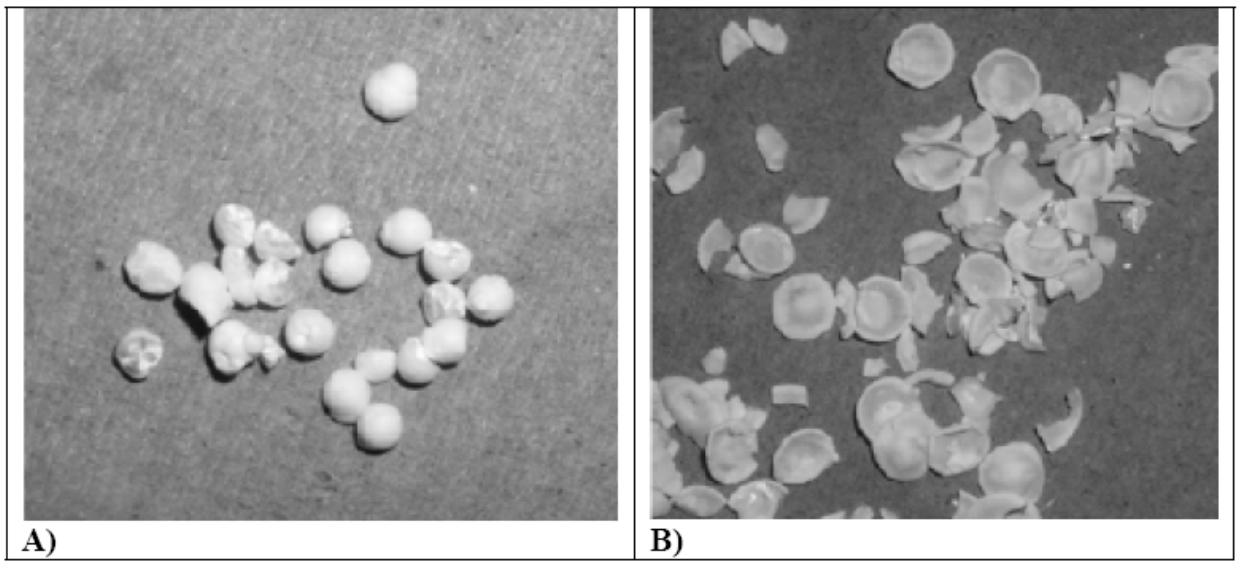

Figure 2.7: Droplets frozen by the falling droplet process into LN2 (A) and i-C5 (B). Feed formulation was 50 mg/mL lysozyme.

Rayleigh and atomization boundaries were determined and correlated in terms of Z^{**} versus Re (Fig. 2.8) (38).

In Fig. 2.8 it is shown that each SFD spray condition with the two-fluid nozzle was in the atomization regime. The 10, 40, and 130 μm droplets are all much smaller than the original 0.7 mm diameter nozzle for the liquid jet, which is consistent with atomization, rather than Rayleigh breakup. As shown in Fig. 2.8, the SFD sprays approach the atomization-transition boundary as the Re number decreases with a decrease in U. The Re values, based on the jet properties, were identical for the SFL sprays regardless of the cryogen since the liquid flow rate and nozzle diameter were fixed (Table 2.5). The SFL-*i*-C5 spray was in the atomization region in Fig. 2.8, consistent with the rapid jet break up in Fig. 2.4.

The SFL-LN2 spray formed a liquid jet ~10 cm long within an inverted gaseous cone of evaporating nitrogen as shown in Fig. 2.4. Therefore, two limits were considered for nitrogen at -196ºC, either gaseous or liquid conditions. The Z^{**} number calculated for gaseous properties (SFL-GN2) was in the Rayleigh regime. It was 2 orders of magnitude lower than the Z^{**} numbers for liquid properties (SFL-LN2), which were in the atomization regime. The spray patterns in Fig. 2.4 suggested that the jet did not fan out within the gaseous N_2 cone, as would have been the case for spraying into a viscous liquid. Thus, the determination of Z^{**} with gaseous properties is more indicative of the behavior in Fig. 2.4 than Z^{**} calculated with liquid properties. The low viscosity of the nitrogen within the cone produced by excessive boiling (Leidenfrost effect) caused the SFL spray to behave like an SFL-GN2 spray.

It is possible that the turbulent cone consisted of gaseous voids mixed with pockets of LN2 droplets. In this case, the properties of the continuous N_2 phase would correspond to those of a mixture of liquid and gas. The very low interfacial tension of

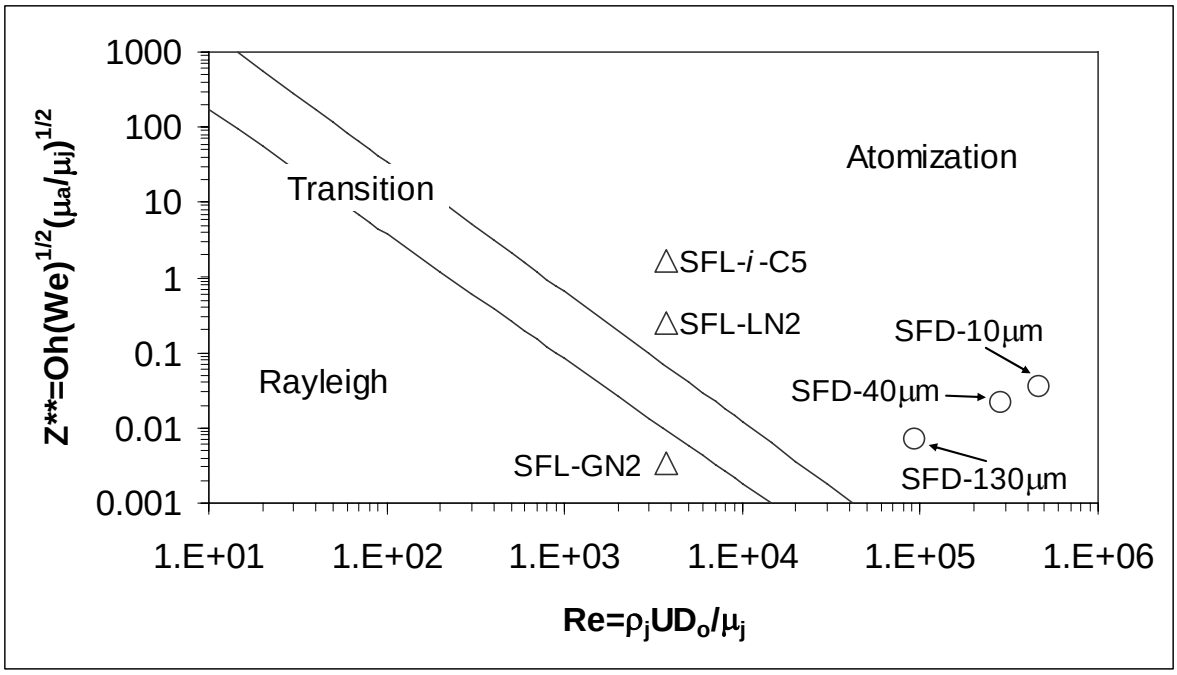

Figure 2.8: Jet breakup regimes correlated with Z** and Re for SFL sprays into *i*-C5, LN2, and GN2 and SFD sprays for 10, 40, and 130 μm diameter droplets.

Table 2.5: Calculation of Reynolds (Re), Weber (We) and Z** numbers for SFL and SFD sprays

Nozzle	**Ambient Fluid/ Temp. (°C)**	**Air Flow Rate (mL/s)**	**U (m/s)**	**σ (mJ/m^2)**	**ρ_a (g/cm^3)**	**We**	**Re**	**Z****
SFD	Air (25ºC)	250	611	74	0.0011	2.8×10^3	4.7×10^5	3.6×10^{-2}
SFD	Air (25ºC)	150	366	74	0.0011	1.0×10^3	2.8×10^5	2.1×10^{-2}
SFD	Air (25ºC)	50	122	74	0.0011	1.1×10^2	9.4×10^4	7.1×10^{-3}
SFL	*i*-C5 (-155ºC)		53	50	0.77	2.8×10^3	3.7×10^3	1.7
SFL	LN2 (-196ºC)		53	74	0.81	2.0×10^3	3.7×10^3	0.25
SFL	GN2 (-196ºC)		53	74	0.0044	11	3.7×10^3	3.4×10^{-3}

The property value μ_j=0.91 (mPa·s) was used for water at 25°C to calculate Re and Z**.

LN2 and turbulence of the boiling N_2 would facilitate mixing of the liquid and gaseous domains.

2.4.2 Cooling rate calculation

For SFD and SFL a forced convective heat transfer coefficient (h) was calculated with spherical droplets moving through a cryogenic medium at constant velocity. Droplet sizes were measured for SFD whereas the droplet sizes for SFL were inferred as explained below. The correlation for h is given below and is valid for gaseous or liquid flow past spheres (40, 41):

$$\frac{hD_d}{k_a} = 2 + (0.4\,\mathrm{Re}_a^{0.5} + 0.06\,\mathrm{Re}_a^{0.67})\,\mathrm{Pr}^{0.4}\left(\frac{\mu_a}{\mu_s}\right)^{0.25} \qquad (2)$$

where D_d, k_a, Pr, and μ_s are the droplet diameter, ambient thermal conductivity, Prandtl number using ambient fluid properties, and ambient viscosity corresponding to the temperature of the droplet surface, respectively. Re_a is calculated with ambient fluid properties and the velocity of the liquid droplets, U. U is the velocity of the liquid jet exiting the nozzle for SFL. For SFD, it was assumed that the atomized liquid droplets moved at the same velocity as the air. The velocity of the air stream 10 cm away from the nozzle was calculated with the continuity equation for a cone of expanding air where UA is constant.

The h was used to determine if the droplets were cooled in a convective-limited or conductive-limited regime. In the convective-limited regime the temperature gradients throughout the liquid droplet are negligible as it cools, whereas in the conductive-limited regime the temperature gradients are significant (41, 42). The cooling regime can be determined by calculating the Biot number for spheres, $Bi = hD_d / 6k_d$, which is a ratio

of convective to conductive heat transfer where k_d is the droplet thermal conductivity (41, 42). In the regime where Bi<1 the cooling of the droplet is convection-limited although some sources place the boundary at Bi<0.1 (40-43). In this work both the convection-limited and conduction-limited calculations are presented when the calculated Bi number is in the range 0.1< Bi <1 (Table 2.6). For the convection-limited regime, with no resistance in the droplet phase, the average cooling rate for the droplet at an initial temperature T_i is estimated as (42, 43):

$$\frac{dT}{dt} \approx \frac{A}{V} h(T_i - T_a) \frac{1}{\rho \cdot C_p} \qquad (3)$$

where T is the droplet temperature at time t and ρ, C_p, A, and V are the droplet density, heat capacity, surface area, and volume, respectively. In the regime where $Bi \geq 1$ the heat transfer mode is conduction-limited. For the cooling rate in the conduction-limited regime (42, 43), with no resistance in the cryogen phase,

$$\frac{dT}{dt} \approx \left(\frac{A}{V}\right)^2 k(T_i - T_a) \frac{1}{\rho \cdot C_p} \qquad (4)$$

The cooling rate calculations (Table 2.6) neglect the latent heat of fusion of water and assume complete vitrification of the aqueous droplets, as has been assumed previously (42, 44). Experimental studies of samples plunged into cryogens have shown that cooling rates of samples that undergo a phase change are not significantly different from those that do not (42, 45). In this work, cooling times in the convective-limited and conductive-limited regime were calculated by integrating equations 3 and 4 over the temperature range from 298 to 173 K (Table 2.6). The lower temperature limit of 173 K

Table 2.6: Calculated Reynolds number (Re), Prandtl number (Pr), average convective heat transfer coefficient (h) and Biot number (Bi) for each spray process

Nozzle	Cryogen	Droplet Diameter (μm)	Re	Pr	$h/10^4$ (W/m^2-K)	Bi	Cooling Time (ms)	Cooling Rate/10^4 (K/s)
SFD	*i*-C5	10	1.7	35	12	0.37[a]	0.014-0.038	330-890
SFD	*i*-C5	40	4.2	35	4.4	0.53[a]	0.22-0.43	29-56
SFD	*i*-C5	130	4.5	35	1.4	0.54[a]	2.4-4.4	2.9-5.3
SFD	GN2	10	6.6	0.75	0.21	0.0062[b]	1.9	6.6
SFD	GN2	40	16	0.75	0.061	0.0073[b]	26	0.49
SFD	GN2	130	17	0.75	0.019	0.0074[b]	270	0.047
SFD	LN2	10	41	2.4	12	0.36[a]	0.012-0.033	380-1100
SFD	LN2	40	97	2.4	4.4	0.53[a]	0.19-0.36	35-66
SFD	LN2	130	110	2.4	1.4	0.54[a]	2.0-3.6	3.4-6.3
SFL	*i*-C5	10	120	35	87	2.6[c]	0.014	890
SFL	GN2	100	4400	0.75	0.23	0.067[b]	17	0.72
SFL	LN2	100	27000	2.4	35	10[c]	1.2	11

[a]Cooling times and cooling rates are represented as a range where the lower limit is the convection-limited regime and the upper limit is the conduction-limited regime.
[b]For Bi numbers <0.1 only convection-limited cooling was calculated.
[c]For Bi numbers >1 only conduction-limited cooling was calculated.

was chosen for the cooling calculations (Table 2.6) since the major amount of ice crystallization occurs in the temperature range of 273 to 173 K for slow cooling (24). Thus, it was of interest to know the cooling times for this dangerous temperature range where it is desirable to avoid ice crystallization.

As shown on Table 2.6 for 10 and 40 μm diameter droplets, the calculated cooling times for SFD-*i*-C5 and SFD-LN2 sprays were similar, consistent with the similar SSAs and particle morphologies (Tables 2.2 and 2.3 and Fig. 2.6). The Leidenfrost effect may be expected to be relatively small for the 10 μm diameter atomized droplets in SFD-LN2 because of their small diameter. The SFD droplets that were 130 μm in size produced smaller morphological features and higher SSAs in *i*-C5 verses LN2 indicating faster cooling (Fig. 2.6C and D) despite similar calculated cooling times. An explanation for this discrepancy is that the droplets were large enough for some evaporation of nitrogen to slow the cooling rate in LN2 versus *i*-C5 leading to a lower powder SSA. If the solutions were sprayed into gaseous N_2 at -196°C, the calculated cooling times would be at least 2 orders of magnitude slower (Table 2.6) versus liquid N_2.

To calculate SFL cooling times, the droplet sizes in each cryogen were estimated from the images shown in Fig. 2.4. For SFL-*i*-C5 the cooling time was calculated for 10 μm spheres due to the intense breakup of the liquid jet from the 63 μm nozzle whereas the SFL-LN2 and SFL-GN2 cooling times were calculated for 100 μm spheres since liquid jet breakup was minimal. Calculated cooling rates for SFL-*i*-C5 sprays were the same order of magnitude as for the SFD-LN2-10 and SFD-*i*-C5-10 sprays. This result is consistent with the similar 100 nm morphological features in Fig. 2.5D and Fig. 2.6A and B. Given these similar morphologies and cooling times, it is likely that these sprays are frozen primarily by liquid-liquid contact with a minimal, if any, Leidenfrost effect for N_2.

The calculated SFL-LN2 cooling time was an order of magnitude slower than for SFL-*i*-C5, as a result of the larger droplet size. For SFL-GN2, it was 3 orders of magnitude slower. The resulting SFL morphology (Fig. 2.5C) and SSA (Table 2.2) were similar to those for the SFD-LN2-130 morphology (Fig. 2.6C and Table 2.3). Thus, it is likely that some of the nitrogen also evaporated about the 130 μm drops in SFD. As droplet sizes increased to 3.6 mm in the falling droplet experiments the same difference in powder SSA resulted from liquid-gas contact in falling droplet-LN2 versus liquid-liquid contact for falling droplet-*i*-C5.

2.4.3 Mechanism of vitrification of aqueous solutions

The morphology of an aqueous solution in the frozen state depends on the cooling rate (45). Fig. 2.9 shows a phase diagram for sucrose, a non-crystallizing solute in water (45-48). Protein and sugar solutions subjected to slow cooling rates on a temperature controlled shelf in a tray lyophilizer have a low degree of supercooling beneath the equilibrium freezing curve (48). The water in the supercooled solution nucleates and forms crystalline ice (45). The latent heat of crystallization causes the temperature of the supercooled solution to rise to the equilibrium freezing curve (45, 48). Globular proteins and most sugars remain in the unfrozen solution known as the freeze concentrate and are usually kinetically hindered from crystallizing (45). As liquid water moves from the unfrozen phase to the ice phase during freezing, the composition of the freeze concentrate follows the equilibrium freezing curve toward T_g', the point where the solution is maximally freeze concentrated (Fig. 2.9) (48). At this point the unfrozen domains become sufficiently viscous that they vitrify (48).

Ultra rapid cooling rates of aqueous solutions, for example in jet sprays, do not follow the equilibrium path as described above (45, 47). Rapid cooling minimizes the time for the formation and growth of ice crystals as the aqueous solution passes through

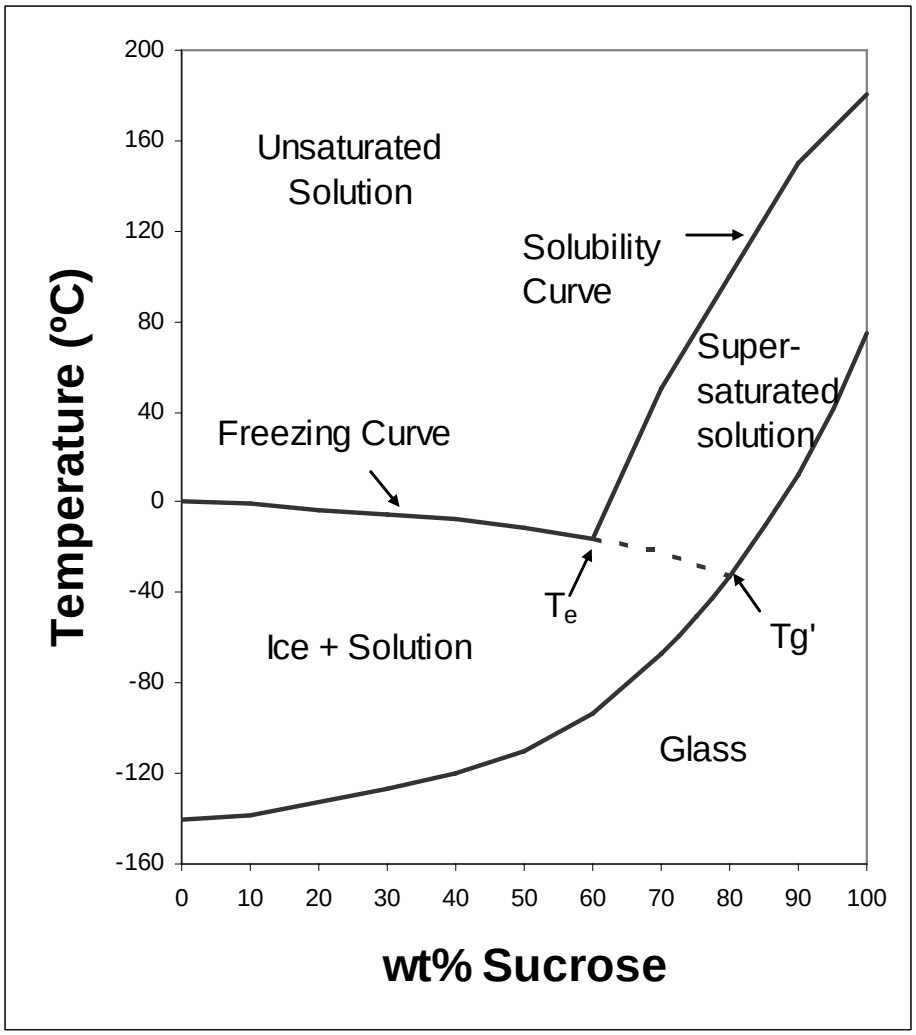

Figure 2.9: Solid-liquid diagram for the sucrose-water system. Adapted from Fig. 7 of Nail et al. (48).

the critical temperature zone (9, 19, 49), which is the region between the equilibrium freezing curve and the T_g curve where liquid water can nucleate to form crystalline ice. The temperature may pass below the T_g curve fast enough to minimize, or even fully prevent, nucleation of ice crystals (45). Fletcher calculated that to vitrify a 1 μm diameter water droplet and prevent ice crystal formation requires a cooling rate of 10^{10} K/s (50). The presence of sugar and/or water miscible polymers in solution can help facilitate vitrification and slow crystal growth which could decrease the cooling rate for vitrification (45). Liquid water jets with diameters sufficiently small (~10 um) sprayed at velocities of 250 m/s led mostly to vitrified water (51). The cryogens were propane and ethane, to avoid the Leidenfrost effect, and the frozen water was analyzed by X-ray diffraction (XRD) (45, 51).

When a supercooled aqueous solution passes through the critical temperature zone, the solute may become supersaturated from a decrease in solubility before the water vitrifies. As shown in Fig. 2.9, the solubility curve decreases with decreasing temperature and ends at the eutectic temperature, T_e. For temperatures well below T_e, it is not possible to measure a true equilibrium sucrose solubility in liquid water. However, for rapid non-equilibrium supercooling of the water without time to freeze, the solubility of sucrose in hypothetical supercooled liquid water would be expected to decrease with temperature. For example, the ideal solubility of a solid in a liquid decreases as the difference between the melting point of the solid and the temperature increases. Furthermore, the decrease in solubility with temperature is evident in Fig. 2.9 above T_e. The decrease in solubility with temperature may even lead to supersaturation and nucleation and growth of solute from the unfrozen solution even before a significant amount of vitrification of water occurs. For a liquid-liquid phase separation two glasses with two separate T_g values can be formed upon vitrification (52). For PEG/dextran

formulations used to stabilize recombinant hemoglobin, increasing the cooling rate of the formulations lead to increased stability (22). The increased hemoglobin stability has been attributed to prevention of phase separation of the polymer, dextran and PEG, from the protein due to increased cooling rates (22).

In the SFD and SFL processes, the high degree of supercooling rapidly leads to temperatures far below the T_g curve in Fig. 2.9. Vitrified water domains form as relatively few water molecules have enough time to reach the crystalline state. The detailed relaxation dynamics for rapid vitrificaton of sucrose and lysozyme solutions are the subject of current study (53). Therefore, in this study, the SEMs of the lysozyme morphology are utilized to shed insight into the vitrification mechanism during the spray freezing processes. Although changes in the morphology of the lysoyzme are possible during lyophilization, the temperature was maintained below T_g' during lyophilization to minimize such changes.

Based on the SEM results and above discussion of freezing processes, a proposed schematic of the role of solute concentration and cooling rate is presented in Fig. 2.10. For all of the cryogens and spray freezing processes in this study, dilute 5 mg/mL lysozyme solutions led to particles on the order of 50 nm in diameter and surface areas greater than 100 m^2/g (Table 2.2). As shown in Fig. 2.10A, for dilute aqueous solutions subjected to a high degree of supercooling, the high nucleation rates lead to small glassy domains of water and small solute domains in the unfrozen water between the finely divided glassy water domains. Between the vitrified water domains, the thin films of unfrozen water, containing solute particles, limit the collisions and hence aggregation/coalescence of the solute particles. The rapid heat transfer vitrifies all of the water quickly, limiting the time for coalescence of solute particles.

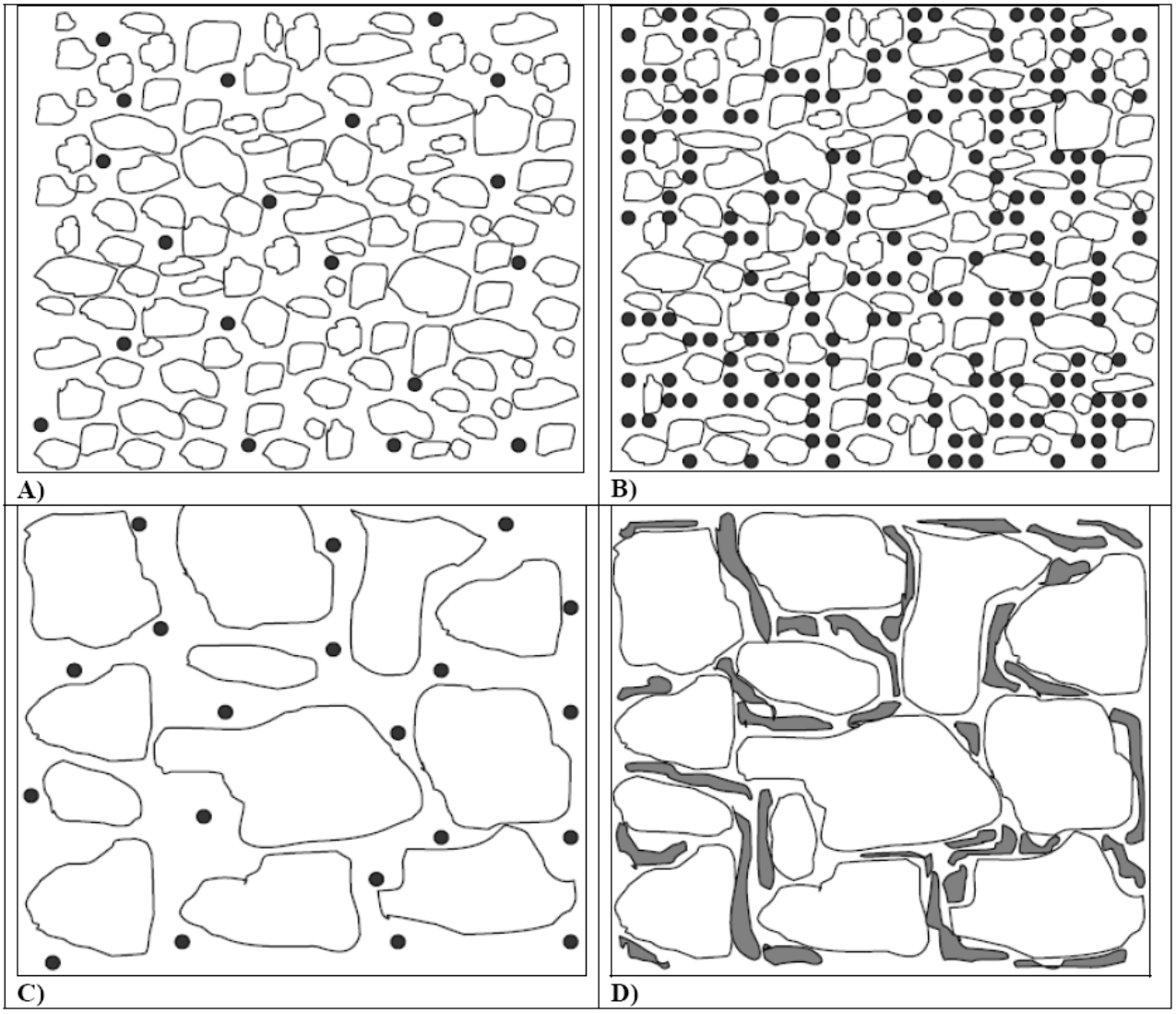

Figure 2.10: Frozen morphologies of dilute solution with high supercooling (A), concentrated solution with high supercooling (B), dilute solution with low supercooling (C), and concentrated solution with low supercooling (D). Amorphous ice particles are represented as white domains and solute precipitate as solid dots or gray regions.

For more concentrated solutions, in this case 50 mg/mL, the lysozyme particles formed a web with 100 nm connecting necks as shown in Fig. 2.5D, 2.6A and B. In Fig. 2.5D which was the SFL-*i*-C5 spray for a 50 mg/mL lysozyme formulation, protein threads are formed as opposed to the more spherical protein domains as seen in Fig. 2.5B. Here the larger solute concentration leads to a greater volume fraction of vitrified solute domains in the unfrozen water channels, and thus a greater collision frequency and increased aggregation/coalescence. The higher concentration also leads to more rapid transport of solute molecules to these growing domains. The result is larger and more aggregated particles after lyophilization as shown in Fig. 2.10B.

For dilute solutions, the morphologies were similar for the slower SFL-LN2 process and the other three more rapid spray processes. The final particle size is on the order of 100 nm. Here the low concentration of the solute leads to a small number of growing solute particles, a low collision rate, and consequently a low aggregation rate, as shown schematically in Fig. 2.10C. The aggregation rates are slow despite the thick channels of unfrozen water between particles. The entire matrix becomes vitrified before significant growth of the small number of particles takes place.

For concentrated solutions, for example 50 mg/mL, subjected to slower rates of cooling in the SFL-LN2 process, as a consequence of the Leidenfrost effect, large plates of particles with significantly smaller surface areas were observed in Fig. 2.10D, relative to the other conditions in Fig. 2.10B. For a slower cooling rate, the lower degree of supercooling decreases the nucleation rate. A longer time is available for the smaller number of nucleated vitrified water domains and precipitated solute domains to grow. As shown schematically in Fig. 2.10D, the solute particles that nucleate and grow in the relatively large channels between vitrified water particles have significant time to coalesce and form thin plates before vitrification is complete.

2.5 CONCLUSIONS

The SFL and SFD spray processes were utilized to produce high surface area lysozyme particles over a wide range of feed concentrations for two cryogens, LN2 and isopentane (*i*-C5). For dilute aqueous solutions up to 5 mg/mL, the focus of most previous studies, the dried powder SSAs were > 100 m^2/g in SFL for each cryogen indicating cooling was rapid enough to prevent substantial particle growth. Even for viscous feeds with concentrations as high as 100 mg/mL, powders with SSAs greater than 100 m^2/g were produced in the SFD and SFL-*i*-C5 processes indicating sufficient atomization for rapid cooling and quenching relative to particle growth. For SFD with either cryogen, powder SSAs and SEMs were shown to be negligibly impacted by the droplet diameter for droplets less than 100 μm suggesting the Leidenfrost effect was unimportant. For SFL, LN2 was found to form a turbulent gaseous N_2 cone around the sprayed jet. The low viscosity gas layer reduced the degree of jet atomization for N_2, but not for the non-evaporating cryogen *i*-C5. The calculated cooling rate for SFL in LN2 was 3 orders of magnitude lower than in *i*-C5 or SFD with either cryogen. For 50 mg/mL concentrated feed solutions, SSAs were on the order of 34 m^2/g for SFL into LN2 and the features in the SEMs were coarser, consistent with the slower cooling rates. The ability to adjust the cooling rate to vary the final particle surface area will be beneficial for designing particles for controlled release applications. The high protein feed concentrations offer the potential of high production rates, as well as smaller volumes of solvent that must be sublimated in lyophilization.

2.6 REFERENCES

1. Y.-F. Maa and H. R. Costantino. Spray freeze-drying of biopharmaceuticals: applications and stability considerations. In H. R. Costantino and M. J. Pikal (eds.), *Biotechnology: Pharmaceutical Aspects. 2. Lyophilization of Biopharmaceuticals*, American Association of Pharmaceutical Scientists, Arlington, 2004, pp. 519-561.

2. X. C. Nguyen, J. D. Herberger, and P. A. Burke. Protein powders for encapsulation: a comparison of spray-freeze drying and spray drying of darbepoetin alfa. *Pharm. Res.* **21:**507-514 (2004).

3. Y.-F. Maa and S. J. Prestrelski. Biopharmaceutical powders: particle formation and formulation considerations. *Curr. Pharm. Biotechnol.* **1:**283-302 (2000).

4. Y.-F. Maa, P.-A. Nguyen, T. Sweeney, S. J. Shire, and C. C. Hsu. Protein inhalation powders: spray drying vs spray freeze drying. *Pharm. Res.* **16:**249-254 (1999).

5. Y.-F. Maa and P.-A. Nguyen. Method of spray freeze drying proteins for pharmaceutical administration. United States Patent. 6,284,282 (2001).

6. H. R. Costantino, L. Firouzabadian, K. Hogeland, C. C. Wu, C. Beganski, K. G. Carrasquillo, M. Cordova, K. Griebenow, S. E. Zale, and M. A. Tracy. Protein spray-freeze drying. Effect of atomization conditions on particle size and stability. *Pharm. Res.* **17:**1374-1383 (2000).

7. H. R. Costantino, L. Firouzabadian, C. C. Wu, K. G. Carrasquillo, K. Griebenow, S. E. Zale, and M. A. Tracy. Protein spray freeze drying. 2. Effect of formulation variables on particle size and stability. *J. Pharm. Sci.* **91:**388-395 (2002).

8. S. D. Webb, S. L. Golledge, J. L. Cleland, J. F. Carpenter, and T. W. Randolph. Surface adsorption of recombinant human interferon-γ in lyophilized and spray-lyophilized formulations. *J. Pharm. Sci.* **91:**1474-1487 (2002).

9. Z. H. Chang and J. G. Baust. Ultra-rapid freezing by spraying/plunging: pre-cooling in the cold gaseous layer. *J. Microsc.* **161:**435-444 (1991).

10. W. Wang. Lyophilization and development of solid protein pharmaceuticals. *Int. J. Pharm.* **203:**1-60 (2000).

11. W. T. Leach, D. T. Simpson, T. N. Val, E. C. Anuta, Z. Yu, R. O. Williams III, and K. P. Johnston. Uniform encapsulation of stable protein nanoparticles produced by spray freezing for the reduction of burst release. *J. Pharm. Sci.* **94:**56-69 (2005).

12. W. T. Leach, D. T. Simpson, T. N. Val, Z. Yu, K. T. Lim, E. J. Park, R. O. Williams III, and K. P. Johnston. Encapsulation of protein nanoparticles into uniform-sized microspheres formed in a spinning oil film. *AAPS Pharm. Sci. Tech.* **6:**605-617 (2005).

13. B. S. Chang, B. S. Kendrick, and J. F. Carpenter. Surface-induced denaturation of proteins during freezing and its inhibition by surfactants. *J. Pharm. Sci.* **85:**1325-1330 (1996).

14. R. O. Williams III, K. P. Johnston, T. J. Young, T. L. Rogers, M. K. Barron, Z. Yu, and J. Hu. Process for production of nanoparticles and microparticles by spray freezing into liquid. 2,004,022,861 (2004).

15. J. Hu, T. L. Rogers, J. Brown, T. Young, K. P. Johnston, and R. O. Williams III. Improvement of dissolution rates of poorly water soluble APIs using novel spray freezing into liquid technology. *Pharm. Res.* **19:**1278-1284 (2002).

16. J. Hu, K. P. Johnston, and R. O. Williams III. Rapid dissolving high potency danazol powders produced by spray freezing into liquid process. *Int. J. Pharm.* **271:**145-154 (2004).

17. T. L. Rogers, J. Hu, Z. Yu, K. P. Johnston, and R. O. Williams III. A novel particle engineering technology: spray-freezing into liquid. *Int. J. Pharm.* **242:**93-100 (2002).

18. T. L. Rogers, A. C. Nelsen, J. Hu, J. N. Brown, M. Sarkari, T. J. Young, K. P. Johnston, and R. O. Williams III. A novel particle engineering technology to enhance dissolution of poorly water soluble drugs: spray-freezing into liquid. *Eur. J. Pharm. Biopharm.* **54:**271-280 (2002).

19. Z. Yu, T. L. Rogers, J. Hu, K. P. Johnston, and R. O. Williams III. Preparation and characterization of microparticles containing peptide produced by a novel process: spray freezing into liquid. *Eur. J. Pharm. Biopharm.* **54:**221-228 (2002).

20. Z. Yu, A. S. Garcia, K. P. Johnston, and R. O. Williams III. Spray freezing into liquid nitrogen for highly stable protein nanostructured microparticles. *Eur. J. Pharm. Biopharm.* **58:**529-537 (2004).

21. Z. Yu, K. P. Johnston, and R. O. Williams III. Spray freezing into liquid versus spray-freeze drying: Influence of atomization on protein aggregation and biological activity. *Eur. J. Pharm. Sci.* **27:**9-18 (2006).

22. M. C. Heller, J. F. Carpenter, and T. W. Randolph. Protein formulation and lyophilization cycle design: prevention of damage due to freeze-concentration induced phase separation. *Biotechnol. Bioeng.* **63:**166-174 (1999).

23. H. Sitte, L. Edelmann, and K. Neumann. Cryofixation without pretreatment at ambient pressure. In R. A. Steinbrecht and K. Zierold (eds.), *Cryotechniques in Biological Electron Microscopy*, Springer-Verlag, Berlin, 1987, pp. 87-113.

24. M. J. Costello and J. M. Corless. The direct measurement of temperature changes within freeze-fracture specimens during rapid quenching in liquid coolants. *J. Microsc.* **112:**17-37 (1978).

25. H. Gieseler, PhD Thesis, University of Erlangen-Nuremburg, 2004.

26. M. K. Barron, T. J. Young, K. P. Johnston, and R. O. Williams III. Investigation of processing parameters of spray freezing into liquid to prepare polyethylene glycol polymeric particles for drug delivery. *AAPS Pharm. Sci. Tech.* **4:**1-13 (2003).

27. S. Mawson, S. Kanakia, and K. P. Johnston. Coaxial nozzle for control of particle morphology in precipitation with a compressed fluid antisolvent. *J. Appl. Polym. Sci.* **64:**2105-2118 (1997).

28. J. D. Engstrom, D. T. Simpson, C. Cloonan, E. Lai, R. O. Williams III, G. B. Kitto, and P. Johnston Keith. Stable high surface area lactate dehydrogenase particles produced by spray freezing into liquid nitrogen. *Eur. J. Pharm. Biopharm.* **65:**163-174 (2007).

29. S. Brunauer, P. H. Emmett, and E. Teller. Adsorption of gases in multimolecular layers. *J. Am. Chem. Soc.* **60:**309-319 (1938).

30. A. A. Elkordy, R. T. Forbes, and B. W. Barry. Integrity of crystalline lysozyme exceeds that of a spray-dried form. *Int. J. Pharm.* **247:**79-90 (2002).

31. Y.-H. Liao, M. B. Brown, A. Quader, and G. P. Martin. Protective Mechanism of Stabilizing Excipients Against Dehydration in the Freeze-Drying of Proteins. *Pharm. Res.* **19:**1854-1861 (2002).

32. A. H. Lefebvre. *Atomization and Sprays*, Hemisphere Publishing Corporation, New York, 1989.

33. R. D. Reitz and F. V. Bracco. Mechanisms of breakup of round liquid jets. In N. P. Cheremisinoff (ed.), *Encyclopedia of Fluid Mechanics*, Gulf Publishing Co., Book Division, Houston, 1986, pp. 233-249.

34. B. J. Meister and G. F. Scheele. Drop formation from cylindrical jets in immiscible liquid systems. *AIChE J.* **15:**700-706 (1969).

35. D. J. Dixon, K. P. Johnston, and R. A. Bodmeier. Polymeric materials formed by precipitation with a compressed fluid antisolvent. *AIChE J.* **39:**127-139 (1993).

36. C. S. Lengsfeld, J. P. Delplanque, V. H. Barocas, and T. W. Randolph. Mechanism governing microparticle morphology during precipitation by a compressed antisolvent: atomization vs. nucleation and growth. *J. Phys. Chem. B* **104:**2725-2735 (2000).

37. E. Badens, O. Boutin, and G. Charbit. Laminar jet dispersion and jet atomization in pressurized carbon dioxide. *J. Supercrit. Fluids* **36:**81-90 (2005).

38. N. Czerwonatis and R. Eggers. Disintegration of liquid jets and drop drag coefficients in pressurized nitrogen and carbon dioxide. *Chem. Eng. Tech.* **24:**619-624 (2001).

39. J. Baldyga, M. Henczka, and B. Y. Shekunov. Fluid dynamics, mass transfer, and particle formation in supercritical fluids. *Drugs Pharm. Sci.* **138:**91-157 (2004).

40. F. Kreith and M. S. Bohn. *Principles of Heat Transfer*, Harper and Row, Publishers, Inc., New York, 1986.

41. F. P. Incropera and D. P. DeWitt. *Fundamentals of Heat and Mass Transfer*, John Wiley and Sons, New York, 2002.

42. J. A. N. Zasadzinski. A new heat transfer model to predict cooling rates for rapid freezing fixation. *J. Microsc.* **150:**137-149 (1988).

43. S. M. Bailey and J. A. N. Zasadzinski. Validation of convection-limited cooling of samples for freeze-fracture electron microscopy. *J. Microsc.* **163:**307-320 (1991).

44. H. Y. Elder, C. C. Gray, A. G. Jardine, J. N. Chapman, and W. H. Biddlecombe. Optimum conditions for cryoquenching of small tissue blocks in liquid coolants. *J. Microsc.* **126:**45-61 (1982).

45. F. Franks. *Biophysics and Biochemistry at Low Temperatures*, Cambridge University Press, New York, 1985.

46. C. A. Angell. Liquid fragility and the glass transition in water and aqueous solutions. *Chem. Rev.* **102:**2627-2649 (2002).

47. A. P. MacKenzie. Non-equilibrium freezing behavior of aqueous systems. *Philos. Trans. R. Soc. London, B: Biol. Sci.* **278:**167-189 (1977).

48. S. L. Nail, S. Jiang, S. Chongprasert, and S. A. Knopp. Fundamentals of freeze-drying. In S. L. Nail and M. J. Akers (eds.), *Pharmaceutical Biotechnology. 14.*

Development and Manufacture of Protein Pharmaceuticals, Kluwer Academic/Plenum Publishers, New York, 2002, pp. 281-360.

49. M. C. Heller, J. F. Carpenter, and T. W. Randolph. Application of a thermodynamic model to the prediction of phase separations in freeze-concentrated formulations for protein lyophilization. *Arch. Biochem. Biophys.* **363:**191-201 (1999).

50. N. H. Fletcher. Structural aspects of the ice-water system. *Rep. Prog. Phys.* **34:**913-994 (1971).

51. E. Mayer and P. Brueggeller. Vitrification of pure liquid water by high pressure jet freezing. *Nature* **298:**715-718 (1982).

52. J. F. Carpenter, K.-i. Izutsu, and T. W. Randolph. Freezing- and drying-induced perturbations of protein structure and mechanisms of protein protection by stabilizing additives. In L. Rey and J. C. May (eds.), *Drugs and the Pharmaceutical Sciences. 137. Freeze-Drying/Lyophilization of Pharmaceutical and Biological Products*, Marcel Dekker, Inc., New York, 2004, pp. 147-186.

53. M. T. Cicerone and C. L. Soles. Fast dynamics and stabilization of proteins: Binary glasses of trehalose and glycerol. *Biophys. J.* **86:**3836-3845 (2004).

Chapter 3: Stable High Surface Area Lactate Dehydrogenase Particles Produced by Spray Freezing into Liquid Nitrogen

Enzyme activities were determined for lactate dehydrogenase (LDH) powder produced by lyophilization, and two fast freezing processes, spray freeze-drying (SFD) and spray freezing into liquid (SFL) nitrogen. The 0.25 mg/mL LDH aqueous feed solutions included either 30 or 100 mg/mL trehalose. The SFL process produced powders with very high enzyme activities upon reconstitution, similar to lyophilization. However, the specific surface area of 13 m^2/g for SFL was an order of magnitude larger than for lyophilization. In SFD activities were reduced in the spraying step by the long exposure to the gas-liquid interface for 0.1 to 1 s, versus only 2 ms in SFL. The ability to produce stable high surface area submicron particles of fragile proteins such as LDH by SFL is of practical interest in protein storage and in various applications in controlled release including encapsulation into bioerodible polymers. The SFL process has been scaled down for solution volumes <1 mL to facilitate studies of therapeutic proteins.

3.1 INTRODUCTION

Due to the limited physical and chemical stability of proteins in solution, it is often necessary to produce a solid protein formulation to achieve an acceptable shelf life (1-6). Protein particles are also of interest for encapsulation into bioerodible microspheres or other matrix geometries for subcutaneous, intramuscular, transdermal and pulmonary delivery (7-14). To achieve high protein loadings and to minimize burst release, high surface area, submicron protein particles have been encapsulated uniformly into 10 to 50 μm diameter microspheres (8, 9, 15-17). However, it is challenging to produce stable submicron protein particles when the surface area exceeds 10 m^2/g (9, 18, 19), relative to the less than 1 m^2/g for powders produced by lyophilization.

Protein particles may be precipitated from aqueous solution by a variety of processes including spray-drying (20-23), supercritical CO_2-assisted aerosolization and bubble drying (scCO_2A-BD) (24), spray freeze-drying (SFD) (5, 18-20), and spray freezing into liquids (SFL) (25-27). The spraying, freezing and drying steps in these processes must be designed to minimize stresses that cause destabilization (1, 3, 4, 6). Loss in stability may be characterized in terms of protein denaturation, aggregation, and loss of enzyme activity upon rehydration (4, 20, 28). During spraying and freezing, stresses arise from changes in solute concentration and pH in the remaining unfrozen solution, as well as exposure of protein to gas-liquid and/or ice-liquid interfaces (3, 6). During drying, dehydration stress from removal of water molecules can subsequently lead to protein unfolding (1, 6, 29). Stabilizers, such as disaccharide sugars often increase the thermodynamic stability of the native folded protein during freezing and prevent the protein from unfolding during drying through replacement of hydrogen bonds to the protein upon loss of water (1, 3, 29-31).

In SFD, an aqueous solution containing dissolved protein and stabilizers is atomized into the cold gas above a cryogenic liquid (Fig. 3.1) (18, 19, 32-34). The micron-sized droplets travel through the cryogenic gas, where they may begin to freeze (35), and then freeze completely after contact with the liquid cryogen. Decreasing the aqueous droplet diameter leads to more rapid freezing resulting in a greater specific surface area (SSA) of the final powder (3, 5, 18). As the SSA increases, the particles become more friable and may be micronized into smaller particles upon sonication (9, 18). By systematically studying the effects of the separate spraying, freezing and drying steps in SFD, it was shown that the large gas-liquid interface in the spraying step was the primary cause of protein aggregation for recombinant human interferon γ (rhIFN-γ) (19) and lysozyme (26). The protein adsorbs at this interface and subsequently unfolds and

forms aggregates (19, 36). The freezing and drying steps had a minimal effect on protein stability. For rhIFN-γ, Webb et al. (19) reported that a protein in the freeze concentrate during rapid freezing would not have sufficient time to diffuse to the ice-liquid interface and denature before being trapped in an amorphous glass (19). To minimize gas-liquid interface in the SFD process, the size of the atomized droplets may be increased, but at the expense of the SSA of the powder (5, 18). Therefore, the formation of high SSA protein powder by SFD has often resulted in an undesirable degree of denaturation and aggregation for a variety of proteins (5, 18-21).

In spray-drying, the protein is exposed to the gas-liquid interface of the atomized droplets which are typically on the order of 10 μm in diameter (20, 23). In spite of the relatively large gas-liquid interface formed upon atomization in spray-drying, Nguyen et al. showed that the protein darbepoetin alfa remained stable, whereas it aggregated in the SFD process (21). Adler and Lee produced ~9 μm diameter particles by spray-drying of a formulation of lactate dehydrogenase (LDH) with 100 mg/mL trehalose as an excipicient and showed that approximately 10% of the activity was lost (23). The addition of Tween 80 to the formulation improved the initial activity, but it was harmful to the storage stability (23). Although spray-drying can produce particles that are between 1-10 μm in diameter and relatively stable (21), the SSAs of protein powders are much lower than in SFD and SFL (21, 22).

A novel spray freezing into liquid (SFL) process has been developed to minimize exposure of protein to the gas-liquid interface and yet sustain rapid freezing rates to produce high SSA powder (25-27). As shown in Fig. 3.1, the feed nozzle is immersed under the cryogen surface to minimize the time of exposure to nitrogen gas-liquid interface (25-27). The SFL process has also been used for freezing dilute organic solutions of poorly water soluble drugs (37-40) to produce powders with high SSA and

enhanced dissolution rates. For dilute (5-10 mg/mL) aqueous peptide and protein solutions the resulting powder SSAs have been greater than 100 m^2/g (9, 25-27, 39). For lysozyme, a reduction in the time of exposure to the gas-liquid interface in the spraying step for SFL led to a smaller degree of aggregation and loss in enzyme activity relative to SFD. In addition, the subsequent freezing and drying steps for SFL and SFD were shown to produce an insignificant amount of additional protein destabilization (19, 26). Since lysozyme is a relatively stable protein, it would be interesting to compare protein stabilities for SFL and SFD for much more fragile proteins.

Lyophilization (41-43), spray-drying (23) and SFD (44) of the fragile protein LDH have been studied extensively. LDH consists of 4 subunits that form a tetramer in solution with an approximate molecular weight of 144 kDa and a hydrodynamic radius of approximately 4 nm, as measured by dynamic light scattering (45, 46). It has already been shown to be destabilized by exposure to the gas-liquid interface in both spray-drying and SFD studies (23, 44). In order to achieve high LDH activities, it was necessary to use a high trehalose concentration (>100mg/mL) and a surfactant such as Tween 80 to minimize dissociation of tetrameric LDH at the gas-liquid interface (23, 44).

Proteins such as LDH are much more stable in aqueous buffer solutions in the presence of high sugar concentrations. A recent companion study has shown differences in the morphologies of lysozyme powders produced by SFL and SFD with liquid nitrogen (LN2) for concentrated (>50mg/mL) feed solutions (47). It was shown with flow visualization, calculated heat transfer rates, and SSAs of lysozyme powder that the cooling rate in SFL (7200 K/s) was approximately 2-3 orders of magnitude slower than in SFD (47). The slower cooling rate in SFL was a result of LN2 boiling around the liquid jet forming an insulating gas layer, known as the Leidenfrost effect. For concentrated feed solutions, the slower cooling rate of the SFL process led to surface areas on the

order of 30 m^2/g, compared to 30-120 m^2/g for SFD (47). However, the powder SSA was still more than an order of magnitude higher than in conventional lyophilization. Therefore, it can be expected that LDH formulations processed by SFL will also have high powder SSAs.

The primary objectives of this study were: (1) to produce LDH powders with surface areas greater than 10 m^2/g and high enzyme activities approaching those for low surface area particles (<1 m^2/g) produced in lyophilization, (2) to compare enzyme activities in SFL relative to SFD, particularly in view of differences in the time of exposure to the gas-liquid interface. LDH is a highly fragile tetramer, and thus sugars such as trehalose have been used to stabilize LDH in solution. Two concentrations of trehalose, 30 and 100 mg/mL were utilized to influence the particle surface area and protein stability. Three types of freezing processes were considered in this study. The first type, as exemplified by tray lyophilization and freezing of large slowly falling droplets into liquid nitrogen, is characterized by a slow cooling rate and low exposure to gas-liquid interface during freezing. The second and third types were the rapid freezing processes, SFD and SFL. They will be shown to differ in two primary ways: the longer exposure to the gas-liquid interface in SFD, and the less intense atomization in SFL, as a consequence of the low viscosity of evaporating N_2. The droplet size in the SFD spray was varied to investigate the effect of the gas-liquid interfacial area and the final SSA of the powder. In SFL, the time of exposure of the liquid jet to nitrogen gas will be shown to be orders of magnitude shorter than for exposure of atomized droplets to gas in SFD. This pronounced reduction in exposure to the gas-liquid interface will be shown to lead to high enzyme activities, without the need to add a surfactant such as Tween 80. The ability to minimize the addition of surfactant excipients can often be beneficial, especially as they can be detrimental to long term stability (1, 23). Furthermore, the high

SSAs of particles produced by SFL relative to lyophilization can be advantageous for the dispersion of these particles within drug delivery matrices including bioerodible polymers (9). A secondary objective of this study was to reduce the volume of feed solution to 1 mL relative to volumes greater than 20 mL in previous studies (9, 26, 27) in order to facilitate studies of expensive proteins.

3.2 MATERIALS AND METHODS

3.2.1 Materials

L-LDH from porcine heart suspended in a 3.2 M ammonium sulfate solution was purchased from Roche Applied Science (Indianapolis, IN). Trehalose, NADH and pyruvate were purchased from Sigma Chemical Company (St. Louis, MO). The water was deionized by flowing distilled water through a series of 2x7 L mixed bed DI vessels (Water and Power Technologies, Salt Lake City, UT) containing 60:40 anionic:cationic resin blends.

3.2.2 Enzyme preparation and catalytic activity assay

The LDH in ammonium sulfate was dialyzed against 10 mM KPO_4 buffer (pH 7.5) at 4ºC for 3 hours before use (41, 42) with Spectra/Por® Dialysis Membrane tubing with a molecular weight cutoff of 12,000-14,000 (Fisher Scientific, Houston, TX). Protein concentration was determined with a μQuant Model MQX200 spectrophotometer (Biotek Instruments Inc., Winooski, VT) with an absorbance at 280 nm. A value of 1.37 mL/mg-cm was used for the LDH extinction coefficient (41). LDH samples were then diluted to 0.25 mg/mL in both 30 and 100 mg/mL trehalose solutions in 10 mM KPO_4 buffer (pH 7.5).

The LDH assay was prepared by adding 0.1 mL of 20 mM pyruvate and 0.05 mL of 11 mM NADH prepared in 0.1 M KPO_4 buffer (pH 7) to 2.5 mL of 0.1 M KPO_4 buffer

(pH 7) at 25ºC into 3 plastic cuvettes which were then mixed by inversion (23). Prior to adding LDH to the reagents, each LDH formulation was diluted with 10 mM KPO_4 buffer to form LDH concentrations of 2, 3, and 4 μg/mL. Aliquots of 0.05 mL of each LDH dilution were added simultaneously with an 8 channel Transferpette® pipet (Brand, Wertheim, Germany) to the 3 plastic cuvettes filled with the reagents to make final protein concentrations of 37, 56, and 74 ng/mL, respectively. The 3 samples in the plastic cuvettes with protein were mixed again by inversion and then 3 aliquots of 230 uL of each solution were immediately placed in a 96 well Falcon plate with the Transferpette® pipet and set in the spectrophotometer. The total time from adding the LDH to the reagents to measuring absorbance data was 30 seconds. Units of LDH activity (U) were calculated by measuring the decrease in absorbance of NADH at λ=340 nm every 15 seconds for 1 minute due to the conversion of NADH to NAD over time (U = Δμmol NADH/min) and then dividing by the mass (mg) of the LDH protein in solution to determine specific activity (U/mg). For the protein concentration range tested during the 1 minute the measurements were made, the rate of NADH decrease remained linear and began to show significant deviation from linearity between 2-4 minutes after making the measurement. For final protein concentrations greater than 74 ng/mL, the activity measurement could not be obtained quickly enough since deviation from the linear rate of absorbance occurred in less than 1 min.

For the LDH formulations with 30 and 100 mg/mL trehalose the stability of the LDH in buffer solution over time was measured. For the formulation with 30 mg/mL trehalose the LDH specific activity remained stable for an hour and then began to decrease. For the formulation with 100 mg/mL trehalose the LDH specific activity remained stable for up to 6 hours before LDH activity began to decrease. All experiments were performed in the time period where the LDH specific activity had not

decayed. During this time period, the specific activity was defined as 100%. Here, the measured specific activities of LDH formulated with 30 or 100 mg/mL trehalose were not significantly different.

3.2.3 Freeze procedures

3.2.3.1 Spray freezing into liquid (SFL)

The SFL process was modified slightly from a previous study (25, 47) (Fig. 3.1). To accommodate the smaller volumes of LDH sample, the protein solution was loaded into a 1 mL sample loop in a six port rotary valve (Valco Instruments Company, Inc., Houston, TX). DI water was used to displace the LDH sample through the sample loop and then through the SFL nozzle. The liquid flow rate was 10 mL/min resulting in a pressure drop of 17.2 MPa through a 63 μm ID poly-ether-ether-ketone (PEEK) nozzle 5 cm in length (Upchurch Scientific, Oak Harbor, WA) (Fig. 3.1). A 1 L plastic bottle 8.5 cm in diameter and 17.6 cm in height containing a 2.54 cm length, 0.952 cm diameter octagonal magnetic stir bar (Fisher Scientific, Somerville, NJ) was filled with LN2 and placed in a 4 L insulated bucket (Fisher Scientific, Somerville, NJ) also filled with LN2. The ice bucket was placed on a stir plate. The depth of the LN2 vortex was approximately 2.5 cm and the nozzle was placed 2.5 cm beneath the minimum LN2 vortex level. Once the spray was completed, stirring was stopped allowing the frozen slurry to settle. Excess LN2 was decanted, and the slurry was then transferred to 50 mL polypropylene tubes (Part No. UP2255, United Laboratory Plastics, St. Louis, MO) 2 cm in diameter and 16 cm in height using a spatula pre-cooled in LN2. The plastic tubes were held in a -80°C freezer to remove residual LN2 and then were transferred to the pre-cooled lyophilizer shelf.

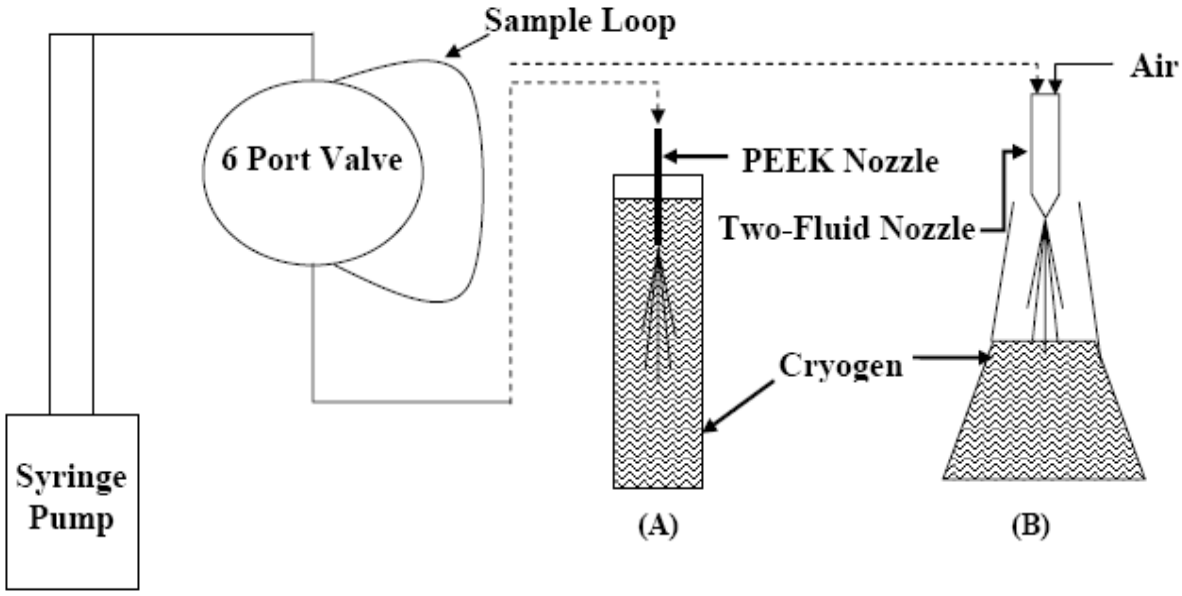

Figure 3.1: Apparatus for SFL (A) and SFD (B) sprays of solution volumes of 1 mL.

3.2.3.2 Spray Freeze-Drying (SFD)

The SFL apparatus described above was also modified for SFD to handle 1 mL sample volumes (Fig. 3.1). The aqueous feed solution was sprayed with a 0.7 mm diameter two-fluid nozzle (Büchi, Laboratory-Techniques, Switzerland) at a constant flow rate of 10 mL/min resulting in a pressure drop of 0.827 MPa (Fig. 3.1). Droplet sizes were tuned by varying the air flow rates. Droplet size distributions were measured by static light scattering (Malvern Mastersizer-S, Malvern Instruments, Ltd., Worcestershire, UK) by mounting the nozzle 10 cm above the laser beam and spraying the droplets normal to the laser beam (47). Obscuration values were between 8-12%.

The SFD setup was comparable to that of Maa et al. (22), who used a flow rate of 15 mL/min, and droplet sizes were shown to be similar (47). The SFD nozzle was mounted 10 cm above the surface of the cryogen. Cryogen preparation and post-spray slurry collection were performed as presented in the SFL spray section, with the exception that 1 L of LN2 was utilized in a 2 L Erlenmeyer flask. For SFD air flow rates of 250 mL/s the LN2 splashed 5 cm above the liquid surface inside the Erlenmeyer flask which quickly dropped the gas temperature surrounding the air plume to -196ºC 10 cm above the cryogen surface. Reducing the air flow rates to 50 mL/s decreased LN2 splashing and increased the gas temperature to -140ºC. For no air flow, the gas temperature above the LN2 was -30ºC.

3.2.3.3 Falling droplets into liquid nitrogen

The aqueous feed solution was passed through a 127 µm ID, 1.59 mm OD PEEK nozzle at a flow rate of 2 mL/min producing 3.6 mm diameter droplets. The nozzle was held 10 cm above a beaker of the stirred cryogen.

3.2.4 Lyophilization

Lyophilization samples were prepared by placing 1 mL of formulation in a 50 mL polypropylene tube (Part No. UP2255, United Laboratory Plastics, St. Louis, MO) and placing it on a pre-cooled -80ºC shelf. The samples remained on the shelf until they had completely frozen which took approximately 20 minutes. The samples were then transferred to the pre-cooled lyophilizer shelf.

3.2.5 Spray into air (SA)

To test the effect of gas-liquid interface on LDH activity independently of the freezing and drying steps in the SFD process, 1 mL of the protein solution was sprayed into an empty beaker with the two-fluid nozzle. In this spray into air (SA) process, 10 μm diameter droplets were produced, and LDH activities were measured immediately after spraying.

3.2.6 Drying and shelf loading

A Virtis Advantage Lyophilizer (The Virtis Company, Inc., Gardiner, NY) was used to dry the frozen slurries. The 50 mL plastic tubes containing the frozen slurries were covered with a single layer Kim-wipe held in place by a rubber-band in order to prevent powder from leaving the vial. Primary drying was carried out at -40ºC for 36 hrs at 300 mTorr and secondary drying at 25ºC for 24 hrs at 100 mTorr. A 12 hour linear ramp of the shelf temperature from -40°C to +25°C was used at 100 mTorr.

3.2.7 Reconstitution and protein concentration assay

Dried LDH powders were reconstituted with 1 mL of DI water and then the enzyme assay was immediately performed. After all protein samples had been assayed, the protein concentration was measured with the BCA analysis kit (Sigma Chemical Company, St. Louis, MO). Once protein concentrations were determined, the specific

activity from each measurement could be calculated. The activity of each LDH sample, formulated either in 30 or 100 mg/mL trehalose, was normalized by the specific activity of the control measured immediately before the freezing process.

3.2.8 Transfer and storage of dried powders

After the lyophilization cycle was complete, the lyophilizer was purged with nitrogen. The 50 mL plastic tubes were then rapidly transferred to a dry box held at 14% RH, and the powders were transferred to 20 mL scintillation vials. The vials were then covered with 24 mm Teflon® Faced Silicone septa (Cat.#W240588, Wheaton, Millville, NJ) which were held in place by open-top screw cap lids (VWR Scientific Products, Austin, TX). Vials were purged with dry nitrogen for 2 minutes by inserting a needle from a dry nitrogen source through the septa with an additional needle for the gas effluent.

3.2.9 Surface area measurement

Surface areas of dried powders were measured with a Quantachrome Nova 2000 (Quantachrome Corporation, Boynton Beach, FL) BET apparatus. Dried powders were transferred to the glass BET sample cells in a dry box. Samples were then degassed under vacuum for a minimum of 12 hours. The Brunauer, Emmett, and Teller (BET) equation (48) was used to fit adsorption data of nitrogen at 77 K over a relative pressure range of 0.05-0.30. The samples were measured two times.

3.2.10 Residual moisture content

Aliquots of methanol were dispensed through the septum of the scintillation vials to form a suspension concentration of 10-100 mg/mL. Vials were then placed in a tub sonicator (Mettler Electronics, Anaheim, CA) for 5 minutes at maximum power to insure complete suspension of the powder. Moisture content was measured for a 200 μL aliquot with an Aquatest 8 Karl-Fischer Titrator (Photovolt Instruments, Indianapolis, IN). The

moisture values were corrected with a 200 μL methanol blank. All samples had a moisture content between 2-3% (w/w) after drying which compared well to the residual moisture contents of 2-7% (w/w) for BSA prepared by SFD as presented by Costantino et al. (18).

3.2.11 Scanning electron microscopy

SEM images were collected on a Hitachi Model S-4500 scanning electron microscope (Hitachi Ltd, Tokyo, Japan). The samples were prepared in a dry-box. Aluminum stages fitted with double adhesive carbon conducting tape were gently dipped into sample vials until covered by powder. Stages were then placed in septum capped vials and purged with nitrogen for transfer. To minimize the time samples were exposed to atmospheric moisture the stages were rapidly transferred to a Pelco Model 3 sputter-coater. A conductive gold layer was applied and the samples were then quickly transferred to the SEM. Total exposure to the atmosphere was less than 1 minute.

3.3 RESULTS

In SFL, the exposure of protein to the gas-liquid interface is minimized by the insertion of the nozzle below the meniscus of the cryogenic liquid. Recently, the characteristics of the spray in SFL were observed visually in a transparent insulated dewar. It was shown (47) that the nozzle tip in the SFL spray was hidden by a large expanding nitrogen gas cone produced by the spray, as shown in Fig. 3.2. The formation of the gaseous N_2 cone was due to the Leidenfrost effect that is an insulating layer of vaporized LN2 which is facilitated by nitrogen's small heat of vaporization. The heat of vaporization is supplied by the liquid aqueous jet. The narrow liquid aqueous jet was observed to penetrate at least 10 cm below the liquid nitrogen surface into the gaseous cone, as shown in Fig. 3.2. The jet breakup is delayed by the low density and viscosity of

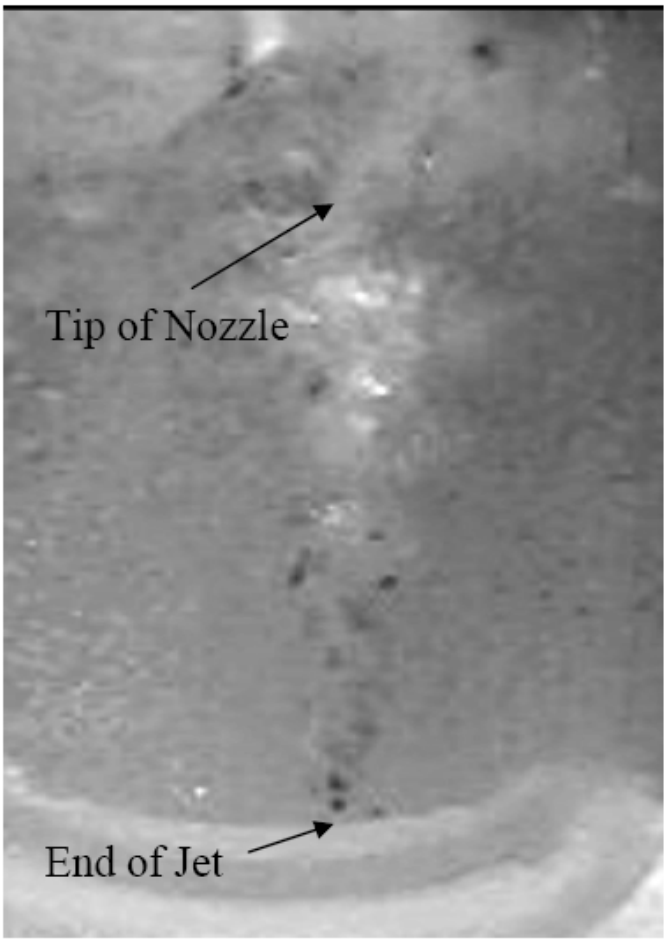

Figure 3.2: SFL of dye solution sprayed at 10 mL/min as seen through double glass dewar in LN2.

Table 3.1: Activities for 0.25 mg/mL LDH, 100 mg/mL trehalose formulations prepared in pH 7.5, 10 mM KPO_4 buffer

Freeze Process	%Activity	Replicates (n)
Lyophilization	107±9.7	3
Falling Droplet	114±6.7	3
SFL	114±6.9	4
SFD-130μm	97±9.3	5
SFD-40μm	87±6.8	5
SFD-10μm	84±6.1	5
SA-10μm	85±7.7	3

Table 3.2: Activities for 0.25 mg/mL LDH, 30 mg/mL trehalose formulations prepared in pH 7.5, 10 mM KPO_4 buffer

Freeze Process	%Activity	Replicates (n)
Lyophilization	97±5.4	3
Falling Droplet	92±6.4	3
SFL	98±5.3	4
SFD-130μm	85±8.2	3
SFD-40μm	74±6.7	5
SFD-10μm	80±5.4	4

the nitrogen gas, relative to the case of a non-evaporating cryogen such as isopentane (47, 49, 50). The delay in jet breakup is evident in the appearance of ice crystals emanating from the bottom of the jet, which were subsequently circulated in the flask by the large gas flux of evaporating LN2. Following the spray, large, dense frozen particles were suspended in the quiescent LN2 (47).

The activities for LDH with 100 mg/mL trehalose frozen by lyophilization, SFL, and falling droplets were extremely high (Table 3.1) and not significantly different ($p<0.05$) fromeach other according to a student's t test where the number of replicates (n) are shown in Table 3.1. The activities are even higher than the measured activities of the original dialyzed formulation. The large trehalose concentration present during drying may have altered the protein conformation resulting in higher activity after drying and reconstitution (41, 51). The very high LDH activities for these three processes demonstrate that the protein did not lose activity from the combined stresses of the freezing, drying and reconstitution steps. As calculated previously (47), the 3 to 4 orders of magnitude increase in cooling rate provided by the SFL process compared to lyophilization suggests that the greater ice-liquid interfacial area created from a faster cooling rate does not result in LDH activity loss.

The SFL activities were significantly higher than those produced for all three droplet sizes in SFD (Table 3.1). For SFD, the LDH activity was significantly higher for a droplet diameter of 130 μm than for the smaller 40 μm and 10 μm diameter droplets. As shown in Table 3.1 for the SA process with 10 μm diameter droplets, the LDH activity was almost equivalent to the LDH activity of the SFD-10 μm process. These results suggest that the activity loss in SFD is from the spraying step and that additional activity loss from the freezing and drying steps was insignificant.

The SEM micrographs in Fig. 3.3 show the effect of increasing the cooling rate on the morphology of the dried powder prepared with 100 mg/mL trehalose without any protein. Since the mass ratio of trehalose:LDH in the LDH formulation was 400:1, it was observed that LDH did not effect the morphology (not shown). For lyophilization, which was the slowest cooling process, large plates were observed that were greater than 15 μm in diameter (Fig. 3.3A). For the SFL process with a much faster cooling rate, the particles were characterized by approximately 1 μm features (Fig. 3.3B), consistent with a measured SSA of 13 m^2/g (Table 3.3). The SSA of the SFL powder was over an order of magnitude higher than for powders prepared by lyophilization (47).

The SEM for the SFD-10 μm process, which had the highest cooling rate (47), revealed spherical particles that ranged 40-100 nm in diameter (Fig. 3.3C). The calculated SSA range between 60 and 150 m^2/g for 100 and 40 nm spheres, respectively, is consistent with the measured lysozyme SSA value of 126 m^2/g in Table 3.3. Therefore, the particles produced by SFD relative to SFL had an approximate 4-fold larger powder SSA and finer features in the SEMs.

Upon lowering the trehalose concentration to 30 mg/mL in the LDH formulation, the LDH activities for the lyophilization, SFL, and falling droplet processes (Table 3.2) were still very high and not significantly different ($p<0.05$) from each other. The SFL activities with the low trehalose concentration were also significantly higher ($p<0.05$) than those for samples prepared by SFD, as reported above for the high 100 mg/mL trehalose concentration. The SFD-130 μm activity was higher than for the two SFD sprays with smaller droplet sizes.

The effect of trehalose concentration on powder morphology for a given cooling rate is shown in the SEMs for the SFL powders (Fig. 3.3B and D). For 30 mg/mL trehalose (Fig. 3.3D), large platelets approximately 1-2 μm in diameter were mixed with

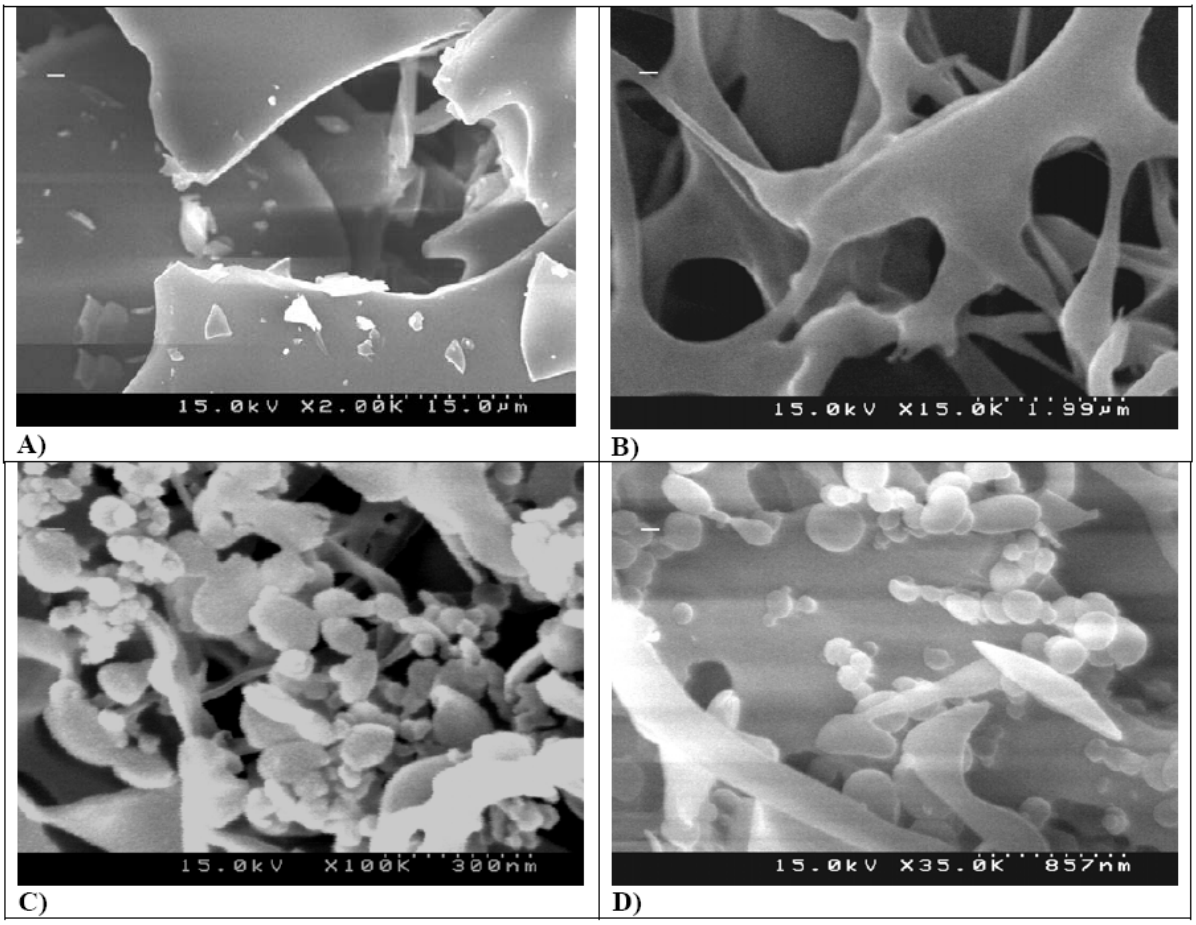

Figure 3.3: 100 mg/mL trehalose formulations processed by Lyophilization (A), SFL (B), and SFD-10 µm (C) and 30 mg/mL trehalose processed by SFL (D).

Table 3.3: Specific surface areas measured on lysozyme and trehalose powders (47)

Process	**Component**	**Feed Concentration (mg/mL)**	**SSA (m^2/g)**
SFL	Lysozyme	50	34 ± 2
SFL	Lysozyme	100	38 ± 2
SFL	Trehalose	50	14 ± 2
SFL	Trehalose	100	13 ± 1
Falling Droplet	Lysozyme	50	4.2 ± 0.02
SFD-130μm	Lysozyme	50	26 ± 1
SFD-40μm	Lysoyzme	50	87 ± 3
SFD-10μm	Lysozyme	50	126 ± 5

spheres as small as 50 nm and threads 200-300 nm in diameter. The 1-2 μm features were comparable to those in Fig. 3.3B for 100 mg/mL trehalose, but submicron particles were not seen. The measured specific surface area (SSA) of trehalose powder sprayed at 50 mg/mL feed concentration was 14 m^2/g which is nearly identical to the value of 13 m^2/g measured for the formulation with 100 mg/mL trehalose (Table 3.3) (47). The submicron particles seen for the dilute 30 mg/mL trehalose formulation in Fig. 3.3D suggest that the measured SSA should have been significantly higher than for the more concentrated 100 mg/mL trehalose formulation shown in Fig. 3.3B. However, the measured SSAs (Table 3.3) were nearly identical. The discrepancy may have been caused by different exposure times of trehalose, which is hygroscopic, to moisture during each analysis. For the SEM analysis the trehalose was exposed to atmospheric moisture for less than 1 minute during transfer to the SEM. For the BET analysis, loading the trehalose powder in BET glass cells took 10-15 minutes to accomplish in the dry box with 14% RH. Even with the relatively low RH in the dry box significant moisture may have been adsorbed by the trehalose resulting in a significant decrease in the expected SSA. Although moisture control was problematic for measuring SSAs, the SEM micrographs indicate that the SFD and SFL processes generate a sufficient degree of atomization and rapid cooling to produce much higher surface areas than in lyophilization, even for concentrated feed solutions.

For the SFD process the intense splashing of the LN2 during the spray did not permit observation of the spray pattern of the liquid droplets. The spray pattern of the droplets was observed by spraying water into air through the SFD nozzle. The atomized liquid droplets for each air flow rate were observed to be well mixed within the air stream plume. When the spray was directed over a sheet of paper 10 cm below the nozzle a

solid wet circle was formed on the paper indicating that the atomized droplets were dispersed throughout the cross sectional area of the plume.

3.4 DISCUSSION

3.4.1 Slow cooling with low surface area: lyophilization and falling droplet

The purpose of the lyophilization and falling droplet experiments was to investigate the effects of a low gas-liquid droplet surface area/volume ratio and a slow cooling rate on LDH activity. The differences in cooling rates for these two processes have been described in detail previously (47). The lyophilization process had the slowest cooling rate in this study; it took 1 mL samples approximately 20 minutes to freeze when placed on a -80ºC shelf. For the falling droplet process with the next fastest cooling rate, the 3.6 mm diameter liquid droplets impacted the LN2 and floated for 30 seconds on the LN2 surface before sinking. The aqueous droplets floated due to the boiling of the cryogen in contact with the droplets as a result of the Leidenfrost effect. As the droplets floated on the LN2 during freezing, two droplets occasionally coalesced into a larger droplet. Therefore, ice formation appeared to require at least 30 seconds after the liquid droplet impacted the LN2 surface. Once the frozen droplets had sufficiently cooled the boiling ceased and the droplets descended to the bottom of the beaker (47). Although the falling droplet process had a relatively long exposure time to the gas-liquid interface during freezing, the surface area/volume ratio of the droplet was sufficiently low that the LDH activity loss was not significant. Relative to tray lyophilization, the slightly faster cooling rate (~1K/s) in the falling droplet experiment does not affect LDH activity.

The high LDH activities for each of these processes at each trehalose concentration in Tables 3.1 and 3.2 indicate that the trehalose concentration was sufficient to protect LDH from denaturing in the freeze concentrate during slow cooling

(~1K/min) and even led to an LDH activity increase. The >100% LDH activities achieved in Table 3.1 have also been achieved in other studies with LDH (52) and the tetramer β-galactosidase (51). The unfavorable free energy of preferential exclusion of the trehalose stabilizes the lower surface area folded state to a greater extent than the greater surface area denatured state (1, 43, 53, 54). For multimeric proteins that form a tetramer such as LDH, the stability of the tetramer is increased in the presence of a preferentially excluded solute since the surface area of the protein is much smaller in the tetramer form (43, 54). It has been suggested that freeze concentration of LDH in the presence of trehalose or sucrose favors the association of dimers to form the active LDH tetramer (52). Upon reconstitution of the dried powder followed by the enzyme assay, the protein activity is increased from the increased formation of the LDH tetramer (51, 52). At trehalose concentrations lower than 30 mg/mL in buffer solution at 25^{o} C, LDH tetramers are known to dissociate. As already mentioned, the LDH formulation with 30 mg/mL trehalose would begin to lose activity in buffer solution after 1 hour. Consequently, lower trehalose concentrations were not investigated in this study. These experiments establish that the concentrations of trehalose studied were sufficient to maintain cryoprotection due to preferential exclusion during slow cooling when the solute concentrations increase in the unfrozen liquid, which is exposed to an ice-liquid interface. In the SFD and SFL processes, the time of exposure to the ice-liquid interface will be much shorter, but the interfacial area will be much larger.

3.4.2 Rapid cooling with large exposure to gas-liquid interface: spray freeze-drying (SFD)

The effect of the gas-liquid and ice-liquid interfaces on protein stability has been the subject of numerous studies (5, 18-20, 23, 25-27, 36, 55, 56); however the mechanisms are not fully understood. In the SFD process, both the area of the gas-liquid interface and cooling rate increase as the droplet diameter is decreased (5). The faster

cooling rates can increase the surface area of the ice-liquid interface (Fig. 3.4) (47). High cooling rates of concentrated feed solutions (> 50 mg/mL) produced with small 10 μm diameter droplets lead to rapid nucleation of amorphous water surrounded by thin channels containing growing protein/excipient clusters that have nucleated from the freeze concentrate (Fig. 3.4A). For larger droplets, lower cooling rates decrease the nucleation rate of amorphous water domains leading to fewer, larger frozen water domains with a smaller area of ice-liquid interface (Fig. 3.4B). Only a few previous studies have separated the effects of the gas-liquid and ice-liquid interfaces on protein stability by analyzing protein stability after the spraying (spray into air), freezing (spray freeze-thaw), and drying steps (spray freeze-drying) (19, 26). It was shown that protein destabilization occurred during the spray into air process and that the freezing and drying steps contributed very little additional destabilization; therefore, exposure to the ice-liquid interface during freezing played a minor role (19, 26). Webb et al. reported that the protein would not have sufficient time to diffuse to the ice-liquid interface to denature before the droplet would be completely frozen (19). Furthermore, X-ray photoelectron spectroscopy (XPS) measurements indicated that the amount of protein within a monolayer of the surface of the dried powder was consistent with the theoretical amount of protein adsorption at the gas-liquid interface (19). For the very large trehalose:LDH ratio used in this study, XPS analysis would not provide sufficient sensitivity to determine the surface LDH concentration. For 10 μm diameter droplets, a comparison of the spray into air and SFD processes in Table 3.1 indicates that the large ice-liquid interface in the rapid SFD freezing process had a negligible effect on LDH activity loss. The loss was caused by the large gas-liquid interface, in agreement with Webb et al.'s conclusion (19), as was also observed for lysozyme (26).

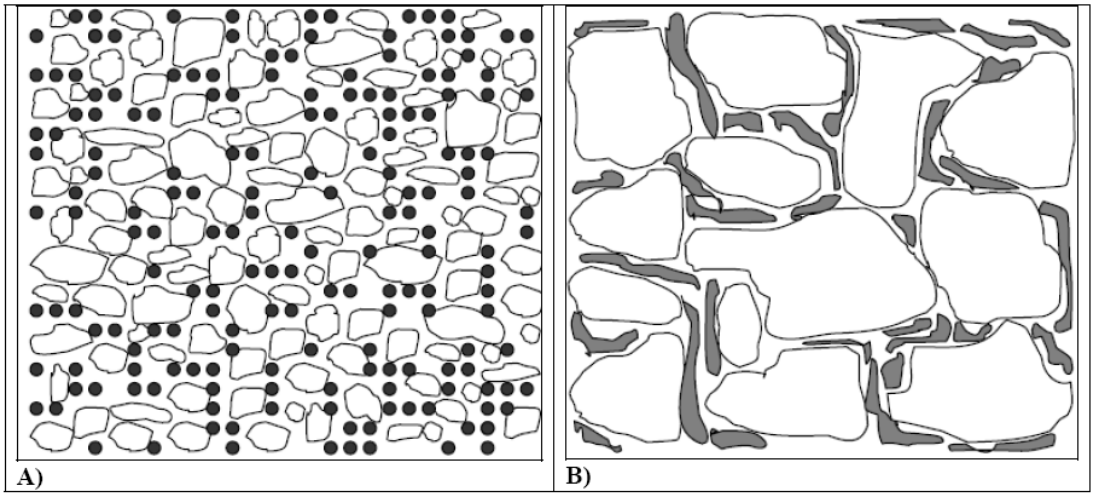

Figure 3.4: Frozen morphologies of concentrated solutions with high supercooling (A) and low supercooling (B). Amorphous ice particles are represented as white domains and solute precipitate as solid dots or gray regions.

The time of flight of the atomized droplets through the gas phase above the cryogen may be calculated assuming the droplets move with the same velocity as the air. From the continuity equation, the product of velocity and area of the conical air jet is constant. The velocity of the air 10 cm below the nozzle exit was 0.80 m/s for the 10 μm diameter droplets and 0.16 m/s forthe 130 μm diameter droplets. The reciprocal of this velocity times this distance, 10 cm, gives time of flight values of ~0.1 s (SFD-10 μm) and ~0.6 s (SFD-130 μm) for the droplets. A greater air flow rate was utilized to atomize the liquid jet into smaller droplets resulting in larger droplet velocities (47). Although the cold LN2 gas above the LN2 meniscus potentially would be able to freeze the surface of the droplets during the time of flight through the gas phase, the warm atomizing air in the conical jet will delay freezing. The similar activity losses in the spray into air and SFD processes suggests that the LDH adsorbed at the gas-liquid interface before the droplet surface froze. Webb et al. explained that adsorption of rhINF-γ, and globular proteins in general, to the gas-liquid interface occurs on the order of milliseconds, which is much shorter than the ~1 second time of flight through the gas phase (19).

For the slowest cooling process (lyophilization) and the fastest cooling process (SFD-10 μm) it was shown that ice-liquid interface had a negligible effect on LDH activity loss. For any intermediate cooling rate it therefore may be expected that the ice-liquid interface would also not affect LDH stability. Thus the higher enzyme activities for the 130 μm droplets versus the smaller droplets may be expected to be caused by the smaller surface area of the gas-liquid interface. The limit of low surface area/volume in the falling droplet experiment produced an even higher enzyme activity.

3.4.3 Rapid cooling with low exposure to nitrogen gas-liquid interface: spray freezing into liquid (SFL)

The stabilities for the SFL powders were very high indicating that none of the steps, spraying, freezing and drying caused much loss in enzyme activity. Thus the SFL

process overcame the key limitation observed in SFD, the destabilization of protein in the spraying step. The exposure time to gas-liquid interface is much shorter for the SFL process relative to SFD according to the following calculation. For SFL, the liquid jet flowed through the boiling LN2 cryogen at 53 m/s upon exiting the nozzle. At this velocity the jet would travel 10 cm below the LN2 surface (Fig. 3.2) in 2 ms before breaking apart into frozen particles. Therefore, the extremely short time of exposure to the nitrogen gas-liquid interface is a result of the very small nozzle I.D. of 63 μm forming a small diameter jet with a high velocity. As already mentioned, for the SFD sprays the time of flight of the droplets through the gas phase above the cryogen varied from ~0.1 to ~0.6 s. Therefore, the time of exposure for the SFD process to the gas-liquid interface was 2 orders of magnitude longer than for the SFL process. Even though the droplets in the SFD-130 μm spray may have similar or even lower surface area/volume ratios than in the SFL spray, the longer time of exposure to the nitrogen gas-liquid interface resulted in lower LDH activities in SFD.

Even if some protein diffused to the gas-liquid interface during its very short exposure of 2 ms, additional factors could have helped prevent unfolding. The very low temperature of the nitrogen gas in the funnel surrounding the jet in SFL may have raised the water viscosity. The high viscosity of the water and the low thermal energy would then slow down the dynamics of protein unfolding and aggregation at the outer surface of the jet. Furthermore, the outer surface of the water may have vitrified preventing the protein from reaching the nitrogen gas-liquid interface. Finally, relative to the SFD process, warm atomizing air was not present, which would otherwise have delayed freezing.

Although the cooling rate in the SFL process (7200 K/s) was reduced by the Leidenfrost effect, it was still 3 to 4 orders of magnitude greater than for lyophilization

(~1 K/min) and the falling droplet (~1 K/s) processes as calculated previously (47). The more rapid nucleation and growth during freezing in SFL produced SSAs an order of magnitude larger than in the falling droplet process (Table 3.3) (47), as was also evident in the SEMs. The LDH activities remained high in spite of the large area of the ice-liquid interface. As seen for SFD (19), the freezing step in SFL also appeared to be too fast for the protein to diffuse to the ice-liquid interface and denature.

Other particle forming processes shown in Table 3.4 including SFD, spray-drying, and $scCO_2$A-BD all required the use of Tween 20 or Tween 80 to achieve high LDH activities for similar protein and sugar concentrations (23, 24, 44). Without a surfactant the LDH activities were significantly lower compared to SFL. Each of these processes exposed the protein to the gas-liquid interface for a sufficiently long time period to produce aggregation. Therefore, the minimization of exposure to the gas-liquid interface in the SFL process removes the need for the addition of a surfactant.

Other reports have indicated that exposure to increased ice-liquid interface significantly destabilizes protein (5, 18, 55). With freeze-thaw studies Chang et al. demonstrated that increasing the cooling rate from slow cooling on a shelf to quench freezing in LN2 increases the ice-liquid interfacial area which decreases LDH activity (55). This study did not use a stabilizing sugar such as trehalose to prevent destabilization during freezing and/or drying. Activity loss was decreased by adding the surfactant Tween 80 to the LDH formulation. From freeze-thaw studies, it was concluded that Tween 80 competes with the protein for ice-liquid interface (55). In the present study in which sufficient trehalose was present the LDH remained stable through the freezing and the drying steps, in spite of the rapid cooling rate. In another study, it has been shown with the SFD process that BSA monomer loss increases with an increase in powder SSA (18). As the diameter of the sprayed droplets decreases, the more rapid

Table 3.4: Activities for porcine LDH (PLDH) or rabbit LDH (RLDH) processed with various freezing and drying processes

Process	Protein	Formulation Composition	Activity
SFD (44)	RLDH	0.015 mg/mL LDH	
		+100 mg/mL trehalose	58%
		+250 mg/mL trehalose	56%
		0.03 mg/mL LDH	
		+250 mg/mL trehalose and 1 mg/mL Tween 80	83%
		+250 mg/mL trehalose and 5 mg/mL Tween 80	92%
SD (23)	PLDH	0.300 mg/mL LDH	
		+100 mg/mL trehalose	90%
		+100 mg/mL trehalose and 0.1 mg/mL Tween 80	93%
		5 mg/mL LDH	
		+95 mg/mL trehalose	90%
		+95 mg/mL trehalose and 0.1 mg/mL Tween 80	98%
$scCO_2$A-BD (24)	RLDH	0.1 mg/mL LDH	15%
		+100 mg/mL mannitol	40%
		+100 mg/mL sucrose	66%
		+100 mg/mL sucrose and 0.1 mg/mL Tween 20	95%

cooling rate produces particles with a finer microstructure (18). It is likely that the gas-liquid interface played an important role in the protein aggregation for BSA, given the results for rhIFN-γ (19), lysozyme (26) and LDH (this study) with SFD.

3.5 CONCLUSIONS

In SFD, the activity loss in the spraying step has been shown to be caused by protein adsorption and aggregation at the gas-liquid interface, as reported for rhIFN-γ (19) and lysozyme (26). In this study, the LDH activity loss was the same as when spraying the protein solution into air without freezing, suggesting that the freezing (ice-liquid interface) and drying steps may not have contributed further to the activity loss. Furthermore, the activity loss increased with a decrease in droplet size, and thus gas-liquid interfacial area, consistent with results for BSA (18), and for rhIFN-γ and lysozyme. Given that long exposure to the gas-liquid interface in SFD and spray-drying can destabilize proteins, the ability to shorten this exposure time is of considerable practical importance.

The SFL process may be used to reduce exposure to the gas-liquid interface. For 0.25 mg/mL LDH with either 30 or 100 mg/mL trehalose, the SFL process produced powders with very high enzyme activities comparable to lyophilization upon reconstitution, despite surface areas that were an order of magnitude higher. The combined spraying, freezing, and drying stresses of the SFL process did not produce any significant loss in LDH activity. The enzyme activities in SFL were higher than for SFD, even with the larger 130 μm droplets, despite the similar powder surface areas in both cases. Although a gas cone was formed about the liquid jet in SFL, as a result of nitrogen evaporation (Leidenfrost effect), the nitrogen gas-liquid contact had a negligible impact on the LDH stability. The exposure time of only 2 ms to the nitrogen gas-liquid interface

in this cone was calculated to be 2 orders of magnitude faster than for SFD. This very short exposure time appeared to prevent loss in activity from protein adsorption and unfolding, even without the use of a surfactant. It is likely the primary cause of the higher LDH activities in SFL versus SFD. The ability to produce stable high surface area submicron particles of fragile proteins such as LDH by SFL, in addition to much more stable proteins such as BSA (27) and lysozyme (26) is of practical interest in protein storage and in controlled release applications including encapsulation in bioerodible polymers. The successful scale down of the SFL process for protein formulation volumes as small as 1 mL will be beneficial for therapeutic proteins available only in limited quantities.

3.6 REFERENCES

1. J. F. Carpenter, B. S. Chang, W. Garzon-Rodriguez, and T. W. Randolph. Rational design of stable lyophilized protein formulations: theory and practice. In J. F. Carpenter and M. C. Manning (eds.), *Pharmaceutical Biotechnology. 13. Rational Design of Stable Protein Formulations*, Kluwer Academic/Plenum Press, New York, 2002, pp. 109-133.

2. M. C. Manning, K. Patel, and R. T. Borchardt. Stability of protein pharmaceuticals. *Pharm. Res.* **6:**903-918 (1989).

3. W. Wang. Lyophilization and development of solid protein pharmaceuticals. *Int. J. Pharm.* **203:**1-60 (2000).

4. R. A. DePaz, D. A. Dale, C. C. Barnett, J. F. Carpenter, A. L. Gaertner, and T. W. Randolph. Effects of drying methods and additives on the structure, function, and storage stability of subtilisin: role of protein conformation and molecular mobility. *Enzyme Microb. Technol.* **31:**765-774 (2002).

5. Y.-F. Maa and H. R. Costantino. Spray freeze-drying of biopharmaceuticals: applications and stability considerations. In H. R. Costantino and M. J. Pikal (eds.), *Biotechnology: Pharmaceutical Aspects. 2. Lyophilization of Biopharmaceuticals*, American Association of Pharmaceutical Scientists, Arlington, 2004, pp. 519-561.

6. M. J. Pikal. Mechanisms of protein stabilization during freeze-drying and storage: the relative importance of thermodynamic stabilization and glassy state relaxation dynamics. *Drugs Pharm. Sci.* **137:**63-107 (2004).

7. Y.-F. Maa, L. Zhao, L. G. Payne, and D. Chen. Stabilization of alum-adjuvanted vaccine dry powder formulations: mechanism and application. *J. Pharm. Sci.* **92:**319-332 (2003).

8. X. M. Lam, E. T. Duenas, A. L. Daugherty, N. Levin, and J. L. Cleland. Sustained release of recombinant human insulin-like growth factor-I for treatment of diabetes. *J. Control. Release* **67:**281-292 (2000).

9. W. T. Leach, D. T. Simpson, T. N. Val, E. C. Anuta, Z. Yu, R. O. Williams III, and K. P. Johnston. Uniform encapsulation of stable protein nanoparticles produced by spray freezing for the reduction of burst release. *J. Pharm. Sci.* **94:**56-69 (2005).

10. O. L. Johnson, W. Jaworowicz, J. L. Cleland, L. Bailey, M. Charnis, E. Duenas, C. Wu, D. Shepard, S. Magil, T. Last, A. J. S. Jones, and S. D. Putney. The

stabilization and encapsulation of human growth hormone into biodegradable microspheres. *Pharm. Res.* **14:**730-735 (1997).

11. X. M. Lam, E. T. Duenas, and J. L. Cleland. Encapsulation and stabilization of nerve growth factor into poly(lactic-co-glycolic) acid microspheres. *J. Pharm. Sci.* **90:**1356-1365 (2001).

12. M. R. Prausnitz. Microneedles for transdermal drug delivery. *Adv. Drug Deliv. Rev.* **56:**581-587 (2004).

13. D. A. Edwards, J. Hanes, G. Caponetti, J. Hrkach, A. Ben-Jebria, M. L. Eskew, J. Mintzes, D. Deaver, N. Lotan, and R. Langer. Large porous particles for pulmonary drug delivery. *Science* **276:**1868-1871 (1997).

14. S. J. Shire, Z. Shahrokh, and J. Liu. Challenges in the development of high protein concentration formulations. *J. Pharm. Sci.* **93:**1390-1402 (2004).

15. H. R. Costantino, O. L. Johnson, and S. E. Zale. Relationship between encapsulated drug particle size and initial release of recombinant human growth hormone from biodegradable microspheres. *J. Pharm. Sci.* **93:**2624-2634 (2004).

16. J. L. Cleland, E. T. Duenas, A. Park, A. Daugherty, J. Kahn, J. Kowalski, and A. Cuthbertson. Development of poly-(d,l-lactide-co-glycolide) microsphere formulations containing recombinant human vascular endothelial growth factor to promote local angiogenesis. *J. Control. Release* **72:**13-24 (2001).

17. W. T. Leach, D. T. Simpson, T. N. Val, Z. Yu, K. T. Lim, E. J. Park, R. O. Williams III, and K. P. Johnston. Encapsulation of protein nanoparticles into uniform-sized microspheres formed in a spinning oil film. *AAPS Pharm. Sci. Tech.* **6:**605-617 (2005).

18. H. R. Costantino, L. Firouzabadian, K. Hogeland, C. C. Wu, C. Beganski, K. G. Carrasquillo, M. Cordova, K. Griebenow, S. E. Zale, and M. A. Tracy. Protein spray-freeze drying. Effect of atomization conditions on particle size and stability. *Pharm. Res.* **17:**1374-1383 (2000).

19. S. D. Webb, S. L. Golledge, J. L. Cleland, J. F. Carpenter, and T. W. Randolph. Surface adsorption of recombinant human interferon-γ in lyophilized and spray-lyophilized formulations. *J. Pharm. Sci.* **91:**1474-1487 (2002).

20. Y.-F. Maa and S. J. Prestrelski. Biopharmaceutical powders: particle formation and formulation considerations. *Curr. Pharm. Biotechnol.* **1:**283-302 (2000).

21. X. C. Nguyen, J. D. Herberger, and P. A. Burke. Protein powders for encapsulation: a comparison of spray-freeze drying and spray drying of darbepoetin alfa. *Pharm. Res.* **21:**507-514 (2004).

22. Y.-F. Maa, P.-A. Nguyen, T. Sweeney, S. J. Shire, and C. C. Hsu. Protein inhalation powders: spray drying vs spray freeze drying. *Pharm. Res.* **16:**249-254 (1999).

23. M. Adler and G. Lee. Stability and surface activity of lactate dehydrogenase in spray-dried trehalose. *J. Pharm. Sci.* **88:**199-208 (1999).

24. S. P. Sellers, G. S. Clark, R. E. Sievers, and J. F. Carpenter. Dry powders of stable protein formulations from aqueous solutions prepared using supercritical CO(2)-assisted aerosolization. *J. Pharm. Sci.* **90:**785-797 (2001).

25. Z. Yu, T. L. Rogers, J. Hu, K. P. Johnston, and R. O. Williams III. Preparation and characterization of microparticles containing peptide produced by a novel process: spray freezing into liquid. *Eur. J. Pharm. Biopharm.* **54:**221-228 (2002).

26. Z. Yu, K. P. Johnston, and R. O. Williams III. Spray freezing into liquid versus spray-freeze drying: Influence of atomization on protein aggregation and biological activity. *Eur. J. Pharm. Sci.* **27:**9-18 (2006).

27. Z. Yu, A. S. Garcia, K. P. Johnston, and R. O. Williams III. Spray freezing into liquid nitrogen for highly stable protein nanostructured microparticles. *Eur. J. Pharm. Biopharm.* **58:**529-537 (2004).

28. M. C. Heller, J. F. Carpenter, and T. W. Randolph. Protein formulation and lyophilization cycle design: prevention of damage due to freeze-concentration induced phase separation. *Biotechnol. Bioeng.* **63:**166-174 (1999).

29. M. J. Akers, V. Vasudevan, and M. Stickelmeyer. Formulation development of protein dosage forms. In S. L. Nail and M. J. Akers (eds.), *Pharmaceutical Biotechnology. 14. Development and Manufacture of Protein Pharmaceuticals*, Kluwer Academic/Plenum Press, New York, 2002, pp. 47-127.

30. T. F. O'Connor, P. G. Debenedetti, and J. D. Carbeck. Simultaneous determination of structural and thermodynamic effects of carbohydrate solutes on the thermal stability of ribonuclease A. *J. Am. Chem. Soc.* **126:**11794-11795 (2004).

31. C. A. Angell and L.-M. Wang. Hyperquenching and cold equilibration strategies for the study of liquid-liquid and protein folding transitions. *Biophys. Chem.* **105:**621-637 (2003).

32. J. D. Andya, Y.-F. Maa, H. R. Costantino, P.-A. Nguyen, N. Dasovich, T. D. Sweeney, C. C. Hsu, and S. J. Shire. The effect of formulation excipients on protein stability and aerosol performance of spray-dried powders of a recombinant humanized anti-IgE monoclonal antibody. *Pharm. Res.* **16:**350-358 (1999).

33. Y.-F. Maa and P.-A. Nguyen. Method of spray freeze drying proteins for pharmaceutical administration. United States Patent. 6,284,282 (2001).

34. H. R. Costantino, L. Firouzabadian, C. C. Wu, K. G. Carrasquillo, K. Griebenow, S. E. Zale, and M. A. Tracy. Protein spray freeze drying. 2. Effect of formulation variables on particle size and stability. *J. Pharm. Sci.* **91:**388-395 (2002).

35. Z. H. Chang and J. G. Baust. Ultra-rapid freezing by spraying/plunging: pre-cooling in the cold gaseous layer. *J. Microsc.* **161:**435-444 (1991).

36. S. Magdassi and A. Kamyshny. Surface activity and functional properties of proteins. In S. Magdassi (ed.), *Surface Activity of Proteins*, Marcel Dekker, New York, 1996, pp. 1-38.

37. J. Hu, T. L. Rogers, J. Brown, T. Young, K. P. Johnston, and R. O. Williams III. Improvement of dissolution rates of poorly water soluble APIs using novel spray freezing into liquid technology. *Pharm. Res.* **19:**1278-1284 (2002).

38. J. Hu, K. P. Johnston, and R. O. Williams III. Rapid dissolving high potency danazol powders produced by spray freezing into liquid process. *Int. J. Pharm.* **271:**145-154 (2004).

39. T. L. Rogers, J. Hu, Z. Yu, K. P. Johnston, and R. O. Williams III. A novel particle engineering technology: spray-freezing into liquid. *Int. J. Pharm.* **242:**93-100 (2002).

40. T. L. Rogers, A. C. Nelsen, J. Hu, J. N. Brown, M. Sarkari, T. J. Young, K. P. Johnston, and R. O. Williams III. A novel particle engineering technology to enhance dissolution of poorly water soluble drugs: spray-freezing into liquid. *Eur. J. Pharm. Biopharm.* **54:**271-280 (2002).

41. T. J. Anchordoquy, K.-I. Izutsu, T. W. Randolph, and J. F. Carpenter. Maintenance of quaternary structure in the frozen state stabilizes lactate dehydrogenase during freeze-drying. *Arch. Biochem. Biophys.* **390:**35-41 (2001).

42. T. J. Anchordoquy and J. F. Carpenter. Polymers protect lactate dehydrogenase during freeze-drying by inhibiting dissociation in the frozen state. *Arch. Biochem. Biophys.* **332:**231-238 (1996).

43. J. F. Carpenter, K.-i. Izutsu, and T. W. Randolph. Freezing- and drying-induced perturbations of protein structure and mechanisms of protein protection by

stabilizing additives. In L. Rey and J. C. May (eds.), *Drugs and the Pharmaceutical Sciences. 137. Freeze-Drying/Lyophilization of Pharmaceutical and Biological Products*, Marcel Dekker, Inc., New York, 2004, pp. 147-186.

44. C. Sonner, PhD Thesis, University of Erlangen-Nuremburg, 2002.

45. T. Dams, R. Ostendorp, M. Ott, K. Rutkat, and R. Jaenicke. Tetrameric and octameric lactate dehydrogenase from the hyperthermophilic bacterium thermotoga maritima: structure and stability of the two active forms. *Eur. J. Biochem.* **240:**274-279 (1996).

46. J. J. Holbrook, A. Liljas, S. J. Steindel, and M. G. Rossmann. Lactate dehydrogenase. In P. D. Boyer (ed.), *Enzymes, 3rd Ed.*, Academic Press, New York, 1975, pp. 191-292.

47. J. D. Engstrom, D. T. Simpson, E. Lai, R. O. Williams III, and K. P. Johnston. Morphology of protein particles produced by spray freezing of concentrated solutions. *Eur. J. Pharm. Biopharm.* **65:**149-162 (2007).

48. S. Brunauer, P. H. Emmett, and E. Teller. Adsorption of gases in multimolecular layers. *J. Am. Chem. Soc.* **60:**309-319 (1938).

49. C. S. Lengsfeld, J. P. Delplanque, V. H. Barocas, and T. W. Randolph. Mechanism governing microparticle morphology during precipitation by a compressed antisolvent: atomization vs. nucleation and growth. *J. Phys. Chem. B* **104:**2725-2735 (2000).

50. H. Sitte, L. Edelmann, and K. Neumann. Cryofixation without pretreatment at ambient pressure. In R. A. Steinbrecht and K. Zierold (eds.), *Cryotechniques in Biological Electron Microscopy*, Springer-Verlag, Berlin, 1987, pp. 87-113.

51. K. A. Pikal-Cleland and J. F. Carpenter. Lyophilization-induced protein denaturation in phosphate buffer systems: monomeric and tetrameric b-galactosidase. *J. Pharm. Sci.* **90:**1255-1268 (2001).

52. B. S. Bhatnagar, S. J. Nehm, M. J. Pikal, and R. H. Bogner. Post-thaw aging affects activity of lactate dehydrogenase. *J. Pharm. Sci.* **94:**1382-1388 (2005).

53. J. F. Carpenter and J. H. Crowe. The mechanism of cryoprotection of proteins by solutes. *Cryobiology* **25:**244-255 (1988).

54. S. N. Timasheff. The control of protein stability and association by weak interactions with water: how do solvents affect these processes? *Annu. Rev. Biophys. Biomol. Struct.* **22:**67-97 (1993).

55. B. S. Chang, B. S. Kendrick, and J. F. Carpenter. Surface-induced denaturation of proteins during freezing and its inhibition by surfactants. *J. Pharm. Sci.* **85:**1325-1330 (1996).

56. S. D. Webb, J. L. Cleland, J. F. Carpenter, and T. W. Randolph. Effects of annealing lyophilized and spray-lyophilized formulations of recombinant human interferon-γ. *J. Pharm. Sci.* **92:**715-729 (2003).

Chapter 4: Novel Ultra-Rapid Freezing Particle Engineering Process for Enhancement of Dissolution Rates of Poorly Water Soluble Drugs[1]

An ultra-rapid freezing (URF) technology, otherwise known as thin film freezing (TFF), has been developed to produce high surface area powders composed of solid solutions of an active pharmaceutical ingredient (API) and a polymer stabilizer. A solution of API and polymer excipient(s) is spread on a cold solid surface to form a thin film that freezes in 50 ms to 1 s. This study provides an understanding of how the solvent's physical properties and the thin film geometry influence the freezing rate and consequently the final physicochemical properties of URF processed powders. Theoretical calculations of heat transfer rates are shown to be in agreement with infrared images with 10 ms resolution. Danazol (DAN)/polyvinylpyrrolidone (PVP) powders, produced from both acetonitrile (ACN) and tert-butanol (T-BUT) as the solvent, were amorphous with high surface areas (~28-30 m^2/g) and had enhanced dissolution rates. However, differences in surface morphology were observed and attributed to the cooling rate (film thickness) as predicted by the model. Relative to spray freezing processes that use liquid nitrogen, URF also offers fast heat transfer rates as a result of the intimate contact between the solution and cold solid surface, but without the complexity of cryogen evaporation (Leidenfrost effect). The ability to produce amorphous high surface area powders with submicron primary particles with a simple ultra rapid freezing process is of practical interest in particle engineering to increase dissolution rates, and ultimately bioavailability.

---

1 Large portions of this chapter have been previously published as, K.A. Overhoff, J.D. Engstrom, B. Chen, T.L. Rogers, K.P. Johnston, and R.O. Williams III. Novel ultra-rapid freezing particle engineering process to enhance the dissolution rates of poorly water-soluble drugs. *Eur. J. Pharm. Biopharm.* 65:57-67 (2007).

4.1 INTRODUCTION

A significant number of active pharmaceutical ingredients (API) being discovered display desirable therapeutic properties, but have undesirable physicochemical properties (e.g. solubility) making formulation into an effective drug product challenging. The Biopharmaceutical Classification System (BCS) class II APIs, which have been reported to account for as many as 40% of new chemical entities (1), present particular challenges in creating successful drug products. For example, BCS class II compounds do not readily dissolve in the biological media of the digestive tract and thus exhibit poor or variable bioavailability. Consequently, the major obstacle in formulating these compounds into successful commercialized products is the difficulty in enhancing the dissolution rate.

A number of strategies and processes have been reported to facilitate the dissolution of these poorly water soluble APIs. These include particle reduction/milling, solution based precipitation techniques, and emulsification/precipitation, etc., as described extensively in reviews (2-6). Cryogenic technologies, in particular, have been shown to enhance the dissolution rates of poorly water soluble APIs by creating highly porous nano-structured particles (7-10). The processes spray freezing into liquid (SFL) and spray freeze-drying (SFD) use cryogens, particularly N_2, to form a solid dispersion or solid solution (11) composed of nanoparticle domains of API within a polymer matrix. The particles are produced by rapidly freezing a feed solution in a cryogenic liquid and removing the solvent(s) through lyophilization. Micronized powders containing nanoparticles of API have been successfully manufactured with the SFL technology using a variety of different types of solvents (12, 13). Early work utilized aqueous co-solvent systems such as tetrahydrofuran (THF):water which has the ability to dissolve both a poorly water soluble API as well as hydrophilic excipients. Subsequently, organic

solvents such as acetonitrile (ACN) which have the unique ability to dissolve both an API and a hydrophilic excipient were used to increase API loading and reduce the risk of liquid-liquid phase separation. However, Hu et al. (14) found that increasing API loading has a profound effect on the surface morphology of the processed powders. Later, Rogers et al. (13) developed an oil-in-water (o/w) emulsion system in which the API and emulsifiers were dissolved in dichloromethane while hydrophilic stabilizers were dissolved in the aqueous phase. High pressure homogenization was used to reduce the mean diameter of the oil droplets to less than 1 μm before freezing the sample via the SFL process.

Ultra-rapid freezing (URF) was recently developed as a particle engineering technology designed to enhance the dissolution rates and bioavailability of poorly water soluble APIs (15). Briefly, the process involves freezing an API contained in a polymer solution onto the surface of a cryogenic substrate with a thermal conductivity k between 10-20 W/(m-K), collecting the frozen particles and removing the solvent. Because of rapid conductive heat transfer, resulting in high supersaturation and nucleation rates, the URF technology has the potential to create powders with superior physico-chemical properties, similar to those produced by other rapid freezing technologies. As in other freezing technologies, the rapid freezing of the API/polymer composition is critical in preventing phase separation during freezing, allowing for the active to be molecularly dispersed with the polymer. Recrystallization of the active is avoided by the inclusion of high glass transition temperature (T_g) polymers such as polyvinylpyrrolidone (PVP) or hypromellose (HPMC).

Previously, criteria for selection of the solvent(s) suitable for the SFL process included sufficient solubility of the solids and the ability to remove the solvent without re-crystallizing the API. These solvents generally have freezing points between 208K

and 273K which are ideal for tray lyophilization. Solvents with freezing points below 208K melt during lyophilization while solvents with freezing points higher than 273K may freeze prematurely within the atomizing nozzle. Because the URF technology applies the droplets directly onto the cryogenic substrate, premature freezing is not a concern and high freezing point solvents may be used. These solvents could prove beneficial by reducing the lyophilization time (16) or eliminating the solvent removal process altogether as some of these solvents sublime at ambient conditions or higher (17).

The objectives of this study are to introduce the URF technology as a novel method to manufacture pharmaceutical powders and to investigate how solvent properties and thin film geometry of the droplet affect the freezing rate and thus the physico-chemical properties of the final micronized powders. To determine the effect of the solvent properties, powders were manufactured from solutions from two solvents, tert-butanol (T-BUT) and ACN. T-BUT was selected for its higher freezing point and good lyophilization characteristics while ACN was selected for its good heat transfer properties. Heat transfer calculations of freezing rates are compared with those measured by infrared imaging. The model and results from imaging with a focal plane array infrared camera are complimentary and are utilized to demonstrate differences in freezing rates between the two solvent systems. The physico-chemical properties of the processed powders were compared to the unprocessed bulk API, and co-ground physical mixtures to assess the potential benefit of the URF technology. The powders were evaluated based on degree of crystallinity, surface area, surface morphologies, wettability and dissolution rate. It is hypothesized that the URF technology can produce powders with enhanced physico-chemical properties, for example low crystallinity and high surface area, leading to faster dissolution rates which could potentially enhance in vivo absorption for the BCS class II compounds.

4.2 MATERIALS AND METHODS

4.2.1 Materials

Micronized danazol (DAN), sodium lauryl sulfate (SLS), and polyvinylpyrrolidone (PVP) K-15 were purchased from Spectrum Chemicals (Gardena, CA). High performance liquid chromatography (HPLC) grade acetonitrile (ACN) was obtained from EM Science (Gibbstown, NJ), and tert-butanol (T-BUT) was purchased from Fisher Scientific (Fair Lawn, NJ).

4.2 Preparation of the URF micronized powders

The compositions were prepared by dissolving DAN and PVP K15 at a 1:2 ratio and 0.55% total solids in either T-BUT heated to 313K or ACN at room temperature. The DAN/PVP feed solutions were processed using the URF apparatus (schematic shown in Fig. 4.1). The feed solutions were applied to a cryogenic solid substrate cooled to a temperature range of 193 K to 243K, collected, and lyophilized using a VirTis Advantage benchtop tray lyophilizer (The VirTis Company, Inc. Gardiner, NY).

4.2.3 Preparation of control powders

The bulk API was used as received while the co-ground physical mixtures were prepared by adding the API and excipients to a glass mortar and pestle and mixed/triturated using the geometric dilution technique until a uniform powder was achieved.

4.2.4 Infrared imaging of freezing droplets

A single droplet of ACN or T-BUT was released from a pipette with a 2 mm diameter tip 10 cm above a cryogenically cooled surface and allowed to impinge on the surface of the cryogenic substrate. An InSb focal plane array (FPA) camera (Phoenix digital acquisition system (DAS) camera, Indigo Systems, Santa Barbara, CA) was

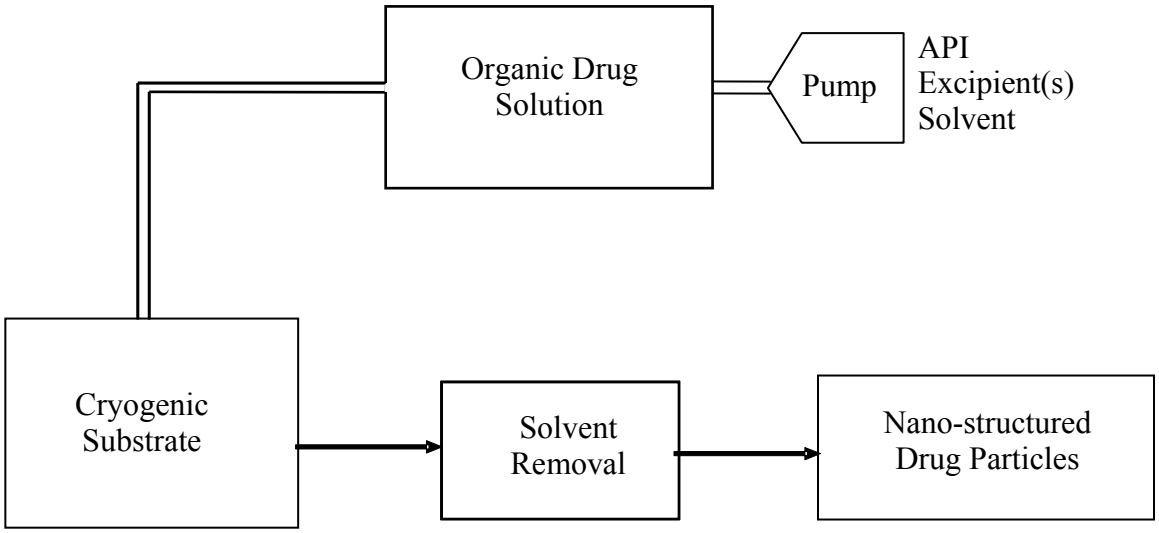

Figure 4.1: Schematic of URF technology

positioned to acquire infrared images from above the freezing droplet on the substrate. The FPA camera detected 3–5 μm radiation, and the images were acquired at 100 frames per second (10 ms/image). The dimensions of each frame were 256 pixels by 256 pixels (15 mm X 15 mm). The image spatial resolution was approximately 40 μm per pixel. Average intensity values were calculated using MATLAB® version 6 (20 x 20 pixel square within the center of the droplet) and plotted versus time to determine the time for the center of the droplet to reach thermal equilibrium with the substrate.

4.2.5 Scanning electron microscopy (SEM)

The powder samples were sputter coated with gold-palladium for 35 seconds and viewed using a Hitachi S-4500 field emission scanning electron microscope. An accelerating voltage of 5-15 kV was used to view the images. All SEMs pictured were representative of the entire sample.

4.2.6 Dissolution testing

Dissolution testing was performed on all powder samples using a United States Pharmacopeia (USP) 24 Type 2 apparatus (VanKel VK6010 Dissolution Tester with a Vanderkamp VK650A heater/circulator). The dissolution medium consisted of 0.3% SLS dissolved in de-ionized water and maintained at 37.0 ± 0.2°C throughout the study. Five ml samples were withdrawn at 2, 5, 10, 20, 30 and 60 minute time points, filtered using a 0.45μm GHP Acrodisc filter and analyzed using a Shimadzu LC-10 liquid chromatograph (Shimadzu Corporation, Kyoto, Japan) equipped with an Alltech ODS-2, 5 μm C_{18} column (Alltech Associates, Inc., Deerfield, IL). A 70:30 ACN:water mobile phase at 1 ml/min eluted the DAN peak at 5 min(11). The maximum absorbance was measured at λ=288 nm. System suitability requirements were met ($R^2 \geq 0.999$, precision $\leq$ 2.0% RSD).

4.2.7 X-Ray powder diffraction (XRD)

The x-ray diffraction patterns of all powder samples were analyzed using a Philips 1710 x-ray diffractometer with a copper target and nickel filter (Philips Electronic Instruments, Inc., Mahwah, NJ). The leveled powder was measured from 5 to 45 2θ degrees using a step size of 0.05 2θ degrees and a dwell time of one second.

4.2.8 Surface area analysis

Specific surface area was measured using a Nova 2000 v.6.11 instrument (Quantachrome Instruments, Boynton Beach, FL). A known weight of powder was added to a 12 mm Quantachrome bulb sample cell and degassed for a minimum of three hours. The sample was then analyzed (n=3) by the NOVA Enhanced Data Reduction Software v. 2.13 via the Brunauer, Emmett, and Teller theory of surface area (18).

4.2.9 Contact angle measurement

A 50 mg aliquot of sample powder was compacted wit a Model M Carver laboratory press (Fred S. Carver, Inc., Menomonee Falls, WI) using a compaction force of 500 kg to form a smooth surfaced tablet. A 3 μl drop of purified water was added to the surface of the tablet and the contact angle was quantitated using a goniometer (Ramè-Hart Inc., Mountain Lakes, NJ) by measuring the tangent to the curve of the droplet on the surface of the tablet.

4.2.10 Statistical analysis

The data were compared using a Student's t-test of the two samples assuming equal variances to evaluate the differences. The significance level ($\alpha = 0.05$) was based on the 95% probability value ($p < 0.05$).

4.3 RESULTS

4.3.1 Infrared measurements of cooling droplets on cryogenic plate

An infrared (IR) camera was used to quantitate the amount of IR energy radiated from the spread droplet over time on a cryogenic plate. The IR camera outputs intensity values assigned on a grayscale with white having a high intensity and black having a low intensity in relation to the amount of radiant energy emitted from the droplet. A thermal equilibrium was established when the intensity value was constant over time, indicating that the rate of heat transfer approached zero. It is estimated that at thermal equilibrium, the temperature of the droplet is near the temperature of the cryogenic substrate and confirmed via direct thermocouple measurement using a surface measuring probe. As the droplets enter the field of view, they appear white for both ACN and T-BUT. Fig. 4.2 and 4.3 contain time lapse IR photographs for ACN and T-BUT, respectively. In addition, IR video for the ACN and TBUT droplets can be seen in MovieACN and MovieTBUT, respectively. The videos more clearly demonstrate the freezing process occurring for the time lapse pictures in Fig. 4.2 and 4.3. For ACN, complete spreading of the droplet occurred within the first 10 ms interval indicating that the time of droplet spreading, tspreading, was much less than the freezing time, tfreeze. Therefore, t = 0 was defined as the first frame in which impingement was observed. When dropped from a height of 10 cm, the diameter for the spread ACN droplet as measured by a ruler and confirmed by IR camera was 1.9 cm. At t = 20 ms, the droplet began to visually darken evenly throughout the entire droplet. Since IR radiation between 3 and 5 microns is not readily absorbed by either ACN or T-BUT, it is believed that the initial darkening is a result of the cooling of the solvent near the droplet-surface interface. Between 20 and 70 ms, a cooling front is observed moving radially inward as the remaining droplet freezes.

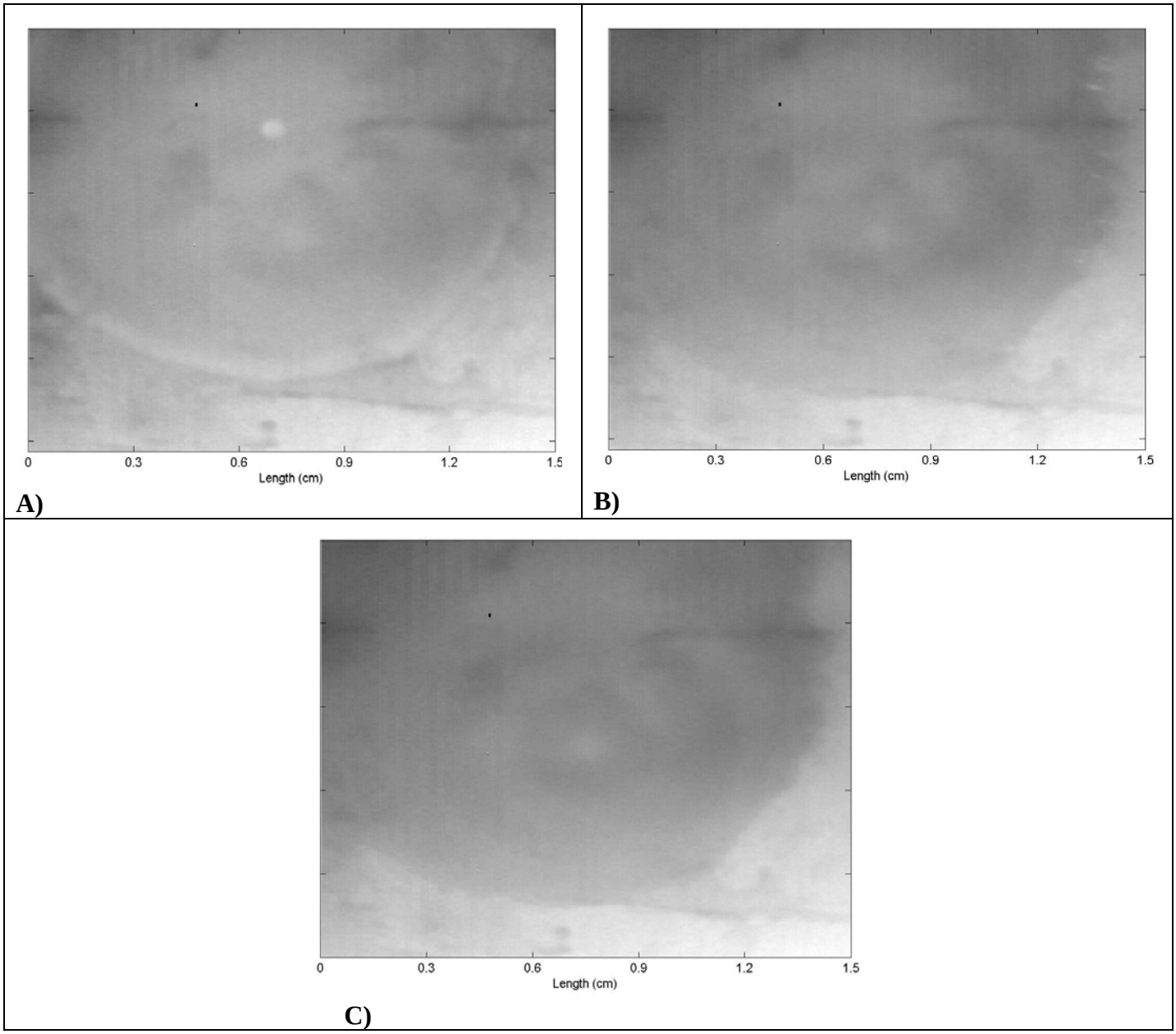

Figure 4.2: IR photographs of ACN droplet impinging and freezing on -60°C surface at t=0 ms (A), t=20 ms (B), t=70 ms (C)

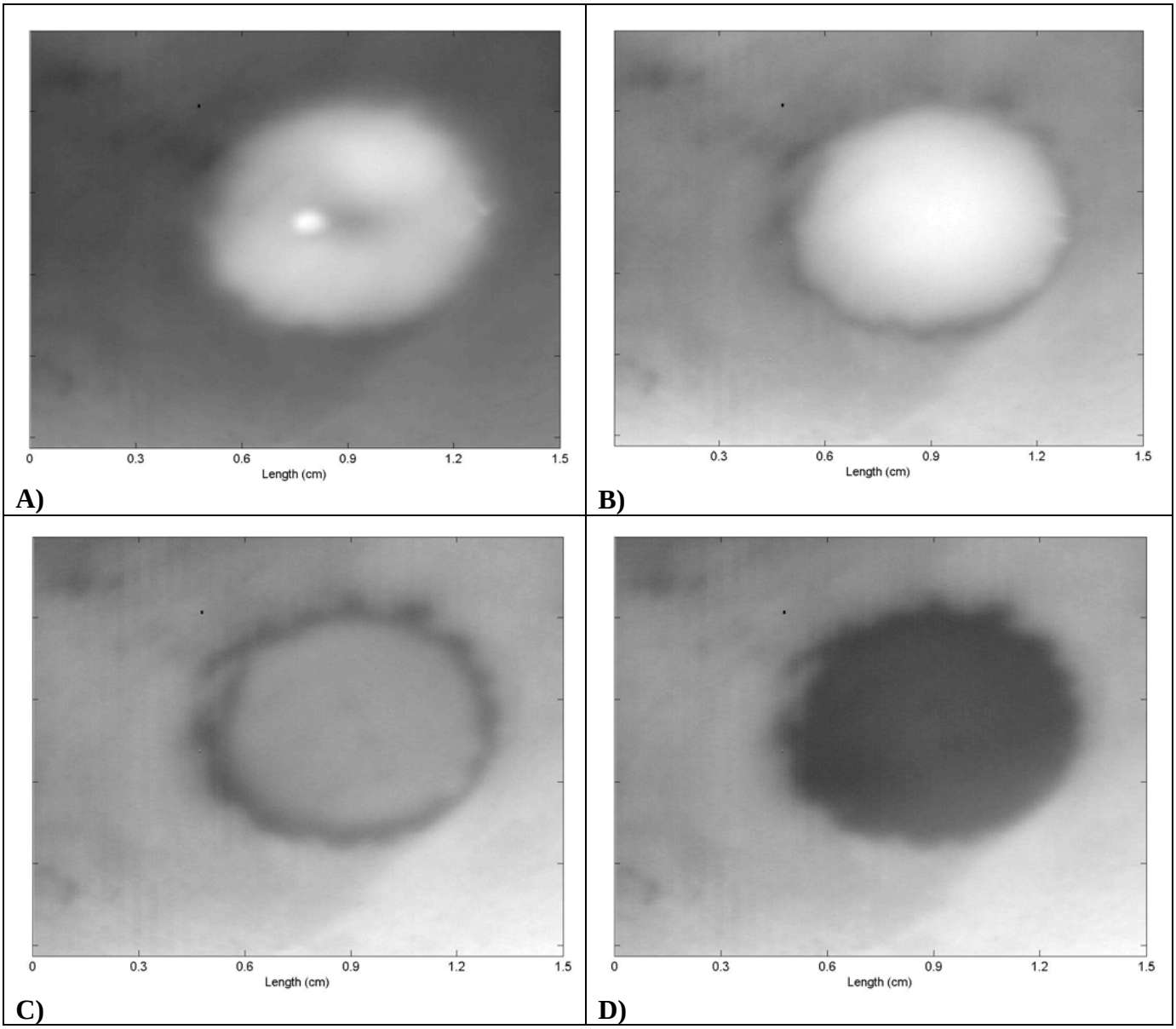

Figure 4.3: IR photographs of T-BUT droplet impinging and freezing on -60°C surface at t = 0 ms (A), t = 150 ms (B), t = 400 ms (C), t = 1000 ms (D)

After 70 ms a slight fluctuation in intensity is observed before thermal equilibrium around 2280 intensity units is established. Fig. 4.4A is a plot of the average intensity at the center of the ACN droplet as a function of time. After a rapid decrease in intensity is initially observed in which the bottom of the solvent immediately freezes, the rate begins to slow slightly until a minimum intensity value of 2280 is reached at 70 ms.

With a melting point near room temperature (296-298 K), the T-BUT samples were heated to 313 K to prevent premature freezing before spreading of the droplet on the cryogenic surface. As in the case of the ACN droplet, impingement and complete spreading of the T-BUT droplet also occurred within the first 10 ms interval. When dropped from a height of 10 cm, the spread diameter for the frozen T-BUT droplet measured 0.8 cm, less than half that of the ACN droplet. At 150 ms, the appearance of a black ring around the edge of the droplet appears indicating that the cooling rate is faster near the edge of the droplet (Fig 4.3B). As cooling continues, the cooling front proceeds radially inward towards the center of the droplet and has much greater contrast than observed with the ACN droplet. At 400 ms, IR intensity throughout the droplet was decreased (Fig 4.3C) and at 1000 ms thermal equilibrium was established (Fig. 4.3D). Similar to the case for the ACN droplet, the first few frames indicate a sharp decrease in intensity as the liquid in contact with the cryogenic surface immediately cools (Fig. 4.4B). After the initial drop in intensity where the droplet freezes instantaneously at the solid liquid interface, the rate of intensity decrease begins to slow and becomes much slower than for the ACN droplet. Since solidification occurs in the axial direction according to this model, the resulting solid solvent and solid API/polymer particles act as an insulating layer (19) decreasing the rate of heat transfer. Ultimately, the droplet thermally equilibrates around 2030 at around 1000 ms.

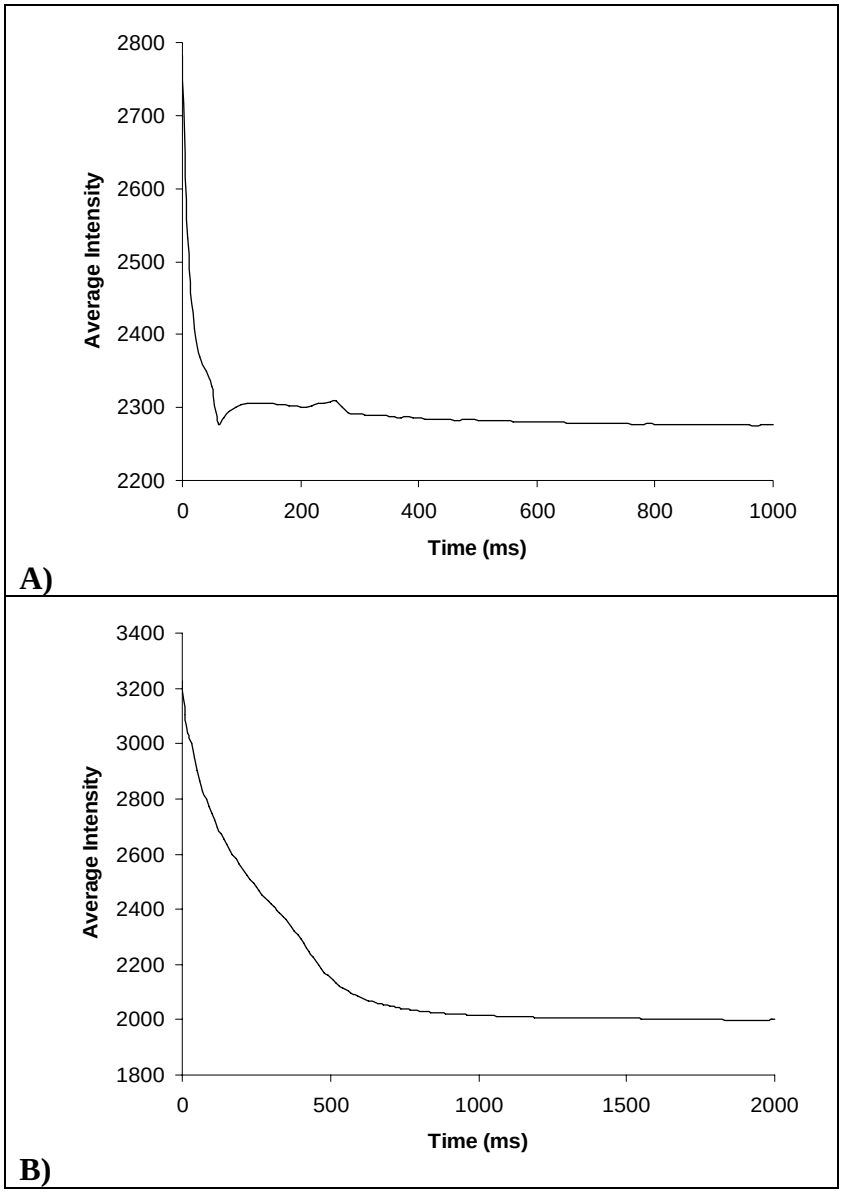

Figure 4.4: IR droplet intensity vs. time for ACN (A) and T-BUT (B)

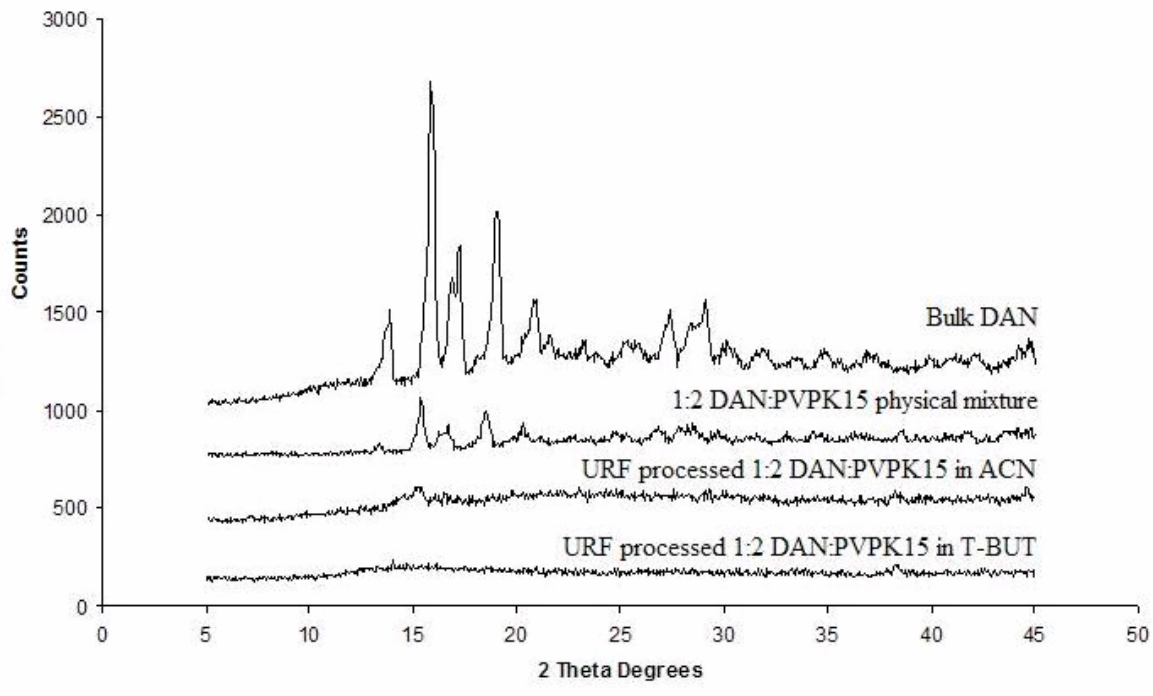

Figure 4.5: X-ray diffraction patterns of processed DAN:PVP compositions compared to bulk DAN

4.3.2 Physico-chemical properties and dissolution rates of URF processed powders

DAN powders were produced using the URF technology, and the physico-chemical properties were compared to the bulk API and the physical mixture. The characteristic crystalline peaks for DAN were found at 15.90 and 19.15 2θ degrees with a doublet peak around 17.30 2θ degrees, as seen in the bulk DAN and physical mixture samples in Fig 4.5. The physical mixture sample showed a reduction in crystalline intensity due to the dilution of PVP in the sample. Both URF processed powders lacked the characteristic crystalline peaks and therefore were considered to contain amorphous DAN. This is attributed to the rapid freezing occurring during the URF process and the ability of PVP to inhibit crystal growth.

As seen in Table 4.1, high specific surface areas (SSA) were reported for both the URF processed powder from T-BUT, with values of 29.3 and 25.9 m^2/g, respectively. The SSA was 50-60X greater than that of the micronized bulk DAN and about 40X greater than that of the physical mixture.

Differences between the two URF processed powders are evident in the surface morphology. The URF processed powder from ACN showed compacted aggregates of uniform nanoparticles with diameters of about 100 nm or smaller (Fig. 4.6A) in all areas of the sample. The surface morphology of the 1:2 DAN:PVP composition dissolved in T-BUT and processed by URF indicated regions of nanoparticles with similar particle sizes (Fig. 4.6B); however, particle sizes were not as uniform as those present from powders produced from ACN. Likewise, other areas of the powder exhibited very thin plate-like domains.

Dissolution rates for the processed powders are compared in Fig. 4.7 with those of the bulk DAN and the physical mixture. Samples processed from URF revealed rapid dissolution with at least 85% API dissolved within 10 minutes and showed statistically

greater release than the bulk DAN and the physical mixture ($p<0.05$). The URF processed powders produced from both T-BUT and ACN had nearly identical dissolution profiles ($p>0.05$). The similar profiles may be rationalized by the observation that both compositions were amorphous and had similar and very high surface areas. These factors produced very rapid dissolution rates. Inclusion of PVP in the physical mixture increased the dissolution only slightly, relative to pure danazol indicating that the low surface area and crystallinity of DAN limited the dissolution rate.

Contact angle measurements for both the processed powders and the physical mixture of 1:2 DAN:PVPK15 showed a statistically significant ($p<0.05$) decrease in contact angle (30.5°-39.5°) compared to the bulk DAN (64.0°) indicating better wettability of the powders as seen in Table 4.1. The contact angles of the powders processed by URF are slightly lower than those of the physical mixture, although there is no statistical difference ($p>0.05$). This is most likely due to the high levels of PVP in both the processed powders and the physical mixture.

4.4 DISCUSSION

4.4.1 Theoretical modeling

The phenomena of droplet spreading and solidifying/freezing for an impinging droplet on a solid substrate have been studied extensively by many research groups (19-32). The fluid dynamics and heat transfer can be coupled requiring a numerical solution. However, in our IR imaging studies the heat transfer was much slower than the droplet spreading. Thus the model can be solved analytically to describe the cooling rate in URF (33). The validity of the model will be evaluated by comparison to the experimental IR data for ACN and T-BUT.

In the model it is first assumed that droplet spreading after impact occurs on a much shorter time scale than heat transfer. Consequently, significant heat transfer does

Table 4.1: Surface area and contact angles of the URF compositions investigated

Composition	Surface Area (m^2/g)	Contact Angle (°)
URF 1:2 DAN:PVPK15 (in ACN)	25.93	30.5 ± 0.5
URF 1:2 DAN:PVPK15 (in T-BUT)	29.33	32.5 ± 0.5
Phys. Mix. 1:2 DAN:PVPK15	0.69	39.5 ± 4.5
Bulk DAN	0.52	64.0 ± 3.0

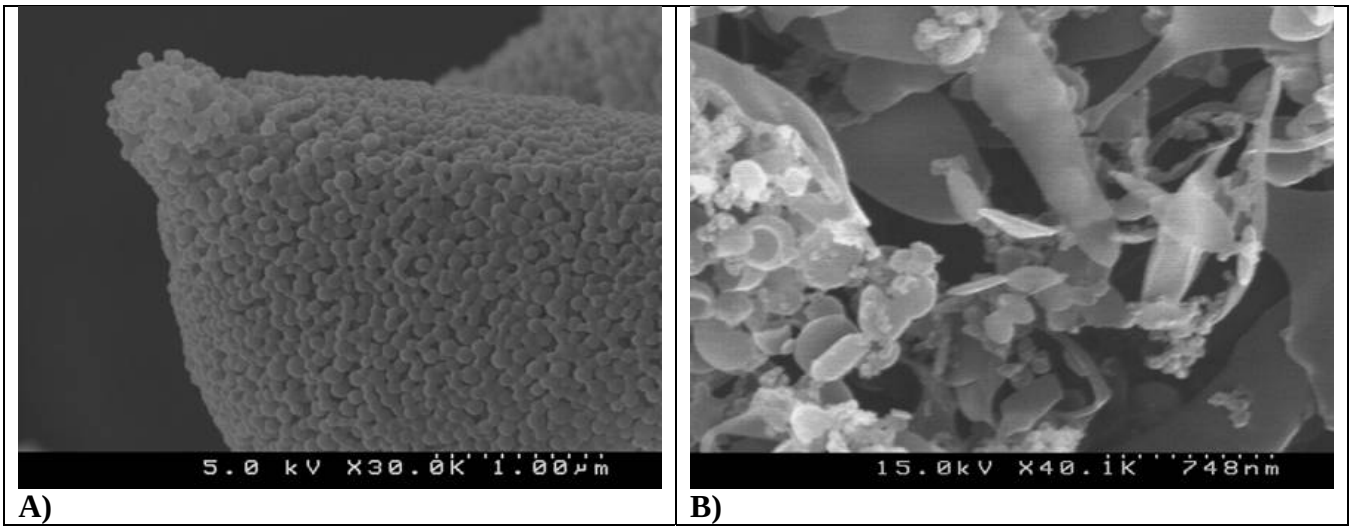

Figure 4.6: SEM micrographs of URF processed 1:2 DAN:PVPK15 in ACN (A), URF processed 1:2 DAN:PVPK15 in T-BUT (B)

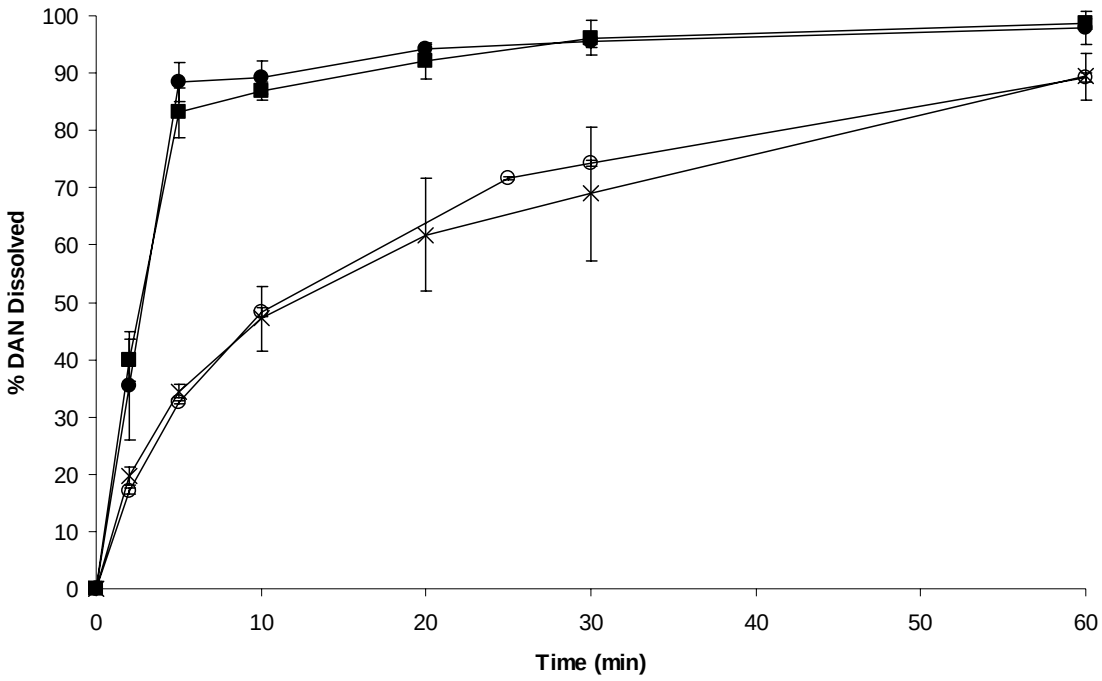

Figure 4.7: Dissolution profile for URF processed 1:2 DAN:PVPK15 in ACN (●), URF processed 1:2 DAN:PVPK15 in T-BUT (■),1:2 DAN:PVPK15 Physical mixture (○), Bulk DAN (x)

not occur until spreading is complete. The second assumption is that the droplet spreads to form a thin cylindrical disk. Because of the small height of the disk relative to the diameter, the third assumption is that only one-dimensional heat transfer is present in the z direction. Conduction in the radial direction through the thin disk parallel to the surface may be neglected. The final assumption is that the thermal diffusivity α is constant over the entire temperature range and remains unchanged during the phase change of freezing. Given the above assumptions the transient heat transfer equation through the cylindrical disk simplifies to (19)

$$\frac{\partial T}{\partial t} = \alpha \frac{\partial^2 T}{\partial x^2} \tag{1}$$

where the temperature T is a function of time t and x is the distance into the disk from the top surface of the thin film exposed to air. The thermal diffusivity of the spread droplet is defined as $\alpha = k / \rho \cdot C_p$, where k is the thermal conductivity, ρ is the density, and C_p is the heat capacity.

The first boundary condition for Eq. 1 assumes that heat transfer through the top surface of the disk exposed to the air is negligible. Therefore, the air is assumed to act as an insulator. The second boundary condition assumes the cryogenic plate temperature, T_{plate}, remains constant during the cooling process with negligible heat transfer resistance between the plate and spread droplet. These boundary conditions are

$$\left.\frac{\partial T}{\partial x}\right|_{x=0} = 0 \tag{2}$$

$$T(L,t) = T_{plate} \tag{3}$$

Here x = L is the bottom surface of the disk in contact with the plate. The initial condition assumes that the droplet temperature is uniform before impact and is defined as:

$$T(x,0) = T_i \tag{4}$$

where T_i is the initial solvent temperature. Equation 1 is then solved analytically for a finite disk thickness (33) to give

$$T(x,t) = T_{plate} + \frac{2}{L}\sum_{n=0}^{\infty} e^{-\alpha(2n+1)^2\pi^2 t/4L^2} \cos\frac{(2n+1)\pi x}{2L}\left\{\frac{2L(-1)^{n+1}T_{plate}}{(2n+1)\pi} + \int_0^L T_i \frac{\cos(2n+1)\pi x'}{2L}dx'\right\} \tag{5}$$

where L is the disk thickness. Cooling times are then determined by calculating the time, t, it takes for the surface of the solvent film at x = 0 with thickness L to reach a given temperature T using the software MATHCAD® version 11.

The spread droplet thickness was easily determined with the assumption that the droplet impacting on the cold substrate deformed into a cylinder with an equivalent volume to the original droplet volume before impact. Droplet volume was determined by dropping 100 droplets into a graduated cylinder and measuring the total volume. Frozen spread droplet diameters were measured with a ruler across two directions and averaged for 10 droplets. Droplet thicknesses were then calculated from the known volume of the falling droplet and the diameter of the frozen spread droplet and were 109 ± 10 μm and 403 ± 32 μm for ACN and T-BUT, respectively. Modeling the frozen spread droplet as a thin cylindrical disk has been used in many previous models (21-23, 26, 34) and has been experimentally justified when the Weber number, $We = \rho V^2 D/\gamma$ (inertial to interfacial forces), of the impacting droplet is >>1 (27) where V is the impact velocity, D is the

droplet diameter, and γ is the droplet interfacial tension. The impact velocity, V was calculated from the free-fall equation in a gravitational field, $V = (2gH)^{1/2}$ (34) where the falling height, H, of the droplet was 10 cm resulting in an impact velocity of 1.4 m/s. The densities and interfacial tensions for each solvent were determined using the DIPPR database (Brigham Young University, Provo, UT) at the initial temperatures of 298 K and 313 K for ACN and T-BUT, respectively. The resulting We numbers were 207 and 274 for the ACN and the T-BUT droplets, respectively, which supports the assumption that the impinging droplets deform into thin cylindrical disks (27). The thermal diffusivity, α, used for each solvent in this model was determined by first taking the average of each property in the definition of α evaluated between the initial droplet temperature to the freezing temperature of each solvent.(Table 4.2). The α for each solid solvent was not determined since thermal conductivity values were not available for each solvent in solid form.

The calculation of cooling times for each solvent was based on the time it takes for the top of the spread droplet at x = 0 to reach a given temperature, T. The cooling time to reach the freezing point of each solvent was calculated first. Fig. 4.8A is the calculated temperature profile for an ACN spread droplet. After 72 ms the top of the spread droplet defined at x = 0 reaches the freezing point of ACN, 230 K. For T-BUT (Fig. 4.8B) the cooling time to reach the freezing temperature of 299 K was 483 ms. Since the freezing points of each solvent are greater than the surface temperature of the solid substrate, 213 K, the spread droplet will continue to cool below the freezing point until an equilibrium temperature is reached. Therefore, a cooling time was calculated for the droplet to reach an arbitrary temperature of 225 K, which is approximately 5% greater than the cryogenic substrate temperature. These times were 86 and 3037 ms for ACN and T-BUT, respectively.

Table 4.2: Thermal and physical properties used to calculate t_{freeze} for ACN and T-BUT.

Property	**ACN[a]**	**T-BUT[b]**
k (W/m-K)	0.218	0.121
ρ (g/cm^3)	0.811	0.774
C_p (J/g-K)	2.182	3.057
α (cm^2/s)	0.0012	0.00051
Estimated t_{freeze} (ms)	61	629
Measured t_{equil} (ms)	70	1000

[a]For ACN, the average values calculated at T_{freeze}=229K and T_i =298K.
[b]For T-BUT, the average values calculated at T_{freeze}=298K and T_i=313K

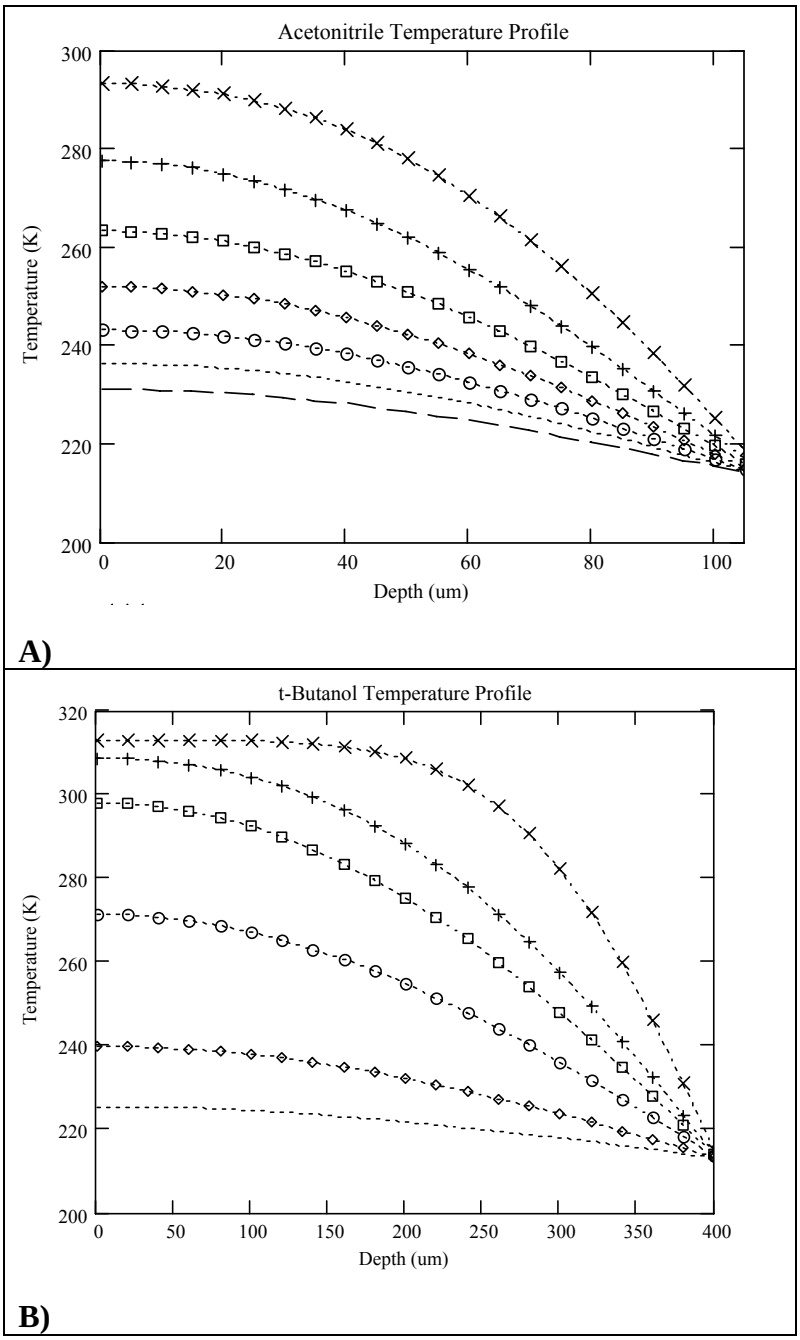

Figure 4.8: Theoretical temperature profile of ACN droplet (A) on a cryogenic surface at 10 ms (×), 20 ms (+), 30 ms (□), 40 ms (◊), 50 ms (○), 60 ms (···), 70 ms (-). Theoretical temperature profile of T-BUT droplet (B) on a cryogenic surface at 100 ms (×), 300 ms (+), 500 ms (□), 1000 ms (○), 2000 ms (◊), 3000 ms (···)

4.4.2 Comparison of ACN IR data to calculated cooling times

To evaluate the accuracy of the predictions of the proposed model, the calculated cooling times were compared to the IR images. The initial intensity of 2783 for time t = 0 ms correlated to the initial ACN temperature of 25ºC (Fig. 4.4). Due to the small thickness of the spread droplet it is reasonable to assume that the equilibrium intensity of 2280 at the top surface of the spread droplet is close to the temperature of the cryogenic substrate (213 K). The calculated cooling times to reach the freezing point, 230 K, and 225 K were 72 and 86 ms, respectively. The similarity in these times is consistent with the small difference in temperature between the freezing temperature and 225 K. The calculated cooling time is located at the bottom of the initial steep descent for the experimental curve in Fig. 4.4A. The calculated equilibrium cooling time occurs shortly thereafter at the beginning of the flat part of the intensity curve. The abrupt change in slope of the intensity curve near 70 ms may be an indication of ACN changing from the liquid to solid phase. The discontinuity in the slope of the intensity curve was confirmed when the experiment was repeated a second time. The good agreement between the calculated cooling times and the shape of the intensity curve supports the assumption that the heat transfer time is considerably slower, and essentially uncoupled, from the rapid spreading of the droplet on impact. Frame by frame analysis of the impinging ACN droplet showed that complete spreading occurred in less than 10 ms. Furthermore, the spreading diameter on the cryogenic substrate was similar to that on the same substrate at room temperature, indicating that cooling and freezing of the droplet did not inhibit spreading. Although the model calculates cooling times that are consistent with experimental IR data, it does not account for the radial cooling front observed during the latter stages of cooling of the spread ACN droplet. In spite of the radial cooling front

observed during cooling, the calculated cooling times do not vary significantly from the experimental cooling times.

4.4.3 Comparison of T-BUT IR data to calculated cooling times

The cooling behavior was substantially different for T-BUT compared to ACN. As shown in Fig. 4.3, cooling along the radial direction of the spread T-BUT droplet appeared to be significant. Also, after the T-BUT droplet impacted the cryogenic substrate the final spread droplet diameter was only 0.8 cm which was significantly smaller compared to the 1.9 cm formed on the same substrate at room temperature. The smaller spread diameter corresponds to a frozen spread droplet thickness 4X greater than ACN. The calculated cooling time to freezing (299 K) for T-BUT was 483 ms starting from an initial droplet temperature of 313 K. In (Fig. 4.4B) the approximate intensity value at t = 483 ms was 2185 which was slightly above the asymptotic equilibrium intensity (~213 K) of 2016, but well below the initial intensity of 3227 correlated to 313 K. The intensity curve reaches equilibrium at approximately t = 1000 ms which is assumed to correlate to an approximate spread droplet surface temperature of 213 K. The calculated time for the top droplet surface to reach the defined equilibrium temperature of 225 K was 3037 ms which is about 3 fold the experimental value of 1000 ms. However, the model correctly predicted that the experimental observation that the cooling was much slower than for ACN.

Various factors may contribute to the faster cooling in the experiments versus the model. The difference cannot be explained by cooling of the droplet during free fall. The free fall cooling effect on droplets, initially at 313 K, according to the model of Bennett and Poulikakos (34), would produce an insignificant change of less than 1K. The more rapid cooling for the experimental measurements may be the result of radial cooling as the droplet spread, and even after spreading. The movement of the radial

cooling front was about 30X slower for T-BUT than for ACN. Thus radial cooling appeared to play a greater role for T-BUT, which is consistent with the thicker disk for T-BUT, which corresponds to a greater cross-sectional surface area for radial conduction, and a smaller surface area for axial conduction.

The effect of radial cooling was shown for molten metal droplets impinging on a cold substrate by other research groups (19, 32). It was determined that significant heat transfer can occur during spreading of the droplet after impact (19, 32). Zhao et al. described that the radial cooling front occurs because during impaction high temperature solvent is continuously supplied to the center region of impact while the spreading front cools at a faster rate by contacting the low temperature surface of the substrate (32). Fukai et al. determined that the spreading diameter of droplets can be arrested on a cold substrate as the edges freeze (19). It is likely that the spreading diameter was reduced for T-BUT by freezing of the droplet edge, since the temperature difference from the initial droplet temperature (313 K) to freezing point (299 K) is only 14 K versus 68 K for ACN. The effect of radial cooling and partial cooling before complete spreading led to an overestimation by the model; however, it gave a reasonable result that was instructive for explaining the slower cooling for T-BUT versus ACN.

4.4.4 Influence of solvent system on powder properties

Even though there are substantial differences in the freezing characteristics of each solvent, both solvents produced powders comprising DAN and PVP with similar physico-chemical properties indicating sufficient cooling rates in both solvents. The URF technology was used to manufacture micronized powders containing DAN and PVPK15 in a 1:2 ratio using both ACN and T-BUT as the solvent system.

The rapid freezing of the URF technology produced powders with amorphous characteristics which can enhance dissolution rates through increasing the solubility

driving force (35) and lowering the heat of solution of the API (36). According to the contact angle measurements, wetting of the DAN was improved through the use of the hydrophilic polymer PVP which also acts as a stabilizer to prevent recrystallization of DAN. Even though no statistical difference was seen between the contact angles for the processed powders and the physical mixtures, higher potency powders produced from URF (not published) or SFL (11, 14) have shown significant differences in wetting compared to their physical mixture counterparts. Therefore, the decrease in contact angle was attributed to the high amount of PVP included in the composition which masked the increased in wetting attributed to the process. Despite the similar surface areas, the particle morphologies were very different. Both processed powder SEMs revealed discrete nanoparticle domains containing DAN. However, flat plate-like regions were also observed throughout the powder sample in Fig. 4.6B for T-BUT. This is attributed to a difference in cooling rates between the two solvents.(20, 29) The temperature decrease over time at the top of the droplet (x=0) is much slower for the T-BUT droplet which drops 17 degrees Kelvin in 600 ms compared to the ACN which drops 75 degrees Kelvin within 70 ms. The slower cooling for T-BUT provided time for growth to form the plate-like regions. The growth may have been non-uniform, as more time for growth was available closest to the air surface where the temperature was the highest. However, the freezing rates appeared to be sufficiently fast in both solvents to produce high surface area powders with low crystallinity. Differences in surface morphology could also be attributed to possible differences in solubility within the solvent based on the temperature-composition phase diagram of the API/polymer solution (37, 38). However, these diagrams were not determined and therefore, the extent of this phenomenon on the particle morphology is not known at this time.

4.5 CONCLUSIONS

Sample powders were prepared by URF technology from two different solvents with different thermal and physical properties, T-BUT and ACN. The differences in the thermal properties of the solvent and droplet dimensions had a dramatic effect on the cooling rate of the droplets as evidenced by the heat transfer model and IR studies. An axial heat transfer model for the spread droplets indicated ACN droplets cooled in 72 ms while T-BUT droplets required a much greater time of 483 ms. The much longer cooling time for T-BUT was also observed by FTIR imaging. However, it was found that the rate of cooling was sufficiently rapid in both solvents to produce amorphous powders with high surface areas on the order of 25.9-29.3 m^2/g and high wettability. Relative to physical mixtures, the URF processed powders had much more rapid dissolution profiles, which were attributed to nano-structured amorphous API domains, and the improved surface areas and wettability. The surface morphology of the powders was different for the two processing solvents, despite the similar surface areas. The primary particles in powders produced from ACN were spherical and uniform in size as a result of the more rapid and uniform cooling of the droplet relative to T-BUT. The use of ACN as a solvent allows for high heat transfer rates, which is beneficial for producing small rapidly dissolving particles, however, its low melting point can cause loss in particle surface area prior to solvent removal. T-BUT, on the other hand, has a lower (but sufficient) heat transfer rate compared to ACN, but is less susceptible to melting at ambient conditions prior to solvent removal. As a result of fast cooling rates and thus high supersaturation, the URF technology is a viable and robust process for producing high surface area nano-structured powders of poorly water soluble APIs with rapid dissolution rates, which will likely lead to enhanced bioavailability in vivo.

4.6 REFERENCES

1. C. Lipinski. Poor aqueous solubility - an industry wide problem in drug discovery. *Am. Pharm. Rev.* **5:**82-85 (2002).

2. R. H. Muller, K. Mader, and S. Gohla. Solid lipid nanoparticles (SLN) for controlled drug delivery - a review of the state of the art. *Eur. J. Pharm. Biopharm.* **50:**161-177 (2000).

3. A. A. Date and V. B. Patravale. Current strategies for engineering drug nanoparticles. *Curr. Opin. Colloid Interface Sci.* **9:**222-235 (2004).

4. K. S. Soppimath, T. M. Aminabhavi, A. R. Kulkarni, and W. E. Rudzinski. Biodegradable polymeric nanoparticles as drug delivery devices. *J. Control. Release* **70:**1-20 (2001).

5. J. M. Vaughn and R. O. Williams III. Nanoparticle Engineering. In J. Swarbrick (ed.), *Encyclopedia of Pharmaceutical Technology*, Dekker, In Press.

6. N. Rasenack and B. W. Mueller. Micron-Size Drug Particles: Common and Novel Micronization Techniques. *Pharm. Develop. Tech.* **9:**1-13 (2004).

7. J. Hu, P. Johnston Keith, and O. Williams Robert, 3rd. Nanoparticle engineering processes for enhancing the dissolution rates of poorly water soluble drugs. *Drug Dev. Ind. Pharm.* **30:**233-245 (2004).

8. H. Leuenberger. Spray Freeze-drying - The Process of Choice for Low Water Soluble Drugs? *J. Nanoparticle Res.* **4:**111-119 (2002).

9. Y.-F. Maa, P.-A. Nguyen, T. Sweeney, S. J. Shire, and C. C. Hsu. Protein inhalation powders: spray drying vs spray freeze drying. *Pharm. Res.* **16:**249-254 (1999).

10. T. L. Rogers, K. P. Johnston, and R. O. Williams III. Solution-based particle formation of pharmaceutical powders by supercritical or compressed fluid CO2 and cryogenic spray-freezing technologies. *Drug Dev. Ind. Pharm.* **27:**1003-1015 (2001).

11. J. M. Vaughn, X. Gao, M.-J. Yacaman, K. P. Johnston, and R. O. Williams. Comparison of powder produced by evaporative precipitation into aqueous solution (EPAS) and spray freezing into liquid (SFL) technologies using novel Z-contrast STEM and complimentary techniques. *Eur. J. Pharm. Biopharm.* **60:**81-89 (2005).

12. J. Hu, K. P. Johnston, and R. O. Williams. Spray freezing into liquid (SFL) particle engineering technology to enhance dissolution of poorly water soluble drugs: organic solvent versus organic/aqueous co-solvent systems. *Eur. J. Pharm. Sci.* **20:**295-303 (2003).

13. T. L. Rogers, K. A. Overhoff, P. Shah, P. Santiago, M. J. Yacaman, K. P. Johnston, and R. O. Williams III. Micronized powders of a poorly water soluble drug produced by a spray-freezing into liquid-emulsion process. *Eur. J. Pharm. Biopharm.* **55:**161-72 (2003).

14. J. Hu, K. P. Johnston, and R. O. Williams III. Rapid dissolving high potency danazol powders produced by spray freezing into liquid process. *Int. J. Pharm.* **271:**145-154 (2004).

15. J. C. Evans, B. D. Scherzer, C. D. Tocco, G. B. Kupperblatt, J. N. Becker, J. N. Wilson, S. A. Saghir, and E. J. Elder. Preparation of nanostructured particles of poorly water soluble drugs via a novel ultra-rapid freezing technology. In S. Svenson (ed.), *Polymeric Drug Delivery Volume II - Polymeric Matrices and Drug Particle Engineering*, American Chemical Society, Washington D.C., In Press.

16. N. Ni, M. Tesconi, S. E. Tabibi, S. Gupta, and S. H. Yalkowsky. Use of pure t-butanol as a solvent for freeze-drying: a case study. *Int. J. Pharm.* **226:**39-46 (2001).

17. M. S. Tesconi, K. Sepassi, and S. H. Yalkowsky. Freeze-Drying above Room Temperature. *J. Pharm. Sci.* **88:**501-506 (1999).

18. S. Brunauer, P. H. Emmett, and E. Teller. Adsorption of gases in multimolecular layers. *J. Am. Chem. Soc.* **60:**309-319 (1938).

19. J. Fukai, T. Ozaki, H. Asami, and O. Miyatake. Numerical simulation of liquid droplet solidification on substrates. *J. Chem. Eng. Jpn.* **33:**630-637 (2000).

20. G. X. Wang and E. F. Matthys. Numerical modeling of phase change and heat transfer during rapid solidification processes: use of control volume integrals with element subdivision. *Int. J. Heat Mass Transfer* **35:**141-53 (1992).

21. T. Bennett and D. Poulikakos. Splat-quench solidification: estimating the maximum spreading of a droplet impacting a solid surface. *J. Mater. Sci.* **28:**963-970 (1993).

22. B. Kang, Z. Zhao, and D. Poulikakos. Solidification of liquid metal droplets impacting sequentially on a solid surface. *J. Heat Transfer* **116:**436-45 (1994).

23. J. Madejski. Solidification of droplets on a cold surface. *Int. J. Heat Mass Transfer* **19:**1009-1013 (1976).

24. M. Pasandideh-Fard, R. Bhola, S. Chandra, and J. Mostaghimi. Deposition of tin droplets on a steel plate : simulations and experiments. *Int. J. Heat Mass Transfer* **41:**2929-2945 (1998).

25. M. Pasandideh-Fard, S. Chandra, and J. Mostaghimi. A three-dimensional model of droplet impact and solidification. *Int. J. Heat Mass Transfer* **45:**2229-2242 (2002).

26. C. Sanmarchi, H. Liu, E. J. Lavernia, R. H. Rangel, A. Sickinger, and E. Muehlberger. Numerical analysis of the deformation and solidification of a single droplet impinging onto a flat substrate. *J. Mater. Sci.* **28:**3313-21 (1993).

27. D. Sivakumar and H. Nishiyama. Numerical analysis on the impact behavior of molten metal droplets using a modified splat-quench solidification model. *J. Heat Transf.-Trans. ASME* **126:**1014-1022 (2004).

28. G. Trapaga and J. Szekely. Mathematical modeling of the isothermal impingement of liquid droplets in spraying processes. *Metall. Trans. B* **22B:**901-14 (1991).

29. G. X. Wang and E. F. Matthys. Modeling of heat transfer and solidification during splat cooling: effect of splat thickness and splat/substrate thermal contact. *Int. J. Rapid Solid.* **6:**141-74 (1991).

30. H. Zhang, X. Y. Wang, L. L. Zheng, and X. Y. Jiang. Studies of splat morphology and rapid solidification during thermal spraying. *Int. J. Heat Mass Transfer* **44:**4579-4592 (2001).

31. Z. Zhao, D. Poulikakos, and J. Fukai. Heat transfer and fluid dynamics during the collision of a liquid droplet on a substrate. II. Experiments. *Int. J. Heat Mass Transfer* **39:**2791-2802 (1996).

32. Z. Zhao, D. Poulikakos, and J. Fukai. Heat transfer and fluid dynamics during the collision of a liquid droplet on a substrate. I. Modeling. *Int. J. Heat Mass Transfer* **39:**2771-2789 (1996).

33. H. S. Carslaw and J. C. Jaeger. *Conduction of Heat in Solids*, Oxford University Press, London, 1959.

34. T. Bennett and D. Poulikakos. Heat transfer aspects of splat-quench solidification: modeling and experiment. *J. Mater. Sci.* **29:**2025-39 (1994).

35. B. C. Hancock and M. Parks. What is the true solubility advantage for amorphous pharmaceuticals? *Pharm. Res.* **17:**397-404 (2000).

36. K. Terada, H. Kitano, Y. Yoshihashi, and E. Yonemochi. Quantitative correlation between initial dissolution rate and heat of solution of drug. *Pharm. Res.* **17:**920-924 (2000).

37. C.-Y. Gao, A. Li, L.-X. Feng, X.-S. Yi, and J.-C. Shen. Factors controlling surface morphology of porous polystyrene membranes prepared by thermally induced phase separation. *Polym. Int.* **49:**323-328 (2000).

38. Y. S. Nam and T. G. Park. Porous biodegradable polymeric scaffolds prepared by thermally induced phase separation. *J. Biomed. Mater. Res.* **47:**8-17 (1999).

Chapter 5: Formation of Stable Submicron Protein Particles by Thin Film Freezing

Highly stable, submicron lactate dehydrogenase (LDH) and lysozyme particles may be produced by thin film freezing (TFF) of aqueous solutions followed by lyophilization. The LDH activity was determined by measuring the decrease in absorbance of NADH over time for the reaction of pyruvate to lactate. For lysozyme the particle morphology was determined by scanning electron microscopy (SEM) and compared with the specific surface area (BET) and the particle size, as measured by laser light scattering. Protein particles with an average diameter of 300 nm and 100% enzyme activity upon reconstitution (for LDH) were formed by TFF. Droplets of protein solutions, 3.6 mm in diameter, spread upon impact with 223 and 133 K metal surfaces to form cylindrical disks with thicknesses of 200-300 μm. Calculated cooling rates of the disks of 10^2 K/s were confirmed experimentally with infrared measurements. The cooling rates of 10^2 K/s, intermediate to those in lyophilization (1 K/min) and spray freeze-drying (SFD) (10^6 K/s), were sufficiently fast to produce sub-micron protein particles with surface areas of 31-73 m^2/g, an order of magnitude higher than in lyophilization. In addition, the low surface area/volume ratio (32-45 cm^{-1}) of the gas-liquid interface led to minimal protein adsorption and denaturation relative to SFD.

5.1 INTRODUCTION

The ability to produce high surface area stable submicron and micron-sized protein particles would create new opportunities for depot, pulmonary, and transdermal delivery applications (1-9). In pulmonary delivery, high surface area porous particles with aerodynamic diameters between 1-3 μm may be deposited more efficiently in the

deep lung compared to dense particles with similar aerodynamic diameters (1, 8). In depot delivery, 300-500 nm submicron protein particles have been encapsulated uniformly into 10-50 μm diameter microspheres to achieve high protein loadings, while minimizing burst release (4, 6, 10, 11).

Solid protein particles, stabilized by cryoprotectants including sugars, are often less susceptible to destabilization during storage (1, 12-17) relative to proteins in solution. However, the formation of stable submicron protein particles with surface areas exceeding 10 m^2/g (4, 18, 19) is highly challenging, as the removal of water exposes protein molecules to large interfacial areas. Adsorption of protein at gas-liquid and ice-liquid interfaces often results in unfolding and aggregation (1, 18-22). In lyophilization, the most common process for producing stable protein particles, particle growth during slow cooling (~1 K/min) limits the particle diameter to a minimum of a few microns with surface areas less than 1 m^2/g (21). The same limitation is true when drop freezing small aliquots (~20-50 μL) of protein solution into liquid nitrogen (23), freezing thick (>500 μm) films on a cooled shelf (24), and plunge freezing ultra-thin walled PCR tubes filled with protein solution into liquid nitrogen (23). In these techniques, the protein solution was cooled at rates between 1 to 10 K/s (23, 24). Although the dried particles may be milled to form submicron particles, yields can be limited, size distributions are often broad, and the mechanical stress can lead to denaturation (1, 21).

Submicron protein particles may be precipitated from aqueous solution by a variety of processes including spray-drying (11, 21, 22, 25), supercritical CO_2-assisted aerosolization and bubble drying (scCO_2A-BD) (26), spray freeze-drying (SFD) (1, 18, 19, 21), and spray freezing into liquids (SFL). In SFD, an aqueous solution containing dissolved protein is atomized into the cold gas above a cryogenic liquid (18, 19, 27-29). The 10 to 100 μm diameter atomized droplets travel through the cryogenic gas, where

they may begin to freeze (30), and freeze completely at a cooling rate of ~10^6 K/s after contacting the liquid cryogen. By systematically studying the effects of the separate spraying, freezing and drying steps in SFD, the large gas-liquid interface in the spraying step was shown to be the primary cause of protein aggregation for recombinant human interferon γ (rhIFN-γ) (19), lysozyme (31), and more recently lactate dehydrogenase (LDH) (32). The interfacially active protein adsorbs at this interface and subsequently unfolds and forms aggregates (1, 11, 18, 19, 21, 33).

To minimize exposure to the gas-liquid interface, the spray nozzle was immersed under the surface of the cryogenic liquid in the SFL process. This modification resulted in less protein adsorption, denaturation and aggregation, and consequently, higher enzymatic activities than in SFD (31, 32, 34, 35). The jet dimensions in SFL led to a cooling rate of ~10^3 K/s as a result of the Leidenfrost effect, in which evaporation of liquid nitrogen produced an insulating layer (32, 36, 37). The cooling rate was sufficiently fast to arrest the growth of submicron protein particles, without the need for ultra rapid cooling rates of 10^6 K/s in SFD (36). Thus, additional novel processes with cooling rates intermediate between those in SFD and lyophilization would be attractive for forming high surface area submicron particles, while mitigating the limitation of protein denaturation in SFD (31, 32, 36). Other freezing techniques such as plunge freezing into liquid cryogens, and thin film freezing (TFF), also known as cold metal block freezing, have been used to cool ~100 μm thick tissue samples at rates between 100 to 10,000 K/s (38-41), but protein solutions were not studied. The TFF process has been studied experimentally and modeled extensively for water and liquid metals (24, 42-44), but not for pharmaceutical formulations.

In the TFF process (Fig. 5.1) liquid droplets fall from a given height and impact, spread, and freeze on a cooled solid substrate. Recently TFF was used to form high SSA

powder (25-29 m^2/g) of the poorly water soluble drug danazol (45). Liquid droplets (~2-4 mm in diameter) were dispensed from a pipet above a cryogenically cooled metal surface (46, 47). Upon impact, the droplets spread out into thin films (~100-400 μm) that froze on time scales of 70 to 1000 ms, which corresponds to a cooling rate of $\sim 10^2$ K/s (42-44, 47-57). The cooling rates predicted with a 1-D heat transfer model were in agreement with experimental measurements with an infrared (IR) camera (45). Since the cooling rates in TFF and SFL are comparable, TFF may be expected to be a desirable process for forming high surface area protein particles.

The primary objective of this study was to demonstrate submicron LDH and lysozyme particles (>10 m^2/g) with 100% enzyme activity may be formed with TFF followed by lyophilization. The cooling rate was designed to be sufficiently fast to arrest particle growth, whereas the relatively small liquid-gas interfacial surface area helps prevent protein adsorption, unfolding and aggregation. The results section presents dimensions of the thin films, stabilities (enzyme activity) of LDH powders after reconstitution, and morphologies of lysozyme particles determined by SEM and BET measurements of surface area. The discussion section gives cooling rates of the thin films determined by a 1-D heat transfer model and IR measurement. A secondary objective was to compare the cooling rates, particle morphologies and protein stabilities for the intermediate cooling rate processes TFF and SFL, relative to the ultra-rapid cooling process, SFD, and in the slow process, lyophilization. A protein nucleation and growth mechanism is presented to explain the particle morphologies in terms of the cooling rates. In TFF, the much smaller area of the gas-liquid interface of the falling droplet and spread film relative to the atomized droplets in SFD will be shown to result in significantly less protein adsorption, and consequently, minimal denaturation and

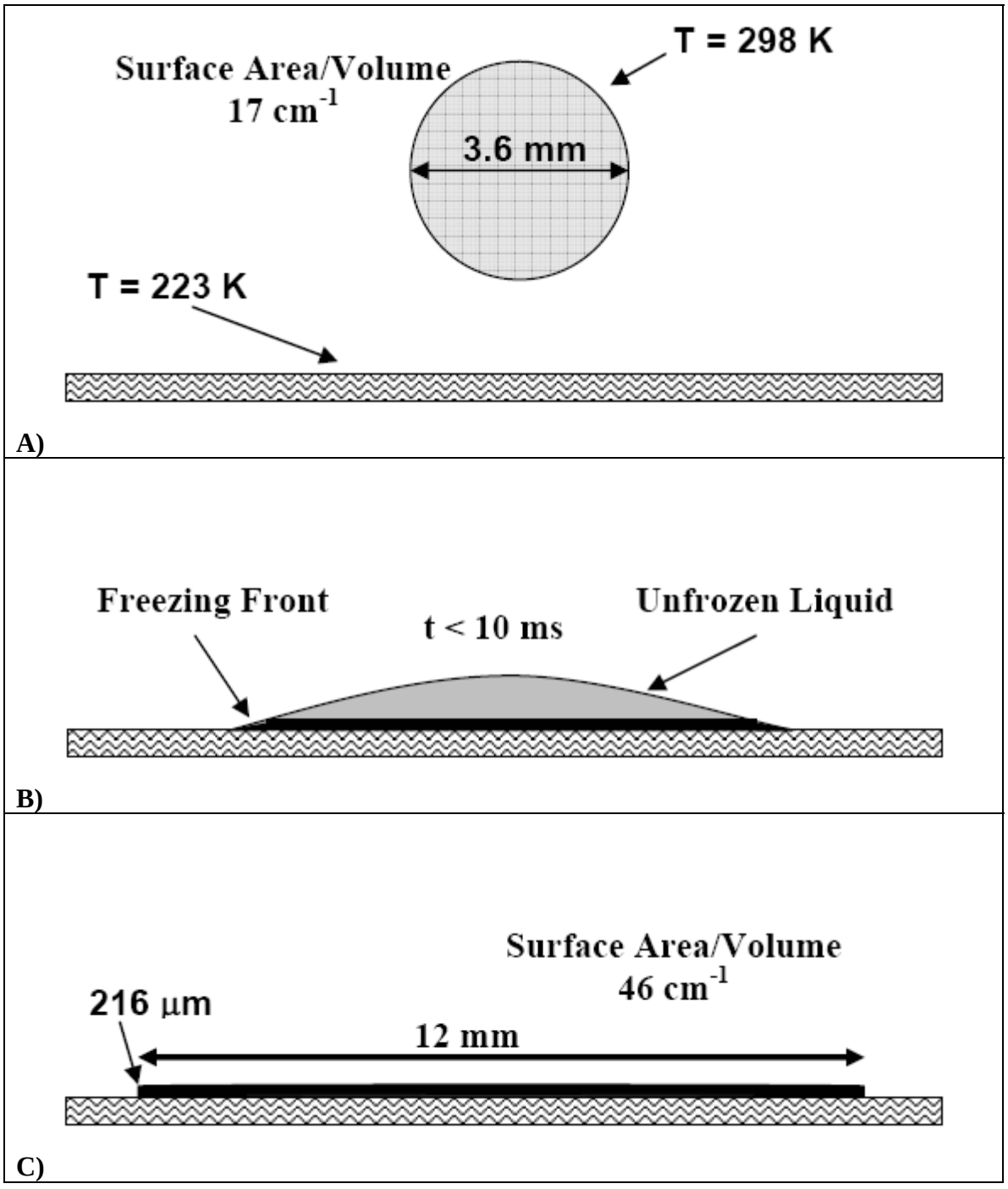

Figure 5.1: Diagram of the thin film freezing process displaying the falling droplet (A), spreading after impact on the stainless steel surface (B), and during cooling and freezing as a thin film (C) (drawn to scale).

aggregation. Furthermore, the intermediate cooling rate (~10^2 K/s) will be shown to be sufficient to arrest particle growth to give surface areas >30 m^2/g.

Compared to SFD and SFL, TFF offers the advantage of simplification in the processing steps, in addition to improvement in the stability of the protein. TFF on a cold metal surface bypasses the need to maintain aseptic conditions of a liquid cryogen, for example liquid nitrogen (24). The cooling rate of the thin films in TFF may be controlled readily by varying the temperature of the metal surface. Also, the surface temperature of the film may be measured directly (45). For SFL and SFD, the complex geometry of the turbulent spray in the liquid nitrogen (LN2) combined with the Leidenfrost effect can be somewhat difficult to control and monitor (36). In TFF, more concentrated and thus more viscous solutions may be processed, as the droplets are not atomized. In TFF, collection of the frozen films leads to nearly 100% yields. However, in SFD process yields were only about 80% as the result of entrainment of uncaptured particles in the atomized aqueous stream, particles sticking to the sides of collection vessels, and inefficient separation of the cryogen from the 10-100 μm frozen particles (11, 21). TFF is a simple, efficient and robust process for freezing either small (<1 mL) quantities of protein solution or commercial quantities, by freezing droplets in parallel.

5.2 MATERIALS AND METHODS

5.2.1 Materials

Lysozyme was purchased from Sigma (St. Louis, MO) and L-LDH from porcine heart suspended in a 3.2 M ammonium sulfate solution from Roche Applied Science (Indianapolis, IN). Trehalose, NADH and pyruvate were purchased from Sigma (St. Louis, MO). The water was deionized by flowing distilled water through a series of 2x7

L mixed bed vessels (Water and Power Technologies, Salt Lake City, UT) containing 60:40 anionic:cationic resin blends.

5.2.2 LDH enzyme preparation and catalytic activity assay

The LDH enzyme preparation and catalytic activity assay used in this study is described in detail in a previous study (32). The LDH in ammonium sulfate was dialyzed against 10 mM KPO_4 buffer (pH 7.5) at 4ºC for 3 hours before use (58, 59). LDH activities were measured for the reaction of pyruvate and NADH into lactate and NAD^+. Units of LDH activity (U) were calculated by measuring the decrease in absorbance of NADH at λ=340 nm every 15 seconds for 1 minute due to the conversion of NADH to NAD over time (U = $\Delta\mu$mol NADH/min) and then dividing by the mass (mg) of the LDH protein in solution to determine specific activity (U/mg). The stability of the LDH formulation in 30 mg/mL trehalose was measured over time. The LDH specific activity remained stable for an hour and then began to decrease. All experiments were performed in the time period where the LDH specific activity had not decayed. During this time period, the specific activity was defined as 100%.

5.2.3 Thin film freezing (TFF) procedure

Aqueous protein solutions of LDH or lysozyme were passed at a flow rate of 4 mL/min either through a 17 gauge (1.1 mm ID, 1.5 mm OD) stainless steel syringe needle producing 3.6 mm diameter droplets or through 3.9 mm ID, 6.4 mm OD stainless steel tubing producing 5.6 mm diameter droplets. The droplets fell from a height of 10 cm above a rotating stainless steel drum 17 cm long and 12 cm in diameter. The stainless steel drum was hollow with 0.7 cm thick walls and was filled with dry ice or liquid nitrogen to maintain drum surface temperatures of 223 K or 133 K, respectively. Before each run, the surface temperature of the drum was verified with a DiGi-Sense® Type K thermometer using a 45º angle surface probe thermocouple attachment (Eutech

Instruments, Vernon Hills, IL). The drum rotated at approximately 12 rpm and was powered by a Heidolph RZR2041 mechanical overhead stirrer (ESSLAB, Essex, UK) connected to a speed reducer (Cat. No. GS6013G, Baldor, Fort Smith, AR). On impact the droplets deformed into thin films (Fig. 5.1) and froze. The frozen thin films were removed from the drum by a stainless steel blade mounted along the rotating drum surface. The frozen thin films then fell 5 cm into a 400 mL Pyrex® beaker filled with liquid nitrogen. For lysozyme, the frozen thin films in the 400 mL Pyrex® beakers were transferred directly to a -80 °C freezer to evaporate excess liquid nitrogen. For LDH, the frozen thin films were transferred from the 400 mL Pyrex® beakers into 50 mL polypropylene tubes (Part No. UP2255, United Laboratory Plactics, St. Louis, MO) 2 cm in diameter and 16 cm in height using a spatula pre-cooled in liquid nitrogen.

5.2.4 Infrared imaging of cooling thin films

An InSb focal plane array (FPA) camera (Phoenix digital acquisition system (DAS) camera, Indigo Systems, Santa Barbara, CA) was positioned to acquire infrared images from above the cooling thin film on a flat plate. The FPA camera detected 3–5 μm radiation, and the images were acquired at 100 frames per second (10 ms/image). The dimensions of each frame were 256 pixels by 256 pixels (15 mm x 15 mm). The image spatial resolution was approximately 40 μm per pixel. Average intensity values were calculated using MATLAB® version 6 (20 x 20 pixel square within the center of the droplet) and plotted versus time to determine the time for the center of the thin film to reach thermal equilibrium with the plate.

5.2.5 Drying and shelf loading

A Virtis Advantage Lyophilizer (The Virtis Company, Inc., Gardiner, NY) was used to dry the frozen slurries. The 400 mL beakers containing frozen slurries of lysozyme and the 50 mL polypropylene tubes containing the frozen slurries of LDH were

covered with a single layer Kim-wipe. Primary drying was carried out at -40ºC for 36 hrs at 300 mTorr and secondary drying at 25ºC for 24 hrs at 100 mTorr. A 12 hour linear ramp of the shelf temperature from -40°C to +25°C was used at 100 mTorr.

5.2.6 LDH reconstitution and concentration assay

Dried LDH powders were reconstituted with 1 mL of DI water and the enzyme assay was performed immediately. After all protein samples had been analyzed for enzymatic activity, the protein concentration was measured with the BCA (bicinchoninic acid) protein analysis kit (Sigma Chemical Company, St. Louis, MO). Once protein concentrations were determined, the specific activity from each measurement could be calculated. The activity of each LDH sample was normalized by the specific activity of the control measured immediately before the freezing process.

5.2.7 Transfer and storage of dried powders

After the lyophilization cycle was complete, the lyophilizer was purged with nitrogen upon releasing the vacuum to reduce the exposure time of the protein powders to water vapor in the ambient air before transfer. The samples were then rapidly transferred to a dry box held at 14% RH, and the powders were transferred to 20 mL scintillation vials. The vials were then covered with 24 mm Teflon® Faced Silicone septa (Wheaton, Millville, NJ) which were held in place by open-top screw cap lids. Vials were purged with dry nitrogen for 2 minutes via a needle through the septa and an additional needle for the gas effluent.

5.2.8 Surface area measurement

Surface areas of dried powders were measured with a Quantachrome Nova 2000 (Quantachrome Corporation, Boynton Beach, FL) BET apparatus. Dried powders were transferred to the glass BET sample cells in a dry box. Samples were then degassed under vacuum for a minimum of 12 hours. The Brunauer, Emmett, and Teller (BET)

equation (60) was used to fit adsorption data of nitrogen at 77 K over a relative pressure range of 0.05-0.30. The samples were measured two times.

5.2.9 Residual moisture content

Aliquots of methanol were dispensed through the septum of the scintillation vials to form a suspension concentration of 10-100 mg/mL. Vials were then placed in a bath sonicator (Mettler Electronics, Anaheim, CA) for 5 minutes at maximum power to insure complete suspension of the powder. Moisture content was measured for a 200 μL aliquot with an Aquatest 8 Karl-Fischer Titrator (Photovolt Instruments, Indianapolis, IN). The moisture values were corrected with a 200 μL methanol blank control. All samples had a moisture content between 6-8% (w/w) after drying, comparable to values of 2-7% (w/w) for BSA prepared by SFD (18).

5.2.10 Particle size analysis

The size distribution of dried powders was measured by multiangle laser light scattering with a Malvern Mastersizer-S (Malvern Instruments, Ltd.,Worcestershire, UK). A mass of 30-100 mg of powder was suspended in 10 mL of acetonitrile and the suspension was then sonicated on ice for 1 minute using a Branson Sonifier 450 (Branson Ultrasonics Corporation, Danbury, CT) with a 102 converter and tip operated in pulse mode at 35 W. Typical obscuration values ranged from 11% to 13%. Aliquots of the sonicated suspension were then dispensed into a 500 mL acetonitrile bath for analysis.

5.2.11 Scanning electron microscopy

SEM images were collected on a Hitachi Model S-4500 scanning electron microscope (Hitachi Ltd, Tokyo, Japan). The samples were prepared in a dry-box. Aluminum stages fitted with double adhesive carbon conducting tape were gently dipped into sample vials until covered by powder. Stages were then placed in septum capped vials and purged with nitrogen for transfer. To minimize the time samples were exposed

to atmospheric moisture the stages were rapidly transferred to a Pelco Model 3 sputter-coater. A conductive gold layer was applied and the samples were then quickly transferred to the SEM. Total exposure to the atmosphere was less than 1 minute.

5.3 RESULTS

The thin films formed from DI water droplets were characterized as a function of surface temperature and droplet diameter (Table 5.1). The droplets spread on the cold metal surface and formed a cylindrical thin disk. The disk diameter decreased with a decrease in surface temperature from 223 K to 133 K and increased with an increase in falling droplet radius. By assuming the frozen thin films were cylindrical disks, the thicknesses of the thin films were calculated from the known volume of the liquid droplet and the measured disk diameter. The volumes of the falling droplets were determined by counting the number of droplets required to occupy 1 mL in a graduated cylinder. The average thin film thickness for the 223 K and 133 K surfaces were 220 μm and 320 μm, respectively. The corresponding surface area/volume ratios for the top surfaces of the cylinders are also shown (Table 5.1). The film thicknesses were essentially independent of the falling droplet diameter. For aqueous samples containing concentrations of lysozyme between 5 and 50 mg/mL or trehalose at 30 mg/mL, the droplet volumes, disk diameters, and thus film thicknesses did not change relative to pure water. The surface area/volume ratios for the 3.6 mm and 5.6 mm falling droplets in TFF were 17 cm^{-1} and 11 cm^{-1}, respectively. As shown in Table 5.1, upon impact the falling droplets spread into thin films with final surface area/volume ratios between 31 and 46 cm^{-1}. In a previous study (36) of SFD and SFL, the corresponding surface area/volume ratios were 6000 and 600 cm^{-1}, respectively (Table 5.1). Relative to these values, the much smaller

Table 5.1: Geometries of the freezing domains for the SFD, SFL, and thin film freezing processes

	SFD[a]	SFL[a]	Thin Film from 3.6 mm Drop[b]		Thin Film from 5.6 mm Drop[c]	
			223 K[d]	133 K[d]	223 K[d]	133 K[d]
Droplet or Thin Film Disk Diameter (μm)	10	100	12000	10000	23000	19000
Film Thickness (μm)	--	--	216	311	221	324
Droplet or Thin Film Surface Area to Volume (cm^{-1})	6000	600	46	32	45	31

[a]Values taken from Engstrom et al. (36)
[b]Surface Area to Volume of 3.6 mm droplet is 17 cm^{-1}
[c]Surface Area to Volume of 5.6 mm droplet is 11 cm^{-1}
[d]Temperatures of stainless steel plate

surface area/volume ratio for TFF may be expected to lower the degree of protein destabilization from exposure to the gas-liquid interface.

The thin films were further characterized by determining the cooling rates from infrared measurements. The IR camera outputs intensity values with white indicating a high intensity and black a low intensity in relation to the amount of radiant energy *E* (energy density per unit time per unit wavelength) emitted from the droplet (45, 61). The radiant energy E is related to the temperature of the object according to Planck's law:

$$E(\lambda, T) = (2\pi hc^2) / \left\{ \lambda^5 \left[\exp(hc / \lambda kT) - 1 \right] \right\} \qquad (1)$$

where λ is the wavelength, c is the speed of light, k is the Boltzmann constant, h is Planck's constant and T is the temperature in Kelvin (61). Therefore, the intensity output of the IR camera is related directly to the temperature.

For the thin film on the 223 K surface (Fig. 5.2A) the diameter of the film was 12 mm and the edge was uniform and smooth. As cooling progressed (Fig. 5.2A) a cooling front moved radially inward from the edge of the film toward the center. The center of the film reached thermal equilibrium in 1.6 s (Fig. 5.2A and Fig. 5.3). For the thin film on the 133 K surface (Fig. 5.2B), the diameter was 10 mm (Fig. 5.2B) and dark jagged "fingers" were observed at the edge, indicating the coldest domains. The cooling front moved radially inward from the edge to the center at first. Next the center turned black, and an annular region between the center and the outer jagged edge remained gray. The cooling front then reversed direction by moving from the center toward the edge of the film. The center of the film reached thermal equilibrium a little more slowly, in about 3 s (Fig. 5.3), relative to 223 K. In each case at the center of the film, a plateau was observed and then an abrupt final decay to thermal equilibrium.

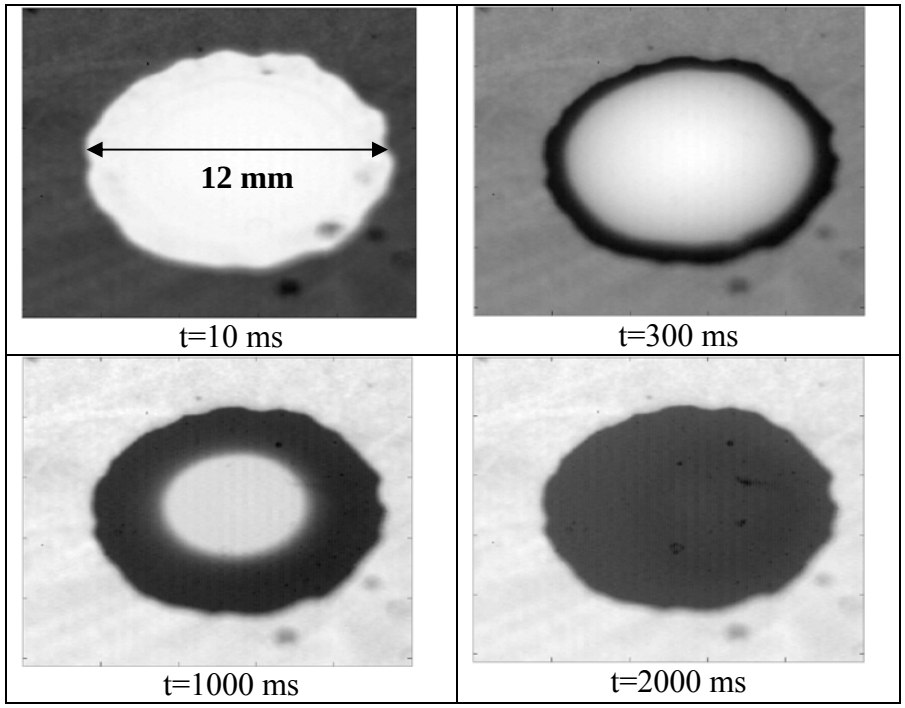

A)

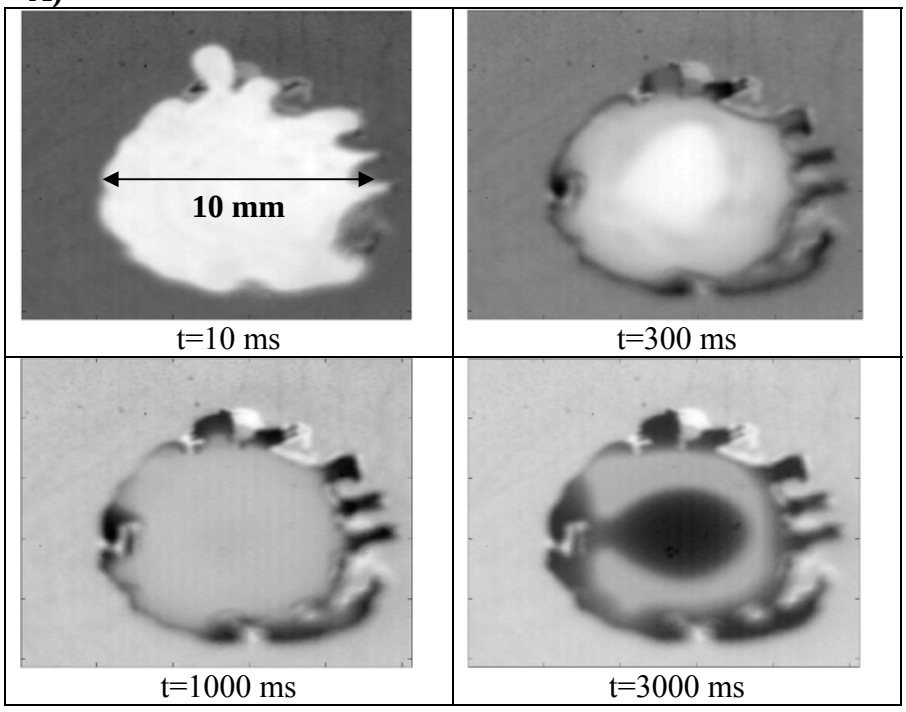

B)

Figure 5.2: IR photographs of an aqueous droplet impinging and freezing on a stainless steel surface at 223 K (A) and 133 K (B).

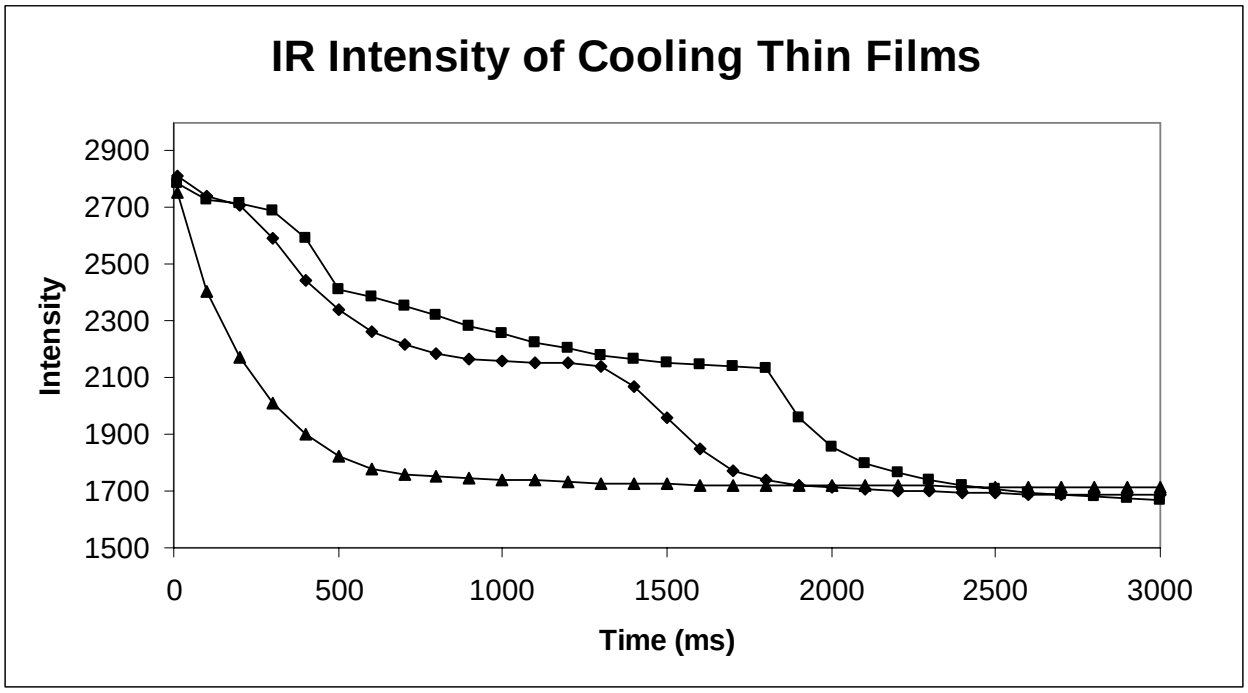

Figure 5.3: IR intensity versus time for an aqueous thin film on stainless steel surface at 223 K measured at the center of the film ◆ and near the edge of the film ▲ and at 133 K at the center of the film

Table 5.2: Activities for 0.25 mg/mL LDH, 30 mg/mL trehalose formulations frozen by various techniques in pH 7.5, 10 mM KPO_4 buffer in replicates of 3

	%Activity	
Freezing Process	**223 K**	**133 K**
Thin Film (3.6 mm drop)	100 ± 3.9	104 ± 12.0
Thin Film (5.6 mm drop)	97 ± 9.5	100 ± 8.4
SFL[a,d]	98 ± 5.3	
SFD-130 μm[a]	85 ± 8.2	
SFD-40 μm[a,e]	74 ± 6.7	
SFD-10 μm[a,d]	80 ± 5.4	
Falling Droplet (3.6 mm)[c]	98 ± 2.1	
Spray into Air (10 μm)[a,b,c]	85 ± 7.7	
Lyophilization	99 ± 2.1	

[a]Values taken from Engstrom et al. (32)
[b]100 mg/mL trehalose used in LDH formulation
[c]The droplets were not frozen in these two controls
[d]Replicate of 4
[e]Replicate of 5

The LDH activities for an aqueous formulation of 0.25 mg/mL LDH with 30 mg/mL trehalose frozen by lyophilization, SFL (32), and TFF were extremely high (Table 5.2) and not significantly different ($p < 0.05$) according to a Student's *t* test. Compared to the SFD process for three droplet sizes, the LDH activities for each TFF condition were significantly higher ($p < 0.05$). The very high LDH activities were maintained in the TFF process throughout the serial stresses of droplet falling and spreading, freezing, drying, and reconstitution.

Given the high enzyme activities for LDH particles formed by TFF, the other key goal was to demonstrate particle morphologies with submicron particle sizes and large particle surface areas (Table 5.3). In the case of LDH, the ratio of LDH:trehalose was 1:120 by mass. As discussed previously (32, 36), the particle surface area for trehalose decreased upon exposure to atmospheric moisture which lowers the T_g sharply. (This limitation may be overcome in the future with the use of lyostoppers to seal the vials from moisture.) Thus, we chose lysozyme as a model protein to investigate powder morphology instead of LDH:trehalose. Lysozyme samples obtained and transfered at room temperature had moisture contents between 6-8% as determined by Karl Fischer titration. For moisture contents between 7-8% by weight, the T_g remained high, between 50-60 ºC (62). Therefore the loss in lysozyme SSA during transfer may be expected to be negligible. For most cases, the SSA values were similar ranging between 30 and 55 m^2/g. For 5 mg/mL lysozyme, the thinner films at 223 K produced a significantly higher SSA of 73 m^2/g relative to the films at 133 K. In a previous study (36), 5 and 50 mg/mL lysozyme solutions processed by SFL had measured powder SSAs of 114 m^2/g and 34 m^2/g, respectively, similar to the values produced by TFF (36). Although the SSA of 126 m^2/g for SFD was about 2 fold larger than for TFF, the enzyme activity was much smaller, as shown in Table 5.2.

As shown in Table 5.3, the volume percentage of submicron particles, determined by laser light scattering, after sonication of the 5 mg/mL lysozyme formulation prepared by TFF at 223 K, ranged from 88 to 92%. The similarity in these two values was expected since the nearly identical thin film thicknesses would be expected to produce similar cooling rates. These values were similar to those for the SFL powders (36). For TFF, the protein powders were friable and could be broken up readily into submicron particles with minimal sonication. As shown in Fig. 5.4 the d(v,50) was 300 nm. In contrast, the same 5 mg/mL lysozyme formulation prepared by lyophilization had a very low fraction of 7% submicron particles (Fig. 5.4 and Table 5.3). As the lysozyme feed concentration was raised to 50 mg/mL the submicron fraction decreased to 66 and 62% on the 223 K and 133 K surfaces, respectively (Table 5.3). The corresponding value for SFL was lower (48%), whereas for SFD it was higher (74%) (36). For the SFD powders, the d(v,50) was approximately 300 nm (36). A second peak with micron-sized particles was present for the 50 mg/mL lysozyme solution prepared by SFL and TFF as shown in Table 5.3. However, 50 mg/mL is an unusually high protein concentration and TFF would ordinarily be applied to concentrations on the order of 5 mg/mL, where the second larger peak is not present (Fig. 5.4).

Selected SEM images from the results in Table 5.3 are shown in Fig. 5.5 and 5.6. For 5 mg/mL lysozyme, fine 50 nm primary particles were produced by TFF at 223 K (Fig. 5.5A), comparable to those produced by SFL (36) (Fig. 5.5C). At 133 K, larger 50-100 nm diameter particles were mixed with rods 50-100 nm in diameter and more than 500 nm long (Fig. 5.5B). The larger particles sizes shown in Fig. 5.5B compared to Fig. 5.5A are consistent with the slightly lower content of submicron particles measured by light scattering in Table 5.3.

Table 5.3: Specific surface area measurements and particle size distributions for lysozyme powders formed by thin film freezing, SFL, and SFD

		SSA (m^2/g)		Size (μm)	
Freeze Process	**Lysozyme Concentration (mg/mL)**	**223 K[a]**	**133 K[a]**	**223 K[a]**	**133 K[a]**
Thin Film (3.6 mm drop)	5	73±0.8	45±0.4	0.050-1.0 (88%) 1.0-10 (12%)	0.050-1.0 (81%) 1.0-12 (19%)
Thin Film (5.6 mm drop)	5	--	--	0.050-1.0 (92%) 1.0-12 (8%)	0.050-1.0 (84%) 1.0-10 (16%)
Thin Film (3.6 mm drop)	50	31±0.1	55±0.4	0.050-1.0 (66%) 1.0-30 (34%)	0.050-1.0 (62%) 1.0-30 (38%)
SFL[b]	5	114±11		0.050-1.0 (85%) 2.0-10 (15%)	
SFL[b]	50	34±2		0.050-1.0 (48%) 4.0-12 (52%)	
SFD-10 μm[b]	50	126±5		0.050-1.0 (74%) 1.0-10 (26%)	
Lyophilization	5	4.4±0.2		0.05-1.0 (7%) 4.8-120 (93%)	

[a]Temperatures of stainless steel plate
[b]Values taken from Engstrom et al. (36)

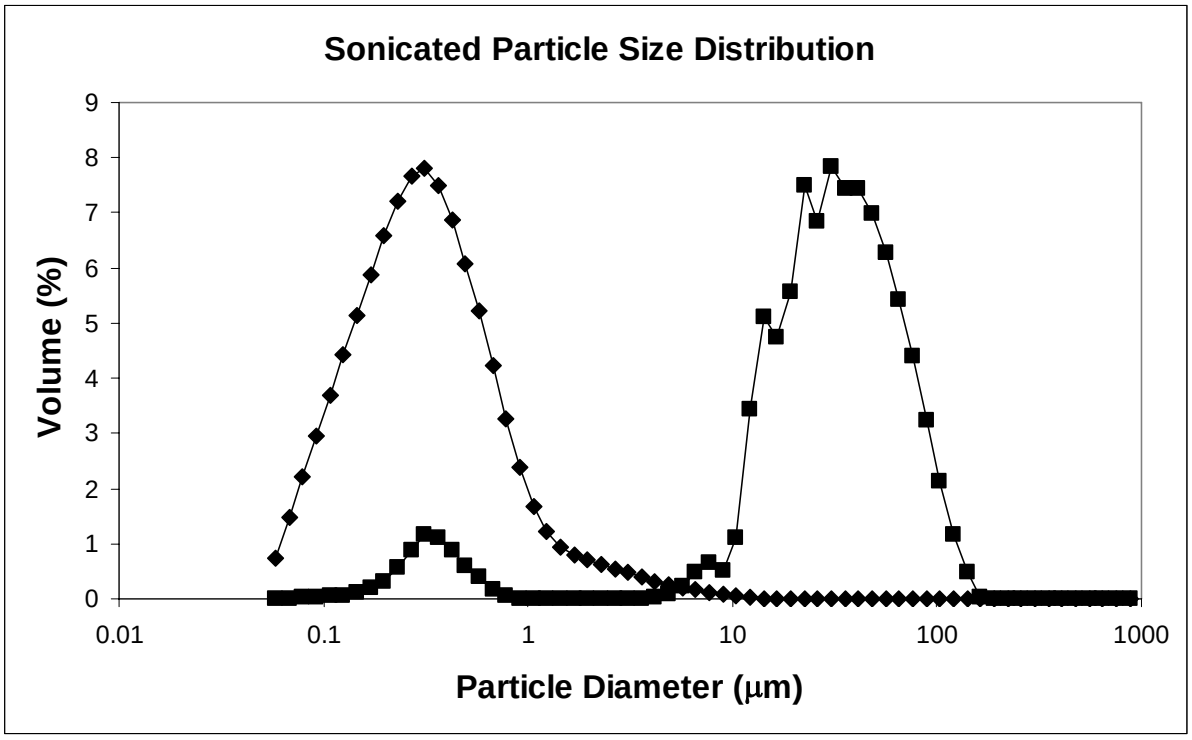

Figure 5.4: Laser light scattering of particles formed by thin film freezing (◆) and lyophilization (■)of 5 mg/mL lysozyme solutions followed by sonication.

For highly concentrated 50 mg/mL lysozyme solutions and a surface temperature of 223 K (Fig. 5.6A), large sheets were observed with features between 1 and 2 μm. Similar features were observed for SFL (36). In contrast, a fine web with 100 nm features were produced by SFD (36) (Fig. 5.6C) consistent with the smaller particle sizes measured by light scattering in Table 5.3. The larger features observed in the TFF and SFL processes for 50 mg/mL versus 5 mg/mL solutions are consistent with the particle size distributions measured by light scattering. The similarity of the particle morphologies for the powders prepared by the SFL and TFF processes at both the 5 and 50 mg/mL concentrations will now be examined in terms of cooling rates.

5.4 DISCUSSION

5.4.1 Modeling the cooling rate of thin films

Droplet spreading to form thin films of liquid metal and water droplets has been described in term of the Weber number, $We = \rho V^2 D / \gamma$ (inertial to interfacial forces) where V is the impact velocity, D is the droplet diameter, and γ is the droplet interfacial tension in air. For We > 30 immediately before impacting the cooled solid substrate (42, 48-50, 56, 63) the droplets deformed into cylindrical thin films before freezing. For the low We < 1 regime, impacting droplets froze as spherical domes with minimal droplet spreading (49, 64). For the falling liquid droplets in this study γ(air-water) = 72 mN/m and $V = (2gH)^{1/2}$ (65) where the falling height, H, of the droplet was 10 cm, resulting in V= 1.4 m/s. The observed formation of thin cylindrical disks was consistent with this We of 97, but when H was reduced to less than 1 cm (We = 9.8) the impacting water droplets froze as spherical domes that were only 4 mm in diameter.

Previously it was shown with IR imaging studies of thin films formed with acetonitrile and t-butanol that droplet spreading occurred within the first 10 ms interval

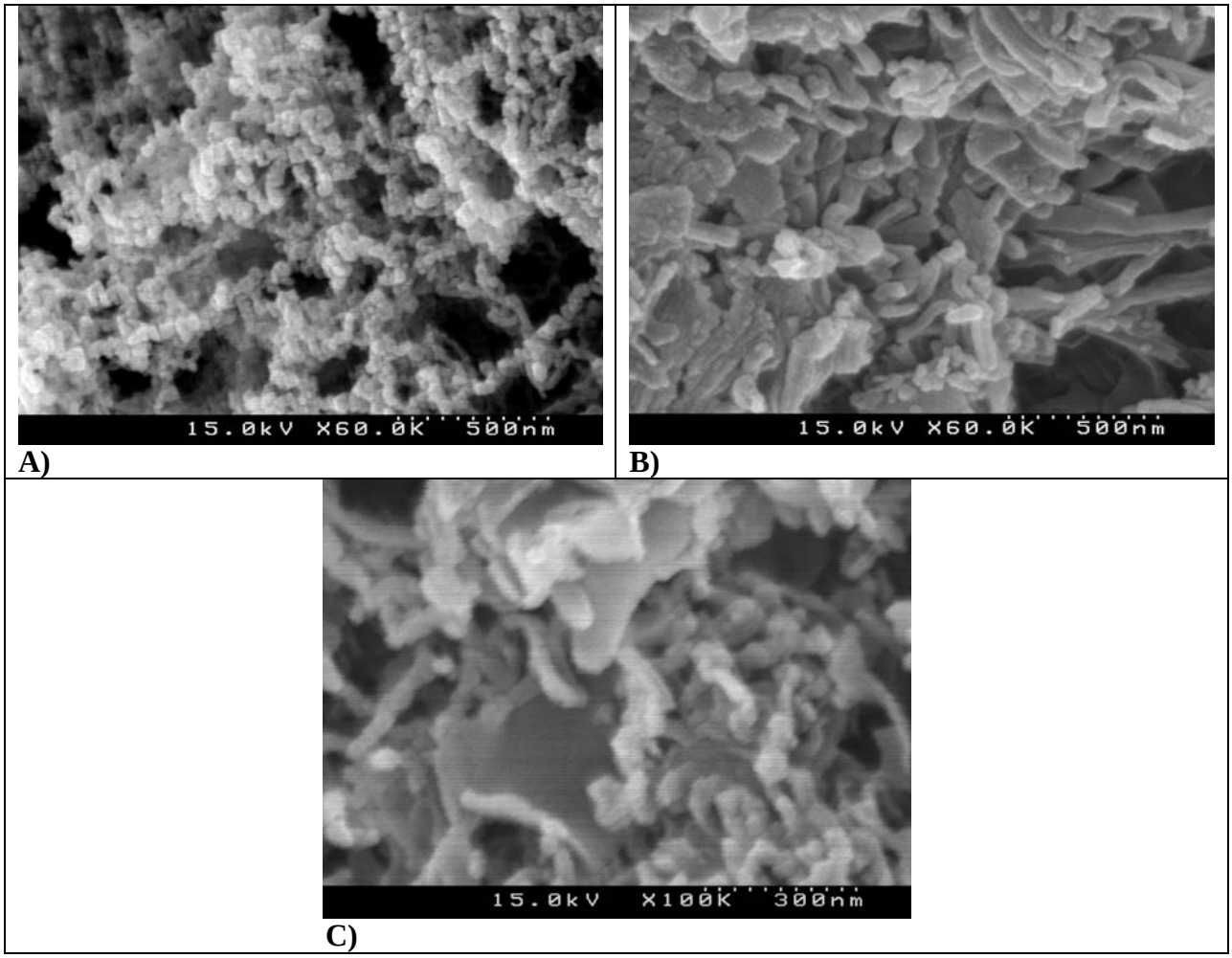

Figure 5.5: SEM of particles from 5 mg/mL lysozyme solutions processed by thin film freezing at surface temperatures of 223 K (A) and 133K (B), and SFL-LN2 (C).

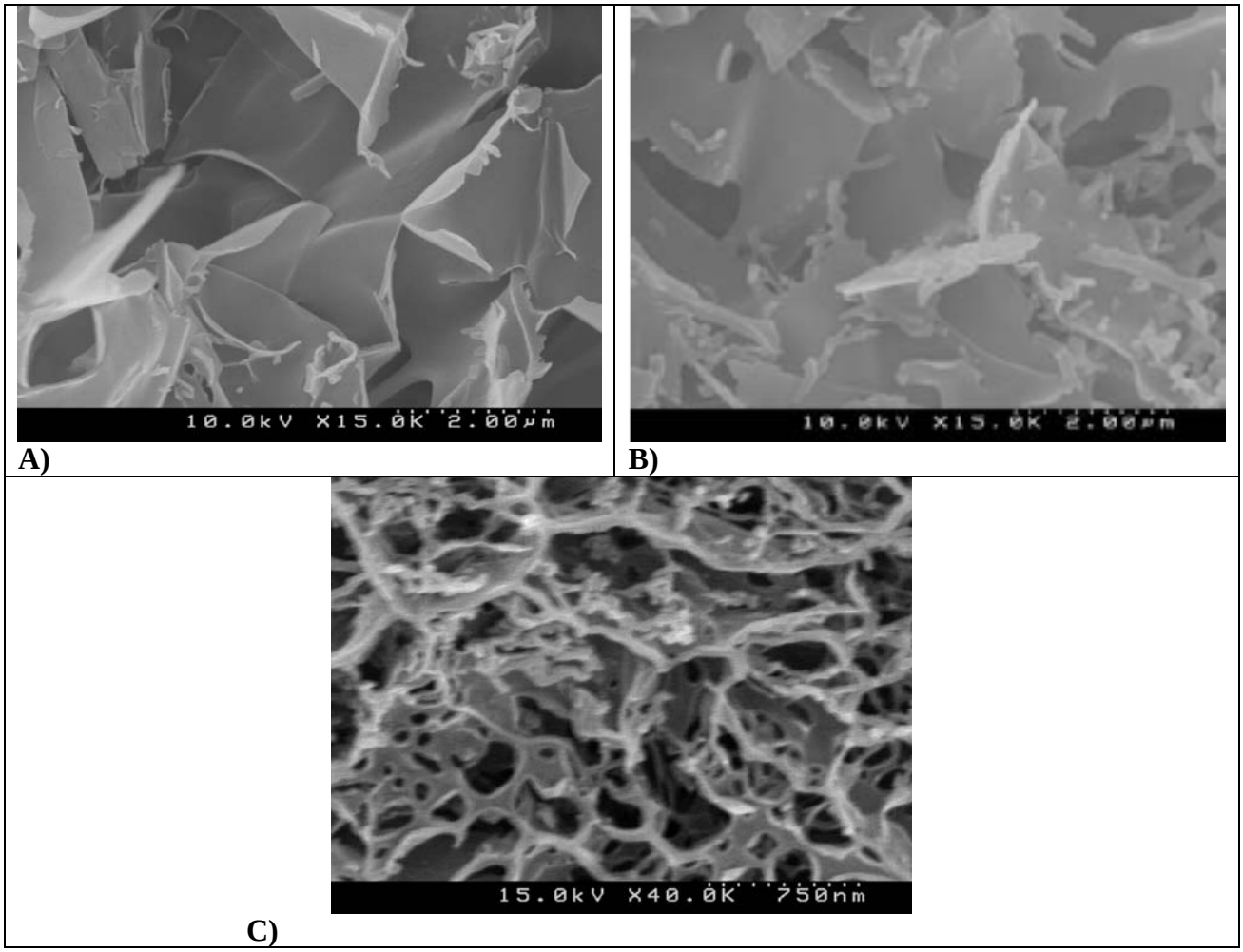

Figure 5.6: SEM of particles from 50 mg/mL lysozyme solution processed by thin film freezing at a surface temperature of 223 K (A), SFL-LN2 (B), and SFD-10 µm into LN2 (C).

indicating that the droplet spreading time was much less than the freezing time (45). (The same behavior was observed in Fig. 5.2 for water. The prediction of the cooling rate of the film with a simplified analytical heat transfer model was in good agreement with experimental IR data (45). Herein, this approach is extended to thin film freezing of water droplets.

Briefly, based on the experimental results observed above, the model assumes that the droplet spreads to form a cylindrical film on a much shorter time scale than heat transfer. Since the height (thickness) of the thin film is on the order of 200-400 μm, relative to a much larger diameter of 10-12 mm, radial heat transfer is neglected. The thermal diffusivity, $\alpha = k / \rho \cdot C_p$, where k is the thermal conductivity, ρ is the density, and C_p is the heat capacity, is treated as constant over the entire temperature range. For the case of freezing water the thermal diffusivities of water and ice are averaged. One-dimensional heat transfer for a finite slab with an insulating boundary condition on the top surface of the thin film (air) and a constant temperature boundary condition on the bottom is described by (66):

$$T(x,t) = T_p + \frac{2}{L}\sum_{n=0}^{\infty} e^{-\alpha(2n+1)^2\pi^2 t/4L^2} \cos\frac{(2n+1)\pi x}{2L}\left\{\frac{2L(-1)^{n+1}T_p}{(2n+1)\pi} + \int_0^L T_i \frac{\cos(2n+1)\pi x'}{2L}dx'\right\} \quad (2)$$

where x is the distance from the top of the spread droplet, T is the temperature in the film, T_p is the plate temperature in contact with the bottom thin film surface, and L is the film thickness.

The calculated temperature profiles from Eq. 2 are shown in Fig. 5.7 and the calculated cooling rates and times are shown in Table 5.4. The cooling time was defined as the time for the temperature of the top surface of the film, T(0,t), to decrease from room temperature (25ºC) to a value 5% greater than that of the metal surface. The

cooling rate (K/s) was then determined by dividing the temperature difference at the top of the film by the cooling time. As shown in Fig. 5.7A and Table 5.4 the predicted time to cool the top surface of the 220 μm thick thin film on the 223 K surface is $2.0x10^2$ ms (cooling rate of $3.9x10^2$ K/s). The calculated cooling rate is an order of magnitude less than for SFL ($7.2x10^3$ K/s) and 4 orders of magnitude less than for SFD ($3.8x10^6$ K/s). The much smaller cooling rates in TFF versus SFD may be explained by a 100 fold smaller surface area/volume ratio and a film thickness on the order of 20-30 times larger than the droplet radius in SFD (Table 5.1).

The particle morphologies shown in Fig. 5.5 and particle SSAs in Table 5.3 were similar for freezing on the 223 K and 133 K surfaces, as a consequence of the rapid cooling in each case. However, for completeness, we discuss small differences in the cooling behavior for these two surface temperatures (Fig. 5.2) in the supplemental section.

The experimental cooling times to reach thermal equilibrium were longer by a factor of 3-4 compared to the modeled cooling times (Table 5.4). This difference is small compared to difference in orders of magnitude relative to other processes such as SFL and lyophilization. The difference may be the result of uncertainty in the calibration of the temperature measurement, differences in definitions of the final temperature for the model and IR camera, and the release of the heat of fusion of water which was not factored into the model. For extremely rapid cooling rates of water, the water may form a glass with limited crystallization (67). As shown by experiment and calculation a cooling rate of 10^6 K/s is necessary to vitrify water (67-70). The 10^2 K/s cooling rate observed experimentally in TFF indicates that the latent heat of fusion may have been significant.

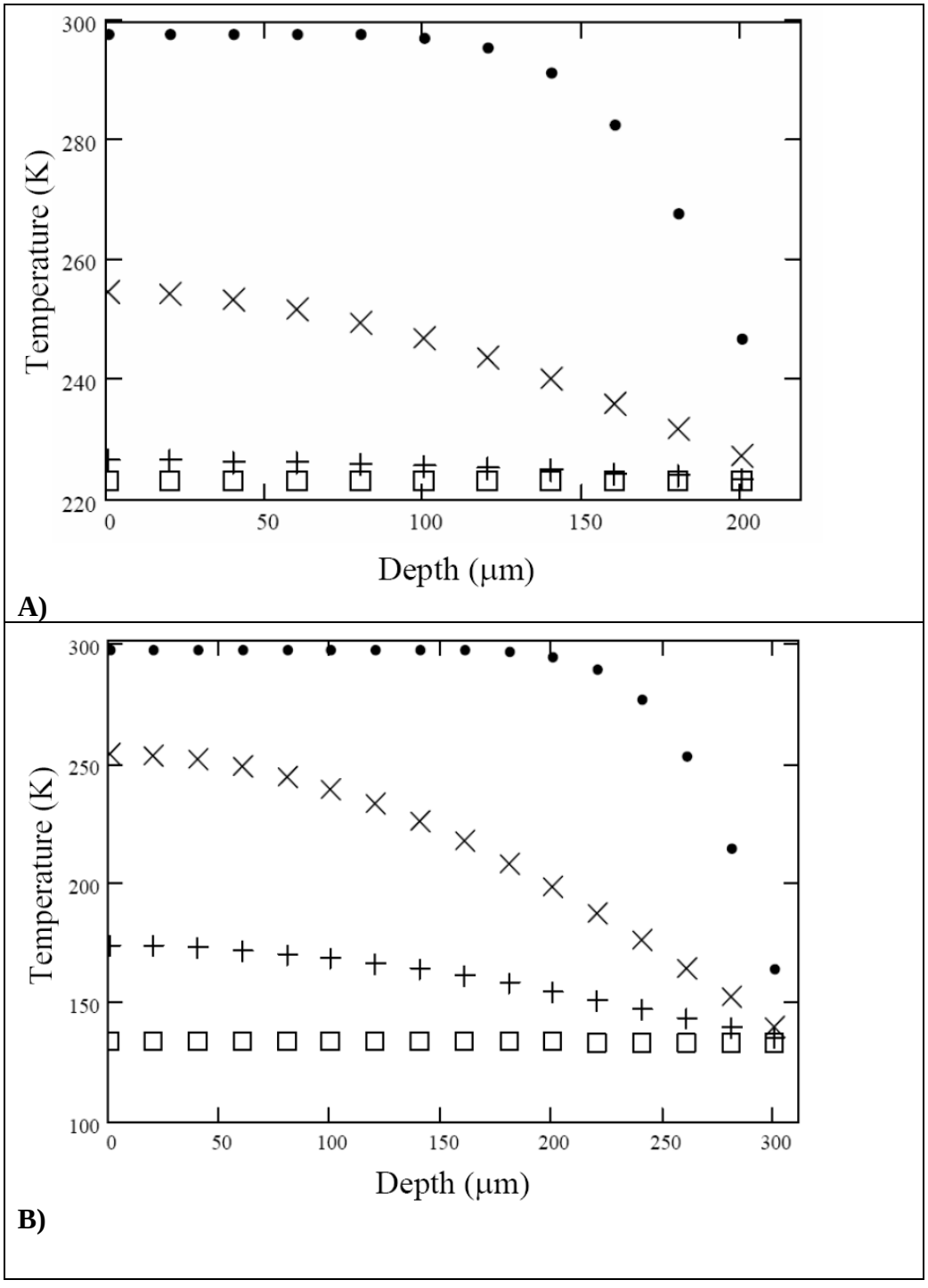

Figure 5.7: Temperature versus depth profiles of thin aqueous films cooled on a surface at 223 K (A) for a 220 μm thin film and 133 K (B) for a 320 μm thin film. Time profiles were calculated after droplet impact at t = 10 ms (●), 100 ms (×), 300 ms (+), and 1000 ms (□).

Table 5.4: Calculated cooling rates, cooling times, and exposure time to the gas-liquid interface for SFD, SFL, and TFF. The droplet dimensions are given in Table 5.1.

	SFD[a]	**SFL[a]**	**Thin Film from 3.6 mm Drop 223 K**	**Thin Film from 3.6 mm Drop 133 K**
Cooling Rate (K/s)	3.8×10^6	7.2×10^3	3.9×10^2	2.0×10^2
Cooling Time (ms)	0.033	17	2.0×10^2	6.2×10^2
Droplet Gas-Liquid Exposure Time (ms)	10-1000	2	~1000	~1000

[a] Values taken from Engstrom et al. (36)

5.4.2 Nucleation and growth mechanisms versus cooling rate

To place the TFF results in perspective, it is instructive to consider the boundary conditions of extremely rapid vitrification/freezing in SFD and slow freezing in lyophilization. Previously, the morphologies of lysozyme powders prepared by SFL and SFD were shown to be similar for dilute 5 mg/mL lysozyme solutions. The SSAs were >100 m^2/g for 50-100 nm spherical primary particles, despite a cooling rate of 10^3 K/s for SFL versus 10^6 K/s for SFD, as shown in Table 5.4 (36).

The freezing mechanism involves many simultaneous changes in the properties of the unfrozen solution. As the water freezes, it changes concentrations, pH, ionic strength, viscosity, diffusion coefficients, collisions between nucleated particles and geometric size and shape of the unfrozen solution. The growth rate of the protein particles depends upon all of these factors, such that it would be challenging to develop a model for the final particle size. The thin liquid channels between the frozen water domains reduce the number of collisions between protein (sugar) particles and thus inhibit growth by coagulation, as shown in Fig. 5.8. Furthermore, the viscosity of the thin channels increases rapidly to arrest particle growth and the channel fully freezes. Furthermore, the sugar in the water raises the viscosity over that of pure water. For the case of slow cooling in lyophilization, the very low degree of supercooling creates relatively few nucleated ice domains compared to the rapid cooling processes, leaving thick channels of liquid solution between these domains (Fig. 5.8). For a cooling rate of 1 K/min, as for the case of slowly cooling a 5 mg/mL solution in a -20ºC freezer, the lyophilized particle sizes were on the order of 30-100 μm. In these thick channels, the protein particles have sufficient time to aggregate and grow forming large particles before the channels are fully frozen. Although it is theoretically possible to mitigate this particle growth partially by

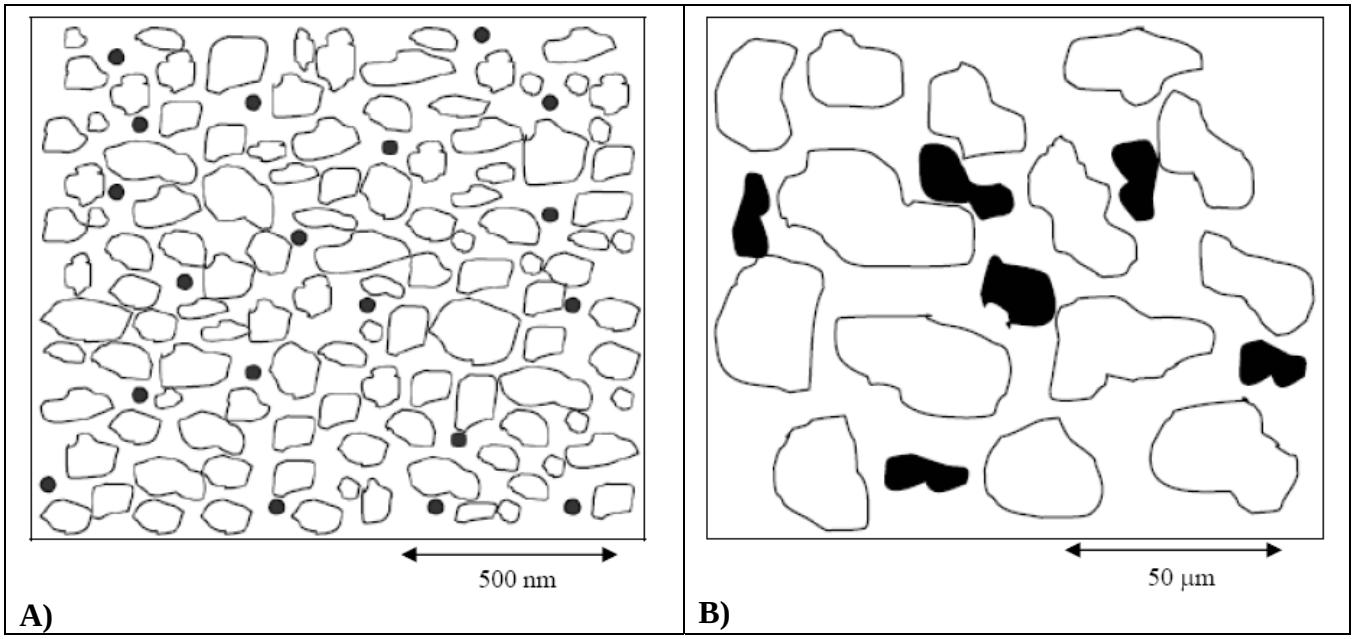

Figure 5.8: Nucleation and growth of protein particle in unfrozen channels between glassy frozen water domains with high supercooling in the thin film freezing, SFL, and SFD processes(A), and with low supercooling in shelf lyophilization (B). Ice particles are represented as white domains and solute precipitate as solid black dots or regions.

reducing the protein solution concentration significantly below 1 mg/mL, such low protein concentrations can lead to excessive lyophilization requirements (21).

In SFD, various studies found that exposure of the protein to the gas-liquid interface has a larger effect on protein stability than to the ice-liquid or glassy water-liquid interface (19, 31, 32). It is unclear whether ice-liquid versus glassy water-liquid interfaces have different effects on protein stabilities (19, 20, 71). As described by previous studies (68, 69), cooling rates on the order of 10^6 K/s are needed to vitrify water, but the cooling rate necessary for vitrification can be lowered in the presence of sugar in solution (67, 70). For the slower cooling rates observed in TFF (10^2 K/s) relative to SFD, it is likely that ice particle domains instead of vitrified water domains are formed. The LDH activities were on the order of 100% for TFF. Thus, our results do not suggest that the ice-liquid interface has a detrimental effect on protein stability.

For the 5 mg/mL lysozyme formulation at 223 K, the SSA was quite large, although modestly smaller than for SFD, and the particle sizes after sonication were similar to those of both SFL and SFD (Table 5.3). The lower cooling rate in TFF (10^2 K/s) compared to SFD (10^6 K/s) and SFL (10^3 K/s) was still sufficient to produce rapid nucleation and to prevent significant particle growth during freezing. However, for TFF, the size of the unfrozen channels was sufficiently thin and the increase in the viscosity of the unfrozen solution sufficiently fast to achieve similar particle sizes and morphologies as for the moderately faster process, SFL and much faster process, SFD. Thus, the extremely rapidly cooling rates in SFD were much faster than necessary to form submicron protein particles. A similar conclusion was reached in the comparison of SFL and SFD (32).

For 50 mg/mL highly concentrated solutions the larger volume fraction of vitrified solute domains in the unfrozen water channels lead to a greater collision

frequency and increased particle growth (36). As observed previously (36), the slower cooling rate in SFL compared to SFD leads to greater particle growth before the large unfrozen liquid channels vitrify, leading to larger protein particles and lower powder SSAs (36). As shown in Table 5.3, the SSAs were similar for TFF and SFL. For these highly concentrated solutions, the larger particles formed in TFF (and SFL) versus SFD results from more time for growth in the thicker unfrozen channels. This limitation is typically not encountered in rapid freezing processes, as most previous studies examined much lower concentrations on the order of 5 mg/mL.

5.4.3 Minimization of gas-liquid interface in TFF process

The LDH stabilities were essentially 100% after TFF indicating that none of the steps, droplet falling, spreading and freezing, and drying caused a measurable loss in enzyme activity. From previous calculations (32) it was shown that the exposure of the atomized droplets to the gas-liquid interface was an order of magnitude less in the SFL process (600 cm^{-1}) relative to SFD (6000 cm^{-1}) (19). This larger exposure to the gas-liquid interface resulted in lower LDH activities in SFD (32). In TFF the surface area/volume ratio of the gas-liquid interface of TFF (46 cm^{-1}) was 2 orders of magnitude lower than in SFD, leading to far less protein adsorption and aggregation (Table 5.4). As shown in Fig. 5.9, the intermediate cooling rates in TFF and SFL offer a means to produce high surface area submicron particles as opposed to lyophilization, with smaller amounts of protein adsorption at gas-liquid interfaces compared to SFD resulting in higher protein stability.

Minimizing gas-liquid interface can improve protein stability by limiting the amount of protein that can adsorb to the interface. For surface active radiolabeled proteins, the surface excess concentration, Γ, (72, 73) at full saturation for β-casein, lysozyme, and BSA were 2.6, 3.0, and 3.3 mg/m^2, respectively (33, 72, 73). For LDH,

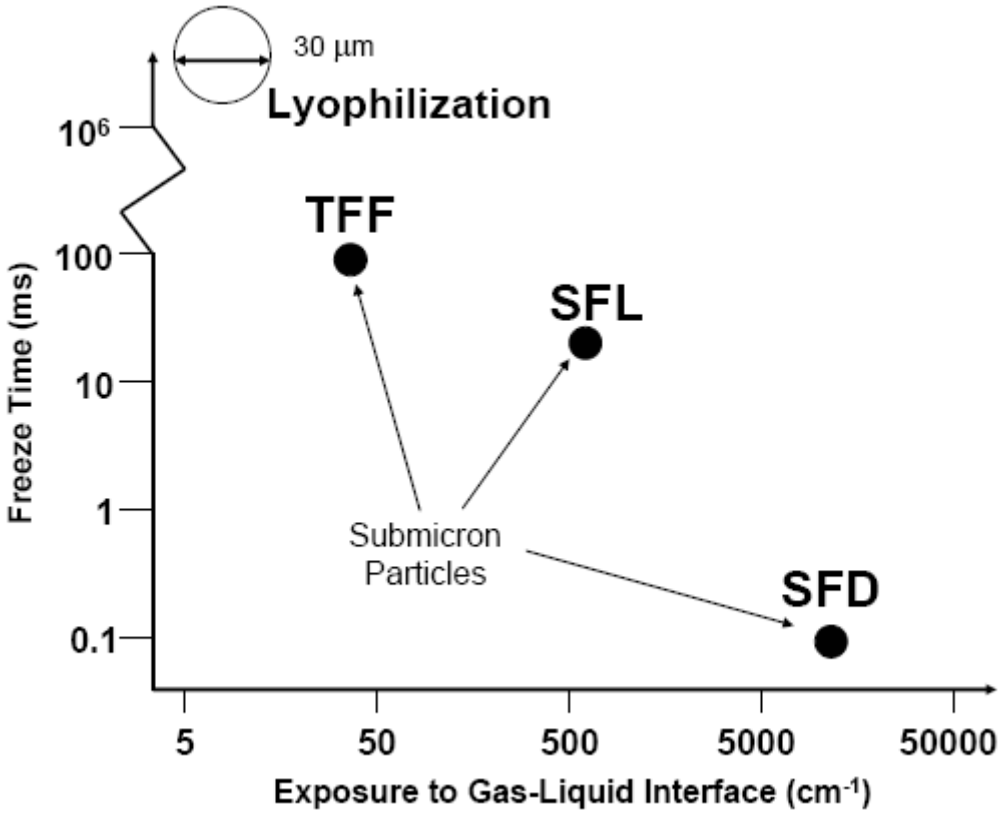

Figure 5.9: Freezing time versus exposure to gas-liquid interface for lyophilization, thin film freezing (TFF), spray freezing into liquid (SFL), and spray freeze-drying (SFD).

we assumed a similar value of approximately 3 mg/m^2. For the top surface of a 12 mm diameter film, where the surface area is $1.13x10^{-4}$ m^2, the total adsorbed protein at equilibrium would be $3.4x10^{-4}$ mg. For a starting 3.6 mm liquid droplet containing 0.25 mg/mL LDH, the total protein is $6.2x10^{-3}$ mg. Therefore, if all of the protein reached the interface and was denatured, the maximum decrease in protein activity would be 5.5%. The exposure of 1 s may not lead to full equilibrium adsorption. Furthermore, the increase in viscosity as a function of height and time with freezing will arrest diffusion of protein to the air-water interface. For ~10 μm diameter droplets in SFD, it was determined that 25-30% of the total LDH in the droplet adsorbs to the gas-liquid interface in only 0.4 ms (22). Denaturation of part of the adsorbed protein is consistent with the significant decreases in protein activity observed in the SFD process in Table 5.2.

5.5 CONCLUSIONS

The TFF process was utilized to produce 300 nm lysozyme particles with surface areas on the order of 31 - 73 m^2/g and 100% LDH activities. Despite a cooling rate of ~10^2 K/s in TFF, the particle sizes and surface areas were similar to those observed in the widely reported process, spray freeze drying SFD, where cooling rates reach 10^6 K/s. In TFF, the thin liquid channels between the ice domains were sufficiently thin and freezing rates of the thin channels sufficiently fast to achieve the similar particle morphologies. Therefore, the extremely rapid cooling rate in the SFD process was not necessary to form the desired submicron protein particles. Although LDH was exposed to the gas-liquid interface of the thin film for a maximum of ~1 s in TFF, the surface area/volume of 45 cm^{-1} was sufficiently small that adsorption produced neglible aggregation and denaturation. Even if this gas-liquid interface became saturated with protein, followed by irreversible denaturation, the maximum activity loss for a 0.25 mg/mL LDH formulation would be 5%. For SFD with a droplet size of 10 μm, the maximum loss could reach 25%

in just 0.4 ms from diffusion to the interface and adsorption (22), consistent with the significant decrease in enzyme activity (80%). In SFD, losses in protein stability have been observed in several previous studies (1, 11, 18, 19, 21). Although LDH stabilities are high in conventional lyophilization, cooling rates are on the order of 1 K/min resulting in large 30 to 100 μm sized particles (21). Thus, the intermediate cooling rate regime for TFF (and likewise for SFL), relative to SFD and lyophilization, offers a promising route to form stable submicron protein particles of interest in pulmonary and parenteral delivery applications.

5.6 SUPPLEMENTAL SECTION

5.6.1 Observed cooling patterns of thin films

The radial cooling pattern of the thin film on the 223 K surface in Fig. 5.2, as described further in Fig. 5.3, indicates that the edge of the film may have been thinner than the center and thus cooled more quickly. Alternatively, previous studies have determined experimentally and theoretically that the edge of a spreading droplet cools at a greater rate than the center even when the thin film deforms into a cylinder (42, 56). To understand how the cooling rate difference across the top of the cooling thin film affects the powder morphology, a thin aqueous film containing lysozyme was frozen on an SEM stage and was then dried by lyophilization. The morphology of the top of the dried lysozyme film as observed by SEM (Fig. 5.10) was uniform across the diameter of the film and had morphological features identical to Fig. 5.5. Therefore, the small cooling rate difference at the edge of the film versus the center had a negligible effect on the dried particle morphology. Thus it is reasonable to model the cooling in the z direction only.

As shown in a previous study, the droplet spreading may terminate as the edge freezes (42). Furthermore, freezing may occur simultaneously with droplet spreading

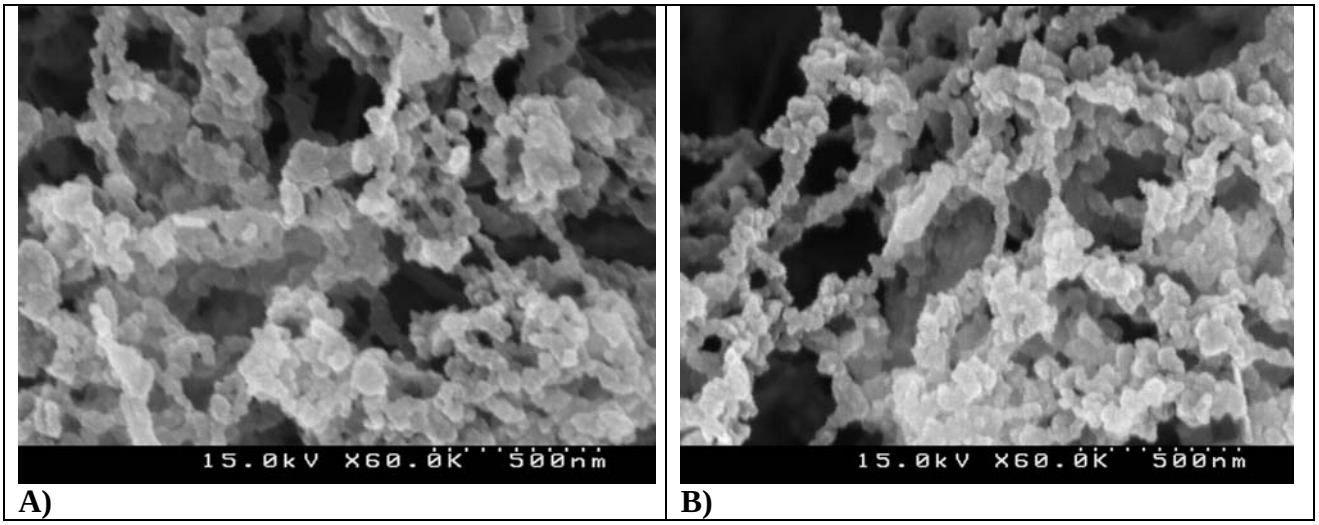

Figure 5.10: SEM of top of dried lysozyme thin film at the center (A) and approximately 10 μm from the edge (B) prepared from a 5 mg/mL lysozyme solution frozen and dried by lyophilization as a thin film on an SEM stage.

(44). For molybdenum thin films, this edge freezing produced patterns with jagged edges (44), as was also observed in this study at 133 K. The jagged edge indicates fingers of liquid water spread outwards between islands of frozen edges. For a warmer surface (T of 223 K), the edge spread evenly to form a circle without frozen islands, which otherwise would have produced jagged edges. In this case, the radial cooling front moves from the edge of the film to the center (42, 56) as was observed experimentally in this study (Fig. 5.2).

5.7 REFERENCES

1. Y.-F. Maa and H. R. Costantino. Spray freeze-drying of biopharmaceuticals: applications and stability considerations. In H. R. Costantino and M. J. Pikal (eds.), *Biotechnology: Pharmaceutical Aspects. 2. Lyophilization of Biopharmaceuticals*, American Association of Pharmaceutical Scientists, Arlington, 2004, pp. 519-561.

2. Y.-F. Maa, L. Zhao, L. G. Payne, and D. Chen. Stabilization of alum-adjuvanted vaccine dry powder formulations: mechanism and application. *J. Pharm. Sci.* **92:**319-332 (2003).

3. X. M. Lam, E. T. Duenas, A. L. Daugherty, N. Levin, and J. L. Cleland. Sustained release of recombinant human insulin-like growth factor-I for treatment of diabetes. *J. Control. Release* **67:**281-292 (2000).

4. W. T. Leach, D. T. Simpson, T. N. Val, E. C. Anuta, Z. Yu, R. O. Williams III, and K. P. Johnston. Uniform encapsulation of stable protein nanoparticles produced by spray freezing for the reduction of burst release. *J. Pharm. Sci.* **94:**56-69 (2005).

5. O. L. Johnson, W. Jaworowicz, J. L. Cleland, L. Bailey, M. Charnis, E. Duenas, C. Wu, D. Shepard, S. Magil, T. Last, A. J. S. Jones, and S. D. Putney. The stabilization and encapsulation of human growth hormone into biodegradable microspheres. *Pharm. Res.* **14:**730-735 (1997).

6. X. M. Lam, E. T. Duenas, and J. L. Cleland. Encapsulation and stabilization of nerve growth factor into poly(lactic-co-glycolic) acid microspheres. *J. Pharm. Sci.* **90:**1356-1365 (2001).

7. M. R. Prausnitz. Microneedles for transdermal drug delivery. *Adv. Drug Deliv. Rev.* **56:**581-587 (2004).

8. D. A. Edwards, J. Hanes, G. Caponetti, J. Hrkach, A. Ben-Jebria, M. L. Eskew, J. Mintzes, D. Deaver, N. Lotan, and R. Langer. Large porous particles for pulmonary drug delivery. *Science* **276:**1868-1871 (1997).

9. S. J. Shire, Z. Shahrokh, and J. Liu. Challenges in the development of high protein concentration formulations. *J. Pharm. Sci.* **93:**1390-1402 (2004).

10. J. L. Cleland, E. T. Duenas, A. Park, A. Daugherty, J. Kahn, J. Kowalski, and A. Cuthbertson. Development of poly-(d,l-lactide-co-glycolide) microsphere formulations containing recombinant human vascular endothelial growth factor to promote local angiogenesis. *J. Control. Release* **72:**13-24 (2001).

11. X. C. Nguyen, J. D. Herberger, and P. A. Burke. Protein powders for encapsulation: a comparison of spray-freeze drying and spray drying of darbepoetin alfa. *Pharm. Res.* **21:**507-514 (2004).

12. S. L. Lee, A. E. Hafeman, P. G. Debenedetti, B. A. Pethica, and D. J. Moore. Solid-State Stabilization of a-Chymotrypsin and Catalase with Carbohydrates. *Ind. Eng. Chem. Res.* **45:**5134-5147 (2006).

13. J. F. Carpenter, B. S. Chang, W. Garzon-Rodriguez, and T. W. Randolph. Rational design of stable lyophilized protein formulations: theory and practice. In J. F. Carpenter and M. C. Manning (eds.), *Pharmaceutical Biotechnology. 13. Rational Design of Stable Protein Formulations*, Kluwer Academic/Plenum Press, New York, 2002, pp. 109-133.

14. M. C. Manning, K. Patel, and R. T. Borchardt. Stability of protein pharmaceuticals. *Pharm. Res.* **6:**903-918 (1989).

15. W. Wang. Lyophilization and development of solid protein pharmaceuticals. *Int. J. Pharm.* **203:**1-60 (2000).

16. R. A. DePaz, D. A. Dale, C. C. Barnett, J. F. Carpenter, A. L. Gaertner, and T. W. Randolph. Effects of drying methods and additives on the structure, function, and storage stability of subtilisin: role of protein conformation and molecular mobility. *Enzyme Microb. Technol.* **31:**765-774 (2002).

17. M. J. Pikal. Mechanisms of protein stabilization during freeze-drying and storage: the relative importance of thermodynamic stabilization and glassy state relaxation dynamics. *Drugs Pharm. Sci.* **137:**63-107 (2004).

18. H. R. Costantino, L. Firouzabadian, K. Hogeland, C. C. Wu, C. Beganski, K. G. Carrasquillo, M. Cordova, K. Griebenow, S. E. Zale, and M. A. Tracy. Protein spray-freeze drying. Effect of atomization conditions on particle size and stability. *Pharm. Res.* **17:**1374-1383 (2000).

19. S. D. Webb, S. L. Golledge, J. L. Cleland, J. F. Carpenter, and T. W. Randolph. Surface adsorption of recombinant human interferon-γ in lyophilized and spray-lyophilized formulations. *J. Pharm. Sci.* **91:**1474-1487 (2002).

20. B. S. Chang, B. S. Kendrick, and J. F. Carpenter. Surface-induced denaturation of proteins during freezing and its inhibition by surfactants. *J. Pharm. Sci.* **85:**1325-1330 (1996).

21. Y.-F. Maa and S. J. Prestrelski. Biopharmaceutical powders: particle formation and formulation considerations. *Curr. Pharm. Biotechnol.* **1:**283-302 (2000).

22. M. Adler and G. Lee. Stability and surface activity of lactate dehydrogenase in spray-dried trehalose. *J. Pharm. Sci.* **88:**199-208 (1999).

23. J. Deng, D. R. Davies, G. Wisedchaisri, M. Wu, W. G. J. Hol, and C. Mehlin. An improved protocol for rapid freezing of protein samples for long-term storage. *Acta Crystallogr., Sect. D: Biol. Crystallogr.* **D60:**203-204 (2004).

24. Y. Yamagata, T. Doen, N. Asakawa, and S. Takada. Process for producing protein powder United States Patent. 6,723,347 (2004).

25. Y.-F. Maa, P.-A. Nguyen, T. Sweeney, S. J. Shire, and C. C. Hsu. Protein inhalation powders: spray drying vs spray freeze drying. *Pharm. Res.* **16:**249-254 (1999).

26. S. P. Sellers, G. S. Clark, R. E. Sievers, and J. F. Carpenter. Dry powders of stable protein formulations from aqueous solutions prepared using supercritical CO(2)-assisted aerosolization. *J. Pharm. Sci.* **90:**785-797 (2001).

27. J. D. Andya, Y.-F. Maa, H. R. Costantino, P.-A. Nguyen, N. Dasovich, T. D. Sweeney, C. C. Hsu, and S. J. Shire. The effect of formulation excipients on protein stability and aerosol performance of spray-dried powders of a recombinant humanized anti-IgE monoclonal antibody. *Pharm. Res.* **16:**350-358 (1999).

28. Y.-F. Maa and P.-A. Nguyen. Method of spray freeze drying proteins for pharmaceutical administration. United States Patent. 6,284,282 (2001).

29. H. R. Costantino, L. Firouzabadian, C. C. Wu, K. G. Carrasquillo, K. Griebenow, S. E. Zale, and M. A. Tracy. Protein spray freeze drying. 2. Effect of formulation variables on particle size and stability. *J. Pharm. Sci.* **91:**388-395 (2002).

30. Z. H. Chang and J. G. Baust. Ultra-rapid freezing by spraying/plunging: pre-cooling in the cold gaseous layer. *J. Microsc.* **161:**435-444 (1991).

31. Z. Yu, K. P. Johnston, and R. O. Williams III. Spray freezing into liquid versus spray-freeze drying: Influence of atomization on protein aggregation and biological activity. *Eur. J. Pharm. Sci.* **27:**9-18 (2006).

32. J. D. Engstrom, D. T. Simpson, C. Cloonan, E. Lai, R. O. Williams III, G. B. Kitto, and P. Johnston Keith. Stable high surface area lactate dehydrogenase particles produced by spray freezing into liquid nitrogen. *Eur. J. Pharm. Biopharm.* **65:**163-174 (2007).

33. S. Magdassi and A. Kamyshny. Surface activity and functional properties of proteins. In S. Magdassi (ed.), *Surface Activity of Proteins*, Marcel Dekker, New York, 1996, pp. 1-38.

34. Z. Yu, A. S. Garcia, K. P. Johnston, and R. O. Williams III. Spray freezing into liquid nitrogen for highly stable protein nanostructured microparticles. *Eur. J. Pharm. Biopharm.* **58:**529-537 (2004).

35. Z. Yu, T. L. Rogers, J. Hu, K. P. Johnston, and R. O. Williams III. Preparation and characterization of microparticles containing peptide produced by a novel process: spray freezing into liquid. *Eur. J. Pharm. Biopharm.* **54:**221-228 (2002).

36. J. D. Engstrom, D. T. Simpson, E. Lai, R. O. Williams III, and K. P. Johnston. Morphology of protein particles produced by spray freezing of concentrated solutions. *Eur. J. Pharm. Biopharm.* **65:**149-162 (2007).

37. H. Sitte, L. Edelmann, and K. Neumann. Cryofixation without pretreatment at ambient pressure. In R. A. Steinbrecht and K. Zierold (eds.), *Cryotechniques in Biological Electron Microscopy*, Springer-Verlag, Berlin, 1987, pp. 87-113.

38. J. C. Gilkey and L. A. Staehelin. Advances in ultrarapid freezing for the preservation of cellular ultrastructure. *J. Electron Microsc. Tech.* **3:**177-210 (1986).

39. J. A. N. Zasadzinski. A new heat transfer model to predict cooling rates for rapid freezing fixation. *J. Microsc.* **150:**137-149 (1988).

40. J. E. Heuser, T. S. Reese, and D. M. Landis. Preservation of synaptic structure by rapid freezing. *Cold Spring Harbor Symp. Quant. Biol.* **40:**17-24 (1976).

41. J. Escaig. New instruments which facilitate rapid freezing at 83 K and 6 K. *J. Microsc.* **126:**221-230 (1982).

42. J. Fukai, T. Ozaki, H. Asami, and O. Miyatake. Numerical simulation of liquid droplet solidification on substrates. *J. Chem. Eng. Jpn.* **33:**630-637 (2000).

43. T. Bennett and D. Poulikakos. Splat-quench solidification: estimating the maximum spreading of a droplet impacting a solid surface. *J. Mater. Sci.* **28:**963-970 (1993).

44. H. Zhang, X. Y. Wang, L. L. Zheng, and X. Y. Jiang. Studies of splat morphology and rapid solidification during thermal spraying. *Int. J. Heat Mass Transfer* **44:**4579-4592 (2001).

45. K. A. Overhoff, J. D. Engstrom, B. Chen, T. L. Rogers, K. P. Johnston, and R. O. Williams III. Development and Optimization of the Novel Ultra-rapid Freezing Particle Engineering Process to Enhance the Dissolution Rates of Poorly Water Soluble Drugs. *Eur. J. Pharm. Biopharm.* **65:**57-67 (2007).

46. J. Fukai, M. Tanaka, and O. Miyatake. Maximum spreading of liquid droplets colliding with flat surfaces. *J. Chem. Eng. Jpn.* **31:**456-461 (1998).

47. M. Pasandideh-Fard, R. Bhola, S. Chandra, and J. Mostaghimi. Deposition of tin droplets on a steel plate : simulations and experiments. *Int. J. Heat Mass Transfer* **41:**2929-2945 (1998).

48. M. Pasandideh-Fard, S. Chandra, and J. Mostaghimi. A three-dimensional model of droplet impact and solidification. *Int. J. Heat Mass Transfer* **45:**2229-2242 (2002).

49. D. Sivakumar and H. Nishiyama. Numerical analysis on the impact behavior of molten metal droplets using a modified splat-quench solidification model. *J. Heat Transf.-Trans. ASME* **126:**1014-1022 (2004).

50. B. Kang, Z. Zhao, and D. Poulikakos. Solidification of liquid metal droplets impacting sequentially on a solid surface. *J. Heat Transfer* **116:**436-45 (1994).

51. J. Madejski. Solidification of droplets on a cold surface. *Int. J. Heat Mass Transfer* **19:**1009-1013 (1976).

52. C. Sanmarchi, H. Liu, E. J. Lavernia, R. H. Rangel, A. Sickinger, and E. Muehlberger. Numerical analysis of the deformation and solidification of a single droplet impinging onto a flat substrate. *J. Mater. Sci.* **28:**3313-21 (1993).

53. G. X. Wang and E. F. Matthys. Modeling of heat transfer and solidification during splat cooling: effect of splat thickness and splat/substrate thermal contact. *Int. J. Rapid Solid.* **6:**141-74 (1991).

54. G. X. Wang and E. F. Matthys. Numerical modeling of phase change and heat transfer during rapid solidification processes: use of control volume integrals with element subdivision. *Int. J. Heat Mass Transfer* **35:**141-53 (1992).

55. Z. Zhao, D. Poulikakos, and J. Fukai. Heat transfer and fluid dynamics during the collision of a liquid droplet on a substrate. I. Modeling. *Int. J. Heat Mass Transfer* **39:**2771-2789 (1996).

56. Z. Zhao, D. Poulikakos, and J. Fukai. Heat transfer and fluid dynamics during the collision of a liquid droplet on a substrate. II. Experiments. *Int. J. Heat Mass Transfer* **39:**2791-2802 (1996).

57. G. Trapaga and J. Szekely. Mathematical modeling of the isothermal impingement of liquid droplets in spraying processes. *Metall. Trans. B* **22B:**901-14 (1991).

58. T. J. Anchordoquy and J. F. Carpenter. Polymers protect lactate dehydrogenase during freeze-drying by inhibiting dissociation in the frozen state. *Arch. Biochem. Biophys.* **332:**231-238 (1996).

59. T. J. Anchordoquy, K.-I. Izutsu, T. W. Randolph, and J. F. Carpenter. Maintenance of quaternary structure in the frozen state stabilizes lactate dehydrogenase during freeze-drying. *Arch. Biochem. Biophys.* **390:**35-41 (2001).

60. S. Brunauer, P. H. Emmett, and E. Teller. Adsorption of gases in multimolecular layers. *J. Am. Chem. Soc.* **60:**309-319 (1938).

61. E. H. Snell, R. A. Judge, M. Larson, and M. J. van der Woerd. Seeing the heat - preliminary studies of cryocrystallography using infrared imaging. *J. Synch. Radiat.* **9:**361-367 (2002).

62. A. A. Elkordy, R. T. Forbes, and B. W. Barry. Integrity of crystalline lysozyme exceeds that of a spray-dried form. *Int. J. Pharm.* **247:**79-90 (2002).

63. J. Fukai, Y. Shiiba, T. Yamamoto, O. Miyatake, D. Poulikakos, C. M. Megaridis, and Z. Zhao. Wetting effects on the spreading of a liquid droplet colliding with a flat surface - experiment and modeling. *Phys. Fluids* **7:**236-247 (1995).

64. S. Schiaffino and A. A. Sonin. Motion and arrest of a molten contact line on a cold surface: an experimental study. *Phys. Fluids* **9:**2217-2226 (1997).

65. T. Bennett and D. Poulikakos. Heat-Transfer Aspects of Splat-Quench Solidification - Modeling and Experiment. *J. Mater. Sci.* **29:**2025-2039 (1994).

66. H. S. Carslaw and J. C. Jaeger. *Conduction of Heat in Solids*, Oxford University Press, London, 1959.

67. F. Franks. *Biophysics and Biochemistry at Low Temperatures*, Cambridge University Press, New York, 1985.

68. P. G. Debenedetti. Supercooled and glassy water. *J. Phys.: Condens. Matter* **15:**R1669-R1726 (2003).

69. E. Mayer and P. Brueggeller. Vitrification of pure liquid water by high pressure jet freezing. *Nature* **298:**715-718 (1982).

70. C. A. Angell. Liquid fragility and the glass transition in water and aqueous solutions. *Chem. Rev.* **102:**2627-2649 (2002).

71. C. A. Angell and L.-M. Wang. Hyperquenching and cold equilibration strategies for the study of liquid-liquid and protein folding transitions. *Biophys. Chem.* **105:**621-637 (2003).

72. D. E. Graham and M. C. Phillips. Proteins at liquid interfaces. I. Kinetics of adsorption and surface denaturation. *J. Colloid Interface Sci.* **70:**403-14 (1979).

73. D. E. Graham and M. C. Phillips. Proteins at liquid interfaces. II. Adsorption Isotherms. *J. Colloid Interface Sci.* **70:**415-426 (1979).

Chapter 6: Templating Open Flocs of Nanorods for Enhanced Pulmonary Delivery with Pressurized Metered Dose Inhalers

A novel concept is presented for the formation of stable suspensions composed of very low density flocs of rod-shaped drugs in hydrofluoroalkane propellants for pressurized meter dose inhalers (pMDI), and for templating the flocs to achieve high fine particle fractions in pulmonary delivery. The flocculated suspensions in HFA 227 are stable against settling for one year. Bovine serum albumin (BSA) nanorods, 50 nm in diameter and 480 nm in length, produced by thin film freezing (TFF), are shown by theory and experiment to form space filling flocs with protein particle volume fractions of only 0.0020, which are one order of magnitude lower than for flocs composed of spheres. The rods are flocculated reversibly, as they were found to break up into individual submicron primary rod particles in a polar solvent acetonitrile. Actuation of the HFA suspension with a pMDI produces high fine particle fractions (38-48%) with an emitted dose of 0.7 mg for particles with 3-4 μm aerodynamic diameters (d_a), as determined with an Andersen cascade impactor (ACI). The atomized 25 μm HFA droplets break apart and template the highly open flocs, which are held together by extremely weak van der Waals forces. Upon evaporation of the HFA, capillary forces shrink the ~25 μm templated flocs resulting in porous particles with optimal d_a = 3-4 μm for deep lung delivery. The corresponding geometric diameters d_g are on the order of 10 μm, as shown by SEM and static light scattering measurements. This novel concept for forming extremely stable suspensions of open flocs of rod shaped particles, and templating and shrinking the flocs to produce particles for efficient pMDI deep lung delivery is applicable to a wide variety of drugs without the need for surfactants or cosolvents to stabilize the primary particles.

6.1 INTRODUCTION

Until recently, the delivery of protein therapeutics has been largely limited to parenteral delivery due to the chemical and physical instabilities of proteins and challenges in permeating biological membranes (1). Among the non-invasive routes, pulmonary delivery offers advantages of large alveolar surface area (~100 m^2), rapid absorption across the thin alveolar epithelium (0.1-0.5 μm), avoidance of first pass metabolism, and sufficient bioavailabilities (1-8). For pulmonary delivery pressurized meter dose inhalers (pMDI) remain the most popular delivery device, relative to dry powder inhalers (DPI) and nebulizers, because of low cost, portability, and disposability (4, 9). Because most drugs, including proteins, are insoluble in hydrofluoroalkane (HFA) propellants, most effort has focused on the design of stable suspensions (10-13). The lack of understanding of how to form these stable suspensions has limited the development of viable formulations (4, 11, 14). Although certain proteins in suspensions may potentially be natured by HFAs (4), the low degree of contact in the solid state with the solvent, relative to solutions, is highly beneficial. For example, insulin, lysozyme, catalase and rhDNase I have been shown to be stable (15-17).

To achieve high deposition of aerosolized particles in the deep lung, the aerodynamic diameter (d_a) should range between 1-5 μm (18). Such protein particles may be produced by milling (11, 17), spray drying (3, 19-21), and spray freeze-drying (SFD) (22, 23). Milling processes can generate significant amounts of heat on localized areas of the protein particle which can lead to denaturation (23, 24). In spray drying and SFD processes, proteins may adsorb and subsequently denature and aggregate at the large gas-liquid interface created upon atomization of droplets on the order of 10-100 μm (24-28), although this effect may be mitigated with interfacially active excipients (23, 25, 29). Limited process yields, in terms of weight of protein, for spray drying (50-70%) (22, 29)

and SFD (~80%) (22, 24, 29) are a major concern for highly valuable proteins. Currently, the production of protein particles with over 90% yield, optimal d_a for deep lung delivery, and high stability against aggregation at the particle and the molecular level remains a significant challenge.

To date, relatively few examples have been given of suspensions with 1-5% (w/w) mass loadings in HFAs that are stable against settling on time scales of over 60 s (11). As the mass loading increases up to and above 5% (w/w), particles often aggregate within aerosolized droplets leading to substantial increases in d_a and thus reduction in fine particle fraction (FPF) (11, 30). Suspensions of spherical particles formed by milling or spray drying often flocculate and settle in less than 60 s (21). Flocculation and settling can lead to irreversible particle aggregation as well as variable dosing between actuations (21, 31). Consequently, the efficiency of pMDIs is often limited for suspensions of proteins, as well as low molecular weight drugs, with typical FPFs between 5-30% (32). Although surfactants and cosolvents, such as ethanol, could potentially stabilize the suspension, the surfactants currently approved by the FDA for inhalation are insoluble in HFAs (33, 34). Even for soluble surfactants, the surfactant tails are often not solvated well enough by HFAs, which have low polarizabilities and van der Waals forces, to provide steric stabilization (35, 36). Thus, a key goal has been to design new surfactant structures by achieving a fundamental understanding of the molecular interactions with atomic force microscopy and theory (11, 35, 36). It would also be desirable to minimize the use of cosolvents, as they can chemically destabilize drugs and modify protein conformation (21, 36).

An alternative approach is to modify the particle morphology to enhance the colloidal stability of the primary particles (11, 21, 37). Large porous particles (37, 38) or hollow particles with porous or nonporous shells (21) formed by spray drying were stable

against settling for at least 4 hours when suspended in HFAs. Respirable fractions were as high as 68%. Here, the presence of pores filled with HFA decreases the density difference of the particle with the surrounding HFA media and reduces van der Waals attractive forces between particles (21). Additional reports of settling rates, primary particle aggregation, and changes in fine particle fraction, especially after storage, will be beneficial for further understanding this approach (21, 37, 38). Recently, large porous nanoparticle (LPNP) aggregates, with d_a optimized for dry powder inhaler (DPI) pulmonary delivery (20, 30), have been formed by spray drying of aqueous suspensions of submicron particles. Upon contact with lung tissue, these "Trojan particles" break up into nanoparticles to facilitate dissolution and absorption (20). To extend this approach to delivery with a pMDI, each LPNP could be stabilized as an individual entity in a colloidal dispersion as shown in Fig. 6.1, if the LPNPs do not aggregate and settle. An alternative approach for efficient nanoparticle delivery to the deep lung is to nebuilize nanoparticle dispersions in aqueous media (39).

Maa et al. demonstrated that DPI delivery of high surface area particles formed by spray freeze drying (SFD) gave higher respirable fractions compared to spray dried particles (22). Two recent particle engineering processes, spray freezing into liquids (SFL) (40-44), and thin film freezing (TFF) (45), were shown to produce high surface area, stable rod-like particles with 50-100 nm diameters and high aspect ratios, despite slower cooling rates than in SFD. The stability of lactase dehydrogenase, based on enzymatic activity, was increased in these processes relative to SFD. This increase was achieved by lowering the area of (42, 45) the gas-liquid interface, which has been shown to denature proteins (28, 42). To our knowledge, dispersible powders produced by these rapid (SFD) or intermediate (SFL and TFF) cooling processes have not been explored for pMDI delivery.

In all of the pMDI methods discussed so far, the goal has been to stabilize a colloidal dispersion of primary particles, or of individual LPNP particles in a HFA (11, 14), often with surfactant stabilization. It would also be of interest to design novel types of particles that do not require surfactants to form stable suspensions.

The primary objective of this study was to form stable suspensions (against settling) of BSA particles in HFA 227 without stabilizing surfactants or cosolvents in order to achieve high fine particle fractions in pMDI delivery. This approach is fundamentally the opposite of previous ones (11), in that we purposely flocculate the particles in the HFA to prevent settling. Spheres, produced by milling or spray drying, were added to HFA 227, but they produced dense flocs that settled rapidly. Asymmetric particles, such as rods, may be expected to pack less efficiently to form much lower density flocs with greater free volume (46-50) than spheres. Rods were produced by TFF. The goal was to form very light open flocs in an HFA that occupy the entire vial and stack upon each other to prevent settling for months, as illustrated in Fig. 6.1. The morphology was determined by SEM of the original particles and after solvent removal of particles suspended and sonicated in acetonitrile or HFA 227. As will be shown by light scattering, the flocculation is reversible, in that the flocs break up into submicron primary rod particles upon transfer to a more polar solvent acetonitrile. The particles were also studied in 2H,3H perfluoropentane (HPFP), a non-volatile surrogate for HFA 227, to analyze floc size by optical microscopy and static light scattering. The d_a values were determined with an Andersen cascade impactor (ACI) and aerodynamic particle sizer (APS) and d_g values with static light scattering and SEM micrographs. The emitted HFA droplets, on the order of 25 μm, were utilized to break apart and template the highly open flocs (Fig. 6.1). Upon evaporation of the HFA, the shrinkage of the flocs

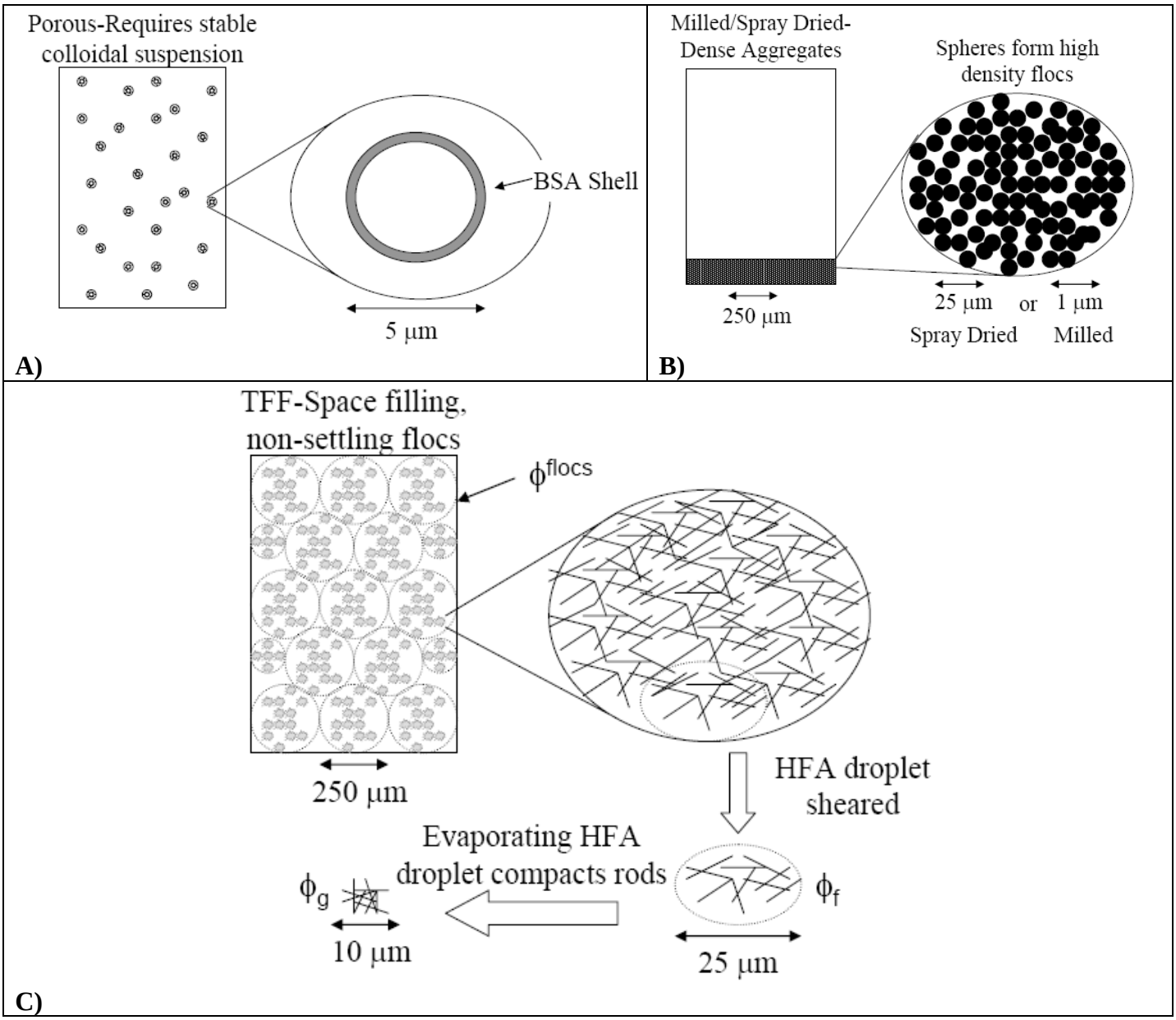

Figure. 6.1: Particle suspensions of hollow sphere particles (A), milled or spray dried particles (B), and TFF rod particles (C).

from capillary forces will be shown to produce smaller and denser porous particles with desirable d_a.

In the discussion section, experimental and calculated settling rates are utilized to characterize particle volume fractions and fractal dimensions for flocs composed of either cylindrical (rods) or spherical primary particles. Calculations of van der Waals energies between suspended particles are presented to explain floc formation, suspension stability of low density flocs, and break up of the floc into subdomains upon templating the flocs with the HFA droplets. The particle shrinkage during HFA evaporation will be shown to lead to the final aerosolized particle size and porosity as explained with a material balance. This novel approach of flocculating, templating, and shrinking the particles results in proper d_a with low polydispersities (Fig. 6.1) without surfactants or cosolvents. Thus it circumvents the classical paradigm of attempting to stabilize colloidal dispersions of preformed primary particles with surfactants. The flocculation concept for achieving stable suspensions and high fine particles fractions without the need for surfactants is of practical interest for wide classes of low and high molecular weight pharmaceuticals and biopharmaceuticals that may be formed into nanorods (45, 51, 52).

6.2 MATERIALS AND METHODS

6.2.1 Materials

Bovine serum albumin (BSA), trehalose, and polyoxyethylene sorbitan monolaurate (Tween 20) were purchased from Sigma (St. Louis, MO). The propellant 1,1,1,2,3,3,3-heptafluoroprane (HFA 227) was purchased from Hoechst (Frankfurt, Germany) and 2H,3H-Perfluoropentane (HPFP) was purchased from SynQuest Labs Inc. (Alachua, FL). The Micro BCA Protein Assay Reagent Kit was obtained from Pierce (Rockford, IL). The water was deionized by flowing distilled water through a series of

2x7 L mixed bed vessels (Water and Power Technologies, Salt Lake City, UT) containing 60:40 anionic:cationic resin blends.

6.2.2 Powder preparation

6.2.2.1 Thin film freezing (TFF)

BSA powders were prepared by the thin film freezing (TFF) process described previously (45). Briefly, 5 mg/mL feed solution of BSA in 10 mM pH = 7.4 potassium phosphate buffer was passed at a flow rate of 4 mL/min through a 17 gauge (1.1 mm ID, 1.5 mm OD) stainless steel syringe needle. The droplets fell from a height of 10 cm above a rotating stainless steel drum (12 rpm) 17 cm long and 12 cm in diameter. The hollow stainless steel drum was filled with dry ice to maintain a drum surface temperature of 223 K. On impact, the droplets deformed into thin films and froze. The frozen thin films were removed from the drum by a stainless steel blade and transferred to a 400 mL Pyrex® beaker filled with liquid nitrogen. The excess liquid nitrogen was evaporated in a -80 °C freezer.

A Virtis Advantage Lyophilizer (The Virtis Company, Inc., Gardiner, NY) was used to dry the frozen slurries. Primary drying was carried out at -40ºC for 36 hrs at 300 mTorr and secondary drying at 25ºC for 24 hrs at 100 mTorr. A 12 hour linear ramp of the shelf temperature from -40°C to +25°C was used at 100 mTorr.

6.2.2.2 Spray drying

Spray drying was performed with a Buchi Model 190 mini spray dryer (Brinkmann, Westbury, NY). A 10 mg/mL BSA feed solution in 10 mM potassium phosphate buffer (pH = 7.4) was atomized using a 0.5 mm ID two fluid nozzle with an atomizing air flow rate of 200 mL/s. The liquid protein formulation was pumped through the nozzle by a peristaltic pump (VWR, Bridgeport, NJ) at a flow rate of 5 mL/min using 5 mm ID silicone tubing. The inlet temperature for the heated aspirator air was set to

150ºC at a flow rate of 1000 L/hr. The resulting outlet temperature from the above conditions was 80ºC.

6.2.2.3 Milling

Bulk BSA powder as received was suspended at 5 mg/mL in acetonitrile. The BSA suspension was placed in a mill filled with 50 ceramic balls approximately 1 cm in diameter and milled on a mechanical roller for 24 hours. The milled BSA suspension was dried in the Virtis Advantage Lyophilizer at a shelf temperature of 30ºC for 12 hrs at 1000 mTorr.

6.2.3 Particle size analysis and preparation of protein HFA suspensions

Dry powders were placed in 60 mL glass bottles (Qorpak, Bridgeville, PA) and pre-cooled in a -80ºC freezer. HFA 227 was also pre-cooled in a -80ºC freezer and poured into the bottles containing the protein powders to form 0.7% (w/w) suspensions. The bottles were packed in dry ice and the suspensions were then sonicated for 2 min. using a Branson Sonifier 450 (Branson Ultrasonics Corporation, Danbury, CT) with a 102 converter and tip operated in pulse mode at 35 W. Approximately 5 mL aliquots of the suspension were then dispensed into a 500 mL acetonitrile bath for particle size analysis by static light scattering with a Malvern Mastersizer-S (Malvern Instruments, Ltd.,Worcestershire, UK). Typical obscuration values ranged from 11 to 13%. Next, 10 mL of the cooled protein formulations were dispensed into 17 mL glass pMDI aerosol vials (SGD, Paris, France) and fitted with metering valves containing 100 μL metering chambers (DF10 RC 150, Valois of America, Inc., Congers, NY). The vials were then allowed to warm up to room temperature.

The dried powders were also suspended in acetonitrile at a concentration of 5 mg/mL and sonicated for 2-3 min. in the same manner described above. Approximately

2 mL of the sonicated suspension was dispersed into a 500 mL acetonitrile bath and the particle sizes were analyzed by static light scattering.

6.2.4 Quantitation of BSA

The amount of BSA was measured using the Micro BCA Protein Assay following protocols provided by Pierce (Rockford, IL). Each sample was measured in triplicate with relative standard deviations (%RSD) < 2%. The absorbance of the solutions was measured at 562 nm in a 96 well plate spectrophotometer (μQuant Model MQX200; Biotek Instruments Inc., Winooski, VT). Untreated BSA was used to prepare the protein standards at concentrations between 2 and 30 μg/mL.

6.2.5 Dose delivered through the valve (DDV) determination

The protein suspensions in HFA were actuated once through the firing adaptor of a dosage unit sample tube (26.6 mm ID x 37.7 mm OD x 103.2 mm length; 50 mL volume; Jade Corporation, Huntingdon, PA) (53). The firing adaptor was removed, and 40 mL of DI water was added to dissolve the protein. The sampling tube was shaken and allowed to sit for at least 30 min. to assure that the protein was dissolved in water. The protein concentration was determined using the Micro BCA protein assay in conjunction with the μQuant spectrophotometer. The glass vial containing the HFA protein suspension was weighed before and after each actuation to assure that the proper dose had been released. The measurement was repeated 3 times to get an average dose delivered through the valve (DDV) for each formulation.

6.2.6 Aerodynamic diameter characterization of protein aerosol

To characterize the aerodynamic properties of the particles, an eight-stage Andersen cascade impactor (ACI) (Thermo-Andersen, Smyrna, GA) with an attached 15 cm spacer and an air flow-rate of 28.3 L/min was used to quantify mass median aerodynamic diameter (MMAD), geometric standard deviation (GSD), fine particle

fraction (FPF), and emitted dose (ED). Initially 3 shots were sent to waste, and the next 5 shots were made into the ACI. The interval between shots was between 15-30 s to prevent cooling of the metering chamber and subsequent moisture condensation. After the last dose was discharged, the glass vial was removed from the impactor and the valve stem and actuator were rinsed separately with a known volume of DI water. Each plate of the impactor was placed in a separate container with a known volume of DI water and soaked for 30 min. to assure complete dissolution. The protein concentrations were then measured with the Micro BCA Protein Assay.

The d_a of the protein particles were also determined in triplicate with an Aerodynamic Particle Sizer (APS) 3321 (TSI, Shoreview, MN). The throat and spacer from the ACI were placed over the inlet of the APS and the airflow rate through the inlet was 5 L/min. Each formulation was shot once through the spacer and throat. The particle size range by mass was determined with the Aerosol Instrument Manager (AIM) software provided by TSI.

6.2.7 Geometric diameter characterization of protein aerosol

To obtain aerosolized particles for scanning electron microscopy (SEM) (Hitachi Model S-4500, Hitachi Ltd, Tokyo, Japan) analysis, double carbon adhesive tape was applied to stage 3 of the ACI. Each formulation was actuated once through the ACI with an air flow rate of 28.3 L/min. The carbon tape was removed from stage 3 and applied to an aluminum SEM stage, which was transferred rapidly to a Pelco Model 3 sputter-coater to minimize exposure to moisture. Total exposure to the atmosphere was less than 1 minute. The SEM micrographs were then characterized with imaging software (Scion, Frederick, MD) to determine the particle size distribution of at least 100 particles.

The aerosolized particles were also characterized by static light scattering. Each formulation was actuated once through the ACI spacer and throat. The aerosol exited the

outlet of the throat downwards 5 cm directly above the laser beam of the Malvern Mastersizer S. For each formulation 100 measurements of the aerosolized spray were made every 5 ms. The recorded measurements were then averaged to give the final profile of the aerosolized particles on a volume basis.

6.2.8 Moisture content in pressurized metered dose inhalers

Moisture contents in the vials of each formulation were tested with an Aquatest 8 Karl-Fischer Titrator (Photovolt Instruments, Indianapolis, IN) according to the method described by Kim et al. (54). A 19 gauge needle was inserted through the septum of the titration cell with the needle tip placed below the reagent, and each formulation was measured in triplicate. For all formulations tested the moisture content was approximately 500 ppm. The pure HFA was found to have a moisture content of 250 ppm. The total amount of moisture to the amount of protein particles was 7% (w/w).

6.2.9 Microscope images of protein suspended in HFA

The particles were initially dispersed by pipette mixing in HPFP and were observed for 2 min. with a Nikon OPTIPHOT 2-POL optical microscope with an attached MTI CCD-72X camera (Nikon, Tokyo, Japan). Pictures were taken 30 and 60 seconds after initial dispersion in HPFP.

6.2.10 Optical density measurements of protein

The μQuant spectrophotometer was used to measure turbidity at 350 nm to characterize BSA aggregation. Dry powders of BSA were reconstituted to 1 mg/mL and 3 x 300 uL aliquots of each formulation were placed in a 96 well Falcon plate which was set in the spectrophotometer.

6.2.11 Dynamic light scattering

Particles of BSA suspended in acetonitrile were analyzed by a custom-built dynamic light scattering (DLS) apparatus (55). The scattering angle was set to 90º and the data were analyzed a digital autocorrelator (Brookhaven BI-9000AT) and a non-negative least-squares (NNLS) routine (Brookhaven 9KDLSW32). The suspension concentration was 0.5 mg/mL which gave a measured count rate of approximately 150 kcps. Measurements were made over a period of 2 min.

6.2.12 Tap density

Approximately 100-300 mg of protein powder was loaded into a 100 mL graduated cylinder. The tap density of the protein particles was measured with a Vankel tap density meter (Varian, Palo Alto, CA).

6.3 RESULTS

6.3.1 Particle morphology produced by thin film freezing, spray drying and milling

The fluffy BSA particles made by TFF shown in Fig. 6.2A had a low tap density of 0.0064 g/cm^3. The morphology of the BSA powder prepared by TFF was interconnected rods 50 nm in diameter (Fig. 6.3A). With the addition of 5 mg/mL trehalose to the BSA feed solution, similar rods were produced, as well as fine 50-100 nm relatively spherical particles (Fig. 6.3B). Similar morphologies were observed previously for lysozyme produced by TFF at 223 K (45). The BSA particles prepared by wet milling (Fig. 6.3C) did not have high external porosity like the TFF particles, but were in the form of cubes with smooth sides with 400-800 nm dimensions. Lastly, spray drying BSA at a feed concentration of 10 mg/mL formed protein particle spheres 3-6 μm in diameter with smooth surfaces (Fig. 6.3D).

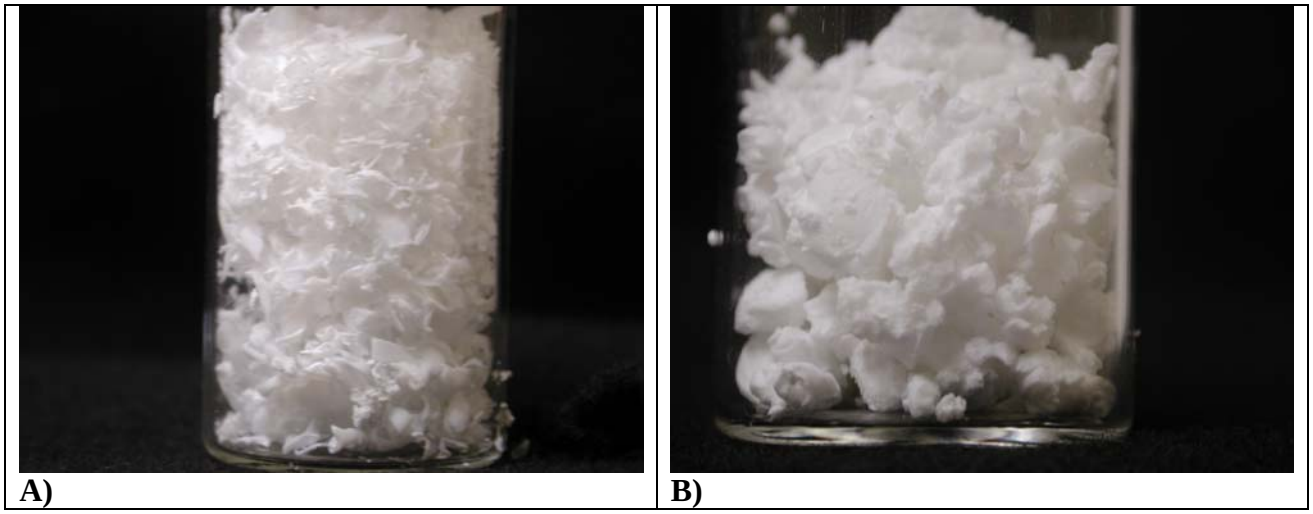

Figure 6.2: TFF particles after lyophilization loaded into vial (A) and TFF particles after drying from acetonitrile (B)

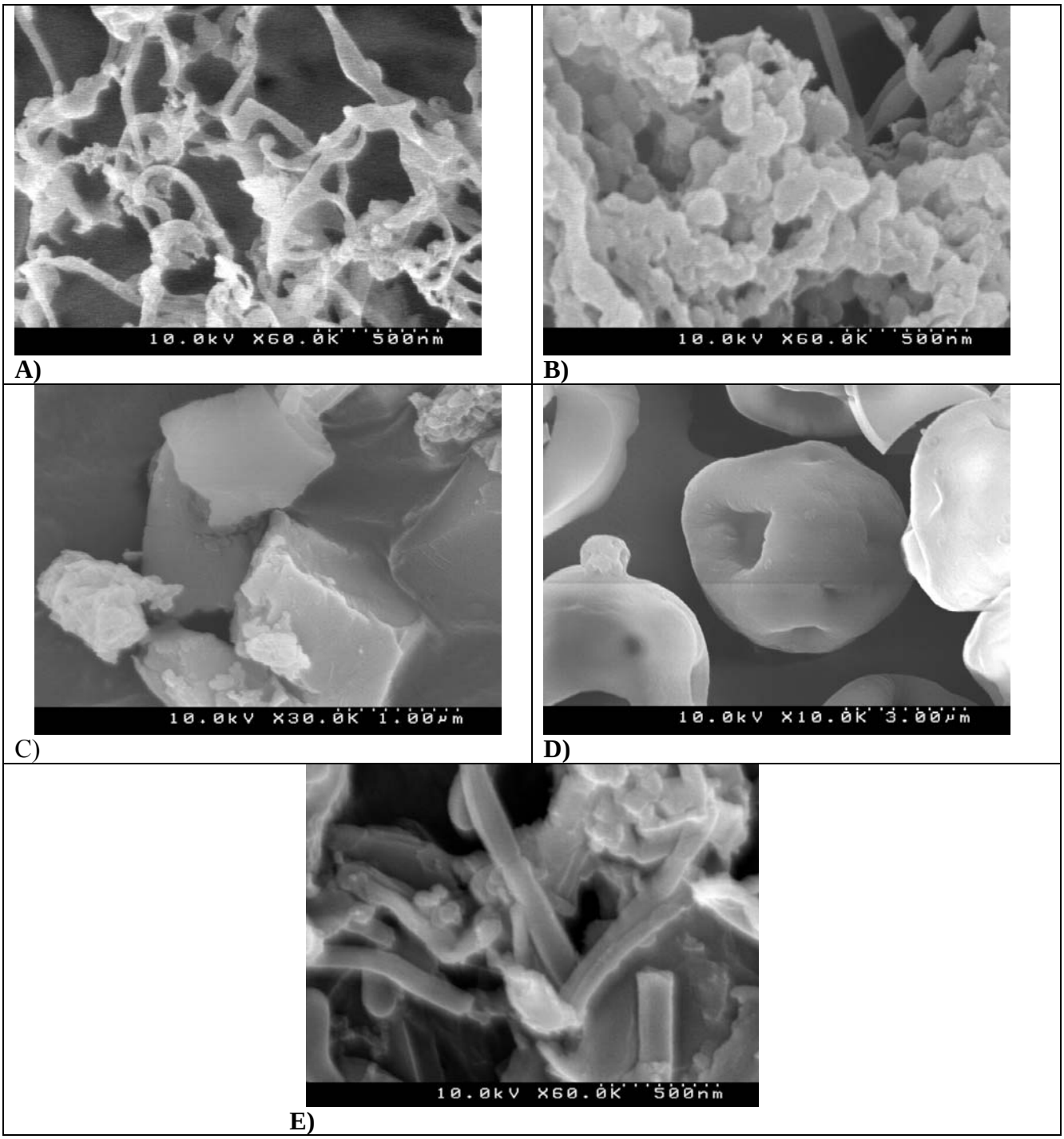

Figure 6.3: TFF particles of BSA (A) and BSA:Trehalose 1:1 (B), milled BSA particles (C), spray dried BSA particles (D), and TFF particles after drying from acetonitrile

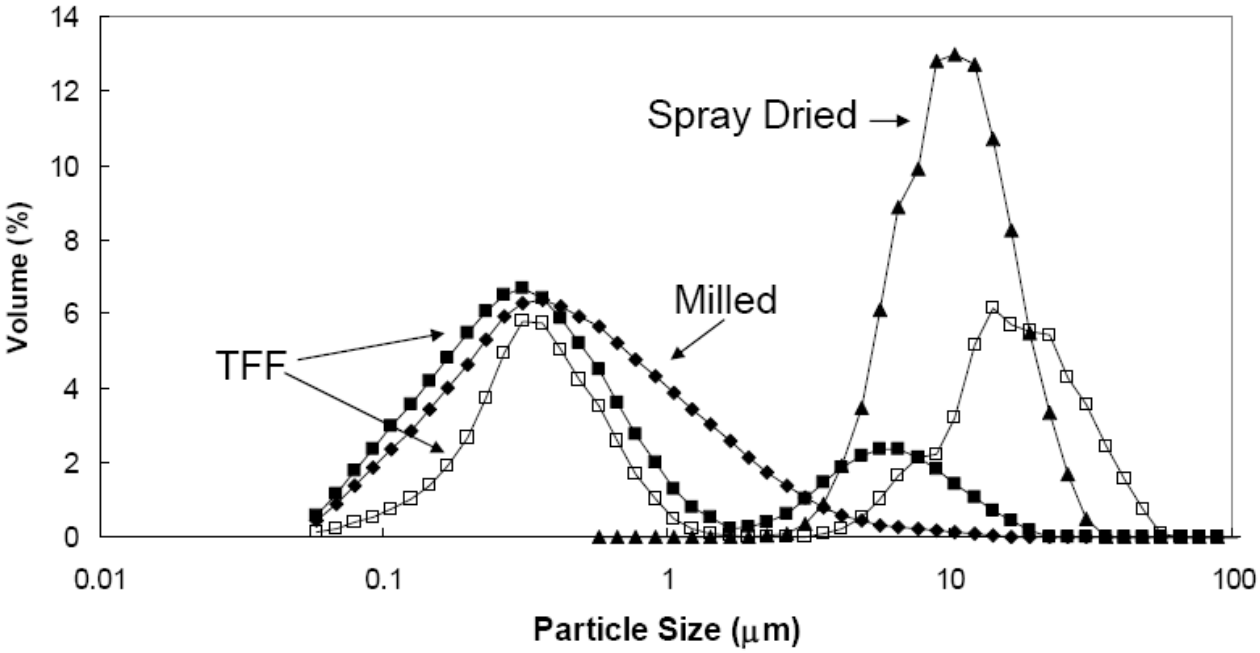

Figure 6.4: Particle sizes measured by static light scattering for BSA spheres formed by milling and spray drying and BSA nanorods formed by thin film freezing (TFF) suspended in acetonitrile where closed symbols indicate sonicated powder and open circles indicate unsonicated powder

For characterization by static light scattering, the various BSA particles suspended in acetonitrile were sonicated for 2 min. As shown in Fig. 6.4 the d(v,50) values were 330 nm, 410 nm and 6.3 μm for the TFF, milled and spray dried BSA particles, respectively, consistent with the sizes in the SEMs. Thus, the primary particles remain dispersed in acetonitrile and do not aggregate. As demonstrated previously with lysozyme (45), the cooling rate in the TFF process for BSA was sufficiently fast to form high surface area powders that redisperse to 330 nm particles in acetonitrile, with little sonication (<2 min). As a further indication of high tendency of the nanorods to deaggregate and disperse in acetonitrile, even with no sonication 2 peaks were observed with maxima at 330 nm and 20 μm, with approximately 50% of the particles by volume below 1 μm (Fig. 6.4). Thus the aggregation of the nanorods in the powder state is highly reversible.

To compliment the light scattering results by SEM, the sonicated suspensions in ACN were frozen by drip freezing into liquid nitrogen. The acetonitrile was then removed by lyophilization leaving fluffy particles with an approximate tap density of 0.012 g/cm^3 (Fig. 6.2B). When the particles were redispersed in acetonitrile the measured particle size profile was d(v,50) = 330 nm which was similar to the profile in Fig. 6.4 of the original TFF dispersion, indicating that the lyophilization process did not cause irreversible particle aggregation. As observed by SEM, the morphology in Fig. 6.3E were 50-100 nm diameter rods, similar to the interconnected rods of the original TFF powder in Fig. 6.3A, and consistent with the sizes from light scattering results in Fig. 6.4. Thus exposure to acetonitrile followed by sonication does not alter the morphology significantly

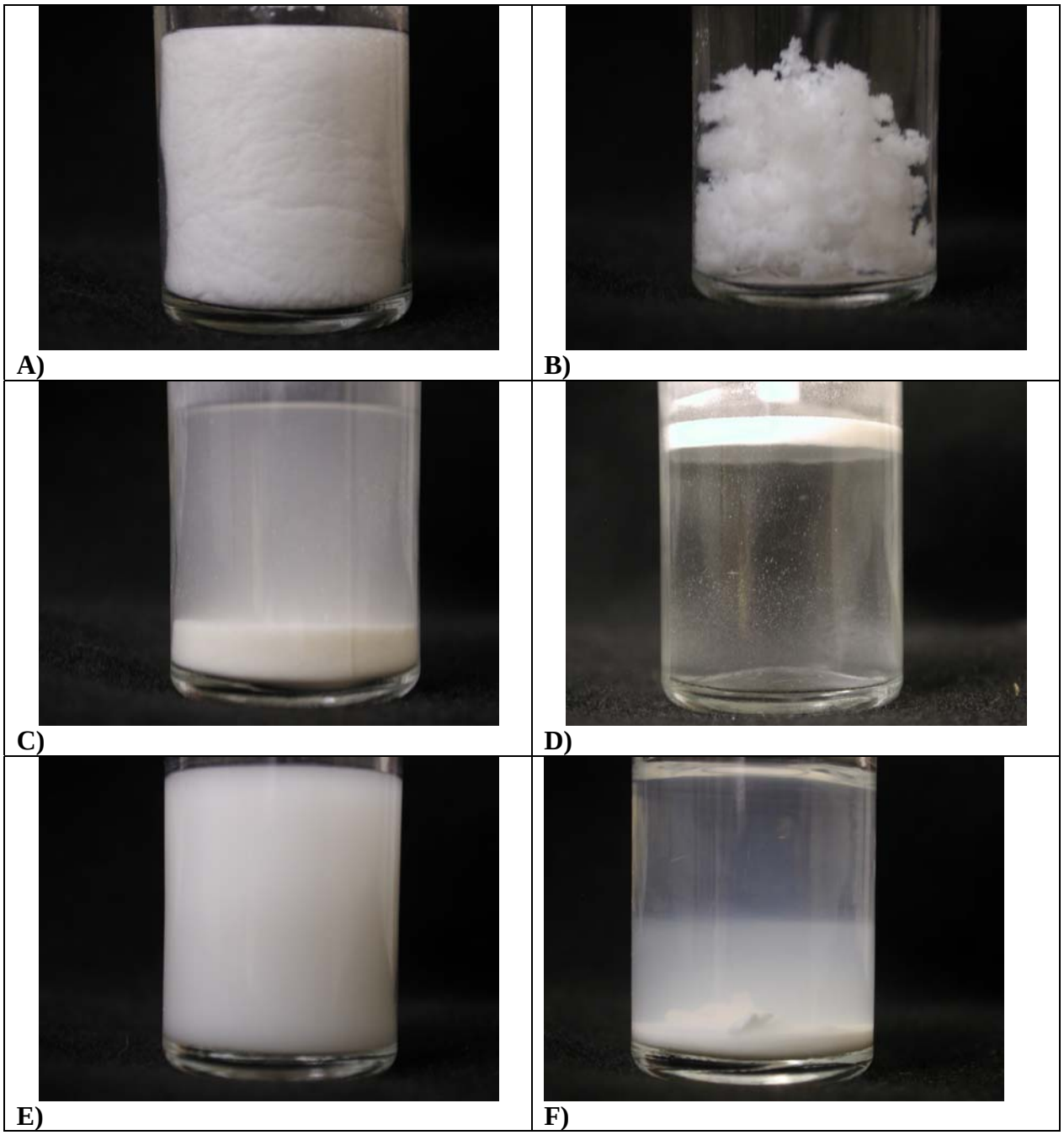

Figure 6.5: Suspensions in HFA 227 of TFF particles at ϕ_v = 0.0077 (A) and ϕ_v = 0.00077 (B), milled particles 5 minutes after shaking (C) and spray dried particles at 2 minutes after shaking (D) at ϕ_v = 0.0077, and TFF particles in acetonitrile at ϕ_v = 0.0077 immediately after shaking (E) and 3 days after shaking (F).

6.3.2 Visual observation of the particles suspended in HFA and acetonitrile

The dried TFF BSA particles were suspended in HFA 227 and acetonitrile (ACN) at 0.70% (w/w) corresponding to a volume fraction in the vial ϕ_v of 0.0077, as determined from the true density of BSA ρ_p = 1.3 g/cm^3 (56) (Fig. 6.5). The particles did not settle even after 1 year in storage in HFA 227 (Fig. 6.5A). Immediately upon adding HFA, the particles formed flocs that filled the entire volume of the vial. For a control with an extremely low ϕ_v of only 0.070% (w/w) (Fig. 6.5B) the loose buoyant flocs still filled approximately half the HFA volume. For the milled BSA nanoparticles, the suspension initially appeared to be uniform (like Fig. 6.5A), but the particles settled to the bottom after only 5 min. (Fig. 6.5C). Since these particles settled in HFA 227 (1.41 g/cm^3) (57), the milling may have compacted the particles to ρ above 1.3 g/cm^3. These particles creamed in HPFP (1.59 g/cm^3) (57). Thus, it was estimated that ρ_p ~ 1.50 g/cm^3, the average of the two solvent densities. The spray dried particles dispersed well with shaking, but creamed after only 2 min. (Fig. 6.5D). The TFF nanorods suspended in acetonitrile and sonicated for 2 min. formed a milky uniform dispersion (Fig. 6.5E). After 3 days the particles had settled (Fig. 6.5F). The dispersion/settling behavior shown in Fig. 6.5E and F was also observed for milled and spray dried particles in acetonitrile (data not shown) with settling in ~3 days and ~30 min., respectively.

6.3.3 Optical microscopy and light scattering of HFA suspensions

Because the vapor pressure of HFA 227 is above ambient at 25^o C(~500 kPa) (57), the particles were not studied *in situ* by microscopy or light scattering. Instead, the particles were studied at ambient pressure in HPFP, a surrogate nonvolatile solvent. Because HPFP has a similar polarity and polarizability as HFA 227, attractive forces between solutes such as budesonide are similar in both solvents on the basis of atomic

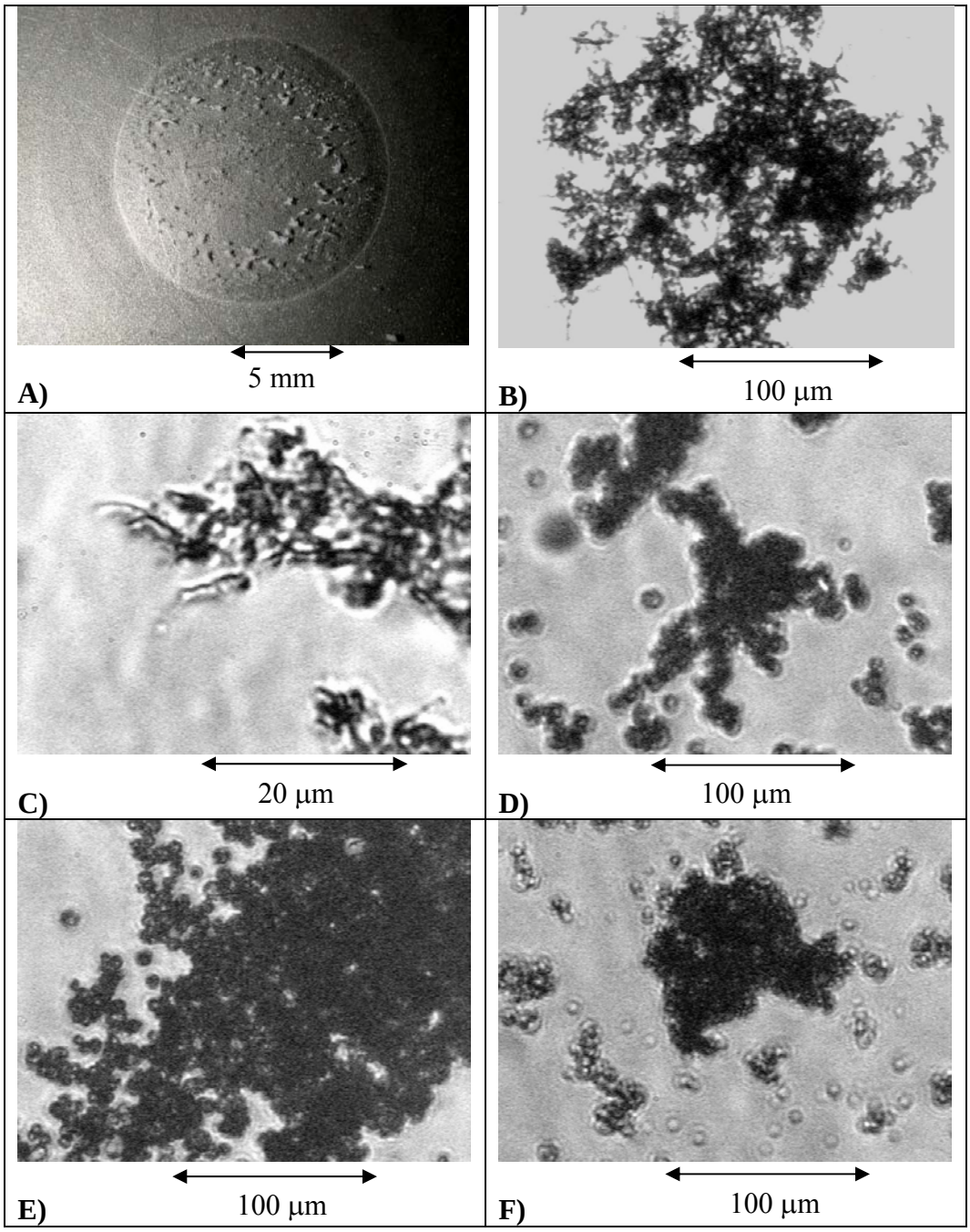

Figure 6.6: Optical microscopy images of BSA particles suspended in HPFP with TFF particles magnified 4x (A), 10x (B), and 60x (C), spray dried BSA particles after 30 seconds at 10x (D), and after 60 seconds (E), and milled BSA particles after 30 seconds at 10x (F)

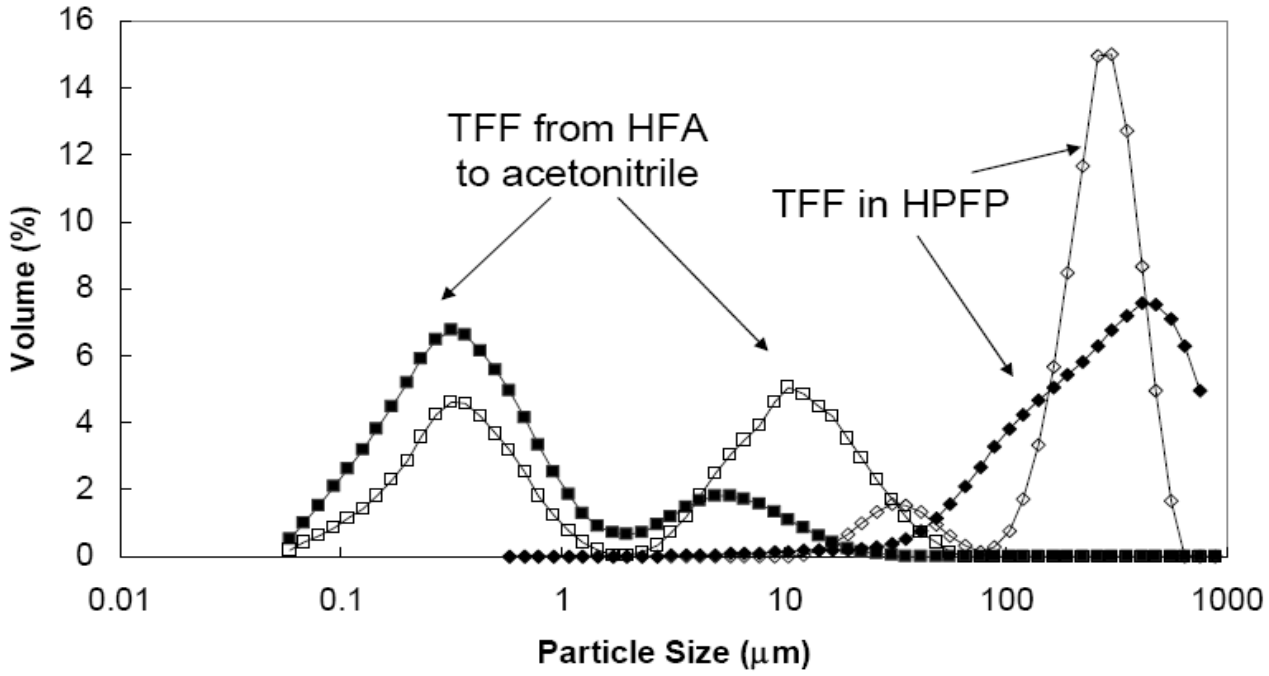

Figure 6.7: Particle sizes measured by static light scattering for BSA nanorods from thin film freezing (TFF) suspended in HFA 227 or HPFP where closed symbols indicate sonicated powder and open circles indicate unsonicated powder

force microscopy (AFM) (57-59). According to light microscopy (Fig. 6.6A), the TFF particles in HPFP were in the form of loosely packed aggregates of rods (Fig. 6.6B and C). The particles were in 200-300 μm flocs with subdomains on the order of 25 μm within 5 s. after dispersing the particles by pipette mixing (Fig. 6.6A and B). These sizes were consistent with static light scattering measurements of the sonicated and unsonicated suspensions in HPFP with d(v,50) values between 215-259 μm (Fig. 6.7). For the spray dried (Fig. 6.6D and E) and milled (Fig. 6.6F) particles, 100 μm flocs formed in 30 seconds and grew to over 200 μm in 60 seconds. These flocs were more densely packed and composed of larger primary particles than those formed from TFF particles.

6.3.4 Reversibility of flocs formed from TFF nanorods suspended in HFA 227

To better anticipate the fate of particles throughout the pMDI delivery process, it would be beneficial to determine how reversibly the nanorods are bound together in the flocs, for example with SEM or light scattering. The elevated pressure of the HFA complicates *in situ* light scattering. Furthermore, the HFA suspension could not be lyophilized since the freezing point (-131ºC) of HFA 227 is too low to for conventional shelf lyophilizers (57, 60). To investigate the effect of HFA evaporation on the particles, HFA was cooled to -80ºC, well below the boiling point of -16ºC (57), and completely evaporated. The TFF particle residue only occupied approx. 1 mL (tap density of 0.10 g/cm^3, Fig. 6.8A), an order of magnitude less than that of the starting TFF bulk powder (Fig. 6.2A). The morphology shown in Fig. 6.8A was rods with 100 nm diameters (Fig. 6.8B), similar to the original TFF particles in Fig. 6.3A. Therefore, exposure to HFA 227 followed by sonication did not significantly alter the microscopic nanorod morphology. However, the densified aggregates of nanorods formed by capillary forces upon evaporation (Fig. 6.5B) of HFA were not redispersible in HFA or in acetonitrile. For a

A)

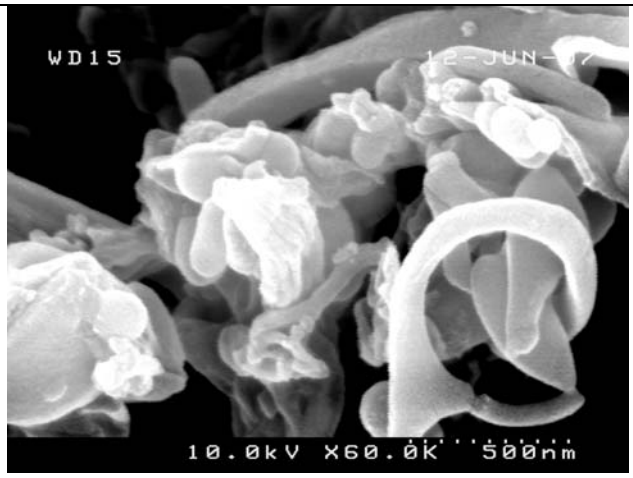

B)

Figure 6.8: TFF particles after HFA 227 evaporation (A) and SEM of TFF particles after sonication and HFA 227 evaporation (B)

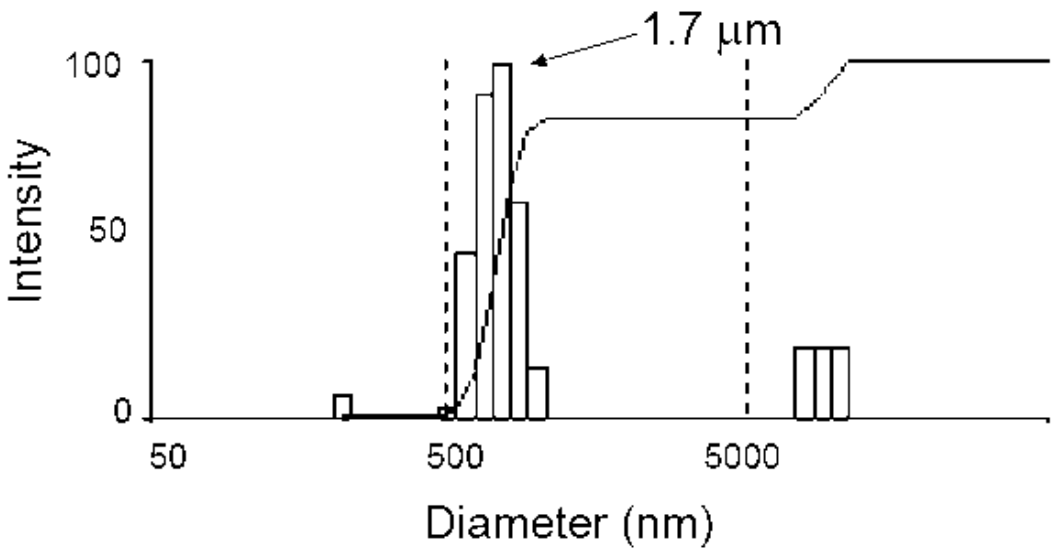

Figure 6.9: DLS of TFF particles actuated through the pMDI valve submerged beneath acetonitrile

sonicated TFF particle dispersion in acetonitrile, the lyophilized powder was redispersible in acetonitrile and HFA, forming suspensions identical to Fig. 6.5A. Thus it appeared that the capillary forces during HFA evaporation and perhaps moisture produced irreversible aggregation of the nanorods.

Given the challenges of *in situ* high pressure light scattering, lyophilization of HFA 227, and compaction of the TFF rods by capillary forces upon HFA evaporation, a more practical approach was to transfer the suspension from HFA 227 to a less volatile solvent. If the nanorods redisperse to primary particles in a good solvent such as acetonitrile, then they were not aggregated irreversibly in HFA 227. A 2 mL aliquot of the cold TFF suspension was mixed directly with 500 mL of acetonitrile at 25^{o}C. The flocs deaggregated nearly completely to individual primary particles with over 80% of the volume distribution between 100 nm and 1 μm, and a maximum at 11 μm (Fig. 6.7). A relatively small peak was centered at 5 μm. The distributions nearly matched those of the original TFF particles in acetonitrile. In a complimentary experiment, the valve of the pMDI containing was submerged into acetonitrile and actuated. A slightly turbid dispersion was formed with an approximate particle concentration of 0.5 mg/mL, too low for detection by static light scattering, but not for DLS. From DLS, the particle size was 1-2 μm (Fig. 6.9) much smaller than the 250 μm floc size in HFA. Therefore, both experiments indicate the loosely connected flocculated nanorods in HFA were reversible and broke up into primary nanorods, which will be shown to be beneficial for lung delivery.

Aggregates of protein molecules did not appear to form according to optical density (OD) measurements at 350 nm of 1 mg/mL BSA (43, 61). The OD was the same at 0.042 for aqueous solutions in 10 mM phosphate pH = 7.4 buffer prepared from bulk and TFF powder, both before and after storage in HFA 227 for 1 week. In the glassy

state, BSA is less susceptible to aggregation (60, 62). The total moisture to BSA content was 7% (w/w) for the suspended BSA particles in HFA 227 as determined by Karl-Fischer titration. Even at particle moisture contents of 8% (w/w), BSA glass transition temperatures T_g range between 80-100ºC (63). Thus the temperature was well below T_g, assuming the HFA 227 did not contribute to plasticization.

6.3.5 Properties of the particles after actuation through the pMDI

The suspension must be stable for consistent dosing with a pMDI, which is commonly characterized by the dose (mass) delivered through the valve (DDV) (Table 6.1). The concentration was 10 mg/mL or 0.7% (w/w) in each HFA suspension. Therefore, the theoretically delivered dose per actuation would be 1 mg with the 100 μL valve. For the BSA TFF particles, the DDV values were 92% and 63% of the theoretical delivery dose for the sonicated and unsonicated TFF particles, respectively (Table 6.1). For the BSA:Trehalose 1:1 formulation, it was 90%, and the delivered dose was 450 μg/actuation as a consequence of the lower amount of BSA loaded into the vial. For the milled and spray dried suspensions with rapid settling, the DDV was only 30-31% of the theoretical loading. Here, the formulation was actuated less than 5 seconds after vigorous shaking. Therefore, these suspensions were not tested further for aerosol properties.

As shown in Table 6.2 and Fig. 6.10, the d_a determined from the Andersen cascade impactor (ACI) and the Aerodynamic Particle Sizer (APS) were in good agreement and ranged from 3 to 4 μm, within the optimal 1-5 μm range for pulmonary delivery. As determined by the ACI, the fine particle fraction (FPF) (particles less than 4.7 μm) was unusually high (32) for an HFA suspension, ranging from 38 to 48%, compared to 5 to 30% for typical suspensions (32), producing a fine particle dose/actuation of approximately 300 μg for the first two formulations in Table 6.1. The emitted dose (ED) (amount of drug that exited the actuator) was approximately 70% of

Table 6.1: Dosage and aerodynamic properties of TFF, milled, and spray dried particle suspensions in HFA 227

Formulation	DDV (μg)	%Theoretical DDV	FPF (%)	Fine Particle Dose/Actuation (μg)	ED (μg)
TFF BSA	915 ± 21	92	47 ± 4.0	318 ± 31	695 ± 133
TFF BSA Tween 20	826 ± 58	83	43 ± 4.2	292 ± 16	690 ± 71
TFF BSA:Tre 1:1 Tween 20	452 ± 54	90	38 ± 2.1	132 ± 19	350 ± 56
TFF BSA unsonicated	625 ± 95	63	--	--	--
Milled BSA	295 ± 17	30	--	--	--
Spray Dried BSA	308± 38	31	--	--	--

Table 6.2: Aerodynamic particle sizes determined by ACI and APS and geometric particle sizes determined by laser diffraction and SEM

Formulation	ACI MMAD (μm)	ACI GSD	APS MMAD (μm)	APS GSD	d(v,50) Particle Diameter (μm)	SEM Particle Diameter (μm)	ρ_g (g/cm^3)
BSA	3.1 ± 0.1	1.9 ± 0.1	3.2 ± 0.03	1.6 ± 0.01	9.1 ± 0.9	9.4	0.19
BSA Tween 20	3.6 ± 0.1	1.9 ± 0.2	--	--	9.9 ± 0.8	9.3	--
BSA:Tre 1:1 Tween 20	3.2 ± 0.2	1.8 ± 0.1	4.0 ± 0.15	1.7 ± 0.01	7.3 ± 0.5	7.4	--

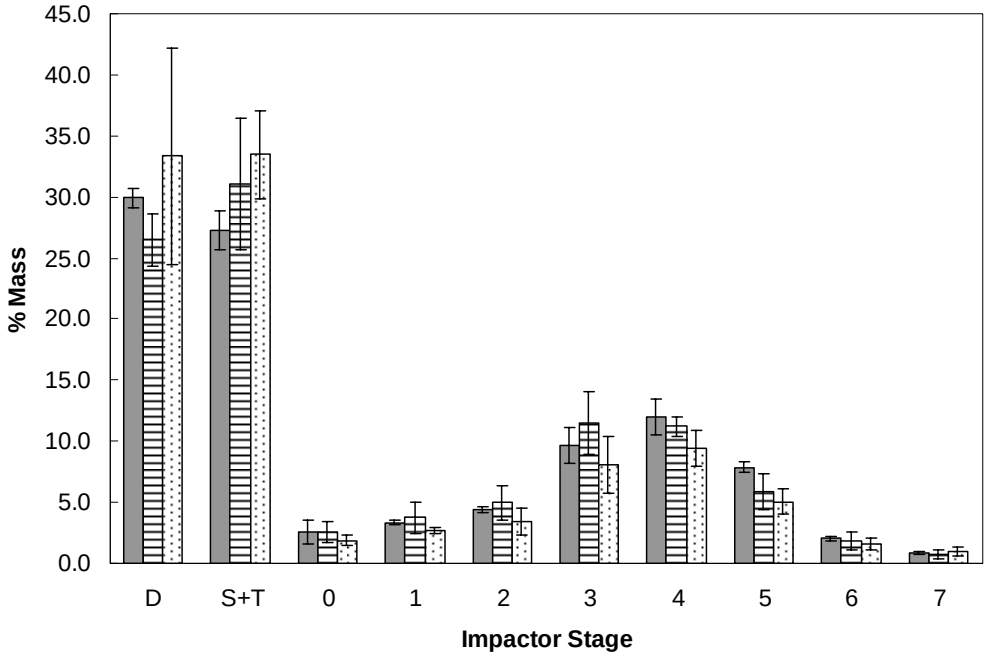

A)

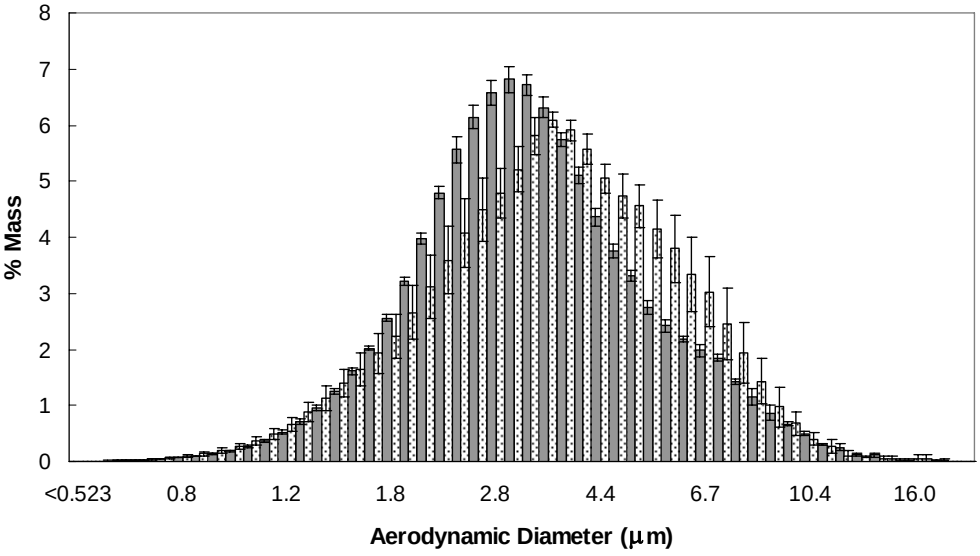

B)

Figure 6.10: ACI mass deposition profiles for device (D) and spacer and throat (S+T) and stages 0-7 (A), and APS mass distribution (B). Formulations on bar charts include BSA (diagonal lines), BSA + Tween 20 (horizontal lines), and BSA:Trehalose 1:1 + Tween 20 (dotted).

the DDV upon actuation (Table 6.1 and Fig. 6.10A). The addition of Tween 20 did not affect any of the properties of the aerosolized TFF powders in Table 6.1 significantly or the suspension stability, indicating that it was not needed as a stabilizer.

The particles were recovered from the ACI for SEM analysis. The peak drug mass in the ACI was deposited on stages 3 and 4, with d_a between 2.0-4.7 μm (Fig. 6.10A). Therefore, particles were collected on stage 3 (d_a = 3-4 μm). The particles were porous and composed of rods with diameters less than 500 nm (Fig. 6.11 A and B), similar in morphology to the original nanorods in Fig. 6.3A. For BSA:Trehalose 1:1 the fine 50-100 nm primary particles, shown in Fig. 6.3B, changed morphology to include curved plates with features on the order of more than one micron as shown in Fig. 6.11 C and D.

The SEMs were analyzed by Scion software to determine the volume average diameter (64, 65)

$$D_{Vol} = \frac{\sum d^4}{\sum d^3} \tag{1}$$

where d is the measured diameter of the particle. The D_{vol} for BSA was approximately 9 μm, while for BSA:Trehalose 1:1 it was slightly smaller at 7 μm (Table 6.2). The d_g of the aerosolized particles were also measured by static light scattering. An effective refractive index n_e was calculated according to the Bruggeman mixing rule (66) based on the volume fraction of BSA in the aerosolized particle ϕ_g (Appendix). From the d_g and the d_a (Table 6.2), the particle density ρ_g can be defined by (38)

$$d_a = d_g \sqrt{\rho_g} \tag{2}$$

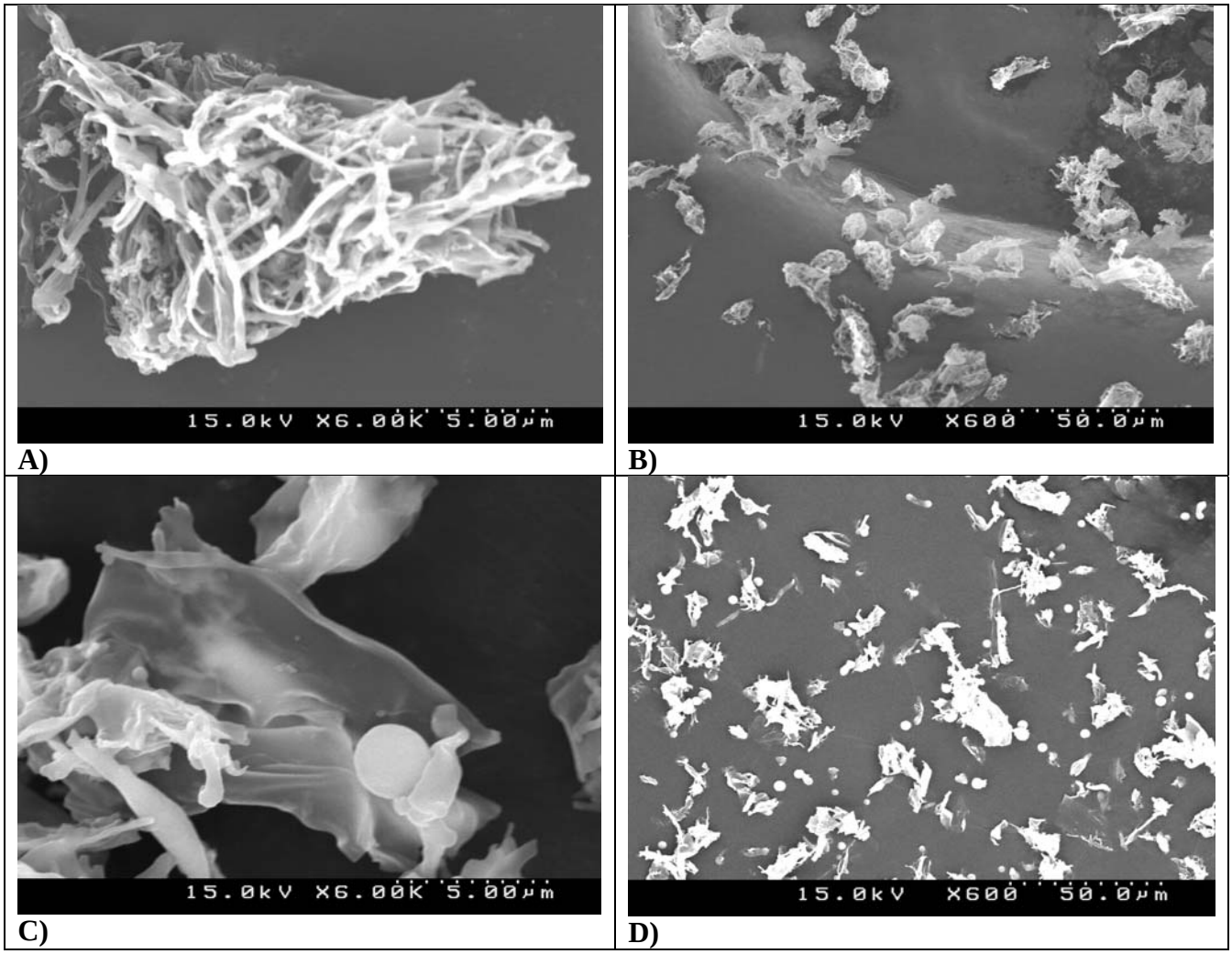

Figure 6.11: BSA aerosol particles collected from stage 3 of Andersen cascade impactor for BSA (A,B) and BSA:Trehalose 1:1 (C,D).

where ρ_g = 0.19 g/cm^3. The resulting $\phi_g = \rho_g / \rho_p$ = 0.14. With n = 1.45 and 1.00 for pure BSA and air, respectively, n_e = 1.1. As shown in Table 6.2 the volume average d(v,50) particle sizes varied by less than 1 μm from the values determined from the SEM micrographs. The consistent d_g and d_a, each measured by two techniques, indicate that TFF particles form large porous particles, and with the optimal size range for pulmonary delivery upon aerosolization. When the TFF particles were actuated above 10 mM phosphate buffer (pH = 7.4) the porous particles were observed to dissolve in less than 5 seconds. The high surface area favors rapid dissolution, which could be advantageous for rapid dissolution rates of proteins that have low solubilities in water (6).

6.4 DISCUSSION

The van der Waals forces between particles play a key role in the differences in colloidal stabilities of various types of primary particles and the behavior of the flocs in this study, as depicted in the summary in Fig. 6.1 (14, 48, 67). According to the Derjaguin-Landau-Verwey-Overbeek (DLVO) theory, particle stability depends on counteracting the attractive van der Waals forces by electrostatic and/or steric repulsion (14, 48, 67). If attractive van der Waals (VdW) forces are dominant at all separation distances, particles flocculate and may then settle (14). Currently, electrostatic stabilization in HFAs is not well understood (11), but atomic force microscopy (AFM) measurements indicate that electrostatic forces may be negligible compared to attractive VdW forces (11, 68). The understanding of steric stabilization in HFAs is in its infancy (33, 36). While novel surfactants are being discovered, developed and approved (35, 36), alternative mechanisms form the formation of stable suspensions in HFAs without surfactants would be useful (11).

6.4.1 Suspension stability for porous or hollow sphere particles

The destabilizing van der Waals attractive forces between suspended are weaker for porous particles or hollow particles with thin solid shells (21, 37). These particles can be stable for hours in HFAs, compared to non-porous 1-5 micron particles, which often flocculate and settle rapidly in less than 1 minute (21, 37) (see Table 6.2). Dellamary et al. (21) suggested that the increased suspension stability resulted from a weaker attractive VdW energy potential Φ_{vdw} between the particles (Fig. 6.1A), but quantitative calculations were not presented (11).

As shown in the Appendix the van der Waals energy Φ_{vdw} is directly proportional to the Hamaker constant A_{121}. In order to compare values of Φ_{vdw} it is necessary to choose a separation distance, h, between particles. Table 6.3 gives the h where Φ_{vdw} becomes equivalent to the thermal energy 3/2 k_BT at 298K. An increase in h required to overcome thermal energy indicates stronger attraction between particles. In Table 6.3, the porous particles with ϕ = 0.5 had a calculated A_{121} (Eq. A.3 in Appendix) that was nearly a factor of 4 lower than for the non-porous particles. Consequently, h was a factor of 3 smaller. The hollow spheres from TEM images (21) were estimated to have 2-5 μm diameters and ~100 nm thick shells. Although the A_{121} for the hollow sphere particles with solid shells was the same as for the non-porous particles, the calculated h was still lower by a factor of 2 as a consequence of the differences in the geometries (Eq. A.5 in Appendix). Therefore, the Φ_{vdw} calculations quantify the benefits of weaker attraction for porous particles or for particles with hollow cores. A reduction in Φ_{vdw} or in h to overcome thermal energy can reduce the rate of flocculation over orders of magnitude as described by the stability ratio (48, 67, 69).

Although, the porous or hollow sphere particles can effectively prevent flocculation, the particles are still subject to settling by gravity (11, 21). If porous or

Table 6.3: Calculation of the van der Waals (VdW) interaction potential Φ_{vdw} of BSA particles in HFA 227

Particle Type	**Particle Diameter (μm)**	**Hamaker Constant 10^{21} x A_{121} (J)**	**Separation Distance (nm) at $\Phi_{vdw} = 3/2k_BT$**
Spray Dried-Non-Porous	5.0	14	270
Spray Dried-Porous $\phi = 0.50$	5.0	3.8	100
Spray Dried-Hollow Sphere[a] $\phi_{shell} = 1.0$	5.0	14	120
Spray Dried-Hollow Sphere[a] $\phi_{shell} = 0.50$	5.0	3.8	60
TFF Nanorods	0.33	14	23
TFF Nanorods[b]	0.33	2.6	6.9

[a]Shell thickness 100 nm
[b]TFF nanorods in acetonitrile

Table 6.4: Settling behavior of BSA particles prepared by TFF, milling, and spray drying and calculations for porous shell particles prepared by spray drying

Particle Type	d_p (μm)	d^{floc} (μm)	$(\rho_L-\rho_f)$ (g/cm^3)	U_f (mm/s)	U_p (mm/s)	ϕ_v	ϕ^{flocs}	ϕ_f	D_f
TFF	0.33[a]	250	0.00022	0.023	2.4×10^{-5}	0.00077	0.38	0.0020	2.4
Milled	0.41	100	0.0080[b]	0.13	3.7×10^{-5}	0.0067	0.11	0.073	2.5
Spray Dried	6.3	100	0.040	0.80	8.8×10^{-3}	0.0077	0.021	0.36	2.6
Spray Dried-Hollow Sphere	5.0[c]	--	0.013[d]	--	6.4×10^{-4}	--	--	--	--

[a]Value determined from the equivalent volume of a sphere measured from laser light scattering

[b]The density difference was determined by $\rho_f-\rho_L$ with $\rho_p = 1.5$ g/cm^3

[c]Determined from dimensions given by Dellamary et al. (21)

[d]Calculated for primary particle with 100 nm thick shell

hollow sphere BSA particles were suspended at ϕ_v = 0.0077, the particles would occupy ~ 10% of the suspension (Fig. 6.1A) and could potentially settle into a dense sediment. As shown in Table 6.4, the calculated settling rate for a single hollow sphere particle with a solid shell is 6.4 x 10^{-4} mm/s indicating that the particles would settle a distance of 2 cm in ~ 9 hrs. The settled particles would then potentially aggregate irreversibly leading to decreased FPFs upon aerosolization (31).

6.4.2 Suspension stability—low density flocs

The concept in this study of stabilizing suspensions with purposely flocculated rods is based on the space filling properties of the rods and the flocs. Experimental and theoretical studies indicate that rods create extremely low density flocs and thus fill much greater space compared to spheres as illustrated in Fig. 6.1B and C (47, 49, 50). For spheres, the volume fraction of primary particles within a floc ϕ_f is related to the floc diameter d^{floc}, primary particle diameter d_p, and fractal dimension D_f, which characterizes the floc structure, by (70)

$$\phi_f \approx \left(\frac{d^{floc}}{d_p} \right)^{D_f - 3} \tag{3}$$

Philipse et al. modified Eq. 3 to account for the packing physics of cylindrical rods of length L and diameter D with the result (49)

$$\phi_f \approx \frac{1}{r} \cdot \left(\frac{d^{floc}}{V_p^{1/3}} \right)^{D_f - 3} \tag{4}$$

where $r = L/D$ is the aspect ratio (49). The volume of a TFF cylindrical rod, V_p = 0.019 μm^3, was calculated from the equivalent volume of a sphere with particle diameter d(v,50) = 0.33 μm, which was measured by static light scattering (Fig. 6.4A) in acetonitrile. For a rod with volume $V_p = \pi \cdot D^2 L/4$ and D = 0.050 μm (Fig. 6.3A), L is determined as 0.48 μm and thus r = 9.6. For r ~ 10, the predicted ϕ_f in Eq. 4 is ~1 order of magnitude lower than for spherical particles with equivalent d^{floc}, D_f, and where d_p for spheres scales as $V_p^{1/3}$ for rods.

To test the theoretical predictions, the density of a floc ρ_f and ϕ_f can be determined experimentally from the visually observed floc settling rate, U_f, according to Stoke's law (71, 72)

$$U_f = \frac{d^{floc\,2} \cdot (\rho_f - \rho_L) \cdot g}{18 \cdot \mu} \tag{5}$$

where ρ_L and μ are the liquid density and viscosity, respectively, and d^{floc} = 250 μm for TFF flocs and 100 μm for spray dried and milled flocs (Fig. 6.6). After solving for ρ_f in Eq. 5, ϕ_f may be determined by the straightforward material balance $\rho_f = \rho_L + \phi_f \cdot (\rho_p - \rho_L)$ (71, 72). As seen in Table 6.4, ϕ_f for the TFF particles is 1-2 orders of magnitude lower than for the spherical milled and spray dried particles. From Eq. 3 and 4 the calculated D_f values are in a narrow range from 2.4 to 2.6 in each case. Although the milled particles have nearly equivalent d^{floc} and D_f values relative to the rods (Table 6.4), the $1/r$ scaling in Eq. 5 for rods accounts for the 1 order of magnitude decrease in ϕ_f, for a given V_p, which is consistent with theoretical prediction above.

The extremely low ϕ_f means the flocs will fill a huge volume of space for a given ϕ_v (Fig. 6.1C). The open nanorod flocs with low ϕ_f filled large amounts of space in HFA and stacked upon each other like tumbleweeds to prevent settling. The volume

fraction of flocs in the HFA suspension, ϕ^{flocs}, is given by $\phi^{flocs} = \phi_v / \phi_f$ (derivation given in Appendix) where ϕ^{flocs} determines the space filling capability of the flocs. As ϕ^{flocs} approaches 1 the flocs occupy the entire volume of HFA (Fig. 6.1C). For the dilute ϕ_v = 0.00077 suspension (Fig. 6.5B), the calculated ϕ^{flocs} was 0.38 (Table 6.4) in good agreement with Fig. 6.5B. At a loading 10 fold higher, ϕ_v = 0.0077, the entire vial was white without the appearance of spaces between flocs (Fig. 6.5A), as expected from the low ϕ_f. Here it was not possible to observe a settling rate as the visual appearance did not change for 1 year, the maximum time tested, as the ϕ^{flocs} of essentially unity prevented settling. In order for the spherical particles to produce ϕ^{flocs} = 1 the required mass loadings for the milled and spray dried particles would be 6.7% (w/w) and 33% (w/w), respectively, compared to <0.7% (w/w) for the TFF rods. In contrast to the TFF rods, the hollow sphere particles would settle the length of the vial (~2 cm) by gravity in ~9 hours according to Stoke's law (21) for a particle diameter of 5 μm and shell thickness of 100 μm. In the settled state with a high particle volume fraction and contact between protein chains they are more likely to form irreversible particle aggregates by interparticle diffusion and sintering (73).

The open flocs in HFA 227, that gave the stable suspensions, may be shown to be favored by the relatively strong attractive forces between the primary particles (48, 67). At first, this may seem counterintuitive to the normal goal of lowering attractive forces to stabilize colloidal dispersions. Upon addition of the HFA, the relatively strong attractive forces between the primary rods, Φ_{vdw}, cause sticky collisions to "lock in" the open structure rapidly to inhibit collapse of the flocs (48, 74). For weaker attractive forces between primary particles, collapse has been shown to be more prevalent as particles sample a greater number of energetically favorable locations to reduce the interfacial

surface area (48, 74). Therefore, rapid flocculation from sticky collisions facilitates the formation of low density flocs that fill the entire vial and prevent settling.

In contrast to the flocs in HFA 227, colloidal dispersions of primary TFF rods in acetonitrile settled in 3 days (Fig. 6.5F). This settling rate agreed with the predicted settling rate of individual effective spheres with a diameter of 330 nm from light scattering given in Table 6.4. From Table 6.3, the calculated A_{121} values for BSA in acetonitrile are 1 order of magnitude lower than in HFA 227 (Table 6.3). Therefore, the stronger attractive forces between particles in HFA relative to ACN, favors formation of open flocs, resulting in more stable suspensions against settling.

6.4.3 Aerosol formation from stable suspensions

Although the 250 μm flocs form stable suspensions, they are too large to produce optimal d_a. The shear forces in the actuator are needed to break apart the flocs. The calculation of these shear forces is rarely reported because the turbulence from the immediate onset of HFA evaporation produces complex cavitation events (65, 75). According to empirical models, aerosolized HFA droplets are typically 10-30 μm in diameter (75). Thus we choose an HFA droplet diameter of 25 μm. Our hypothesis is that the shear forces acting on the flocs are sufficiently strong to overcome the attractive van der Waals interactions between primary particles within a floc such that the HFA droplets may template the 250 μm flocs into 25 μm subdomains with the same ϕ_f = 0.0020 as illustrated schematically in Fig. 1. From the high ϕ^{flocs} (Table 1C) it is expected that most of the HFA droplets are likely to be filled with a subdomain.

Since direct comparison of calculated shear forces to van der Waals forces of primary particles within a floc is unfeasible, the concept of templating of the 25 μm subdomains is instead supported by a material balance on the protein between the volume

of the HFA droplet, V_{HFA}, and the volume of the dry aerosolized particle, V_g, (Fig. 6.1C) given by

$$V_g \cdot \rho_g = V_{HFA} \cdot \rho_{HFA} \tag{6}$$

where BSA concentrations are given by $\rho_{HFA} = \phi_v \cdot \rho_p$, and $\rho_g = \phi_g \cdot \rho_p$. It is assumed that the volume fraction of particles in HFA droplet is approximately equal to ϕ_v as a result of the break up of the flocs. From the d_g and d_a in Table 6.2 and ρ_g = 0.19 g/cm^3 (Eq. 2), ϕ_g = 0.14. The ϕ_g is nearly 20 times greater than ϕ_v in the vial. Therefore, the capillary forces in the shrinking HFA droplets during evaporation collapse the flocs (30). Eq. 6 is refined to relate ϕ_g to ϕ_v as

$$\phi_g \cdot {d_g}^3 = \frac{f_{BSA}}{f_{HFA}} \cdot \phi_v \cdot {d_{HFA}}^3 \tag{7}$$

where d is a diameter, f_{BSA} = 0.7 accounts for the mass fraction of drug that is emitted from the actuator, and f_{HFA} = 0.5 accounts for the mass fraction of HFA that exits the actuator orifice to form aerosolized liquid droplets (relative to vapor) (65).

From Eq. 7 with d_g = 9.3 μm (Table 6.2), d_{HFA} = 25 μm (75), and ϕ_v = 0.0077 , the calculated ϕ_g = 0.21, which compares reasonably well to the experimentally determined ϕ_g = 0.14. Also the polydispersity in the aerodynamic properties was small. It would be unlikely that any other factor besides templating of the flocs with relatively uniform HFA droplets could explain these low polydispersities.

The control experiment in Fig. 6.8A supports this argument since the TFF particles remained below the meniscus of the evaporating HFA 227. The tap density of the particles was approximately 0.10 g/cm^3 (Fig. 6.8A) which is within a factor of 2 of

the calculated density (0.19 g/cm^3) of the aerosolized particle. Therefore, the capillary forces acting on the TFF particles during HFA evaporation compacted the particles into denser aggregates with a highly desirable value of the d_a. If needed, the d_a may be manipulated further by varying the valve volume and geometry and the HFA droplet generation. If the particles had not collapsed partially, they would have been too large and light for pulmonary delivery. Even after this collapse, the porosity and surface area were still relatively high and favorable for high dissolution rates of small molecules and proteins with limited solubilities, relative to nonporous particles (6).

6.5 CONCLUSIONS

High (38-48%) fine particle fractions in HFA 227 pMDI delivery were achieved with flocculated BSA nanorods stable against settling for up to 1 year, without the use of surfactants and cosolvents. Analysis of experimental settling rates of dilute suspensions indicated that the volume fraction, ϕ_f, of the nanorods in the flocs was an order of magnitude lower than for flocs of spherical particles produced by milling or spray drying. The rapid and sticky attractive collisions of nanorods facilitates the formation of low density flocs (250 μm) which stack upon each other to fill the entire solvent volume to prevent settling (Fig. 6.1C). In contrast, denser flocs of spherical particles filled much less space and rapidly settled within 60 s (Fig. 6.1B). The novel concept of purposely flocculating nanorods to prevent settling is fundamentally opposite the conventional approach of stabilizing colloidal dispersions of primary particles. The reversibility of the nanorod flocs in HFA 227 was demonstrated by break up of the flocs into individual 330 nm primary rod particles upon transfer to the more polar solvent acetonitrile.

A material balance on a shrinking HFA droplet containing a 25 μm floc subdomain predicts a final volume fraction of BSA in the aerosolized particle in

agreement with experiment. Therefore, the attractive van der Waals interactions between primary particles within the floc are sufficiently weak such that the atomized HFA droplets initially template the 250 μm flocs into 25 μm subdomains. The aerosolized particles with a d_a of 3-4 μm and d_g of ~10 μm are optimal for high fine particle fractions via a pMDI. The concept of forming open flocs composed of nanorods, that are stable against settling without surfactants, and templating the flocs to achieve optimal d_as and high FPFs is of practical interest for wide classes of low and high molecular weight pharmaceuticals and biopharmaceuticals.

6.6 APPENDIX

6.6.1 Bruggeman mixing rule

For porous particles or suspensions with a BSA particle volume fraction ϕ, the effective refractive index n_e and dielectric constant ε_e can be calculated from the following Bruggeman mixing relationships

$$(1-\phi)\frac{n_A^{\,2}-n_e^{\,2}}{n_A^{\,2}+2n_e^{\,2}}+\phi\frac{n_B^{\,2}-n_e^{\,2}}{n_B^{\,2}+2n_e^{\,2}}=0 \tag{A.1}$$

$$(1-\phi)\frac{\varepsilon_A-\varepsilon_e}{\varepsilon_A+2\varepsilon_e}+\phi\frac{\varepsilon_B-\varepsilon_e}{\varepsilon_B+2\varepsilon_e}=0 \tag{A.2}$$

where ϕ can be either ϕ_g or ϕ_f, the subscript A denotes air or HFA 227, and B denotes BSA.

6.6.2 Attractive van der Waals equations

The Φ_{vdw} is directly proportional to the Hamaker constant A_{121} for one particle interacting with another (subscript 1) across solvent, such as HFA 227 or acetonitrile, (subscript 2) as a function of the particle geometry (76). The Hamaker constant A_{121} may be approximated by

$$A_{121} = \left(\sqrt{A_{11}} - \sqrt{A_{22}}\right)^2 \tag{A.3}$$

where A_{11} and A_{22} are the pure Hamaker constants for BSA and the suspending media interacting across a vacuum, respectively. These values were calculated from Lifshitz theory (76, 77). To determine A_{11} for porous BSA particles in HFA 227, ε_e and n_e were calculated with the Bruggeman mixing rule (Eq. A.1 and A.2) at ϕ = 0.5 in HFA 227 (37, 66). The van der Waals attractive potential between identical spherical particles (76)

$$\Phi_{vdw} = -\frac{A_{121}R}{12h} \tag{A.4}$$

where R is the spherical particle radius and h is the separation distance between the particle surfaces and for identical hollow spheres with solid shells (78)

$$\Phi_{vdw} = -\frac{A_{121}R}{12}\left(\frac{1}{h+2t} - \frac{2}{h+t} + \frac{1}{h}\right) - \frac{A_{121}}{6}\ln\left(\frac{h(h+2t)}{(h+t)^2}\right) \tag{A.5}$$

where t is the shell thickness. For identical rods, E_{vdw} can be calculated for parallel

$$\Phi_{vdw} = -\frac{A_{121}LR^{1/2}}{24h^{3/2}} \tag{A.6}$$

or crossed cylinders

$$\Phi_{vdw} = -\frac{A_{121}R}{6h} \tag{A.7}$$

where L is the cylinder length. The values from Eq. A.6 and A.7 were averaged to give equal weight to the two orientations (Table 6.4).

6.6.3 Space filling floc derivation

A vial filled with protein particles of total mass m and primary particle density ρ_p into a given volume V of HFA 227 has a volume fraction ϕ_v defined as

$$\phi_v = \frac{m/\rho_p}{V} \tag{A.8}$$

The volume fraction of particles in a floc ϕ_f is

$$\phi_f = \frac{V_p \cdot k}{V_f} \tag{A.9}$$

where V_p and V_f are the volume of a spherical primary particle and a spherical floc, respectively, and k is the number of primary particles in a floc.

The volume fraction of flocs in HFA ϕ^{flocs} is defined as

$$\phi^{flocs} = \frac{V_f \cdot N_f}{V} \tag{A.10}$$

where N_f is the total number of flocs in suspension. $N_f = N_p / k$ where $N_p = m / m_p$ is the total number of primary particles in suspension and $m_p = V_p \cdot \rho_p$ is the mass of a primary particle. Substitution into Eq A.3 gives

$$\phi^{flocs} = \frac{V_f \cdot m}{V_p \cdot k \cdot V \cdot \rho_p} = \frac{\phi_v}{\phi_f} \tag{A.11}$$

6.7 REFERENCES

1. R. U. Agu, M. I. Ugwoke, M. Armand, R. Kinget, and N. Verbeke. The lung as a route for systemic delivery of therapeutic proteins and peptides. *Respiratory Research* **2:**198-209 (2001).

2. A. L. Adjei and P. K. Gupta. *Inhalation Delivery of Therapeutic Peptides and Proteins*, 1997.

3. S. White, D. B. Bennett, S. Cheu, P. W. Conley, D. B. Guzek, S. Gray, J. Howard, R. Malcolmson, J. M. Parker, P. Roberts, N. Sadrzadeh, J. D. Schumacher, S. Seshadri, G. W. Sluggett, C. L. Stevenson, and N. J. Harper. EXUBERA: Pharmaceutical Development of a Novel Product for Pulmonary Delivery of Insulin. *Diabetes Tech. Therapeutics* **7:**896-906 (2005).

4. S. A. Shoyele and A. Slowey. Prospects of formulating proteins/peptides as aerosols for pulmonary drug delivery. *Int. J. Pharm.* **314:**1-8 (2006).

5. H. M. Courrier, N. Butz, and T. F. Vandamme. Pulmonary drug delivery systems: recent developments and prospects. *Crit. Rev. Therapeutic Drug Carrier Systems* **19:**425-498 (2002).

6. M. J. Kwon, J. H. Bae, J. J. Kim, K. Na, and E. S. Lee. Long acting porous microparticle for pulmonary protein delivery. *Int. J. Pharm.* **333:**5-9 (2007).

7. J. S. Patton and P. R. Byron. Inhaling medicines: delivering drugs to the body through the lungs. *Nature Rev. Drug Discovery* **6:**67-74 (2007).

8. V. Codrons, F. Vanderbist, R. K. Verbeeck, M. Arras, D. Lison, V. Preat, and R. Vanbever. Systemic delivery of parathyroid hormone (1-34) using inhalation dry powders in rats. *J. Pharm. Sci.* **92:**938-950 (2003).

9. L. Garcia-Contreras and H. D. C. Smyth. Liquid-spray or dry-powder systems for inhaled delivery of peptide and proteins? *Am. J. Drug Delivery* **3:**29-45 (2005).

10. D. Traini, P. Young, P. Rogueda, and R. Price. The Use of AFM and Surface Energy Measurements to Investigate Drug-Canister Material Interactions in a Model Pressurized Metered Dose Inhaler Formulation. *Aerosol Sci. Tech.* **40:**227-236 (2006).

11. P. Rogueda. Novel hydrofluoroalkane suspension formulations for respiratory drug delivery. *Expert Opinion Drug Del.* **2:**625-638 (2005).

12. R. O. Williams, III and J. Liu. Formulation of a protein with propellant HFA 134a for aerosol delivery. *Eur. J. Pharm. Sci.* **7:**137-144 (1999).

13. R. O. Williams, III, M. Repka, and J. Liu. Influence of propellant composition on drug delivery from a pressurized metered-dose inhaler. *Drug Dev. Ind. Pharm.* **24:**763-770 (1998).

14. K. A. Johnson. Interfacial phenomena and phase behavior in metered dose inhaler formulations. In A. J. Hickey (ed.), *Inhalation Aerosols: Physical and biological basis for therapy*, 2007.

15. E. A. Quinn, R. T. Forbes, A. C. Williams, M. J. Oliver, L. McKenzie, and T. S. Purewal. Protein conformational stability in the hydrofluoroalkane propellants tetrafluoroethane and heptafluoropropane analyzed by Fourier transform Raman spectroscopy. *Int. J. Pharm.* **186:**31-41 (1999).

16. M. J. Oliver, L. McKenzie, W. D. Graffiths, G. R. Morgan, and N. O'Kelly. Initial assessment of a protein formulated in pressurized mdis for pulmonary delivery, *RDD VII*, 2000.

17. C. Benfait. Kos reports achievement of new research and development milestones. *Kos Press Release* (2004).

18. J. Heyder, J. Gebhart, G. Rudolf, C. F. Schiller, and W. Stahlhofen. Deposition of particles in the human respiratory tract in the size range 0.005-15 μm. *J. Aerosol Sci.* **17:**811-825 (1986).

19. A. Ben-Jebria, D. Chen, M. L. Eskew, R. Vanbever, R. Langer, and D. A. Edwards. Large porous particles for sustained protection from carbachol-induced bronchoconstriction in guinea pigs. *Pharm. Res.* **16:**555-561 (1999).

20. N. Tsapis, D. Bennett, B. Jackson, D. A. Weitz, and D. A. Edwards. Trojan particles: large porous carriers of nanoparticles for drug delivery. *Proc. Natl. Acad. Sci. U. S. A.* **99:**12001-12005 (2002).

21. L. A. Dellamary, T. E. Tarara, D. J. Smith, C. H. Woelk, A. Adractas, M. L. Costello, H. Gill, and J. G. Weers. Hollow porous particles in metered dose inhalers. *Pharm. Res.* **17:**168-174 (2000).

22. Y.-F. Maa, P.-A. Nguyen, T. Sweeney, S. J. Shire, and C. C. Hsu. Protein inhalation powders: spray drying vs spray freeze drying. *Pharm. Res.* **16:**249-254 (1999).

23. Y.-F. Maa and H. R. Costantino. Spray freeze-drying of biopharmaceuticals: applications and stability considerations. In H. R. Costantino and M. J. Pikal

(eds.), *Biotechnology: Pharmaceutical Aspects. 2. Lyophilization of Biopharmaceuticals*, American Association of Pharmaceutical Scientists, Arlington, 2004, pp. 519-561.

24. Y.-F. Maa and S. J. Prestrelski. Biopharmaceutical powders: particle formation and formulation considerations. *Curr. Pharm. Biotechnol.* **1:**283-302 (2000).

25. M. Adler and G. Lee. Stability and surface activity of lactate dehydrogenase in spray-dried trehalose. *J. Pharm. Sci.* **88:**199-208 (1999).

26. H. R. Costantino, L. Firouzabadian, K. Hogeland, C. C. Wu, C. Beganski, K. G. Carrasquillo, M. Cordova, K. Griebenow, S. E. Zale, and M. A. Tracy. Protein spray-freeze drying. Effect of atomization conditions on particle size and stability. *Pharm. Res.* **17:**1374-1383 (2000).

27. Y.-F. Maa and P.-A. Nguyen. Method of spray freeze drying proteins for pharmaceutical administration. United States Patent. 6,284,282 (2001).

28. S. D. Webb, S. L. Golledge, J. L. Cleland, J. F. Carpenter, and T. W. Randolph. Surface adsorption of recombinant human interferon-γ in lyophilized and spray-lyophilized formulations. *J. Pharm. Sci.* **91:**1474-1487 (2002).

29. X. C. Nguyen, J. D. Herberger, and P. A. Burke. Protein powders for encapsulation: a comparison of spray-freeze drying and spray drying of darbepoetin alfa. *Pharm. Res.* **21:**507-514 (2004).

30. I. Gonda. Development of a systematic theory of suspension inhalation aerosols. I. A framework to study the effects of aggregation on the aerodynamic behavior of drug particles. *Int. J. Pharm.* **27:**99-116 (1985).

31. Y.-H. Liao, M. B. Brown, S. A. Jones, T. Nazir, and G. P. Martin. The effects of polyvinyl alcohol on the in vitro stability and delivery of spray-dried protein particles from surfactant-free HFA 134a-based pressurised metered dose inhalers. *Int. J. Pharm.* **304:**29-39 (2005).

32. M. Keller. Innovations and perspectives of metered dose inhalers in pulmonary drug delivery. *Int. J. Pharm.* **186:**81-90 (1999).

33. C. Vervaet and P. R. Byron. Drug-surfactant-propellant interactions in HFA-formulations. *Int. J. Pharm.* **186:**13-30 (1999).

34. F. E. Blondino and P. R. Byron. Surfactant dissolution and water solubilization in chlorine-free liquified gas propellants. *Drug Dev. Ind. Pharm.* **24:**935-945 (1998).

35. R. P. S. Peguin, P. Selvam, and S. R. P. da Rocha. Microscopic and Thermodynamic Properties of the HFA134a-Water Interface: Atomistic Computer Simulations and Tensiometry under Pressure. *Langmuir* **22:**8826-8830 (2006).

36. L. Wu, R. P. S. Peguin, P. Selvam, U. Chokshi, and S. R. P. da Rocha. Molecular scale behavior in alternative propellant-based inhaler formulations. In A. J. Hickey (ed.), *Inhalation Aerosols: Physical and biological basis for therapy*, 2007.

37. R. Vanbever, J. D. Mintzes, J. Wang, J. Nice, D. Chen, R. Batycky, R. Langer, and D. A. Edwards. Formulation and physical characterization of large porous particles for inhalation. *Pharm. Res.* **16:**1735-1742 (1999).

38. D. A. Edwards, J. Hanes, G. Caponetti, J. Hrkach, A. Ben-Jebria, M. L. Eskew, J. Mintzes, D. Deaver, N. Lotan, and R. Langer. Large porous particles for pulmonary drug delivery. *Science* **276:**1868-1871 (1997).

39. J. Tam, J. T. McConville, R. O. Williams III, and K. P. Johnston. Amorphous cyclosporin A nanodispersions for enhanced pulmonary deposition and dissolution. Submitted. *J. Pharm. Sci.* (2007).

40. Z. Yu, A. S. Garcia, K. P. Johnston, and R. O. Williams III. Spray freezing into liquid nitrogen for highly stable protein nanostructured microparticles. *Eur. J. Pharm. Biopharm.* **58:**529-537 (2004).

41. J. D. Engstrom, D. T. Simpson, E. Lai, R. O. Williams III, and K. P. Johnston. Morphology of protein particles produced by spray freezing of concentrated solutions. *Eur. J. Pharm. Biopharm.* **65:**149-162 (2007).

42. J. D. Engstrom, D. T. Simpson, C. Cloonan, E. Lai, R. O. Williams III, G. B. Kitto, and P. Johnston Keith. Stable high surface area lactate dehydrogenase particles produced by spray freezing into liquid nitrogen. *Eur. J. Pharm. Biopharm.* **65:**163-174 (2007).

43. Z. Yu, K. P. Johnston, and R. O. Williams III. Spray freezing into liquid versus spray-freeze drying: Influence of atomization on protein aggregation and biological activity. *Eur. J. Pharm. Sci.* **27:**9-18 (2006).

44. Z. Yu, T. L. Rogers, J. Hu, K. P. Johnston, and R. O. Williams III. Preparation and characterization of microparticles containing peptide produced by a novel process: spray freezing into liquid. *Eur. J. Pharm. Biopharm.* **54:**221-228 (2002).

45. J. D. Engstrom, E. S. Lai, B. Ludher, B. Chen, T. E. Milner, G. B. Kitto, R. O. Williams III, and K. P. Johnston. Formation of stable submicron protein particles by thin film freezing. *Pharm. Res.* (Submitted).

46. Z. Jiang and Y. Guan. Flocculation morphology: effect of particulate shape and coagulant species on flocculation. *Water Sci. Technol.* **53:**9-16 (2006).

47. I. Goodarz-Nia and D. N. Sutherland. Floc simulation. Effects of particle size and shape. *Chem. Eng. Sci.* **30:**407-12 (1975).

48. P. C. Hiemenz and R. Rajagopalan. *Principles of colloid and surface chemistry*, 1997.

49. A. P. Philipse and A. M. Wierenga. On the Density and Structure Formation in Gels and Clusters of Colloidal Rods and Fibers. *Langmuir* **14:**49-54 (1998).

50. A. P. Philipse. The Random Contact Equation and Its Implications for (Colloidal) Rods in Packings, Suspensions, and Anisotropic Powders. *Langmuir* **12:**5971 (1996).

51. T. L. Rogers, A. C. Nelsen, J. Hu, J. N. Brown, M. Sarkari, T. J. Young, K. P. Johnston, and R. O. Williams III. A novel particle engineering technology to enhance dissolution of poorly water soluble drugs: spray-freezing into liquid. *Eur. J. Pharm. Biopharm.* **54:**271-280 (2002).

52. T. L. Rogers, K. A. Overhoff, P. Shah, P. Santiago, M. J. Yacaman, K. P. Johnston, and R. O. Williams III. Micronized powders of a poorly water soluble drug produced by a spray-freezing into liquid-emulsion process. *Eur. J. Pharm. Biopharm.* **55:**161-72 (2003).

53. R. O. Williams, III, J. Liu, and J. J. Koleng. Influence of metering chamber volume and water level on the emitted dose of a suspension-based pMDI containing propellant 134a. *Pharm. Res.* **14:**438-443 (1997).

54. Y. Kim, S. H. Atwell, and R. G. Bell. Determination of water in pressurized pharmaceutical metered dose aerosol products. *Drug Dev. Ind. Pharm.* **18:**2185-95 (1992).

55. P. G. Smith, Jr., W. Ryoo, and K. P. Johnston. Electrostatically Stabilized Metal Oxide Particle Dispersions in Carbon Dioxide. *J. Phys. Chem. B* **109:**20155-20165 (2005).

56. E. Berlin and M. J. Pallansch. Densities of several proteins and L-amino acids in the dry state. *J. Phys. Chem.* **72:**1887-9 (1968).

57. P. G. A. Rogueda. HPFP, a model propellant for pMDIs. *Drug Dev. Ind. Pharm.* **29:**39-49 (2003).

58. R. Ashayer, P. F. Luckham, S. Manimaaran, and P. Rogueda. Investigation of the molecular interactions in a pMDI formulation by atomic force microscopy. *Eur. J. Pharm. Sci.* **21:**533-543 (2004).

59. D. Traini, M. Young Paul, P. Rogueda, and R. Price. In vitro investigation of drug particulates interactions and aerosol performance of pressurised metered dose inhalers. *Pharm. Res.* **24:**125-135 (2007).

60. S. L. Nail, S. Jiang, S. Chongprasert, and S. A. Knopp. Fundamentals of freeze-drying. In S. L. Nail and M. J. Akers (eds.), *Pharmaceutical Biotechnology. 14. Development and Manufacture of Protein Pharmaceuticals*, Kluwer Academic/Plenum Publishers, New York, 2002, pp. 281-360.

61. S. D. Webb, J. L. Cleland, J. F. Carpenter, and T. W. Randolph. A new mechanism for decreasing aggregation of recombinant human interferon-g by a surfactant: slowed dissolution of lyophilized formulations in a solution containing 0.03% polysorbate 20. *J. Pharm. Sci.* **91:**543-558 (2002).

62. J. F. Carpenter, B. S. Chang, W. Garzon-Rodriguez, and T. W. Randolph. Rational design of stable lyophilized protein formulations: theory and practice. In J. F. Carpenter and M. C. Manning (eds.), *Pharmaceutical Biotechnology. 13. Rational Design of Stable Protein Formulations*, Kluwer Academic/Plenum Press, New York, 2002, pp. 109-133.

63. A. Farahnaky, F. Badii, I. A. Farhat, J. R. Mitchell, and S. E. Hill. Enthalpy relaxation of bovine serum albumin and implications for its storage in the glassy state. *Biopolymers* **78:**69-77 (2005).

64. B. Y. Shekunov, P. Chattopadhyay, H. H. Y. Tong, and A. H. L. Chow. Particle Size Analysis in Pharmaceutics: Principles, Methods and Applications. *Pharm. Res.* **24:**203-227 (2007).

65. W. H. Finlay. *The mechanics of inhaled pharmaceutical aerosols*, New York, 2001.

66. A. Sihvola. *Electromagnetic mixing formulas and applications*, 1999.

67. W. B. Russel, D. A. Saville, and W. R. Schowalter. *Colloidal dispersions*, 1989.

68. D. Traini, P. Rogueda, P. Young, and R. Price. Surface Energy and Interparticle Forces Correlations in Model pMDI Formulations. *Pharm. Res.* **22:**816-825 (2005).

69. M. A. Bevan, PhD Dissertation, Carnegie Mellon University, 1999.

70. R. G. Larson. *The Structure and Rheology of Complex Fluids*, Oxford University Press Inc., New York, 1999.

71. P. Tang, J. Greenwood, and J. A. Raper. A model to describe the settling behavior of fractal aggregates. *J. Colloid Interface Sci.* **247:**210-219 (2002).

72. C. Fargues and C. Turchiuli. Structural characterization of flocs in relation to their settling performances. *Chem. Eng. Res. Design* **82:**1517 (2004).

73. H. Abramowitz, P. S. Shah, P. F. Green, and K. P. Johnston. Welding Colloidal Crystals with Carbon Dioxide. *Macromolecules* **37:**7316-7324 (2004).

74. D. R. Ulrich. Chemical processing of ceramics. *Chem. Eng. News* **68:**28-40 (1990).

75. H. D. C. Smyth, A. J. Hickey, and R. M. Evans. Aerosol generation from propellant-driven metered dose inhalers. In J. Hickey Anthony (ed.), *Inhalation Aerosols: Physical and Biological Basis for Therapy*, 2007, pp. 399-416.

76. J. Israelachvili. *Intermolecular and surface forces*, Academic Press, San Diego, 1992.

77. S. Takashima. Proton fluctuation in protein. Experimental study of the Kirkwood-Shumaker theory. *J. Phys. Chem.* **69:**2281-6 (1965).

78. R. Tadmor. The London-van der Waals interaction energy between objects of various geometries. *J. Phys.: Condens. Matter* **13:**L195-L202 (2001).

Chapter 7: Conclusions and Recommendations

The research described in this dissertation has improved the understanding of how to produce stable submicron protein particles. It has also demonstrated how rod-shaped particles can be utilized to form suspensions stable against settling in HFAs to achieve high fine particle fractions by pMDI delivery. This chapter summarizes the key advances made in this dissertation as well as recommendations for future research.

7.1 CONCLUSIONS

7.1.1 Morphology of protein particles produced by spray freezing of concentrated solutions

The SFL and SFD spray processes were utilized to produce high surface area lysozyme particles over a wide range of feed concentrations for two cryogens, LN2 and isopentane (*i*-C5). For dilute aqueous solutions up to 5 mg/mL, the focus of most previous studies, the dried powder SSAs were > 100 m^2/g in SFL for each cryogen indicating cooling was rapid enough to prevent substantial particle growth. Even for viscous feeds with concentrations as high as 100 mg/mL, powders with SSAs greater than 100 m^2/g were produced in the SFD and SFL-*i*-C5 processes indicating sufficient atomization for rapid cooling and quenching relative to particle growth. For SFD with either cryogen, powder SSAs and SEMs were shown to be negligibly impacted by the droplet diameter for droplets less than 100 μm suggesting the Leidenfrost effect was unimportant. For SFL, LN2 was found to form a turbulent gaseous N_2 cone around the sprayed jet. The low viscosity gas layer reduced the degree of jet atomization for N_2, but not for the non-evaporating cryogen *i*-C5. The calculated cooling rate for SFL in LN2 was 3 orders of magnitude lower than in *i*-C5 or SFD with either cryogen. For 50 mg/mL

concentrated feed solutions, SSAs were on the order of 34 m^2/g for SFL into LN2 and the features in the SEMs were coarser, consistent with the slower cooling rates. The ability to adjust the cooling rate to vary the final particle surface area will be beneficial for designing particles for controlled release applications. The high protein feed concentrations offer the potential of high production rates, as well as smaller volumes of solvent that must be sublimated in lyophilization.

7.1.2 Stable high surface area lactate dehydrogenase particles produced by spray freezing into liquid nitrogen

In SFD, the activity loss in the spraying step has been shown to be caused by protein adsorption and aggregation at the gas-liquid interface, as reported for rhIFN-γ (1) and lysozyme (2). In this study, the LDH activity loss was the same as when spraying the protein solution into air without freezing, suggesting that the freezing (ice-liquid interface) and drying steps may not have contributed further to the activity loss. Furthermore, the activity loss increased with a decrease in droplet size, and thus gas-liquid interfacial area, consistent with results for BSA (3), and for rhIFN-γ and lysozyme. Given that long exposure to the gas-liquid interface in SFD and spray-drying can destabilize proteins, the ability to shorten this exposure time is of considerable practical importance.

The SFL process may be used to reduce exposure to the gas-liquid interface. For 0.25 mg/mL LDH with either 30 or 100 mg/mL trehalose, the SFL process produced powders with very high enzyme activities comparable to lyophilization upon reconstitution, despite surface areas that were an order of magnitude higher. The combined spraying, freezing, and drying stresses of the SFL process did not produce any significant loss in LDH activity. The enzyme activities in SFL were higher than for SFD, even with the larger 130 μm droplets, despite the similar powder surface areas in both

cases. Although a gas cone was formed about the liquid jet in SFL, as a result of nitrogen evaporation (Leidenfrost effect), the nitrogen gas-liquid contact had a negligible impact on the LDH stability. The exposure time of only 2 ms to the nitrogen gas-liquid interface in this cone was calculated to be 2 orders of magnitude faster than for SFD. This very short exposure time appeared to prevent loss in activity from protein adsorption and unfolding, even without the use of a surfactant. It is likely the primary cause of the higher LDH activities in SFL versus SFD. The ability to produce stable high surface area submicron particles of fragile proteins such as LDH by SFL, in addition to much more stable proteins such as BSA (4) and lysozyme (2) is of practical interest in protein storage and in controlled release applications including encapsulation in bioerodible polymers. The successful scale down of the SFL process for protein formulation volumes as small as 1 mL will be beneficial for therapeutic proteins available only in limited quantities.

7.1.3 Novel ultra-rapid freezing particle engineering process for enhancement of dissolution rates of poorly water soluble drugs

Sample powders were prepared by URF, otherwise known as TFF, technology from two different solvents with different thermal and physical properties, T-BUT and ACN. The differences in the thermal properties of the solvent and droplet dimensions had a dramatic effect on the cooling rate of the droplets as evidenced by the heat transfer model and IR studies. An axial heat transfer model for the spread droplets indicated ACN droplets cooled in 72 ms while T-BUT droplets required a much greater time of 483 ms. The much longer cooling time for T-BUT was also observed by FTIR imaging. However, it was found that the rate of cooling was sufficiently rapid in both solvents to produce amorphous powders with high surface areas on the order of 25.9-29.3 m^2/g and high wettability. Relative to physical mixtures, the URF processed powders had much more rapid dissolution profiles, which were attributed to nano-structured amorphous API

domains, and the improved surface areas and wettability. The surface morphology of the powders was different for the two processing solvents, despite the similar surface areas. The primary particles in powders produced from ACN were spherical and uniform in size as a result of the more rapid and uniform cooling of the droplet relative to T-BUT. The use of ACN as a solvent allows for high heat transfer rates, which is beneficial for producing small rapidly dissolving particles, however, its low melting point can cause loss in particle surface area prior to solvent removal. T-BUT, on the other hand, has a lower (but sufficient) heat transfer rate compared to ACN, but is less susceptible to melting at ambient conditions prior to solvent removal.. As a result of fast cooling rates and thus high supersaturation, the URF technology is a viable and robust process for producing high surface area nano-structured powders of poorly water soluble APIs with rapid dissolution rates, which will likely lead to enhanced bioavailability in vivo.

7.1.4 Formation of stable submicron protein particles by thin film freezing

The TFF process was utilized to produce 300 nm lysozyme particles with surface areas on the order of 31 - 73 m^2/g and 100% LDH activities. Despite a cooling rate of ~10^2 K/s in TFF, the particle sizes and surface areas were similar to those observed in the widely reported process, spray freeze drying SFD, where cooling rates reach 10^6 K/s. In TFF, the thin liquid channels between the ice domains were sufficiently thin and freezing rates of the thin channels sufficiently fast to achieve the similar particle morphologies. Therefore, the extremely rapid cooling rate in the SFD process was not necessary to form the desired submicron protein particles. Although LDH was exposed to the gas-liquid interface of the thin film for a maximum of ~1 s in TFF, the surface area/volume of 45 cm^{-1} was sufficiently small that adsorption produced neglible aggregation and denaturation. Even if this gas-liquid interface became saturated with protein, followed by

irreversible denaturation, the maximum activity loss for a 0.25 mg/mL LDH formulation would be 5%. For SFD with a droplet size of 10 μm, the maximum loss could reach 25% in just 0.4 ms from diffusion to the interface and adsorption (5), consistent with the significant decrease in enzyme activity (80%). In SFD, losses in protein stability have been observed in several previous studies (1, 3, 6-8). Although LDH stabilities are high in conventional lyophilization, cooling rates are on the order of 1 K/min resulting in large 30 to 100 μm sized particles (7). Thus, the intermediate cooling rate regime for TFF (and likewise for SFL), relative to SFD and lyophilization, offers a promising route to form stable submicron protein particles of interest in pulmonary and parenteral delivery applications.

7.1.5 Templating open flocs of nanorods for enhanced pulmonary delivery with pressurized metered dose inhalers

High (38-48%) fine particle fractions in HFA 227 pMDI delivery were achieved with flocculated BSA nanorods stable against settling for up to 1 year, without the use of surfactants and cosolvents. Analysis of experimental settling rates of dilute suspensions indicated that the volume fraction, ϕ_f, of the nanorods in the flocs was an order of magnitude lower than for flocs of spherical particles produced by milling or spray drying. The rapid and sticky attractive collisions of nanorods facilitates the formation of low density flocs (250 μm) which stack upon each other to fill the entire solvent volume to prevent settling (Fig. 6.1C). In contrast, denser flocs of spherical particles filled much less space and rapidly settled within 60 s (Fig. 6.1B). The novel concept of purposely flocculating nanorods to prevent settling is fundamentally opposite the conventional approach of stabilizing colloidal dispersions of primary particles. The reversibility of the nanorod flocs in HFA 227 was demonstrated by break up of the flocs into individual 330 nm primary rod particles upon transfer to the more polar solvent acetonitrile.

A material balance on a shrinking HFA droplet containing a 25 μm floc subdomain predicts a final volume fraction of BSA in the aerosolized particle in agreement with experiment. Therefore, it is likely that the atomized HFA droplets initially template the 250 μm flocs into 25 μm subdomains. The aerosolized particles with a d_a of 3-4 μm and d_g of ~10 μm are optimal for high fine particle fractions via a pMDI. The concept of forming open flocs composed of nanorods, that are stable against settling without surfactants, and templating the flocs to achieve optimal d_as and high FPFs is of practical interest for wide classes of low and high molecular weight pharmaceuticals and biopharmaceuticals.

7.2 RECOMMENDATIONS FOR FUTURE RESEARCH

7.2.1 Stabilization of proteins

The work of this dissertation has focused on a limited number of proteins including BSA, lysozyme and lactate dehydrogenase (LDH). It would be of interest to extend the concepts introduced in this dissertation to mechanisms of stabilization for other model or therapeutic proteins. Further information about protein stabilization could still be gleaned for LDH because of its tetrameric structure. In solution LDH has been known to dissociate into monomers which can also recombine to form the active tetramer (9). Therefore it can be difficult to determine how the protein behaves after freezing and thawing or freezing and drying if the protein is able to recombine in solution. It is therefore additionally proposed that two isoforms of LDH be formulated together. Studies by Anchordoquy et al. showed that when LDH from porcine heart (P-LDH) and from rabbit muscle (R-LDH) were formulated together that LDH hybrids were formed if the LDH tetramers dissociated (10, 11). The formation of the hybrids significantly decreased the activity of the initial LDH formulation after freeze-thaw and freeze-drying

experiments (10). LDH hybrids were analyzed with the SDS-PAGE technique. Since P-LDH and R-LDH are electrophoretically distinct, it was possible to separate the LDH hybrids (10).

It is suggested that the protein β-galoctosidase be used for studying protein activity, secondary and tertiary structure alterations, and aggregation. β-galoctosidase can be formulated at much higher concentrations than LDH and therefore can be analyzed within the detection limits of FTIR and optical density. β-galactosidase can have a monomeric or tetrameric structure depending on how it is produced (12) and has also been processed with freeze-drying and spray-drying and was subsequently analyzed with enzymatic assays and FTIR (12-15) to investigate the secondary structure. It is recommended that enzyme activity and FTIR analysis be completed throughout the SFL and TFF processing steps.

After work with the model proteins is completed, a therapeutic protein such as rhIFN-γ should be processed and analyzed. The protein rhIFN-γ has been investigated thoroughly with the SFD and lyophilization processes by Webb et als. (1, 16, 17). The protein was shown to be destabilized by exposure to gas-liquid interface in the SFD process. It will then be determined if the protein stability barriers of processing rhIFN-γ particles can be overcome with the SFL or TFF processes.

7.2.2 Pulmonary delivery of therapeutic proteins

It is recommended that a study of the long term storage stability of proteins suspended in hydrofluoroalkanes (HFA) be conducted. It is of interest to know if molecular protein aggregates are formed as well as if the flocculated rods can be redispersed as primary particles. This will ensure that protein delivery by pMDIs remains a viable option for the high surface area particles produced by TFF and SFL.

7.3 REFERENCES

1. S. D. Webb, S. L. Golledge, J. L. Cleland, J. F. Carpenter, and T. W. Randolph. Surface adsorption of recombinant human interferon-γ in lyophilized and spray-lyophilized formulations. *J. Pharm. Sci.* **91:**1474-1487 (2002).

2. Z. Yu, K. P. Johnston, and R. O. Williams III. Spray freezing into liquid versus spray-freeze drying: Influence of atomization on protein aggregation and biological activity. *Eur. J. Pharm. Sci.* **27:**9-18 (2006).

3. H. R. Costantino, L. Firouzabadian, K. Hogeland, C. C. Wu, C. Beganski, K. G. Carrasquillo, M. Cordova, K. Griebenow, S. E. Zale, and M. A. Tracy. Protein spray-freeze drying. Effect of atomization conditions on particle size and stability. *Pharm. Res.* **17:**1374-1383 (2000).

4. Z. Yu, A. S. Garcia, K. P. Johnston, and R. O. Williams III. Spray freezing into liquid nitrogen for highly stable protein nanostructured microparticles. *Eur. J. Pharm. Biopharm.* **58:**529-537 (2004).

5. M. Adler and G. Lee. Stability and surface activity of lactate dehydrogenase in spray-dried trehalose. *J. Pharm. Sci.* **88:**199-208 (1999).

6. Y.-F. Maa and H. R. Costantino. Spray freeze-drying of biopharmaceuticals: applications and stability considerations. In H. R. Costantino and M. J. Pikal (eds.), *Biotechnology: Pharmaceutical Aspects. 2. Lyophilization of Biopharmaceuticals*, American Association of Pharmaceutical Scientists, Arlington, 2004, pp. 519-561.

7. Y.-F. Maa and S. J. Prestrelski. Biopharmaceutical powders: particle formation and formulation considerations. *Curr. Pharm. Biotechnol.* **1:**283-302 (2000).

8. X. C. Nguyen, J. D. Herberger, and P. A. Burke. Protein powders for encapsulation: a comparison of spray-freeze drying and spray drying of darbepoetin alfa. *Pharm. Res.* **21:**507-514 (2004).

9. B. S. Bhatnagar, S. J. Nehm, M. J. Pikal, and R. H. Bogner. Post-thaw aging affects activity of lactate dehydrogenase. *J. Pharm. Sci.* **94:**1382-1388 (2005).

10. T. J. Anchordoquy and J. F. Carpenter. Polymers protect lactate dehydrogenase during freeze-drying by inhibiting dissociation in the frozen state. *Arch. Biochem. Biophys.* **332:**231-238 (1996).

11. T. J. Anchordoquy, K.-I. Izutsu, T. W. Randolph, and J. F. Carpenter. Maintenance of quaternary structure in the frozen state stabilizes lactate dehydrogenase during freeze-drying. *Arch. Biochem. Biophys.* **390:**35-41 (2001).

12. K. A. Pikal-Cleland and J. F. Carpenter. Lyophilization-induced protein denaturation in phosphate buffer systems: monomeric and tetrameric b-galactosidase. *J. Pharm. Sci.* **90:**1255-1268 (2001).

13. K. A. Pikal-Cleland, N. Rodriguez-Hornedo, G. L. Amidon, and J. F. Carpenter. Protein Denaturation during Freezing and Thawing in Phosphate Buffer Systems: Monomeric and Tetrameric b-Galactosidase. *Arch. Biochem. Biophys.* **384:**398-406 (2000).

14. K. Izutsu, S. Yoshioka, and S. Kojima. Physical stability and protein stability of freeze-dried cakes during storage at elevated temperatures. *Pharm. Res.* **11:**995-9 (1994).

15. S. Jiang and S. L. Nail. Effect of process conditions on recovery of protein activity after freezing and freeze-drying. *Eur. J. Pharm. Biopharm.* **45:**249-257 (1998).

16. S. D. Webb, J. L. Cleland, J. F. Carpenter, and T. W. Randolph. A new mechanism for decreasing aggregation of recombinant human interferon-g by a surfactant: slowed dissolution of lyophilized formulations in a solution containing 0.03% polysorbate 20. *J. Pharm. Sci.* **91:**543-558 (2002).

17. S. D. Webb, J. L. Cleland, J. F. Carpenter, and T. W. Randolph. Effects of annealing lyophilized and spray-lyophilized formulations of recombinant human interferon-γ. *J. Pharm. Sci.* **92:**715-729 (2003).

References

1. M. C. Manning, K. Patel, and R. T. Borchardt. Stability of protein pharmaceuticals. *Pharm. Res.* **6:**903-918 (1989).

2. J. F. Carpenter, B. S. Chang, W. Garzon-Rodriguez, and T. W. Randolph. Rational design of stable lyophilized protein formulations: theory and practice. In J. F. Carpenter and M. C. Manning (eds.), *Pharmaceutical Biotechnology. 13. Rational Design of Stable Protein Formulations*, Kluwer Academic/Plenum Press, New York, 2002, pp. 109-133.

3. J. F. Carpenter, K.-i. Izutsu, and T. W. Randolph. Freezing- and drying-induced perturbations of protein structure and mechanisms of protein protection by stabilizing additives. In L. Rey and J. C. May (eds.), *Drugs and the Pharmaceutical Sciences. 137. Freeze-Drying/Lyophilization of Pharmaceutical and Biological Products*, Marcel Dekker, Inc., New York, 2004, pp. 147-186.

4. M. J. Pikal. Mechanisms of protein stabilization during freeze-drying and storage: the relative importance of thermodynamic stabilization and glassy state relaxation dynamics. *Drugs Pharm. Sci.* **137:**63-107 (2004).

5. R. A. DePaz, D. A. Dale, C. C. Barnett, J. F. Carpenter, A. L. Gaertner, and T. W. Randolph. Effects of drying methods and additives on the structure, function, and storage stability of subtilisin: role of protein conformation and molecular mobility. *Enzyme Microb. Technol.* **31:**765-774 (2002).

6. Y.-F. Maa and S. J. Prestrelski. Biopharmaceutical powders: particle formation and formulation considerations. *Curr. Pharm. Biotechnol.* **1:**283-302 (2000).

7. Z. Yu, T. L. Rogers, J. Hu, K. P. Johnston, and R. O. Williams III. Preparation and characterization of microparticles containing peptide produced by a novel process: spray freezing into liquid. *Eur. J. Pharm. Biopharm.* **54:**221-228 (2002).

8. W. Wang. Lyophilization and development of solid protein pharmaceuticals. *Int. J. Pharm.* **203:**1-60 (2000).

9. Y.-F. Maa and H. R. Costantino. Spray freeze-drying of biopharmaceuticals: applications and stability considerations. In H. R. Costantino and M. J. Pikal (eds.), *Biotechnology: Pharmaceutical Aspects. 2. Lyophilization of Biopharmaceuticals*, American Association of Pharmaceutical Scientists, Arlington, 2004, pp. 519-561.

10. K. A. Johnson. Preparation of peptide and protein powders for inhalation. *Adv. Drug Deliv. Rev.* **26:**3-15 (1997).

11. S. J. Shire, Z. Shahrokh, and J. Liu. Challenges in the development of high protein concentration formulations. *J. Pharm. Sci.* **93:**1390-1402 (2004).

12. Y.-F. Maa, L. Zhao, L. G. Payne, and D. Chen. Stabilization of alum-adjuvanted vaccine dry powder formulations: mechanism and application. *J. Pharm. Sci.* **92:**319-332 (2003).

13. X. M. Lam, E. T. Duenas, A. L. Daugherty, N. Levin, and J. L. Cleland. Sustained release of recombinant human insulin-like growth factor-I for treatment of diabetes. *J. Control. Release* **67:**281-292 (2000).

14. W. T. Leach, D. T. Simpson, T. N. Val, E. C. Anuta, Z. Yu, R. O. Williams III, and K. P. Johnston. Uniform encapsulation of stable protein nanoparticles produced by spray freezing for the reduction of burst release. *J. Pharm. Sci.* **94:**56-69 (2005).

15. O. L. Johnson, W. Jaworowicz, J. L. Cleland, L. Bailey, M. Charnis, E. Duenas, C. Wu, D. Shepard, S. Magil, T. Last, A. J. S. Jones, and S. D. Putney. The stabilization and encapsulation of human growth hormone into biodegradable microspheres. *Pharm. Res.* **14:**730-735 (1997).

16. X. M. Lam, E. T. Duenas, and J. L. Cleland. Encapsulation and stabilization of nerve growth factor into poly(lactic-co-glycolic) acid microspheres. *J. Pharm. Sci.* **90:**1356-1365 (2001).

17. M. R. Prausnitz. Microneedles for transdermal drug delivery. *Adv. Drug Deliv. Rev.* **56:**581-587 (2004).

18. D. A. Edwards, J. Hanes, G. Caponetti, J. Hrkach, A. Ben-Jebria, M. L. Eskew, J. Mintzes, D. Deaver, N. Lotan, and R. Langer. Large porous particles for pulmonary drug delivery. *Science* **276:**1868-1871 (1997).

19. J. L. Cleland, E. T. Duenas, A. Park, A. Daugherty, J. Kahn, J. Kowalski, and A. Cuthbertson. Development of poly-(d,l-lactide-co-glycolide) microsphere formulations containing recombinant human vascular endothelial growth factor to promote local angiogenesis. *J. Control. Release* **72:**13-24 (2001).

20. H. R. Costantino, L. Firouzabadian, K. Hogeland, C. C. Wu, C. Beganski, K. G. Carrasquillo, M. Cordova, K. Griebenow, S. E. Zale, and M. A. Tracy. Protein spray-freeze drying. Effect of atomization conditions on particle size and stability. *Pharm. Res.* **17:**1374-1383 (2000).

21. S. D. Webb, S. L. Golledge, J. L. Cleland, J. F. Carpenter, and T. W. Randolph. Surface adsorption of recombinant human interferon-γ in lyophilized and spray-lyophilized formulations. *J. Pharm. Sci.* **91:**1474-1487 (2002).

22. X. C. Nguyen, J. D. Herberger, and P. A. Burke. Protein powders for encapsulation: a comparison of spray-freeze drying and spray drying of darbepoetin alfa. *Pharm. Res.* **21:**507-514 (2004).

23. Y.-F. Maa, P.-A. Nguyen, T. Sweeney, S. J. Shire, and C. C. Hsu. Protein inhalation powders: spray drying vs spray freeze drying. *Pharmaceutical Research* **16:**249-254 (1999).

24. M. Adler and G. Lee. Stability and surface activity of lactate dehydrogenase in spray-dried trehalose. *J. Pharm. Sci.* **88:**199-208 (1999).

25. S. P. Sellers, G. S. Clark, R. E. Sievers, and J. F. Carpenter. Dry powders of stable protein formulations from aqueous solutions prepared using supercritical CO(2)-assisted aerosolization. *J. Pharm. Sci.* **90:**785-797 (2001).

26. Z. Yu, K. P. Johnston, and R. O. Williams III. Spray freezing into liquid versus spray-freeze drying: Influence of atomization on protein aggregation and biological activity. *Eur. J. Pharm. Sci.* **27:**9-18 (2006).

27. Z. Yu, A. S. Garcia, K. P. Johnston, and R. O. Williams III. Spray freezing into liquid nitrogen for highly stable protein nanostructured microparticles. *Eur. J. Pharm. Biopharm.* **58:**529-537 (2004).

28. J. D. Engstrom, E. S. Lai, B. Ludher, B. Chen, T. E. Milner, G. B. Kitto, R. O. Williams III, and K. P. Johnston. Formation of stable submicron protein particles by thin film freezing. *Pharm. Res.* (Submitted).

29. K. A. Overhoff, J. D. Engstrom, B. Chen, T. L. Rogers, K. P. Johnston, and R. O. Williams III. Novel ultra-rapid freezing particle engineering process to enhance the dissolution rates of poorly water-soluble drugs. *Eur. J. Pharm. Biopharm.* **65:**57-67 (2007).

30. M. C. Heller, J. F. Carpenter, and T. W. Randolph. Protein formulation and lyophilization cycle design: prevention of damage due to freeze-concentration induced phase separation. *Biotechnol. Bioeng.* **63:**166-174 (1999).

31. M. J. Akers, V. Vasudevan, and M. Stickelmeyer. Formulation development of protein dosage forms. In S. L. Nail and M. J. Akers (eds.), *Pharmaceutical Biotechnology. 14. Development and Manufacture of Protein Pharmaceuticals*, Kluwer Academic/Plenum Press, New York, 2002, pp. 47-127.

32. T. F. O'Connor, P. G. Debenedetti, and J. D. Carbeck. Simultaneous determination of structural and thermodynamic effects of carbohydrate solutes on the thermal stability of ribonuclease A. *J. Am. Chem. Soc.* **126:**11794-11795 (2004).

33. C. A. Angell and L.-M. Wang. Hyperquenching and cold equilibration strategies for the study of liquid-liquid and protein folding transitions. *Biophys. Chem.* **105:**621-637 (2003).

34. F. Franks. *Biophysics and Biochemistry at Low Temperatures*, Cambridge University Press, New York, 1985.

35. C. A. Angell. Liquid fragility and the glass transition in water and aqueous solutions. *Chem. Rev.* **102:**2627-2649 (2002).

36. A. P. MacKenzie. Non-equilibrium freezing behavior of aqueous systems. *Philos. Trans. R. Soc. London, B: Biol. Sci.* **278:**167-189 (1977).

37. S. L. Nail, S. Jiang, S. Chongprasert, and S. A. Knopp. Fundamentals of freeze-drying. In S. L. Nail and M. J. Akers (eds.), *Pharmaceutical Biotechnology. 14. Development and Manufacture of Protein Pharmaceuticals*, Kluwer Academic/Plenum Publishers, New York, 2002, pp. 281-360.

38. Z. H. Chang and J. G. Baust. Ultra-rapid freezing by spraying/plunging: pre-cooling in the cold gaseous layer. *J. Microsc.* **161:**435-444 (1991).

39. M. C. Heller, J. F. Carpenter, and T. W. Randolph. Application of a thermodynamic model to the prediction of phase separations in freeze-concentrated formulations for protein lyophilization. *Arch. Biochem. Biophys.* **363:**191-201 (1999).

40. J. D. Andya, Y.-F. Maa, H. R. Costantino, P.-A. Nguyen, N. Dasovich, T. D. Sweeney, C. C. Hsu, and S. J. Shire. The effect of formulation excipients on protein stability and aerosol performance of spray-dried powders of a recombinant humanized anti-IgE monoclonal antibody. *Pharm. Res.* **16:**350-358 (1999).

41. Y.-F. Maa and P.-A. Nguyen. Method of spray freeze drying proteins for pharmaceutical administration. United States Patent. 6,284,282 (2001).

42. H. R. Costantino, L. Firouzabadian, C. C. Wu, K. G. Carrasquillo, K. Griebenow, S. E. Zale, and M. A. Tracy. Protein spray freeze drying. 2. Effect of formulation variables on particle size and stability. *J. Pharm. Sci.* **91:**388-395 (2002).

43. J. D. Engstrom, D. T. Simpson, C. Cloonan, E. Lai, R. O. Williams III, G. B. Kitto, and P. Johnston Keith. Stable high surface area lactate dehydrogenase particles produced by spray freezing into liquid nitrogen. *Eur. J. Pharm. Biopharm.* **65:**163-174 (2007).

44. S. Magdassi and A. Kamyshny. Surface activity and functional properties of proteins. In S. Magdassi (ed.), *Surface Activity of Proteins*, Marcel Dekker, New York, 1996, pp. 1-38.

45. J. Hu, T. L. Rogers, J. Brown, T. Young, K. P. Johnston, and R. O. Williams III. Improvement of dissolution rates of poorly water soluble APIs using novel spray freezing into liquid technology. *Pharm. Res.* **19:**1278-1284 (2002).

46. J. Hu, K. P. Johnston, and R. O. Williams III. Rapid dissolving high potency danazol powders produced by spray freezing into liquid process. *Int. J. Pharm.* **271:**145-154 (2004).

47. T. L. Rogers, J. Hu, Z. Yu, K. P. Johnston, and R. O. Williams III. A novel particle engineering technology: spray-freezing into liquid. *Int. J. Pharm.* **242:**93-100 (2002).

48. T. L. Rogers, A. C. Nelsen, J. Hu, J. N. Brown, M. Sarkari, T. J. Young, K. P. Johnston, and R. O. Williams III. A novel particle engineering technology to enhance dissolution of poorly water soluble drugs: spray-freezing into liquid. *Eur. J. Pharm. Biopharm.* **54:**271-280 (2002).

49. H. Sitte, L. Edelmann, and K. Neumann. Cryofixation without pretreatment at ambient pressure. In R. A. Steinbrecht and K. Zierold (eds.), *Cryotechniques in Biological Electron Microscopy*, Springer-Verlag, Berlin, 1987, pp. 87-113.

50. M. J. Costello and J. M. Corless. The direct measurement of temperature changes within freeze-fracture specimens during rapid quenching in liquid coolants. *J. Microsc.* **112:**17-37 (1978).

51. J. D. Engstrom, D. T. Simpson, E. Lai, R. O. Williams III, and K. P. Johnston. Morphology of protein particles produced by spray freezing of concentrated solutions. *Eur. J. Pharm. Biopharm.* **65:**149-162 (2007).

52. J. Fukai, M. Tanaka, and O. Miyatake. Maximum spreading of liquid droplets colliding with flat surfaces. *J. Chem. Eng. Jpn.* **31:**456-461 (1998).

53. M. Pasandideh-Fard, R. Bhola, S. Chandra, and J. Mostaghimi. Deposition of tin droplets on a steel plate : simulations and experiments. *Int. J. Heat Mass Transfer* **41:**2929-2945 (1998).

54. M. Pasandideh-Fard, S. Chandra, and J. Mostaghimi. A three-dimensional model of droplet impact and solidification. *Int. J. Heat Mass Transfer* **45:**2229-2242 (2002).

55. J. Fukai, T. Ozaki, H. Asami, and O. Miyatake. Numerical simulation of liquid droplet solidification on substrates. *J. Chem. Eng. Jpn.* **33:**630-637 (2000).

56. D. Sivakumar and H. Nishiyama. Numerical analysis on the impact behavior of molten metal droplets using a modified splat-quench solidification model. *J. Heat Transf.-Trans. ASME* **126:**1014-1022 (2004).

57. B. Kang, Z. Zhao, and D. Poulikakos. Solidification of liquid metal droplets impacting sequentially on a solid surface. *J. Heat Transfer* **116:**436-45 (1994).

58. J. Madejski. Solidification of droplets on a cold surface. *Int. J. Heat Mass Transfer* **19:**1009-1013 (1976).

59. C. Sanmarchi, H. Liu, E. J. Lavernia, R. H. Rangel, A. Sickinger, and E. Muehlberger. Numerical analysis of the deformation and solidification of a single droplet impinging onto a flat substrate. *J. Mater. Sci.* **28:**3313-21 (1993).

60. G. X. Wang and E. F. Matthys. Modeling of heat transfer and solidification during splat cooling: effect of splat thickness and splat/substrate thermal contact. *Int. J. Rapid Solid.* **6:**141-74 (1991).

61. G. X. Wang and E. F. Matthys. Numerical modeling of phase change and heat transfer during rapid solidification processes: use of control volume integrals with element subdivision. *Int. J. Heat Mass Transfer* **35:**141-53 (1992).

62. H. Zhang, X. Y. Wang, L. L. Zheng, and X. Y. Jiang. Studies of splat morphology and rapid solidification during thermal spraying. *Int. J. Heat Mass Transfer* **44:**4579-4592 (2001).

63. Z. Zhao, D. Poulikakos, and J. Fukai. Heat transfer and fluid dynamics during the collision of a liquid droplet on a substrate. I. Modeling. *Int. J. Heat Mass Transfer* **39:**2771-2789 (1996).

64. Z. Zhao, D. Poulikakos, and J. Fukai. Heat transfer and fluid dynamics during the collision of a liquid droplet on a substrate. II. Experiments. *Int. J. Heat Mass Transfer* **39:**2791-2802 (1996).

65. T. Bennett and D. Poulikakos. Splat-quench solidification: estimating the maximum spreading of a droplet impacting a solid surface. *J. Mater. Sci.* **28:**963-970 (1993).

66. G. Trapaga and J. Szekely. Mathematical modeling of the isothermal impingement of liquid droplets in spraying processes. *Metall. Trans. B* **22B:**901-14 (1991).

67. R. U. Agu, M. I. Ugwoke, M. Armand, R. Kinget, and N. Verbeke. The lung as a route for systemic delivery of therapeutic proteins and peptides. *Respiratory Research* **2:**198-209 (2001).

68. J. S. Patton and P. R. Byron. Inhaling medicines: delivering drugs to the body through the lungs. *Nature Rev. Drug Discovery* **6:**67-74 (2007).

69. V. Codrons, F. Vanderbist, R. K. Verbeeck, M. Arras, D. Lison, V. Preat, and R. Vanbever. Systemic delivery of parathyroid hormone (1-34) using inhalation dry powders in rats. *J. Pharm. Sci.* **92:**938-950 (2003).

70. S. A. Shoyele and A. Slowey. Prospects of formulating proteins/peptides as aerosols for pulmonary drug delivery. *Int. J. Pharm.* **314:**1-8 (2006).

71. A. L. Adjei and P. K. Gupta. *Inhalation Delivery of Therapeutic Peptides and Proteins*, 1997.

72. S. White, D. B. Bennett, S. Cheu, P. W. Conley, D. B. Guzek, S. Gray, J. Howard, R. Malcolmson, J. M. Parker, P. Roberts, N. Sadrzadeh, J. D. Schumacher, S. Seshadri, G. W. Sluggett, C. L. Stevenson, and N. J. Harper. EXUBERA: Pharmaceutical Development of a Novel Product for Pulmonary Delivery of Insulin. *Diabetes Tech. Therapeutics* **7:**896-906 (2005).

73. H. M. Courrier, N. Butz, and T. F. Vandamme. Pulmonary drug delivery systems: recent developments and prospects. *Crit. Rev. Therapeutic Drug Carrier Systems* **19:**425-498 (2002).

74. M. J. Kwon, J. H. Bae, J. J. Kim, K. Na, and E. S. Lee. Long acting porous microparticle for pulmonary protein delivery. *Int. J. Pharm.* **333:**5-9 (2007).

75. L. Garcia-Contreras and H. D. C. Smyth. Liquid-spray or dry-powder systems for inhaled delivery of peptide and proteins? *Am. J. Drug Delivery* **3:**29-45 (2005).

76. P. Rogueda. Novel hydrofluoroalkane suspension formulations for respiratory drug delivery. *Expert Opinion Drug Del.* **2:**625-638 (2005).

77. D. Traini, P. Young, P. Rogueda, and R. Price. The Use of AFM and Surface Energy Measurements to Investigate Drug-Canister Material Interactions in a Model Pressurized Metered Dose Inhaler Formulation. *Aerosol Sci. Tech.* **40:**227-236 (2006).

78. E. A. Quinn, R. T. Forbes, A. C. Williams, M. J. Oliver, L. McKenzie, and T. S. Purewal. Protein conformational stability in the hydrofluoroalkane propellants tetrafluoroethane and heptafluoropropane analyzed by Fourier transform Raman spectroscopy. *Int. J. Pharm.* **186:**31-41 (1999).

79. M. J. Oliver, L. McKenzie, W. D. Graffiths, G. R. Morgan, and N. O'Kelly. Initial assessment of a protein formulated in pressurized mdis for pulmonary delivery, *RDD VII*, 2000.

80. C. Benfait. Kos reports achievement of new research and development milestones. *Kos Press Release* (2004).

81. J. Heyder, J. Gebhart, G. Rudolf, C. F. Schiller, and W. Stahlhofen. Deposition of particles in the human respiratory tract in the size range 0.005-15 μm. *J. Aerosol Sci.* **17:**811-825 (1986).

82. A. Ben-Jebria, D. Chen, M. L. Eskew, R. Vanbever, R. Langer, and D. A. Edwards. Large porous particles for sustained protection from carbachol-induced bronchoconstriction in guinea pigs. *Pharm. Res.* **16:**555-561 (1999).

83. N. Tsapis, D. Bennett, B. Jackson, D. A. Weitz, and D. A. Edwards. Trojan particles: large porous carriers of nanoparticles for drug delivery. *Proc. Natl. Acad. Sci. U. S. A.* **99:**12001-12005 (2002).

84. L. A. Dellamary, T. E. Tarara, D. J. Smith, C. H. Woelk, A. Adractas, M. L. Costello, H. Gill, and J. G. Weers. Hollow porous particles in metered dose inhalers. *Pharm. Res.* **17:**168-174 (2000).

85. I. Gonda. Development of a systematic theory of suspension inhalation aerosols. I. A framework to study the effects of aggregation on the aerodynamic behavior of drug particles. *Int. J. Pharm.* **27:**99-116 (1985).

86. Y.-H. Liao, M. B. Brown, S. A. Jones, T. Nazir, and G. P. Martin. The effects of polyvinyl alcohol on the in vitro stability and delivery of spray-dried protein particles from surfactant-free HFA 134a-based pressurised metered dose inhalers. *Int. J. Pharm.* **304:**29-39 (2005).

87. M. Keller. Innovations and perspectives of metered dose inhalers in pulmonary drug delivery. *Int. J. Pharm.* **186:**81-90 (1999).

88. R. P. S. Peguin, P. Selvam, and S. R. P. da Rocha. Microscopic and Thermodynamic Properties of the HFA134a-Water Interface: Atomistic Computer Simulations and Tensiometry under Pressure. *Langmuir* **22:**8826-8830 (2006).

89. R. Vanbever, J. D. Mintzes, J. Wang, J. Nice, D. Chen, R. Batycky, R. Langer, and D. A. Edwards. Formulation and physical characterization of large porous particles for inhalation. *Pharm. Res.* **16:**1735-1742 (1999).

90. W. T. Leach, D. T. Simpson, T. N. Val, Z. Yu, K. T. Lim, E. J. Park, R. O. Williams III, and K. P. Johnston. Encapsulation of protein nanoparticles into uniform-sized microspheres formed in a spinning oil film. *AAPS Pharm. Sci. Tech.* **6:**605-617 (2005).

91. B. S. Chang, B. S. Kendrick, and J. F. Carpenter. Surface-induced denaturation of proteins during freezing and its inhibition by surfactants. *J. Pharm. Sci.* **85:**1325-1330 (1996).

92. R. O. Williams III, K. P. Johnston, T. J. Young, T. L. Rogers, M. K. Barron, Z. Yu, and J. Hu. Process for production of nanoparticles and microparticles by spray freezing into liquid. 2,004,022,861 (2004).

93. H. Gieseler, PhD Thesis, University of Erlangen-Nuremburg, 2004.

94. M. K. Barron, T. J. Young, K. P. Johnston, and R. O. Williams III. Investigation of processing parameters of spray freezing into liquid to prepare polyethylene glycol polymeric particles for drug delivery. *AAPS Pharm. Sci. Tech.* **4:**1-13 (2003).

95. S. Mawson, S. Kanakia, and K. P. Johnston. Coaxial nozzle for control of particle morphology in precipitation with a compressed fluid antisolvent. *J. Appl. Polym. Sci.* **64:**2105-2118 (1997).

96. S. Brunauer, P. H. Emmett, and E. Teller. Adsorption of gases in multimolecular layers. *J. Am. Chem. Soc.* **60:**309-319 (1938).

97. A. A. Elkordy, R. T. Forbes, and B. W. Barry. Integrity of crystalline lysozyme exceeds that of a spray-dried form. *Int. J. Pharm.* **247:**79-90 (2002).

98. Y.-H. Liao, M. B. Brown, A. Quader, and G. P. Martin. Protective Mechanism of Stabilizing Excipients Against Dehydration in the Freeze-Drying of Proteins. *Pharm. Res.* **19:**1854-1861 (2002).

99. A. H. Lefebvre. *Atomization and Sprays*, Hemisphere Publishing Corporation, New York, 1989.

100. R. D. Reitz and F. V. Bracco. Mechanisms of breakup of round liquid jets. In N. P. Cheremisinoff (ed.), *Encyclopedia of Fluid Mechanics*, Gulf Publishing Co., Book Division, Houston, 1986, pp. 233-249.

101. B. J. Meister and G. F. Scheele. Drop formation from cylindrical jets in immiscible liquid systems. *AIChE J.* **15:**700-706 (1969).

102. D. J. Dixon, K. P. Johnston, and R. A. Bodmeier. Polymeric materials formed by precipitation with a compressed fluid antisolvent. *AIChE J.* **39:**127-139 (1993).

103. C. S. Lengsfeld, J. P. Delplanque, V. H. Barocas, and T. W. Randolph. Mechanism governing microparticle morphology during precipitation by a compressed antisolvent: atomization vs. nucleation and growth. *J. Phys. Chem. B* **104:**2725-2735 (2000).

104. E. Badens, O. Boutin, and G. Charbit. Laminar jet dispersion and jet atomization in pressurized carbon dioxide. *J. Supercrit. Fluids* **36:**81-90 (2005).

105. N. Czerwonatis and R. Eggers. Disintegration of liquid jets and drop drag coefficients in pressurized nitrogen and carbon dioxide. *Chem. Eng. Tech.* **24:**619-624 (2001).

106. J. Baldyga, M. Henczka, and B. Y. Shekunov. Fluid dynamics, mass transfer, and particle formation in supercritical fluids. *Drugs Pharm. Sci.* **138:**91-157 (2004).

107. F. Kreith and M. S. Bohn. *Principles of Heat Transfer*, Harper and Row, Publishers, Inc., New York, 1986.

108. F. P. Incropera and D. P. DeWitt. *Fundamentals of Heat and Mass Transfer*, John Wiley and Sons, New York, 2002.

109. J. A. N. Zasadzinski. A new heat transfer model to predict cooling rates for rapid freezing fixation. *J. Microsc.* **150:**137-149 (1988).

110. S. M. Bailey and J. A. N. Zasadzinski. Validation of convection-limited cooling of samples for freeze-fracture electron microscopy. *J. Microsc.* **163:**307-320 (1991).

111. H. Y. Elder, C. C. Gray, A. G. Jardine, J. N. Chapman, and W. H. Biddlecombe. Optimum conditions for cryoquenching of small tissue blocks in liquid coolants. *J. Microsc.* **126:**45-61 (1982).

112. N. H. Fletcher. Structural aspects of the ice-water system. *Rep. Prog. Phys.* **34:**913-994 (1971).

113. E. Mayer and P. Brueggeller. Vitrification of pure liquid water by high pressure jet freezing. *Nature* **298:**715-718 (1982).

114. M. T. Cicerone and C. L. Soles. Fast dynamics and stabilization of proteins: Binary glasses of trehalose and glycerol. *Biophys. J.* **86:**3836-3845 (2004).

115. H. R. Costantino, O. L. Johnson, and S. E. Zale. Relationship between encapsulated drug particle size and initial release of recombinant human growth hormone from biodegradable microspheres. *J. Pharm. Sci.* **93:**2624-2634 (2004).

116. T. J. Anchordoquy, K.-I. Izutsu, T. W. Randolph, and J. F. Carpenter. Maintenance of quaternary structure in the frozen state stabilizes lactate dehydrogenase during freeze-drying. *Arch. Biochem. Biophys.* **390:**35-41 (2001).

117. T. J. Anchordoquy and J. F. Carpenter. Polymers protect lactate dehydrogenase during freeze-drying by inhibiting dissociation in the frozen state. *Arch. Biochem. Biophys.* **332:**231-238 (1996).

118. C. Sonner, PhD Thesis, University of Erlangen-Nuremburg, 2002.

119. T. Dams, R. Ostendorp, M. Ott, K. Rutkat, and R. Jaenicke. Tetrameric and octameric lactate dehydrogenase from the hyperthermophilic bacterium thermotoga maritima: structure and stability of the two active forms. *Eur. J. Biochem.* **240:**274-279 (1996).

120. J. J. Holbrook, A. Liljas, S. J. Steindel, and M. G. Rossmann. Lactate dehydrogenase. In P. D. Boyer (ed.), *Enzymes, 3rd Ed.*, Academic Press, New York, 1975, pp. 191-292.

121. K. A. Pikal-Cleland and J. F. Carpenter. Lyophilization-induced protein denaturation in phosphate buffer systems: monomeric and tetrameric b-galactosidase. *J. Pharm. Sci.* **90:**1255-1268 (2001).

122. B. S. Bhatnagar, S. J. Nehm, M. J. Pikal, and R. H. Bogner. Post-thaw aging affects activity of lactate dehydrogenase. *J. Pharm. Sci.* **94:**1382-1388 (2005).

123. J. F. Carpenter and J. H. Crowe. The mechanism of cryoprotection of proteins by solutes. *Cryobiology* **25:**244-255 (1988).

124. S. N. Timasheff. The control of protein stability and association by weak interactions with water: how do solvents affect these processes? *Annu. Rev. Biophys. Biomol. Struct.* **22:**67-97 (1993).

125. S. D. Webb, J. L. Cleland, J. F. Carpenter, and T. W. Randolph. Effects of annealing lyophilized and spray-lyophilized formulations of recombinant human interferon-γ. *J. Pharm. Sci.* **92:**715-729 (2003).

126. C. Lipinski. Poor aqueous solubility - an industry wide problem in drug discovery. *Am. Pharm. Rev.* **5:**82-85 (2002).

127. R. H. Muller, K. Mader, and S. Gohla. Solid lipid nanoparticles (SLN) for controlled drug delivery - a review of the state of the art. *Eur. J. Pharm. Biopharm.* **50:**161-177 (2000).

128. A. A. Date and V. B. Patravale. Current strategies for engineering drug nanoparticles. *Curr. Opin. Colloid Interface Sci.* **9:**222-235 (2004).

129. K. S. Soppimath, T. M. Aminabhavi, A. R. Kulkarni, and W. E. Rudzinski. Biodegradable polymeric nanoparticles as drug delivery devices. *J. Control. Release* **70:**1-20 (2001).

130. J. M. Vaughn and R. O. Williams III. Nanoparticle Engineering. In J. Swarbrick (ed.), *Encyclopedia of Pharmaceutical Technology*, Dekker, In Press.

131. N. Rasenack and B. W. Mueller. Micron-Size Drug Particles: Common and Novel Micronization Techniques. *Pharm. Develop. Tech.* **9:**1-13 (2004).

132. J. Hu, P. Johnston Keith, and O. Williams Robert, 3rd. Nanoparticle engineering processes for enhancing the dissolution rates of poorly water soluble drugs. *Drug Dev. Ind. Pharm.* **30:**233-245 (2004).

133. H. Leuenberger. Spray Freeze-drying - The Process of Choice for Low Water Soluble Drugs? *J. Nanoparticle Res.* **4:**111-119 (2002).

134. T. L. Rogers, K. P. Johnston, and R. O. Williams III. Solution-based particle formation of pharmaceutical powders by supercritical or compressed fluid CO2 and cryogenic spray-freezing technologies. *Drug Dev. Ind. Pharm.* **27:**1003-1015 (2001).

135. J. M. Vaughn, X. Gao, M.-J. Yacaman, K. P. Johnston, and R. O. Williams. Comparison of powder produced by evaporative precipitation into aqueous solution (EPAS) and spray freezing into liquid (SFL) technologies using novel Z-contrast STEM and complimentary techniques. *Eur. J. Pharm. Biopharm.* **60:**81-89 (2005).

136. J. Hu, K. P. Johnston, and R. O. Williams. Spray freezing into liquid (SFL) particle engineering technology to enhance dissolution of poorly water soluble drugs: organic solvent versus organic/aqueous co-solvent systems. *Eur. J. Pharm. Sci.* **20:**295-303 (2003).

137. T. L. Rogers, K. A. Overhoff, P. Shah, P. Santiago, M. J. Yacaman, K. P. Johnston, and R. O. Williams III. Micronized powders of a poorly water soluble drug produced by a spray-freezing into liquid-emulsion process. *Eur. J. Pharm. Biopharm.* **55:**161-72 (2003).

138. J. C. Evans, B. D. Scherzer, C. D. Tocco, G. B. Kupperblatt, J. N. Becker, J. N. Wilson, S. A. Saghir, and E. J. Elder. Preparation of nanostructured particles of poorly water soluble drugs via a novel ultra-rapid freezing technology. In S. Svenson (ed.), *Polymeric Drug Delivery Volume II - Polymeric Matrices and Drug Particle Engineering*, American Chemical Society, Washington D.C., In Press.

139. N. Ni, M. Tesconi, S. E. Tabibi, S. Gupta, and S. H. Yalkowsky. Use of pure t-butanol as a solvent for freeze-drying: a case study. *Int. J. Pharm.* **226:**39-46 (2001).

140. M. S. Tesconi, K. Sepassi, and S. H. Yalkowsky. Freeze-Drying above Room Temperature. *J. Pharm. Sci.* **88:**501-506 (1999).

141. H. S. Carslaw and J. C. Jaeger. *Conduction of Heat in Solids*, Oxford University Press, London, 1959.

142. T. Bennett and D. Poulikakos. Heat transfer aspects of splat-quench solidification: modeling and experiment. *J. Mater. Sci.* **29:**2025-39 (1994).

143. B. C. Hancock and M. Parks. What is the true solubility advantage for amorphous pharmaceuticals? *Pharm. Res.* **17:**397-404 (2000).

144. K. Terada, H. Kitano, Y. Yoshihashi, and E. Yonemochi. Quantitative correlation between initial dissolution rate and heat of solution of drug. *Pharm. Res.* **17:**920-924 (2000).

145. C.-Y. Gao, A. Li, L.-X. Feng, X.-S. Yi, and J.-C. Shen. Factors controlling surface morphology of porous polystyrene membranes prepared by thermally induced phase separation. *Polym. Int.* **49:**323-328 (2000).

146. Y. S. Nam and T. G. Park. Porous biodegradable polymeric scaffolds prepared by thermally induced phase separation. *J. Biomed. Mater. Res.* **47:**8-17 (1999).

147. S. L. Lee, A. E. Hafeman, P. G. Debenedetti, B. A. Pethica, and D. J. Moore. Solid-State Stabilization of a-Chymotrypsin and Catalase with Carbohydrates. *Ind. Eng. Chem. Res.* **45:**5134-5147 (2006).

148. J. Deng, D. R. Davies, G. Wisedchaisri, M. Wu, W. G. J. Hol, and C. Mehlin. An improved protocol for rapid freezing of protein samples for long-term storage. *Acta Crystallogr., Sect. D: Biol. Crystallogr.* **D60:**203-204 (2004).

149. Y. Yamagata, T. Doen, N. Asakawa, and S. Takada. Process for producing protein powder United States Patent. 6,723,347 (2004).

150. J. C. Gilkey and L. A. Staehelin. Advances in ultrarapid freezing for the preservation of cellular ultrastructure. *J. Electron Microsc. Tech.* **3:**177-210 (1986).

151. J. E. Heuser, T. S. Reese, and D. M. Landis. Preservation of synaptic structure by rapid freezing. *Cold Spring Harbor Symp. Quant. Biol.* **40:**17-24 (1976).

152. J. Escaig. New instruments which facilitate rapid freezing at 83 K and 6 K. *J. Microsc.* **126:**221-230 (1982).

153. E. H. Snell, R. A. Judge, M. Larson, and M. J. van der Woerd. Seeing the heat - preliminary studies of cryocrystallography using infrared imaging. *J. Synch. Radiat.* **9:**361-367 (2002).

154. J. Fukai, Y. Shiiba, T. Yamamoto, O. Miyatake, D. Poulikakos, C. M. Megaridis, and Z. Zhao. Wetting effects on the spreading of a liquid droplet colliding with a flat surface - experiment and modeling. *Phys. Fluids* **7:**236-247 (1995).

155. S. Schiaffino and A. A. Sonin. Motion and arrest of a molten contact line on a cold surface: an experimental study. *Phys. Fluids* **9:**2217-2226 (1997).

156. T. Bennett and D. Poulikakos. Heat-Transfer Aspects of Splat-Quench Solidification - Modeling and Experiment. *J. Mater. Sci.* **29:**2025-2039 (1994).

157. P. G. Debenedetti. Supercooled and glassy water. *J. Phys.: Condens. Matter* **15:**R1669-R1726 (2003).

158. D. E. Graham and M. C. Phillips. Proteins at liquid interfaces. I. Kinetics of adsorption and surface denaturation. *J. Colloid Interface Sci.* **70:**403-14 (1979).

159. D. E. Graham and M. C. Phillips. Proteins at liquid interfaces. II. Adsorption Isotherms. *J. Colloid Interface Sci.* **70:**415-426 (1979).

160. R. O. Williams, III and J. Liu. Formulation of a protein with propellant HFA 134a for aerosol delivery. *Eur. J. Pharm. Sci.* **7:**137-144 (1999).

161. R. O. Williams, III, M. Repka, and J. Liu. Influence of propellant composition on drug delivery from a pressurized metered-dose inhaler. *Drug Dev. Ind. Pharm.* **24:**763-770 (1998).

162. K. A. Johnson. Interfacial phenomena and phase behavior in metered dose inhaler formulations. In A. J. Hickey (ed.), *Inhalation Aerosols: Physical and biological basis for therapy*, 2007.

163. C. Vervaet and P. R. Byron. Drug-surfactant-propellant interactions in HFA-formulations. *Int. J. Pharm.* **186:**13-30 (1999).

164. F. E. Blondino and P. R. Byron. Surfactant dissolution and water solubilization in chlorine-free liquified gas propellants. *Drug Dev. Ind. Pharm.* **24:**935-945 (1998).

165. L. Wu, R. P. S. Peguin, P. Selvam, U. Chokshi, and S. R. P. da Rocha. Molecular scale behavior in alternative propellant-based inhaler formulations. In A. J.

Hickey (ed.), *Inhalation Aerosols: Physical and biological basis for therapy*, 2007.

166. J. Tam, J. T. McConville, R. O. Williams III, and K. P. Johnston. Amorphous cyclosporin A nanodispersions for enhanced pulmonary deposition and dissolution. Submitted. *J. Pharm. Sci.* (2007).

167. Z. Jiang and Y. Guan. Flocculation morphology: effect of particulate shape and coagulant species on flocculation. *Water Sci. Technol.* **53:**9-16 (2006).

168. I. Goodarz-Nia and D. N. Sutherland. Floc simulation. Effects of particle size and shape. *Chem. Eng. Sci.* **30:**407-12 (1975).

169. P. C. Hiemenz and R. Rajagopalan. *Principles of colloid and surface chemistry*, 1997.

170. A. P. Philipse and A. M. Wierenga. On the Density and Structure Formation in Gels and Clusters of Colloidal Rods and Fibers. *Langmuir* **14:**49-54 (1998).

171. A. P. Philipse. The Random Contact Equation and Its Implications for (Colloidal) Rods in Packings, Suspensions, and Anisotropic Powders. *Langmuir* **12:**5971 (1996).

172. R. O. Williams, III, J. Liu, and J. J. Koleng. Influence of metering chamber volume and water level on the emitted dose of a suspension-based pMDI containing propellant 134a. *Pharm. Res.* **14:**438-443 (1997).

173. Y. Kim, S. H. Atwell, and R. G. Bell. Determination of water in pressurized pharmaceutical metered dose aerosol products. *Drug Dev. Ind. Pharm.* **18:**2185-95 (1992).

174. P. G. Smith, Jr., W. Ryoo, and K. P. Johnston. Electrostatically Stabilized Metal Oxide Particle Dispersions in Carbon Dioxide. *J. Phys. Chem. B* **109:**20155-20165 (2005).

175. E. Berlin and M. J. Pallansch. Densities of several proteins and L-amino acids in the dry state. *J. Phys. Chem.* **72:**1887-9 (1968).

176. P. G. A. Rogueda. HPFP, a model propellant for pMDIs. *Drug Dev. Ind. Pharm.* **29:**39-49 (2003).

177. R. Ashayer, P. F. Luckham, S. Manimaaran, and P. Rogueda. Investigation of the molecular interactions in a pMDI formulation by atomic force microscopy. *Eur. J. Pharm. Sci.* **21:**533-543 (2004).

178. D. Traini, M. Young Paul, P. Rogueda, and R. Price. In vitro investigation of drug particulates interactions and aerosol performance of pressurised metered dose inhalers. *Pharm. Res.* **24:**125-135 (2007).

179. S. D. Webb, J. L. Cleland, J. F. Carpenter, and T. W. Randolph. A new mechanism for decreasing aggregation of recombinant human interferon-g by a surfactant: slowed dissolution of lyophilized formulations in a solution containing 0.03% polysorbate 20. *J. Pharm. Sci.* **91:**543-558 (2002).

180. A. Farahnaky, F. Badii, I. A. Farhat, J. R. Mitchell, and S. E. Hill. Enthalpy relaxation of bovine serum albumin and implications for its storage in the glassy state. *Biopolymers* **78:**69-77 (2005).

181. B. Y. Shekunov, P. Chattopadhyay, H. H. Y. Tong, and A. H. L. Chow. Particle Size Analysis in Pharmaceutics: Principles, Methods and Applications. *Pharm. Res.* **24:**203-227 (2007).

182. W. H. Finlay. *The mechanics of inhaled pharmaceutical aerosols*, New York, 2001.

183. A. Sihvola. *Electromagnetic mixing formulas and applications*, 1999.

184. W. B. Russel, D. A. Saville, and W. R. Schowalter. *Colloidal dispersions*, 1989.

185. D. Traini, P. Rogueda, P. Young, and R. Price. Surface Energy and Interparticle Forces Correlations in Model pMDI Formulations. *Pharm. Res.* **22:**816-825 (2005).

186. M. A. Bevan, PhD Dissertation, Carnegie Mellon University, 1999.

187. R. G. Larson. *The Structure and Rheology of Complex Fluids*, Oxford University Press Inc., New York, 1999.

188. P. Tang, J. Greenwood, and J. A. Raper. A model to describe the settling behavior of fractal aggregates. *J. Colloid Interface Sci.* **247:**210-219 (2002).

189. C. Fargues and C. Turchiuli. Structural characterization of flocs in relation to their settling performances. *Chem. Eng. Res. Design* **82:**1517 (2004).

190. H. Abramowitz, P. S. Shah, P. F. Green, and K. P. Johnston. Welding Colloidal Crystals with Carbon Dioxide. *Macromolecules* **37:**7316-7324 (2004).

191. D. R. Ulrich. Chemical processing of ceramics. *Chem. Eng. News* **68:**28-40 (1990).

192. H. D. C. Smyth, A. J. Hickey, and R. M. Evans. Aerosol generation from propellant-driven metered dose inhalers. In J. Hickey Anthony (ed.), *Inhalation Aerosols: Physical and Biological Basis for Therapy*, 2007, pp. 399-416.

193. J. Israelachvili. *Intermolecular and surface forces*, Academic Press, San Diego, 1992.

194. S. Takashima. Proton fluctuation in protein. Experimental study of the Kirkwood-Shumaker theory. *J. Phys. Chem.* **69:**2281-6 (1965).

195. R. Tadmor. The London-van der Waals interaction energy between objects of various geometries. *J. Phys.: Condens. Matter* **13:**L195-L202 (2001).

196. K. A. Pikal-Cleland, N. Rodriguez-Hornedo, G. L. Amidon, and J. F. Carpenter. Protein Denaturation during Freezing and Thawing in Phosphate Buffer Systems: Monomeric and Tetrameric b-Galactosidase. *Arch. Biochem. Biophys.* **384:**398-406 (2000).

197. K. Izutsu, S. Yoshioka, and S. Kojima. Physical stability and protein stability of freeze-dried cakes during storage at elevated temperatures. *Pharm. Res.* **11:**995-9 (1994).

198. S. Jiang and S. L. Nail. Effect of process conditions on recovery of protein activity after freezing and freeze-drying. *Eur. J. Pharm. Biopharm.* **45:**249-257 (1998).

Vita

Joshua David Engstrom was born on September 14, 1978 to Kevin Brent Engstrom and Bonnie Jo Engstrom. After graduating from Centennial High School in Boise, Idaho in 1997, he entered Brigham Young University in Provo, Utah. From May, 1998 to May, 2000 he served a full time mission for his church in Munich, Germany. After his missionary service he returned to Brigham Young University and completed his Bachelor of Science degree in chemical engineering in April, 2003. He also performed research under the supervision of Professor Thomas Fletcher during his undergraduate studies. After graduation he married Jenalyn Renfroe on May 8, 2003 in Salt Lake City, Utah. In August 2003 he entered the University of Texas at Austin in the Department of Chemical Engineering and worked under the supervision of Professors Keith P. Johnston and Robert O. Williams III until August 2007. Upon graduating with his Doctor of Philosophy degree in chemical engineering he will work for Bristol-Myers Squibb in New Brunswick, New Jersey.

Permanent address: 12 Szymanski Dr., Spotswood, NJ 08884

This dissertation was typed by the author.